# Characterisation of immunometabolic responses in astrocytes

Submitted by

**Josephine L. Robb**

to the University of Exeter as a thesis for the degree of

Doctor of Philosophy in Medical Studies

in January 2020.

This thesis is available for Library use on the understanding that it is copyright material and that no quotation from the thesis may be published without proper acknowledgement.

I certify that all material in this thesis which is not my own work has been identified and that any material that has previously been submitted and approved for the award of a degree by this or any other University has been acknowledged.

Signature: ……

## Abstract

Astrocytes play a role in the central nervous system (CNS) inflammatory response. In many immune cell types cellular inflammation and metabolism are linked, a phenomenon termed ‘immunometabolism’. This has led to attempts to reduce chronic inflammation through manipulating cellular metabolism. Proteins of interest for this approach include transcription factor nuclear factor-kappa B (NF-κB) and mitochondrial protein ‘translocator protein (18 kDa)’ (TSPO). TSPO is of particular interest as a therapy for CNS disease as many TSPO ligands can access the CNS and have been demonstrated to have anti-inflammatory effects. However, immunometabolism has not been well described in astrocytes, and the function of TSPO is currently disputed. In this thesis, mouse primary astrocytes were used to characterise immunometabolic responses following treatment with the pro-inflammatory stimulus lipopolysaccharide (LPS). An initial increase in glycolytic metabolism was measured, prior to a shift towards oxidative phosphorylation and away from glucose metabolism, in part mediated by a decrease in glucose transporter GLUT1 expression. Pharmacological inhibition of NF-κB signalling demonstrated that this pathway is important in mediating the cellular metabolic response to inflammation in astrocytes, and may play a role in maintaining basal metabolic function in these cells. Pharmacological or genetic modulation of TSPO signalling in human astroglioma (U373) cells and/or mouse primary astrocytes demonstrated that while TSPO suppressed fatty acid oxidation and promoted glycolytic metabolism, this did not appear to acutely alter the inflammatory response of these cells after LPS treatment; however, the longer term effects remain to be explored. Together these data demonstrate that inflammation and metabolism are intrinsically linked in astrocytes and TSPO plays an important role in regulating metabolism in these cells.

# Table of Contents

# List of Figures

# List of Tables

## Appendices



## Publications arising from thesis

Robb J.L., Hammad N.M., Weightman Potter P.G., Chilton J., Beall C., and Ellacott K.L.J. — *The metabolic response to inflammation in astrocytes is regulated by nuclear factor-kappa B signaling*. **Glia.** (In press at time of submission). DOI:10.1002/glia.23835

Robb J.L., Morrissey N.A., Weightman Potter P.G., Smithers H.E., Beall C., and Ellacott K.L.J. — *Immunometabolic Changes in Glia – A Potential Role in the Pathophysiology of Obesity and Diabetes.* **Neuroscience.** Nov 22 (2019). pii: S0306-4522(19)30708. DOI: 10.1016/j.neuroscience.2019.10.021

## Authors Declaration

All of the work presented in this thesis is a result of experimental work carried out by myself, Josephine L. Robb, with invaluable support from research and academic staff and students at the University of Exeter College of Medicine and Health.

Work carried out with the assistance of others included:

**Chapter 5:** U373 human astroglioma CRISPR/Cas9 TSPO knock out cell line and empty vector controls were created by Daisy Stewart (Professional Training Year, Undergraduate), with the assistance and guidance of Dr Asami Oguro-Ando and Dr Rosemary Bamford.

**Chapter 5:** Immunoblotting experiments presented in **fig. 5.3.9C** and **fig. 5.3.10** were carried out by Daisy Stewart under my guidance.

**Chapter 5:** Seahorse Bioanalyser XFe96 data presented in **fig. 5.3.11** was generated by Daisy Stewart under my guidance.

This has also been stated at the place of presentation, for full transparency.

## Acknowledgements

First and foremost I would like to thank Dr Kate Ellacott, my primary supervisor. Without her help and guidance this work would not exist. I particularly want to thank her for the extra effort she went to, initially finding the funding for me to start my MRes, and then finding further funding and encouraging the University to allow me to transfer onto a PhD to continue the research presented here. Further to this I would like to thank Dr Craig Beall, for taking a risk and letting me work in his lab when I turned up at the RILD L4 door. I also want to thank him for introducing me to Kate and continuing to support my growth as a researcher throughout the past 4 years. I would also like to thank Dr John Chilton for all of his help with coding, imaging, and analysis. Through the support of these three I have grown in confidence and skill as a researcher.

I would also like to thank the amazing team I have been fortunate enough to work with throughout my PhD; Nicole, Nadia, Ana, Katherine, Alastair, Paul and Ben, for encouraging me and supporting me, and particularly Julia who had no small part in training me and starting me on this path. I also want to thank Daisy, who not only created the valuable TSPO knock out cell line used to produce data for some of this thesis but who also pushed me to be a better teacher and scientist.

I would, finally, like to thank my family and Jacob, whose unending support allowed me to start this PhD, and encouragement allowed me to finish it.

# List of Abbreviations

For the convenience of the reader, commonly used abbreviations are listed below.

| Abbreviation | Definition |
|---|---|
| 2-DG | 2-deoxy-6-glucose |
| 2DG6P | 2-deoxyglucose-6-phosphate |
| ACC | Acetyl-CoA carboxylase |
| ACLY | ATP citrate lyase |
| ADP | Adenosine diphosphate |
| Akt | Protein kinase B; see PKB |
| AMP | Adenosine monophosphate |
| AMPK | AMP-activated protein kinase |
| ANOVA | Analysis of variance |
| ANT | Adenosine nucleotide transporter |
| AP | Activator protein |
| APS | Ammonium persulfate |
| ATP | Adenosine triphosphate |
| AUC | Area under the curve |
| BBB | Blood-brain barrier |
| BSA | Bovine serum albumin |
| $Ca^{2+}$ | Calcium ions |
| CaMKK | Calcium-calmodulin dependent protein kinase kinase |
| CD-14 | Cluster of differentiation 14 |
| CNS | Central nervous system |
| COX2 | Cyclooxygenase-2 |
| CPT-1A | Carnitine palmitoyl transferase-1A |
| CRAC motif | Cholesterol Recognition/Interaction Amino Acid Consensus motif |
| CRISPR | Clustered Regularly Interspaced Short Palindromic Repeats |
| CRTAS | Mouse cortical primary astrocytes |
| Cx43 | Connexin 43 |
| DAMP | Damage-associated molecular pattern |

| | |
|---|---|
| DBM | n-dodecyl-beta-maltoside |
| DMEM | Dulbecco’s Modified Eagle’s Medium |
| DMSO | Dimethyl sulfoxide |
| DNA | Deoxyribose nucleotide |
| Drp-1 | Dynamin related protein 1 |
| ECAR | Extracellular acidification rate |
| EDTA | Ethylenediaminetetraacetic acid |
| EGTA | Ethylene glycol-bis(β-aminoethyl ether)-N,N,N’,N’-tetraacetic acid |
| ELISA | Enzyme-linked immunosorbent assay |
| ERK | Extracellular signal regulated kinase |
| ETC | Electron transport chain |
| EV | Empty vector |
| FABP | Fatty acid binding protein |
| FACS | Fluorescence activated cell sorting |
| FAD | Flavin adenine dinucleotide |
| $FADH_2$ | Flavin adenine dinucleotide (reduced) |
| FAO | Fatty acid oxidation |
| FAS | Fatty acid synthase |
| FBS | Foetal bovine serum |
| FCCP | Carbonyl cyanide-4-trifluromethoxyphenylhydrazone |
| FSC | Forward scatter |
| g | Gram |
| GAPDH | Glyceraldehyde 3-phosphate dehydrogenase |
| GFAP | Glial fibrillary acidic protein |
| GDP | Guanosine diphosphate |
| GLAST | Glutamate aspartate transporter |
| GLT | Glutamate transporter |
| GLUT | Glucose transporter |
| GM | Genetically modified |
| GTP | Guanosine triphosphate |
| HBSS | Hanks Balanced Salt Solution |
| HCl | Hydrochloric acid |

| | |
|---|---|
| HEPES | 4-(2-hydroxyethyl)-1-piperazineethanesulfonic acid |
| HFD | High fat diet |
| HFHS | High fat, high sugar |
| HIF-1α | Hypoxia inducible factor 1 alpha |
| iATP | Intracellular adenosine triphosphate |
| IBA-1 | Ionized calcium binding adaptor molecule 1 |
| $IC_{50}$ | Half maximal inhibitory concentration |
| IFN-γ | Interferon gamma |
| lκB | I kappa B |
| IKK | I kappa B kinase |
| IL | Interleukin |
| IL-R | Interleukin receptor |
| IMM | Inner mitochondrial membrane |
| JAK | Janus kinase |
| JNK | c-Jun N-terminal kinases |
| $K^+$ | Potassium ion |
| Kir4.1 | Potassium inwardly rectifying channel 4.1 |
| kDa | Kilo Daltons |
| LDH | Lactate dehydrogenase |
| LPS | Lipopolysaccharide |
| MAPK | Mitogen-activated protein kinase |
| MBP-1 | Myc promoter-binding protein 1 |
| MCP | Monocyte chemoattractant protein |
| MD-2 | Lymphocyte antigen 96 |
| Mfn | Mitofusin |
| mL | Millilitre |
| mM | Millimolar |
| MPTP | Mitochondrial permeability transition pore |
| mRNA | Messenger RNA |
| mTOR | Mammalian target of rapamycin |
| MyD88 | Myeloid differentiation factor 88 |
| $Na_3VO_4$ | Sodium orthovanadate |
| NaCl | Sodium chloride |

| | |
|---|---|
| $NAD^+$ | Nicotinamide adenine dinucleotide (oxidised) |
| NADH | Nicotinamide adenine dinucleotide (reduced) |
| NADPH | Nicotinamide adenine dinucleotide phosphate (reduced) |
| NaF | Sodium fluoride |
| NaOH | Sodium hydroxide |
| NaPPi | Sodium pyrophosphate tetrabasic decahydrate |
| NEMO | NF-κB regulatory subunit; IKKγ |
| NF-κB | Nuclear factor kappa-light-chain-enhancer of activated B cells |
| nM | Nanomolar |
| nm | Nanometer |
| NOX | NADPH oxidase |
| $O_2$ | Oxygen |
| $O_2^{\bullet-}$ | Superoxide |
| OCR | Oxygen consumption rate |
| Oligo | Oligomycin |
| OMM | Outer mitochondrial membrane |
| OPA-1 | Optic atrophy 1 |
| OXPHOS | Oxidative phosphorylation |
| PAMP | Pathogen-associated molecular pattern |
| PBR | Peripheral benzodiazepine receptor; see TSPO |
| PBS | Phosphate buffered saline |
| PCR | Polymerase chain reaction |
| PET | Positron emission tomography |
| PFK2 | Phospho-fructokinase 2 |
| PFKFB3 | 6-phosphofructo-2-kinase/fructose-2,6-biphosphatase |
| PI3K | Phosphoinositide-3-kinase |
| PKB | Protein kinase B |
| PKC | Protein kinase C |
| PKM2 | Pyruvate kinase isozyme M2 |
| PLL | Poly-L-lysine |
| PMSF | Phenylmethylsulfonyl fluoride |
| PPAR | Peroxisome proliferator-activated receptor |
| PPP | Pentose phosphate pathway |

| | |
|---|---|
| PRR | Pattern recognition receptor |
| R/A | Rotenone with antimycin A |
| RET | Reverse electron transport |
| RHD | Rel homology domain |
| RIPA | Radioimmunoprecipitation assay |
| ROS | Reactive oxygen species |
| RXR | Retinoic X receptor |
| SDS | Sodium dodecyl sulphate |
| SEM | Standard error from the mean |
| siRNA | Small interefering RNA |
| Sp | Specificity protein |
| Srepb | Sterol regulatory element binding protein |
| SSC | Side scatter |
| STAT | Signal transducers and activators of transcription |
| TBK1 | TANK binding kinase 1 |
| TBS-T | Tris buffered saline with tween 20 |
| TCA | Tricarboxylic acid |
| TEMED | Tetramethylethylenediamine |
| TIR | Toll/IL-1-receptor domain |
| TLR | Toll-like receptor |
| TMRE | Tetramethylrhodamine ethyl ester |
| TNF | Tumour necrosis factor |
| TSPO | Translocator protein 18 kDa |
| UCP | Uncoupling protein |
| VDAC | Voltage dependent anion channel |

# Chapter 1. Introduction

Many neurodegenerative diseases, including Alzheimer's (Kinney *et al.*, 2018), multiple sclerosis (Matthews, 2019) and Parkinson's disease (Caggiu *et al.*, 2019) are caused by inappropriate and perpetuated immune responses within the central nervous system (CNS). Recent developments in the study of the immune response have revealed that an intrinsic part of inflammation is a change in cellular metabolism (O'Neill *et al.*, 2016). It has therefore been suggested that one way of controlling inflammation to help treat disease is through modulating cellular metabolism (Rhoads *et al.*, 2017).

In the CNS the immune response is in part controlled by a non-neuronal cell type called astrocytes. However, there is currently very little known about the metabolic response to inflammation in astrocytes. This chapter aims to introduce the concept of immunometabolism and consolidate the current knowledge of immunometabolism and its regulation in astrocytes. This will be with particular regard to the nuclear factor kappaB (NF-κB) pathway, although other inflammatory signalling pathways have been shown to play important roles in immunometabolic regulation (Hotamisligil, 2017; Robb *et al.*, 2019). The translocator protein 18 kDa (TSPO) will also be introduced as a potential novel regulator of immunometabolism.

## 1.1 Astrocytes as regulators of CNS function

There are multiple classes of non-neuronal cells in the brain, collectively termed glia. One class of glia are the astrocytes. These are large stellate cells which

reside within the CNS and are ramified and highly plastic, both in function and morphology. Astrocytes were first classified by Santiago Ramon y Cajal and named by Michael von Lenhossek in 1891 (Parpura & Verkhratsky, 2012). Once assumed to be a homogenous class of cell, evidence is emerging that there are subtypes of astrocytes, with specialised roles dependent on receptor expression, location, and interactions with other specialised cells within the brain (Allen, 2014).

### 1.1.1 Maintenance of the extracellular environment

Astrocytes are important for the maintenance of the CNS microenvironment and are key regulators of neuronal physiology and behaviour (Buskila *et al.*, 2019). The position of astrocytes adjacent to blood vessels allows them to be responsive to peripheral cues, such as circulating nutrient, hormone and cytokine levels (Daneman & Prat, 2015). This positioning allows them to play a role in regulating access to the CNS. Astrocyte end feet contact capillaries, and tight junctions between end feet form a barrier called the *glia limitans* which prevents passage of large molecules into the CNS (Alvarez *et al.*, 2013). Many substrates, such as glucose and fatty acids, access the brain by being taken up through specific transporters on astrocyte end feet. This allows astrocytes to regulate provision of nutrients and metabolites to the CNS (Alvarez *et al.*, 2013). Thus astrocytes are an important component of the blood brain barrier (BBB), the selective, semipermeable interface which separates the brain from circulating blood (Daneman & Prat, 2015).

### 1.1.2 Maintenance of neuronal function

Astrocyte end feet are in close proximity to neuronal synaptic clefts, forming a key component of the tripartite synapse. Due to their size and structure, astrocytes can interact with thousands of synapses simultaneously, allowing them to integrate information from across the CNS (Allen, 2014; Bushong *et al.*, 2002). This is in addition to contacting peripheral blood vessels, so allowing a single astrocyte to respond to information from both the periphery and within the CNS, and rapidly provide nutrients and substrate to neurons as needed to fuel their activity (Foo *et al.*, 2011). Astrocytes are thought to ensheath roughly 60%–90% of synaptic clefts in the CNS (Farhy-Tselnicker & Allen, 2018; Nedergaard & Verkhratsky, 2012). As astrocytes are morphologically plastic the interactions between astrocyte end feet and synapses are dynamic, and synapses can be ensheathed and unsheathed as needed (Farhy-Tselnicker & Allen, 2018). This is thought to occur through the receptor tyrosine kinase family eph and ligand ephrin. Astrocytes express multiple members of these families, including ephrin-A1, -A3, -B2, and eph-A4 (Yang *et al.,* 2018). These cell adhesion molecules drive the rearrangement of the astrocyte cytoskeleton (Carmona *et al.*, 2009; Pasquale, 2008). As this interaction is bidirectional, astrocytes can also influence neuronal dendritic spine formation and axon guidance through this mechanism. For example, loss of EphrinA3 from glial cells reduces phosphorylation of EphA4 and disrupts dendritic spine morphology in the mouse hippocampus (Carmona *et al.*, 2009).

Astrocytes express neurotransmitter transporters and receptors, making them capable of detecting, clearing and directly responding to alterations in

neurotransmitter levels (Verkhratsky *et al.*, 2019). In particular, astrocytes regulate clearance of the excitatory neurotransmitter glutamate (Murphy-Royal *et al.*, 2017). Glutamate is taken into astrocytes through glutamate transporters such as glutamate transporter 1 (GLT-1) and glutamate aspartate transporter 1 (GLAST) making these cells important for preventing excitotoxicity (Mahmoud *et al.*, 2019). Indeed, ablation of astrocytes in mice results in neurodegeneration and death due to overstimulation by excitatory neurotransmitters when they are not removed from the synapse (Allen, 2014; Jäkel & Dimou, 2017). This demonstrates that astrocytes are essential for the proper development and maintenance of normal CNS function (Allen, 2014; Jäkel & Dimou, 2017).

In addition to clearing neurotransmitters from the synapse, astrocytes release compounds which can directly modulate both glial and neuronal signalling. These are collectively called gliotransmitters. Major gliotransmitters released by astrocytes include glutamate and adenosine triphosphate (ATP), among others (Covelo & Araque, 2018; Harada *et al.*, 2016). Gliotransmitter release can be regulated by intracellular $Ca^{2+}$ signalling (Harada *et al.*, 2016), which stimulates vesicular exocytosis. Additionally, gliotransmitter release can be regulated by activity of astrocyte transporters such as GLT-1 and GLAST, and hemichannels such as connexin 43 (Cx43) (Harada *et al.*, 2016), which allow bidirectional movement of molecules and ions between cells and into the extracellular space (Cotrina *et al.*, 1998; Xu *et al.*, 2019).

Astrocytes also regulate neuronal firing through maintaining the ion concentration in the CNS extracellular environment. An action potential is propagated by loss

of neuronal membrane polarisation (Øyehaug *et al.*, 2012). Polarisation is maintained by potassium ions ($K^+$). $K^+$ can be taken up into astrocytes through $K^+$ channels, such as the inwardly rectifying Kir4.1 channel and pumps such as $Na^+/K^+$ ATPases (Nwaobi *et al.*, 2016). Low levels of extracellular $K^+$ decrease the membrane potential, increasing polarisation across the membrane (Øyehaug *et al.*, 2012). This decreases neuronal excitability, demonstrating that astrocytes can contribute to the regulation of neuronal firing.

Astrocytic regulation of neuronal firing results in astrocytes orchestrating physiological changes in the whole organism (Liddelow & Barres, 2017). However, inflammation alters astrocyte behaviour. This can result in changes in the CNS environment, which then affects physiology beyond the CNS. These changes to the CNS environment can promote neurodegeneration if inappropriately regulated. Therefore, we need to fully understand the astrocytic response to inflammation in order to develop appropriate interventions aimed at minimising the detrimental changes caused by inflammation.

## 1.2 Inflammation

Inflammation is the response to mechanical, chemical and/or biological damage, or deviations from homeostasis. Its role is to help resolve and restore the organism back to its basal state. This is orchestrated by immune effector cells, such as macrophages and lymphocytes (in the periphery) and astrocytes and microglia (in the CNS), which mediate the complex multifaceted response (Chen *et al.*, 2017). Cellular inflammation is broadly constituted of two phases. The initial 'pro-inflammatory' phase is characterised by immune cell proliferation and

release of cytotoxic agents. These include pro-inflammatory cytokines such as interleukin 1β (IL-1β) and tumour necrosis factor α (TNF-α), and chemokines, a group of small chemoattractive cytokines. This phase is designed to destroy infectious factors such as bacteria and viruses (Chen *et al.*, 2017). Bacteria and viruses are detected by pattern recognition receptors (PRRs) found on immune effector cells which activate downstream pathways leading to the initiation of the pro-inflammatory phase. PRR signalling will be discussed in more depth later in the chapter. A secondary 'anti-inflammatory' phase is aimed at resolving inflammation and promoting tissue repair through the release of immunomodulatory agents such as interleukin 10 (IL-10) (Headland & Norling, 2015). The second phase can be initiated by the increasing concentration of cytotoxic chemicals, including cytokines such as TNF-α released in the first phase.

### 1.2.1 Chronic inflammation in disease

Chronic inflammation is extended activation of the pro-inflammatory response. This can be caused either through failure of the immune response to remove the inflammatory stimulus or repeated persistent exposure to the stimulus (Pahwa & Jialal, 2019). This prolongs exposure of cells to cytokines, although often at relatively low concentrations, often leading to cell death and the development of disease specific to the tissue(s) affected (Newcombe *et al.*, 2018). The effect of chronic inflammation in the CNS is of concern because of the current aging population. There is substantial evidence that chronic low grade inflammation contributes to the pathology of neurodegenerative diseases, including Parkinson's disease (Whitton, 2007), multiple sclerosis (Matthews, 2019), and

dementias including Alzheimer's disease (Kinney *et al.*, 2018). For example, during Alzheimer's disease beta-amyloid protein accumulates in the extracellular matrix, forming 'plaques', resulting cellular stress and leading to activation and perpetuation of the immune response. This immune response recruits both astrocytes and microglia, resulting in chronic inflammation (Johnson *et al.,* 2020; Kinney *et al.,* 2018). Accumulation of pro-inflammatory cytokines, such as IL-1β and IL-6, as a result of this unresolved immune response, can activate signalling pathways leading to the hyperphosphorylation of tau, a microtubule binding protein (Kinney *et al.,* 2018). Hyperphosphorylated tau forms 'tangles' within neurons, disrupting normal neuronal function. Further to this, the prolonged presence of pro-inflammatory cytokines suppresses the expression of anti-apoptotic proteins, promoting apoptosis of neurons (Kinney *et al.,* 2018). This leads to neurodegeneration and advancement of Alzheimer's disease.

Neurodegeneration describes the loss of functional neurons, leading to impairment in motor and/or cerebral function and often resulting in premature death. This class of disease is highly prevalent: around 50 million people worldwide are currently living with a diagnosis of dementia (World Health Organisation, 2019). Beyond the debilitating symptoms mainly characterised by loss of memory and deteriorating physical ability, these diseases place a high burden of care on families. This results in high societal and financial costs, which are estimated to be an average 1.1% of the global GDP (Gross domestic product: US $818 billion) (World Health Organisation, 2019). Predictions currently estimate that there will be 82 million people living with dementia by 2030, emphasising the growing scale of the problem (World Health Organisation, 2019). These data only consider the impact of dementias, and not the other rarer forms

of neurodegeneration. However, they make clear the scale of the current burden of disease. Therefore, understanding CNS inflammation and developing methods to treat it are important.

### 1.2.2 Inflammation in the CNS

Despite the importance of this field of study, inflammation in the CNS is currently less well characterised than inflammation in the rest of the body. When intact, the BBB largely prevents passage of pathogens into the cerebrospinal fluid. However, while there is evidence of leukocyte and macrophage infiltration into the brain during disease (Schmitt *et al.*, 2012; Zattoni *et al.*, 2011), in the non-diseased state the BBB also restricts movement of peripheral immune cells into the brain (Sofroniew, 2015). Typically, immune cell infiltration does not generally occur in sufficient numbers to orchestrate the scale of immune response seen in the CNS during disease. Therefore, CNS inflammation is thought to be mediated by glia, including astrocytes, which are immune competent cells (Engelhardt, 2008; Wilson *et al.*, 2010). An immune competent cell is defined as a cell capable of initiating an immune response when appropriately stimulated by an antigen. The immune response initiated by astrocytes includes recruiting and activating other immune cell types through expression and release of chemokines; presentation of antigens using class II major histocompatibility complex molecules; and removal of damaged structures and pathogens through phagocytosis (Preigo & Valiente, 2019; Wilson *et al.,* 2010; Tremblay *et al.,* 2019). The role of astrocytes in the immune response within the CNS is discussed in further detail below.

### 1.2.3 Astrocytes in CNS inflammation

During inflammation astrocytes undergo morphological and functional adaptations called reactive astrogliosis. Astrogliosis is defined by functional and structural changes to astrocytes, including upregulation of the cytoskeletal intermediate filament protein glial fibrillary acidic protein (GFAP) and a transition to a highly ramified structure. This is caused by activation of intracellular signalling pathways. Signalling pathways activated during astrogliosis include NF-κB, mitogen activated protein kinases (MAPKs) and Janus kinase (JAK) - signal transducers and activators of transcription (STATs). Activation of these signalling pathways vastly alters cellular activity, including the regulation of gene expression (Zamanian *et al.*, 2012).

The *glia limitans* places astrocytes in a unique position to regulate the CNS response to peripheral inflammation as there is evidence that astrocytes can regulate inflammation whilst the *glia limitans* is intact. Astrocytes express PRRs on their end feet both on the *glia limitans* extending into the periphery, and within the CNS. Activation of these PRRs induces inflammatory pathways *in vivo* when subjected to stressors, including metabolic stress or infection (Colombo & Farina, 2016; Zamanian *et al.*, 2012). This leads to cytokine release by astrocytes within the CNS in response to inflammatory stimuli (Sofroniew, 2013). Astrocytes also regulate the migration of monocytes and leukocytes across the BBB whilst the *glia limitans* remains intact, mediated at least in part through expression of monocyte chemoattractant protein-1 (MCP-1). This chemokine attracts immune cells towards the *glia limitans*, and reduces tight junction formation between the cells of the *glia limitans*, impacting the permeability of the BBB (Stamatovic *et al.*,

2005; Yao & Tsirka, 2014). Immune cells attracted by MCP-1 can then bind to adhesion proteins and migrate across the *glia limitans* (Weiss *et al.*, 1998). In response to extensive inflammation and tissue damage astrocytes proliferate to form glial scars to maintain the *glia limitans* and limit further injury of healthy tissue (Adams & Gallo, 2018).

Other regulatory roles that astrocytes play within the CNS are perturbed during inflammation. For example, during CNS inflammation, synaptic glutamate is increased (Matute *et al.*, 2006). This may be exacerbated by impaired glutamate clearance by astrocytes as a result of downregulation of glutamate transporter expression after exposure to pro-inflammatory cytokines such as TNF-α and interleukin 1β (IL-1β) (Matute *et al.*, 2006; Olmos & Lladó, 2014; Tilleux & Hermans, 2007). During inflammation astrocytes also release more gliotransmitters. In amyloid plaque forming mouse models of Alzheimer's disease the opening of the astrocyte hemichannel Cx43 is increased. This results in increased glutamate and ATP release from astrocytes (Yi *et al.*, 2016). This is supported by *in vitro* evidence demonstrating that pro-inflammatory stimulation with bacterial cell wall protein lipopolysaccharide (LPS) or bradykinin also increases glutamate and ATP release from rodent astrocytes, driven through hemichannel opening (Chávez *et al.*, 2019; Liu *et al.*, 2009; Xu *et al.*, 2019). Together these data show that during inflammation changes in astrocytes can directly impact neuronal behaviour in part through gliotransmitter release and changes in neurotransmitter reuptake, which can exacerbate excitotoxicity and cell death (Matute *et al.*, 2006).

During inflammation and neurodegenerative diseases astrocyte control over ion homeostasis is also disrupted. For example, in mouse models of multiple sclerosis and Alzheimer's disease, or after treatment with the inflammatory cytokine IL-1β, the expression of the potassium channel Kir4.1 is downregulated *in vivo*, reducing $K^+$ uptake by astrocytes (Nwaobi *et al.*, 2016). Genetically induced overexpression of Kir4.1 in astrocytes in mouse models of Huntington's disease reduced associated neurodegeneration (Tong *et al.*, 2014). Together these data suggest that perturbations in $K^+$ uptake increase neuronal cell death. Astrocyte synapse ensheathment is heightened during inflammation. During astrogliosis ephrin-B2 and Eph-A4 expression are increased, possibly to encourage axon regrowth and increase astrocyte involvement in neuronal signalling (Bundesen *et al.,* 2003; Frugier *et al.,* 2012). However, this can increase formation of glial scars (Pasquale, 2008; Yang *et al.,* 2018). Loss of these key cell adhesion molecules prevents astrogliosis, suggesting a role of astrocyte-neuron interactions in CNS inflammation.

Together, the data described in this section suggest that inflammation induces changes to astrocyte function, as summarised in **fig. 1.2.3,** resulting in changes to the CNS microenvironment. This in turn impacts neuronal survival and behaviour.

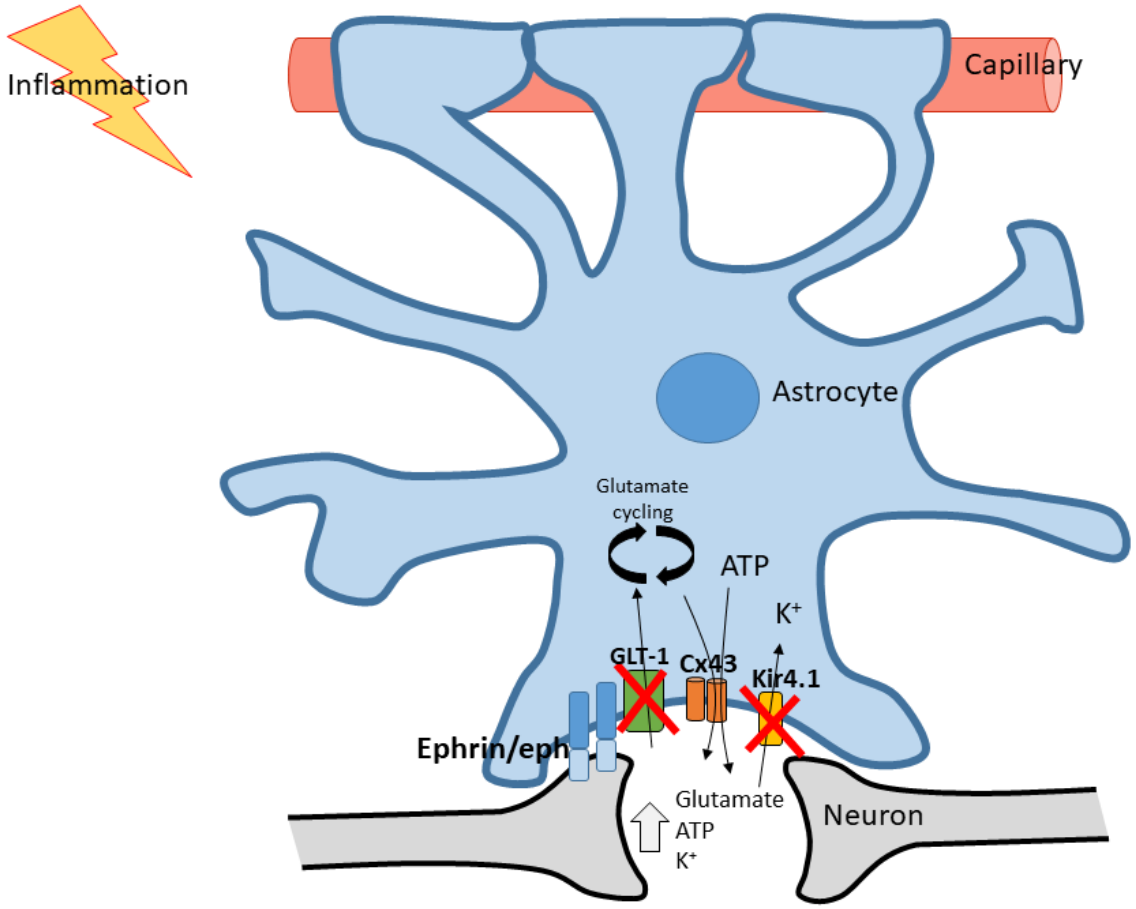


**Figure 1.2.3: A simplified schematic demonstrating alteration in astrocyte function during inflammation**. Glutamate transporter (GLT-1) expression is reduced, reducing glutamate clearance and cycling. Connexin 43 (Cx43) expression is increased, increasing release of gliotransmitters ATP and glutamate into the synapse. Expression of the $K^+$ inwardly rectifying channel (Kir4.1) is decreased, reducing $K^+$ uptake and reducing neuronal membrane polarisation, promoting neuronal excitability. Adhesion molecules ephrin/eph are upregulated, encouraging synapse formation and plasticity but also promoting glial scar formation.

### 1.2.4 Regulation of inflammation

The initiation of inflammation is mediated by multiple receptors, collectively termed PRRs, which detect activators called pathogen-associated molecular patterns (PAMPs; e.g. Lipopolysaccharide [LPS]) or damage-associated molecular patterns (DAMPs; e.g. DNA) (Tang *et al.*, 2012). A well-known class of PRRs are toll-like receptors (TLRs). When stimulated these receptors activate downstream signalling pathways, such as NF-κB and mitogen-activated protein kinase (MAPK) signalling, which interact with each other to give a tightly controlled response (Chen *et al.*, 2017). The signalling pathways used and resultant response differs from cell type to cell type depending on the role the cell plays in the whole-body inflammatory response, and also depending on the type of inflammatory stimulus (Escoll & Buchrieser, 2018; Kim & Harty, 2014; Mosser & Edwards, 2008; Pennock *et al.*, 2013; Vergadi *et al.*, 2017; Wager & Wormley, 2014). This allows an appropriate proportional response to inflammatory stimuli, in both scale and duration, to ensure the long-term health of the organism. However, this process can become dysfunctional due to the failure of individual or multiple pathways. In turn, this may exacerbate inflammation and can result in failure of the response to resolve, leading to the development of chronic inflammation (Cope, 2002).

The following sections will introduce NF-κB as an inflammatory regulator and discuss its role in astrocyte function, specifically regarding control of both cellular and systemic metabolism.

### 1.2.5 Nuclear Factor-kappa B regulation of inflammation

In mammals the NF-κB family is composed of 5 proteins: p65 (RelA), RelB, c-Rel, p105/p50 (NF-κB1) and p100/p52 (NF-κB2) (Lawrence, 2009; Oeckinghaus & Ghosh, 2009; Perkins, 2007). These proteins can form homodimers and heterodimers which regulate cellular function by acting as transcription factors. These proteins all contain a Rel homology domain (RHD) which is bound by IκB (nuclear factor of kappa light polypeptide gene enhancer in B-cells inhibitor) to sequester the molecules in the cytoplasm, preventing them from promoting the unregulated transcription of target genes. NF-κB signalling can be activated by two distinct pathways: canonical or non-canonical activation. During the canonical or classical pathway IκB is phosphorylated by heterodimers of IκB kinase (IKK), IKKα and IKKβ with an IKKγ regulatory subunit (NEMO). This leads to ubiquitination and proteasomal degradation of IκB, releasing NF-κB; commonly p65-p50 heterodimers. NF-κB signalling can also be initiated through the non-canonical or alternative pathway. This is regulated by IKKα homodimers which liberate primarily p52-RelB NF-κB dimers through ubiquitination and proteasomal processing of p100 into p52 (**fig. 1.2.5.1**).

Once activated, NF-κB dimers from both pathways translocate into the nucleus. Here, they can bind to promotors to regulate gene transcription. It is important to note that active NF-κB dimers can also localise within the mitochondria when the tumour suppressor p53 is absent (Tornatore *et al.*, 2012). Localisation to the mitochondria results in inhibition of mitochondrial genes, including those coding for components of the electron transport chain (ETC). This will be described in more detail later in this chapter.

Whilst both the canonical and non-canonical NF-κB pathways are activated by pro-inflammatory stimuli, they are activated by different cell surface receptors. The non-canonical pathway is activated by a subset of tumour necrosis factor (TNF) receptors through highly specific stimuli, including CD40 ligand and B-cell activating factor (Sun, 2017). By contrast, the canonical pathway has a broader range of activating stimuli, including the TNF receptor family, but also TLRs and interleukin receptors (IL-Rs) (Liu *et al.*, 2017c).

Activity of the canonical NF-κB pathway can be regulated by the pro-inflammatory factor LPS (Liu *et al.*, 2017c). This is an endotoxin from the bacterial cell wall which acts as a PAMP and elicits a strong inflammatory response in most cell types. LPS stimulates multiple cell surface receptors, including Toll Like Receptor 4 (TLR4). TLR4 signalling is summarised in **fig 1.2.5.2** and can activate both canonical and non-canonical NF-κB signalling. Proteins CD-14 and MD-2 act as co-receptors to TLR-4. On activation, myeloid differentiation factor 88 (MyD88) is recruited to the Toll/IL-1-receptor domain (TIR) of the receptor to activate IKK and MAPK signalling cascades, c-Jun N-terminal kinases (JNK), extracellular signal regulated kinase (ERK), and p38. This leads to the activation of transcription factors activator protein-1 (AP-1) and NF-κB (Hayden & Ghosh, 2008).

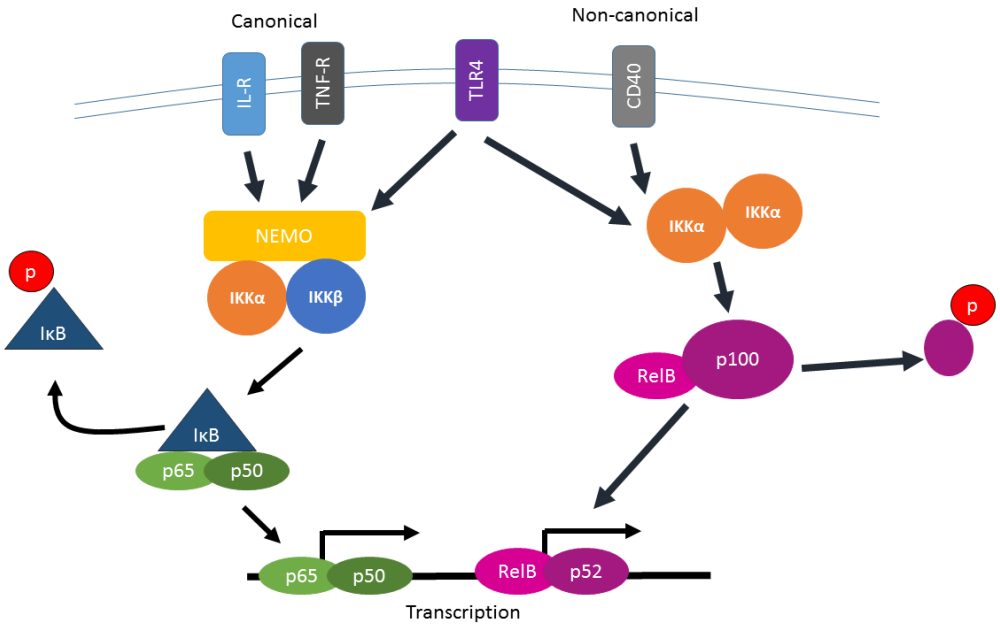


**Figure 1.2.5.1: A simplified schematic of nuclear factor κB (NF-κB) activation signalling pathways.** The canonical signalling pathway is activated by stimulation of receptors such as interleukin receptor (IL-R) or tumour necrosis factor receptor (TNF-R). This leads to phosphorylation of IκB heterodimers (IKKα and IKKβ) bound to the regulatory subunit IKKγ (NEMO), which in turn phosphorylate IκB, allowing heterodimers of NF-κB p65-p50 to be liberated and translocated into the nucleus. The non-canonical signalling pathway is activated by CD40 ligand, leading to phosphorylation of IKKα homodimers. This results in phosphorylation, processing and ubiquitination of p100 NF-κB into p52, allowing translocation of RelB-p52 heterodimers into the nucleus. Both of these pathways can be activated by toll like receptor 4 (TLR4) and result in changes to gene transcription.

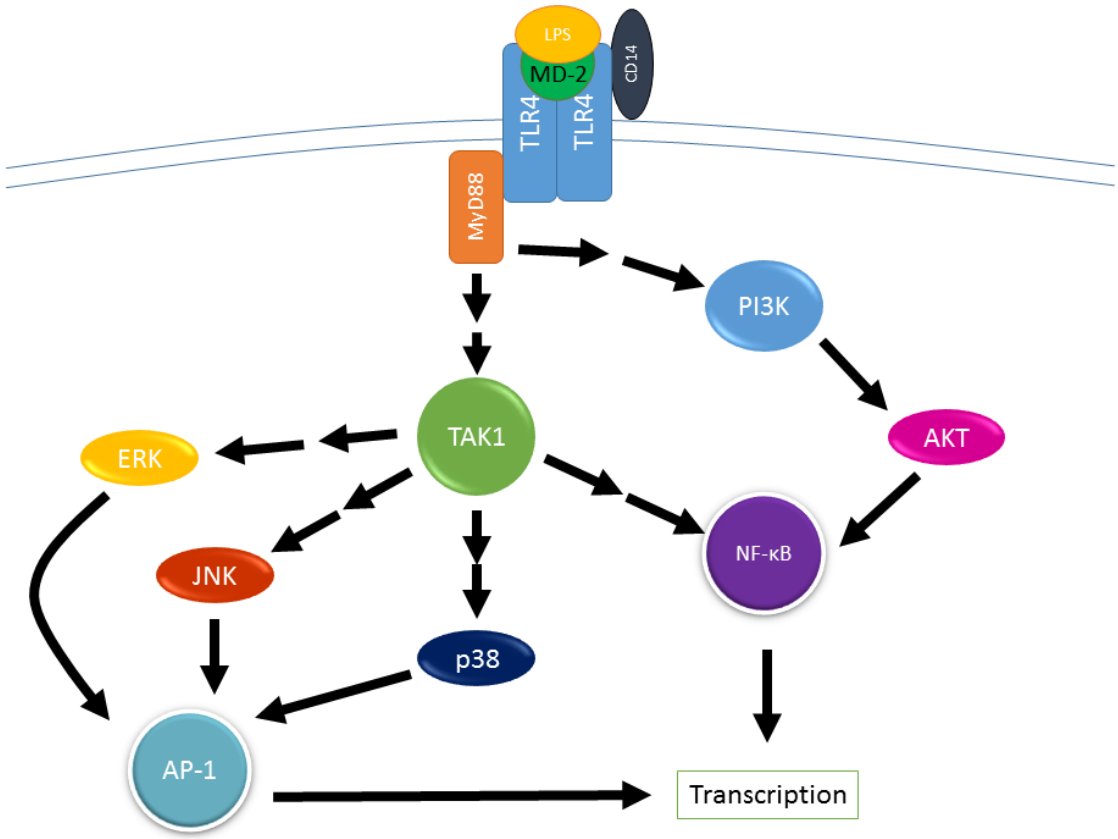


**Figure 1.2.5.2: A simplified representation of signalling pathways downstream of Toll Like Receptor 4 (TLR4).** When TLR4 is activated, it dimerises and recruits the co-receptors CD-14 and MD-2. This leads to recruitment of MyD88, which in turn activates intracellular signalling cascades, resulting in transcription of target genes.

### 1.2.6 Astrocytic NF-κB signalling in the regulation of neuronal function

NF-κB signalling is activated in astrocytes during inflammation. Proteomic profiling of the astrocytic response to pro-inflammatory cytokines and LPS suggests that these stimuli differentially activate the canonical and non-canonical NF-κB signalling pathways, with LPS initially activating the non-canonical pathway, measured by immunoblot detection of p52 after 1 hour, although it is unclear through which mechanism (Dozio & Sanchez, 2018). This study showed no activation of the canonical NF-κB pathway by LPS after 1 hour, 8 hour or 24 hour exposure. However, other studies have shown translocation of p65 to the nucleus and/or phosphorylation of p65 after treatment with LPS in astrocytes, with some studies showing activation persisting after 24 hours (Zhou *et al.,* 2015). This suggests that LPS does activate the canonical NF-κB signalling pathway in astrocytes. Activation of NF-κB leads to genome-wide changes to protein expression, regulating proteins involved in inflammation such as TNF-α and interleukins (IL) including IL-6 and IL-10. It can also lead to activation of the NLRP-3 inflammasome leading to release of IL-1β. Additionally, NF-κB drives transcription of molecules associated with cell growth and survival in astrocytes (Pahl, 1999), and the structural protein vimentin (Zheng *et al.*, 2005); thus, potentially linking changes in inflammatory signalling and morphology in astrocytes.

Preventing inflammation in astrocytes through inhibition of NF-κB signalling can alter the pathophysiological response to disease. For example, inhibition of NF-κB activity in GFAP expressing astrocytes promotes functional recovery of spinal

cord injury in mice, resulting in reduced glial scarring and increased locomotor activity (Brambilla *et al.*, 2005). There is also evidence that loss of NF-κB signalling from astrocytes reduces astrogliosis in mouse models of diet-induced obesity, resulting in reduced disease pathology (Buckman *et al.*, 2014; Douglass *et al.*, 2017; Zhang *et al.*, 2017b). Together these data show that NF-κB signalling plays a role in regulating astrogliosis in response to nutrient excess. This implicates NF-κB as an immunometabolic modulator in astrocytes.

### 1.2.7 The energetic cost of inflammation

Inflammation is an energetically costly process requiring an increase in the production of ATP, the 'molecular currency' of the cell, to fuel the rapid structural and functional changes involved (Romanyukha *et al.*, 2006; Vander Heiden *et al.*, 2009). ATP stores energy liberated from fuel sources, allowing it to be transported in a stable form to a site of use where it can be converted back to adenosine diphosphate (ADP) to release the stored energy (Bonora *et al.*, 2012). Inflammation necessitates a rapid and large supply of intermediate molecules for the synthesis of fatty acids, nucleotides and proteins (Gaber *et al.*, 2017). This facilitates the increased cell replication often associated with inflammation (Gaber *et al.*, 2017). Additionally the cells require more amino acids and oxidative agents for the synthesis of immunomodulatory molecules (Gaber *et al.*, 2017). To allow these changes, the cell must use more energy and/or alter the source of energy, necessitating the reprogramming of metabolic behaviour of the cell during inflammation.

## 1.3 Immunometabolism: Fuelling inflammation

To provide the additional energy needed a metabolic shift is often observed in immune cells during inflammation. Peripheral immune cells of myeloid and lymphoid lineage are dependent on the activity of a variety of metabolic pathways (O'Neill *et al.*, 2016). Inflammatory stimuli are reported to drive metabolic changes, promoting the activity of the essential metabolic pathways (O'Neill *et al.*, 2016; Russell *et al.*, 2019). As is outlined further below, this metabolic change is often characterised as an increase in glucose metabolism through glycolysis, and a decrease in mitochondrial fatty acid metabolism. This bi-directional relationship between immune and metabolic function has become known as 'immunometabolism'.

Immunometabolism is emerging as a therapeutic target for disease. This was first considered after the observation that treatment of rheumatoid diseases with salicylates improved patient glucose tolerance (Williamson, 1901). This has led to anti-inflammatory drugs being investigated to treat metabolic diseases including Type-2 diabetes and obesity (Goldfine *et al.*, 2010; Goldfine *et al.*, 2008; Lee *et al.*, 2018). Additionally pharmaceuticals targeting cellular metabolism (e.g. Metformin) are being repurposed for conditions including cancers (Singer *et al.*, 2018), Alzheimer's disease (Campbell *et al.*, 2018; Koenig *et al.*, 2017), and autoimmune diseases such as multiple sclerosis and lupus (Norata *et al.*, 2015).

Despite the therapeutic potential of this approach there is less understanding of whether the same immunometabolic changes are also seen in the central nervous system (CNS), most notably in astrocytes. A deeper understanding of

immunometabolism and the regulation of immunometabolism in astrocytes may allow a more targeted approach to drug development. Although many inflammatory pathways can regulate metabolism, NF-κB signalling will be the main pathway reviewed in this body of work, although others will be mentioned if they are of particular relevance in the context presented.

### 1.3.1 Glycolysis in immunometabolism

Glycolysis is a series of reactions that occur in the cytoplasm of the cell to break down glucose for ATP generation. Although glycolysis is a less efficient means of generating ATP than another metabolic pathway called oxidative phosphorylation (OXPHOS), it can generate ATP much more rapidly, making it more useful during an acute response to inflammatory stimulation (Pfeiffer *et al.*, 2001). Glycolysis also forms pyruvate and the reducing agents NADH and $FADH_2$ which are transported to the mitochondria and used in the tricarboxylic acid (TCA) cycle and in OXPHOS to generate a further 36 ATP molecules (**fig 1.3.1.11**). Any pyruvate which is not transported into the mitochondria is converted into lactate to regenerate $NAD^+$, allowing glycolysis to continue. Although the pathway is always the same, glycolysis can be classified as anaerobic or aerobic (**fig 1.3.1.12**).

During limited periods of restricted oxygen availability, for example during exercise, cells can use anaerobic glycolysis as an energy source. This is facilitated by the conversion of pyruvate to lactate to regenerate the $NAD^+$ used. This allows the cell to maintain ATP production during short periods of oxygen

deprivation. However, it cannot be used for long as $NAD^+$ is not regenerated rapidly enough to maintain glycolysis through lactate production alone.

Alternatively, cells can use aerobic glycolysis. This is often used during cell proliferation when there is plenty of oxygen available. For example, T cells divert 85% of the product of glycolysis into lactate rather than into the TCA cycle (Fox *et al.*, 2005), but importantly the presence of oxygen allows regeneration of $NAD^+$ from NADH using the ETC, allowing continued glycolysis. This also generates two more ATP than anaerobic glycolysis and is much faster than OXPHOS. Aerobic glycolysis is facilitated by the transcription factor hypoxia inducible factor 1α (HIF-1α) induction, which leads to enhanced expression of lactate dehydrogenase (LDH). This increases conversion of pyruvate to lactate. Interestingly, lactate can act as an immune cell modulator itself, decreasing pro-inflammatory cytokine release and reducing glycolytic flux (Ratter *et al.*, 2018).

HIF-1α is a transcription factor, which among other functions, promotes gene transcription mediating a shift in cellular metabolism towards use of glycolysis over mitochondrial metabolism (Cimmino *et al.*, 2019; Ziello *et al.*, 2007). This helps to maintain oxygen homeostasis and during hypoxia promotes cell survival. HIF-1α can be activated directly through PRR and inflammatory signalling pathways that stabilise HIF-1α, preventing degradation, or indirectly through low oxygen levels (Devraj *et al.,* 2017). During hypoxia, the oxygen dependent prolyl hydroxylases, which lead to ubiquitination and degradation of HIF-1α, are inactivated. Both mechanisms result in increased HIF-1α activity (Devraj *et al.,* 2017).

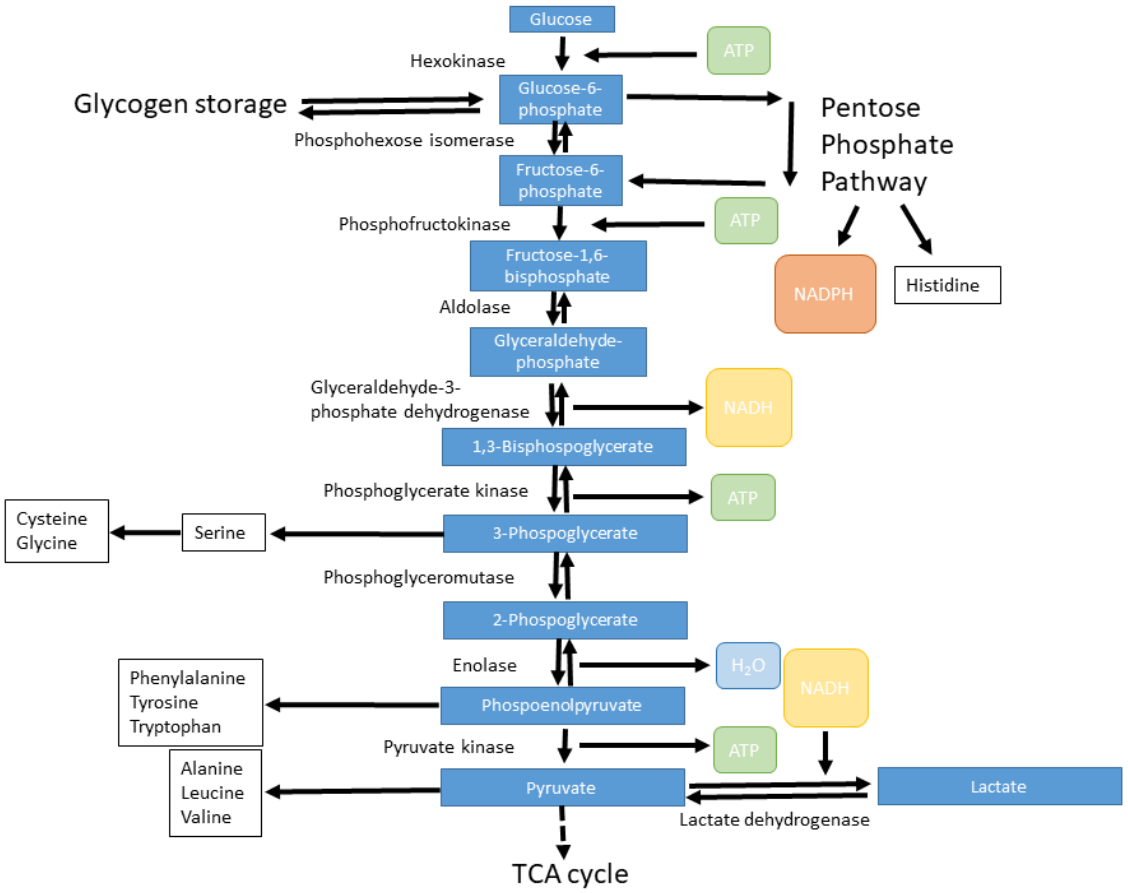


**Figure 1.3.1.11 A simplified schematic of the steps in glycolysis, including products and enzymes involved.** Glycolysis is the metabolism of glucose into pyruvate catalysed by a series of enzymes. This generates reduced nicotinamide adenine dinucleotide ($NAD^+$; Reduced, NADH) and adenosine triphosphate (ATP). The resulting pyruvate can be transported into the mitochondria for use in the tricarboxylic acid (TCA) cycle. Alternatively pyruvate can be further reduced into lactate to replenish the pool of available $NAD^+$. After initial phosphorylation by hexokinase, the resultant glucose-6-phosphate can be introduced into the pentose phosphate pathway, a derivative pathway of glycolysis which generates nicotinamide adenine dinucleotide phosphate (NADPH) for nucleotide synthesis. Intermediates from both the pentose phosphate pathway and glycolysis can be used to synthesise amino acids.

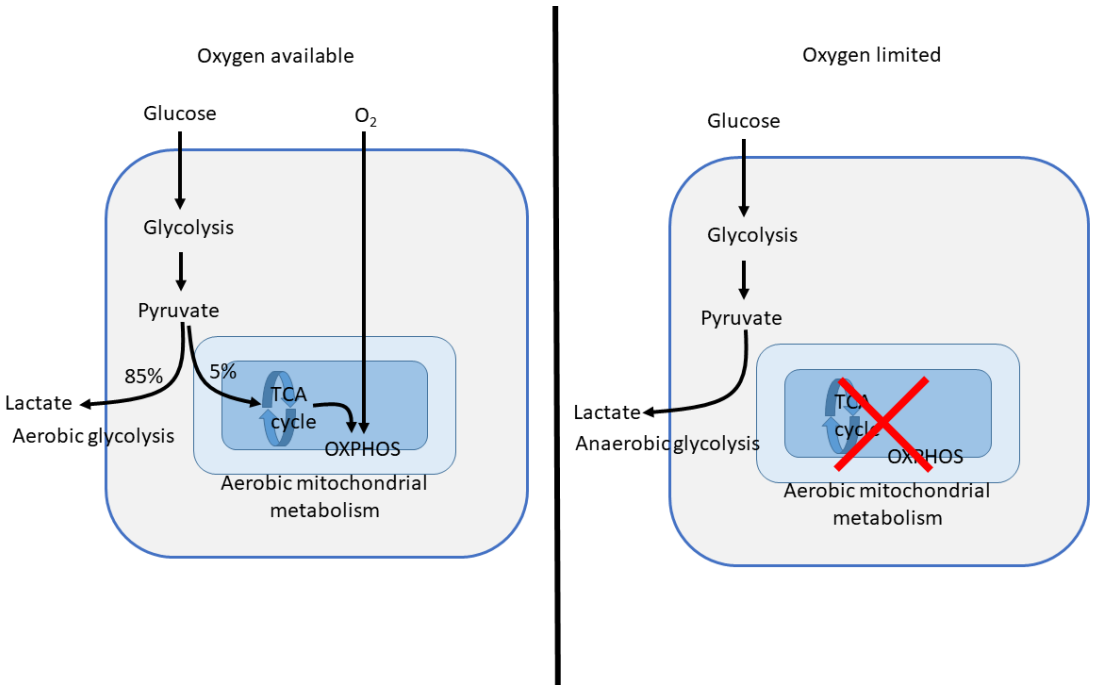


**Figure 1.3.1.12 The difference between aerobic glycolysis, aerobic mitochondrial metabolism and anaerobic glycolysis.** *Aerobic glycolysis* is the metabolism of glucose into lactate, resulting in the reduction of nicotinamide adenine dinucleotide ($NAD^+$; Reduced, NADH), and a small amount of adenosine triphosphate (ATP). A small percentage of the pyruvate produced is trafficked into the mitochondria for metabolism by the tricarboxylic acid cycle (TCA). Oxidative phosphorylation (OXPHOS) uses the reducing agents generated by aerobic glycolysis and the TCA cycle to generate ATP, and restore the reducing agents to their oxidised states. This allows aerobic glycolysis and the TCA cycle to continue. *Anaerobic glycolysis* is the metabolism of glucose into lactate in oxygen restricted environments. The lack of oxygen means NADH cannot be oxidised by the electron transport chain during OXPHOS. Over time the pool of $NAD^+$ is depleted, halting glycolysis.

Although the metabolic response to inflammation varies between cell types, the initial pro-inflammatory phase is typically associated with an increase in glycolytic rate (O'Neill *et al.*, 2016). Inhibition of glycolysis with the non-metabolisable glucose homolog 2-deoxyglucose (2-DG) prevents pro-inflammatory activation of monocytes and macrophages and suppresses NF-κB signalling in fibroblasts indicating that glycolysis is essential for inflammation in many cell types (Hamilton *et al.*, 1986; Kawauchi *et al.*, 2008b; Lee *et al.*, 2019; Liu *et al.*, 2016; Michl *et al.*, 1976; Tannahill *et al.*, 2013). This is probably due to the need for rapid — as opposed to efficient — ATP production during the initial pro-inflammatory phase.

There is evidence that glycolysis is also upregulated to provide substrates for the rapid increase in biomass seen during inflammation (Vander Heiden *et al.*, 2009). In addition to being used as a substrate for the TCA cycle, pyruvate derived from glycolysis can be converted into the amino acids alanine, valine or leucine. Other glycolytic intermediates can also be converted into amino acids: phosphoenolpyruvate is a substrate for phenylalanine, tyrosine and tryptophan synthesis, while 3-phosphoglycerate is converted into serine and further synthesised into cysteine and glycine (Nelson & Cox, 2017). Additionally, the glycolytic intermediate glucose-6-phosphate fuels the pentose phosphate pathway (PPP; **fig. 1.3.1.11**) which is a derivative metabolic pathway of glycolysis. The PPP intermediate ribose 5-phosphate is used to synthesise the amino acid histidine. PPP also synthesises nucleotides and the reducing agent NADPH which protects the cell from oxidative stress (Kuehne *et al.*, 2015). The amino acids produced via these various metabolic pathways can then be used to enable the rapid protein synthesis required during inflammation.

#### 1.3.1.1 Regulation of glycolysis in inflamed peripheral immune cells by NF-κB signalling

To allow the increase in glycolytic rate needed for inflammation, the expression of many glycolytic genes is upregulated in response to an inflammatory stimulus in many cell types (Remels *et al.*, 2015). In dendritic cells c-Myc promotes transcription and expression of glycolytic genes, whereas in macrophages and T-cells an increase in aerobic glycolysis can be driven by HIF-1α (Liu *et al.*, 2016; Rodríguez-Prados *et al.*, 2010; Shi *et al.*, 2019; Shi *et al.*, 2011; Tannahill *et al.*, 2013; Wang *et al.*, 2011; Wang *et al.*, 2017). HIF-1α promotes transcription of genes encoding glycolytic enzymes, including phospho-fructokinase 2 (PFK2) which appears to be essential for macrophage response to inflammation (Rodríguez-Prados *et al.*, 2010). Expression of both of these transcription factors is upregulated by NF-κB signalling, demonstrating a role for NF-κB in regulating the glycolytic response to inflammation.

HIF-1α is also regulated by degradation. HIF-1α is stabilised by TCA intermediate succinate and dimeric pyruvate kinase isozyme M2 (PKM2), the enzyme which catalyses the synthesis of pyruvate (Tannahill *et al.*, 2013; Yang *et al.*, 2014). NF-κB can also promote transcription and expression of PKM2, thus promoting aerobic glycolysis through HIF-1α (Azoitei *et al.*, 2016; Han *et al.*, 2015). Inhibition of dimeric PKM2, the main regulator of aerobic glycolysis, impairs inflammasome activation and inflammation in these cells (Palsson-McDermott *et al.*, 2015; Xie *et al.*, 2016).

The major enzymatic regulator of glycolytic rate is hexokinase II, which introduces glucose into the glycolytic pathway (Roberts & Miyamoto, 2015). This enzyme is both transcriptionally and post-transcriptionally regulated. While hexokinase II can be upregulated by HIF-1α, it is under the direct transcriptional control of p65 NF-κB (Kim *et al.*, 2007b; Londhe *et al.*, 2018; Yeung *et al.*, 2008). However, hexokinase II activity is also inhibited by its product, glucose-6-phosphate, therefore reduced use of glycolytic products will result in accumulation of glucose-6-phosphate, resulting in the inhibition of hexokinase II activity (Roberts & Miyamoto, 2015).

Another limiting factor for hexokinase II activity is the availability of ATP to provide both the phosphate group and the energy to allow phosphorylation of glucose into glucose-6-phosphate. Localisation of hexokinase II to the mitochondria, through binding to the voltage dependent anion channel (VDAC) promotes coupling between mitochondrial metabolism and glycolysis (Arzoine *et al.*, 2009; BeltrandelRio & Wilson, 1992; John *et al.*, 2011; Perevoshchikova *et al.*, 2010; Roberts & Miyamoto, 2015). This physical proximity enables increased movement of ATP from the inside the mitochondria to hexokinase II, through VDAC, allowing increased phosphorylation of glucose, increasing glycolytic flux.

In dendritic cells hexokinase II targeting to the mitochondria is, in part, modulated by phosphoinositide-3-kinase (PI3K)/Protein kinase B (PKB/Akt), TANK binding kinase 1 (TBK1), and IKK signalling (Everts *et al.*, 2014; Huynh *et al.*, 2015; Krawczyk *et al.*, 2010). As described earlier, these signalling pathways are activated by TLR4, and regulate NF-κB signalling (**fig. 1.2.5.2**). Activation of

these kinases promotes hexokinase II association with the mitochondria, increasing glycolytic flux during the inflammatory response (Calmettes *et al.*, 2013; Everts *et al.*, 2014; Majewski *et al.*, 2004; Sun *et al.*, 2008).

PI3K/Akt also regulates T-cell glycolysis during inflammation (Frauwirth *et al.*, 2002). However, unlike in macrophages where PI3K/Akt increases hexokinase II, increased glycolysis in T-cells driven by PI3K/Akt is driven by promotion of glucose transporter 1 (GLUT1) localisation to the plasma membrane of the cell (Frauwirth *et al.*, 2002). GLUT1 is a uniporter which facilitates movement of glucose into the cell. This provides increased substrate for glycolysis, so increasing glycolytic rate. When glucose demand is low GLUT1 can be stored within endosomes inside the cell, ready to be inserted into the cell membrane when glucose demand is increased (Antonescu *et al.*, 2014). This PI3K/Akt regulation of GLUT1 in T-cells is mediated through the mTOR (mammalian target of rapamycin) pathway (Fang, 2015; Makinoshima *et al.*, 2015).

GLUT1 expression is also transcriptionally regulated by mTOR signalling, through activation of c-Myc (Michalek *et al.*, 2011). Overexpression of GLUT transporters increases cytokine production in T-cells (Michalek *et al.*, 2011), whereas glucose limitation and loss of GLUT1 in T-cells prevents inflammation and cell division (Blagih *et al.*, 2015; Macintyre *et al.*, 2014; Siska *et al.*, 2016; Wang *et al.*, 2011). This suggests that GLUT1 expression can regulate inflammation in T-cells. Therefore, c-Myc appears to be essential for T-cell metabolic reprogramming, promoting GLUT expression and hexokinase II expression among other glycolytic genes (Wang *et al.*, 2011).

NF-κB signalling can also increase expression of GLUT transporters during inflammation (Maedera *et al.*, 2019; Zhang *et al.*, 2017a). Loss of p65 significantly decreases glycolytic metabolism through reduced GLUT3 expression in fibroblasts (Kawauchi *et al.*, 2008b). This implies that GLUT3 expression is driven by p65 signalling, as has been previously reported (Moriyama *et al.*, 2018; Zha *et al.*, 2015). Furthermore, loss of the tumour suppressor p53 in fibroblasts increases both NF-κB signalling and glycolytic metabolism (Kawauchi *et al.*, 2008b). In agreement with this work, Mauro *et al*. suggests that p53 represses GLUT3 expression to restrict inflammatory reprogramming of the cell (Kawauchi *et al.*, 2008b; Mauro *et al.*, 2011).

Together these studies indicate that substrate availability is the rate-limiting step of glycolysis in both T-cells and fibroblasts. Hexokinase II regulates glucose uptake and substrate availability in part by metabolising glucose into glycogen, for storage, or glucose-6-phosphate (Roberts & Miyamoto, 2015). This maintains the glucose gradient promoting facilitated diffusion of glucose into the cell. Nevertheless, expression of GLUT transporters in the membrane appears to be more important during inflammation than hexokinase II activity in T-cells and fibroblasts (Kawauchi *et al.*, 2008b; Mauro *et al.*, 2011). GLUT1 mediated glucose uptake is also a regulator of inflammation in macrophages, as overexpression of GLUT1 promotes inflammation in these cells (Freemerman *et al.*, 2014). However, in macrophages GLUT expression is less critical than hexokinase II activity for regulating glycolysis during inflammation, demonstrating signalling differences between these cell types (Van den Bossche *et al.*, 2017).

Beyond fuelling inflammation, glycolytic enzymes also play an important role in immunity directly (Seki & Gaultier, 2017). For example, during inflammation hexokinase II targeted to the mitochondria protects against apoptosis (Miyamoto *et al.*, 2008; Pastorino *et al.*, 2002). Other glycolytic enzymes suppress inflammation, such as glyceraldehyde 3-phosphate dehydrogenase (GAPDH) which binds interferon γ (IFN-γ) and TNF-α messenger RNA (mRNA), suppressing translation. However, during intense glycolytic increases, such as those seen during inflammation, GAPDH becomes unbound from the transcripts, allowing their translation and synthesis (Chang *et al.*, 2013; Millet *et al.*, 2016). Additionally, a truncated form of α-enolase, called myc promoter-binding protein 1 (MBP-1), represses c-Myc transcription, which (as discussed above) regulates GLUT1 transcription (Chaudhary & Miller, 1995; Ray & Miller, 1991). Together these data demonstrate that glycolytic enzymes and intermediates are essential for producing and regulating an inflammatory response in many cell types. However, the regulation of the response is complex and cell-type specific.

#### 1.3.1.2 Canonical NF-κB signalling in basal regulation of glycolysis

In the absence of an inflammatory stimulus, canonical NF-κB signalling is still an important regulator of cellular metabolism. A seminal paper published by Mauro *et al.* demonstrated a role of NF-κB signalling in basal metabolism and during disease. Using IKKβ inhibitor SC-514 and p65 knockout fibroblasts, the group showed that basal NF-κB signalling is essential to prevent cellular metabolic reprogramming to aerobic glycolysis (Mauro *et al.*, 2011).

There is some suggestion that the differential metabolic functions of NF-κB during basal and inflammatory states are mediated through p53 preventing NF-κB from translocating to the mitochondria, and so promoting oxidative phosphorylation (**fig. 1.3.1.2**) (Johnson *et al.*, 2011). NF-κB signalling in mouse fibroblasts promotes p53 expression, increasing OXPHOS, particularly during glucose starvation (Schwartzenberg-Bar-Yoseph *et al.*, 2004). There is additional evidence that in fibroblasts loss of p53 prevents NF-κB from promoting transcription of genes encoding ETC proteins, despite phosphorylation and DNA binding of the NF-κB p65 subunit (Kawauchi *et al.*, 2008a). Furthermore, p53 also inhibits glycolysis and glucose uptake through repression of GLUT transporter expression by repressing p65 signalling (Kawauchi *et al.*, 2008b; Schwartzenberg-Bar-Yoseph *et al.*, 2004). This may suggest that p53 and NF-κB exist in a negative feedback loop to restrain glycolysis and glucose addiction at the cellular level during inflammation. Together, these data suggest that p53-NF-κB signalling orchestrates normal metabolic function.

Other components of NF-κB signalling may restrain aerobic glycolysis when an inflammatory stimulus is not present. The NF-κB regulator IKKβ can phosphorylate 6-phosphofructo-2-kinase/fructose-2,6-biphosphatase (PFKFB3), acting to inhibit the action of this enzyme which synthesises allosteric activators of aerobic glycolysis (Reid *et al.*, 2016). This decreases aerobic glycolysis and increases pyruvate input into the TCA cycle (Reid *et al.*, 2016). This additional data further supports the theory that basal NF-κB signalling maintains normal cellular metabolism.

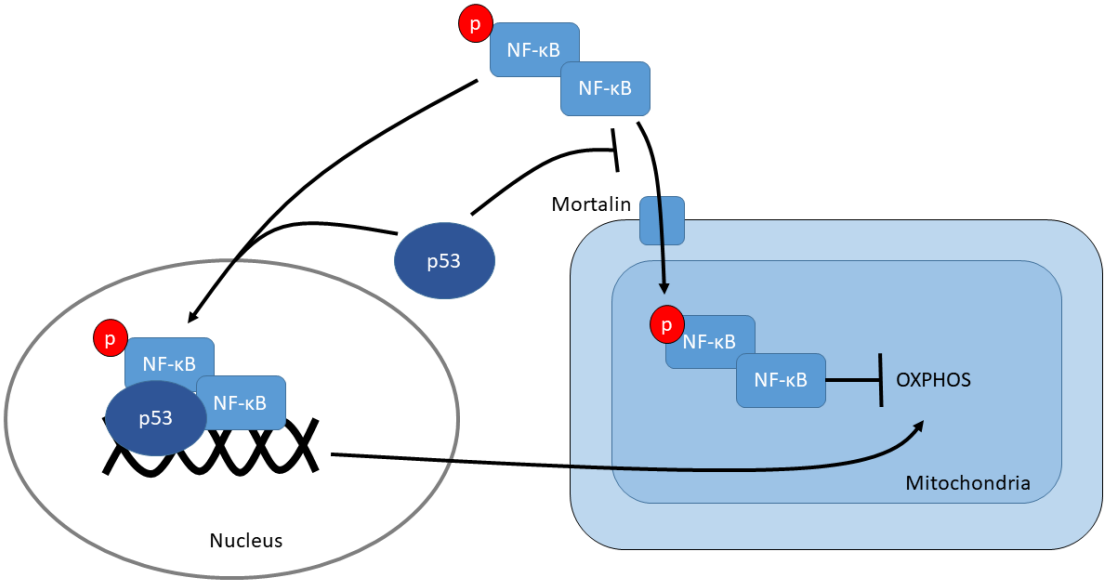


**Figure 1.3.1.2: Presence of p53 determines NF-κB translocation to the mitochondria or nucleus.** After phosphorylation, active NF-κB can be located to the mitochondria through the membrane channel mortalin. If p53 is present this is inhibited, and the active NF-κB instead translocated to the nucleus, where it promotes transcription of target genes.

#### 1.3.1.3 Glycolysis and inflammation in astrocytes

Glucose is the main fuel consumed by the brain. Data suggests that astrocyte glucose metabolism is entirely via aerobic glycolysis, particularly when supporting neuronal signalling (Bélanger *et al.*, 2011a; Fernández-Moncada *et al.*, 2018; Pellerin & Magistretti, 1994; Vardjan *et al.*, 2018; Yellen, 2018). Glucose is metabolised by glycolysis into pyruvate and further oxidised into lactate, which is thought to be released as fuel for the neurons it supplies, rather than being transported into the astrocytic mitochondria for use in the TCA cycle. This is termed the Astrocyte-Neuron Lactate Shuttle, however this is currently a contentious theory (Mason, 2017). Glucose taken up by astrocytes can also be stored as glycogen within the cell if it is not required immediately for energy metabolism (Bak *et al.*, 2018; Falkowska *et al.*, 2015).

Some evidence already exists linking inflammation with changes in glycolytic metabolism in astrocytes. *In vitro* studies in mouse primary astrocytes demonstrate that treatment with pro-inflammatory cytokines increases glucose uptake and depletes intracellular glycogen stores (Bélanger *et al.*, 2011b; Gavillet *et al.*, 2008). This suggests an increase in astrocyte glucose use as a fuel during inflammation. This was coupled with increased flux through the TCA cycle and PPP (Bélanger *et al.*, 2011b; Gavillet *et al.*, 2008). The increase in TCA cycle use suggests that some pyruvate is being used to generate reducing agents for OXPHOS as opposed to lactate production for immediate energy gains. In a related study, Meares *et al.* showed that decreasing substrate availability to astrocytes *in vitro,* by limiting glucose and pyruvate availability, reduces IFN-γ induced inflammatory responses (Meares *et al.*, 2013). This implies that glycolysis is essential for inflammation in astrocytes. Exposure to nitric oxide,

which can be an inflammatory factor at high concentrations (Sharma *et al.*, 2007), also enhances glycolytic pathways in astrocytes, including activity of HIF-1α (Almeida *et al.*, 2004; Brix *et al.*, 2012). Together these data suggest that astrocytes rely on glycolysis to support protein synthesis and achieve full inflammatory activation, but to our knowledge this important question and the mechanisms driving it have never been directly examined.

### 1.3.2 Mitochondria in energy metabolism

Mitochondria are organelles which play an integral role in ATP generation. These organelles are bound with two membranes, an outer mitochondrial membrane (OMM) and an inner mitochondrial membrane (IMM). The IMM contains the mitochondrial matrix, where metabolic processes occur. Substrates for energy generation, including pyruvate, lactate, acyl-coA (derived from fatty acids), and amino acids, are transported into the mitochondrial matrix by either passive diffusion or active transport, dependent on substrate type (Becker & Wagner, 2018; McCommis & Finck, 2015; Palmieri & Monné, 2016).

Once inside the mitochondrial matrix these substrates are converted into acetyl-coA and metabolised through the tricarboxylic acid (TCA) cycle (**fig. 1.3.3**). This generates reducing agents and substrates for the electron transfer chain (ETC; **fig. 1.3.3**). The dual membranes of the mitochondria are essential for mitochondrial function. The space between the two membranes is called the intermembrane space, and the IMM is highly folded into structures called cristae, increasing its surface area. During electron transport protons are pumped into the cristae of the intermembrane space, leading to high concentrations of protons

and establishing a proton gradient. This membrane polarisation is integral for oxidative phosphorylation (OXPHOS) and other metabolic functions, as will be discussed further later in this chapter.

### 1.3.3 TCA cycle in immunometabolism

The TCA cycle uses a sequence of enzymatic reactions to generate reducing agents for OXPHOS. This is fuelled by acetyl-coA which is converted into CoA-SH to replenish levels of the critical TCA substrate citrate, allowing initiation of a new rotation. In addition to providing substrates for OXPHOS the TCA cycle provides precursors for biosynthetic pathways. Intermediates from the TCA cycle can be used to synthesise new amino acids, which are then used for protein synthesis, as is shown in **fig 1.3.3** (Berg *et al.*, 2002; Ryan & O'Neill, 2017). The TCA cycle also contributes to fatty acid synthesis through citrate which can be exported from the mitochondria by ATP citrate lyase (ACLY) and converted into acetyl co-A, for use in fatty acid synthesis (Berg *et al.*, 2002; Infantino *et al.*, 2013; Vittoria *et al.*, 2019; Williams & O'Neill, 2018).

ACLY is an important component of the inflammatory response. ACLY expression is driven through NF-κB and signal transducers and activators of transcription (STAT) signalling (Infantino *et al.*, 2013). In dendritic cells the transcription factor sterol regulatory element binding protein (Srebp) regulates ACLY, and citrate driven lipid synthesis is essential for the full pro-inflammatory immune response (Assmann *et al.*, 2017). There is data showing that in mice on a high fat diet inhibition of ACLY prevents the development of glucose intolerance and obesity, and suppresses inflammatory gene expression (Samsoondar *et al.*,

2017). Together these data demonstrate that in immune cells inflammatory signalling pathways, including NF-κB play a role in regulating TCA cycle activity, and, in common with glycolysis, inflammatory and metabolic pathways are integrated at the level of the TCA cycle.

In peripheral immune cells activity of the TCA cycle is instrumental in inflammation. During fungal infection dendritic cells have altered ratios of TCA cycle intermediates which influence the pro-inflammatory response (Márquez *et al.*, 2019). For example, pyruvate dehydrogenase — the enzyme which converts pyruvate into acetyl-coA for use in the TCA cycle — increases expression of IL-10 and IL-23A in dendritic cells (Márquez *et al.*, 2019). Similarly TCA cycle intermediates accumulate in activated bone-marrow derived macrophages after LPS insult, despite decreased mitochondrial activity (Tannahill *et al.*, 2013). This suggests increased TCA cycle activity during a pro-inflammatory response.

In macrophages, succinate oxidation is instrumental in promoting inflammation (Mills *et al.*, 2016). Succinate accumulates after LPS insult and stabilises HIF-1α to promote macrophage inflammasome activation and HIF-1α driven transcription (Koivunen *et al.*, 2007; Mills *et al.*, 2016; Palsson-McDermott *et al.*, 2015; Selak *et al.*, 2005; Tannahill *et al.*, 2013). The TCA cycle is also essential for T cell activation (Wang *et al.*, 2011). Together these studies demonstrate the importance of the TCA cycle in regulating the function of immune responsive cells. Whilst there is evidence that the TCA cycle is increased in astrocytes during inflammation (Bélanger *et al.*, 2011b; Gavillet *et al.*, 2008), it has not been demonstrated whether this is essential for the inflammatory response.

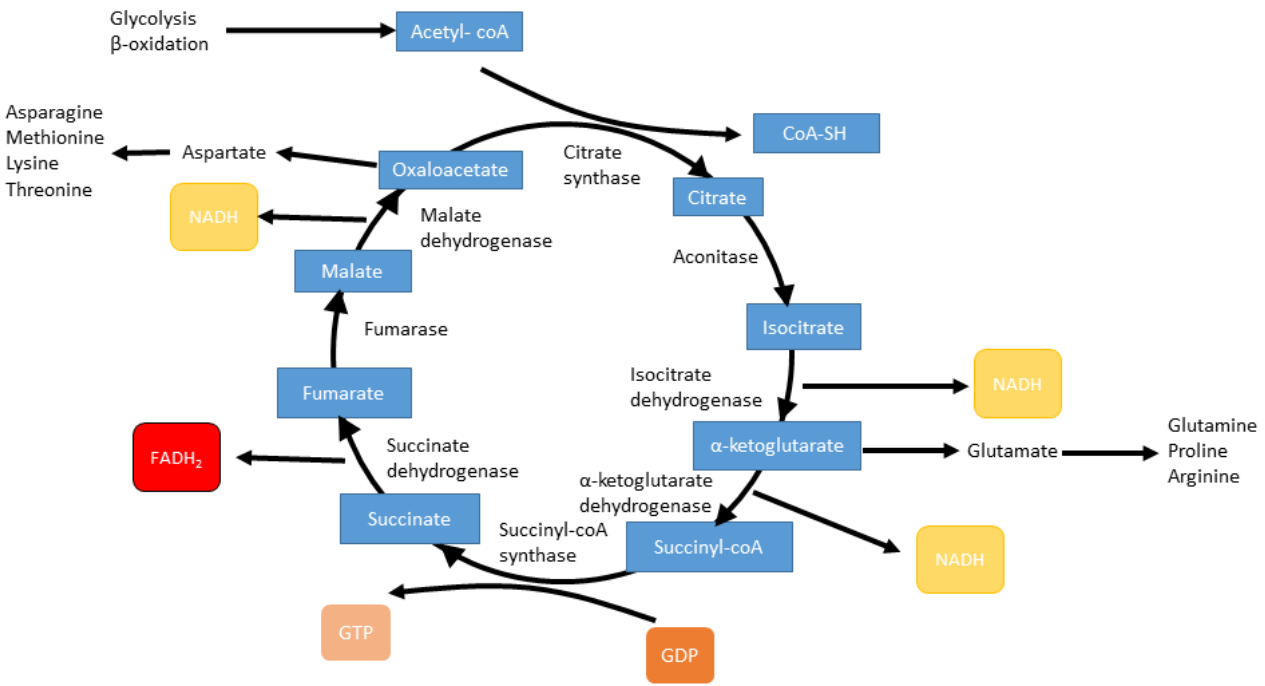


**Figure 1.3.3: A simplified tricarboxylic acid (TCA) cycle showing enzymes and substrates involved.** The TCA cycle uses acetyl-coA provided from upstream metabolic pathways to replenish citrate from oxaloacetate. The citrate generated is metabolised by a sequence of enzymes back into oxaloacetate, generating reduced nicotinamide adenine dinucleotide (NADH), reduced flavin adenine dinucleotide (FADH) and phosphorylating guanosine diphosphate (GDP) into guanosine triphosphate (GTP). Intermediates of the TCA cycle can also be used to generate some amino acids.

### 1.3.4 Oxidative phosphorylation in immunometabolism

OXPHOS is a well characterised process, recently reviewed by Zhao *et al.* (Zhao *et al.*, 2019). Briefly, OXPHOS generates ATP from ADP by capturing the energy generated by proton movement through ATP synthase (Complex V; **fig. 1.3.4**). Use of this pathway increases metabolic efficiency. As mentioned earlier, the ETC pumps protons across the inner mitochondrial membrane and into the intermembrane space using the energy generated through electron transport. Electrons are provided for this from the reducing agents NADH and $FADH_2$ derived from the TCA cycle, FAO and glycolysis. This polarises the inner mitochondrial membrane and creates a proton gradient. Protons flow down this gradient back into the mitochondrial matrix through ATP synthase. This flow of protons provides the energy needed to phosphorylate ADP into ATP. The spare electrons are accepted by oxygen and hydrogen to form water. Therefore, OXPHOS is only possible in the presence of oxygen.

The ETC produces highly damaging reactive oxygen species (ROS). ROS are used as an important bactericidal molecule during the inflammatory response. Inhibition of ATP production by the ETC whilst there is availability of reducing agents and a proton gradient increases production of superoxide ($O_2^{\bullet-}$), a species of ROS (Murphy, 2008). This is formed by incomplete reduction of oxygen. Complex I generates ROS when fully reduced by NADH (Kudin *et al.*, 2004). Therefore the $NAD^+$/NADH ratio determines the rate of ROS production, with increased NADH increasing the production of ROS (Adam-Vizi & Chinopoulos, 2006; Murphy, 2008).

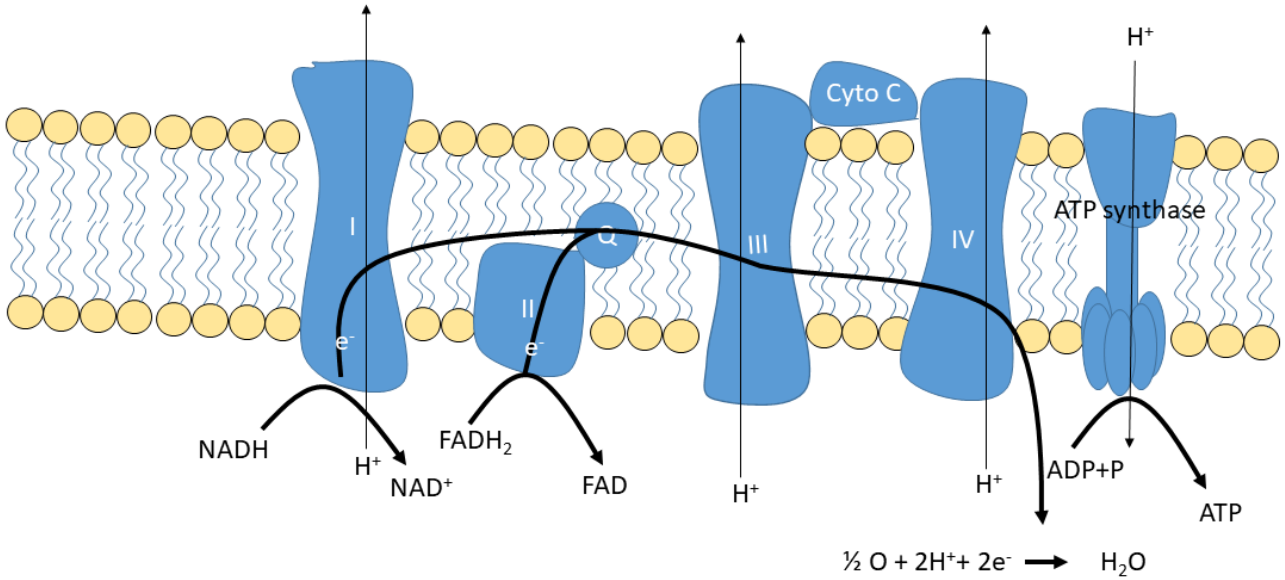


**Figure 1.3.4: The electron transport chain (ETC) used for oxidative phosphorylation.** Reducing agents, nicotinamide adenine dinucleotide (reduced, NADH), flavin adenine dinucleotide (reduced, FADH) from the tricarboxylic acid (TCA) cycle, glycolysis and other metabolic pathways are oxidised into nicotinamide adenine dinucleotide ($NAD^+$) and flavin adenine dinucleotide (FAD) by complex I and II on the ETC. Electrons obtained by this oxidation are transported between the remaining complexes in the chain. This generates sufficient energy to pump protons ($H^+$) across the inner mitochondrial membrane against the concentration gradient. $H^+$ then moves back down the proton gradient through ATP synthase, generating energy to phosphorylate adenosine diphosphate (ADP) into adenosine triphosphate (ATP). The spare electron is accepted by oxygen, which reacts with protons to form water.

In the brain, succinate promotes ROS production by reducing Complex II (Cino & Del Maestro, 1989; Votyakova & Reynolds, 2001). When the mitochondrial membrane is polarised, this leads to reverse electron transport (RET) from Complex II to Complex I. This increases reduction of Complex I, increasing $O_2^{\bullet-}$ production. Astrocytes are capable of producing ROS during the inflammatory response (Lopez-Fabuel *et al.*, 2016; Sheng *et al.*, 2013). Treatment of astrocytes with LPS impairs the $NAD^+$/NADH ratio and increases succinate production, promoting ROS production (Tannahill *et al.*, 2013). Lopez-Fabiel *et al.* suggested that this is due to increased free and inactive Complex I in astrocytes, preventing onward electron transport and encouraging ROS production (Lopez-Fabuel *et al.*, 2016). This suggests that astrocytes can produce high amounts of ROS during inflammation without affecting OXPHOS rate. This would allow astrocytes to maintain OXPHOS during the pro-inflammatory response.

There is extensive evidence that ROS can activate both canonical and non-canonical NF-κB signalling in astrocytes (Morgan & Liu, 2011). This leads to induction of compensatory expression of genes which are protective against ROS, in addition to genes which propagate ROS production (Morgan & Liu, 2011). This encourages cell survival in an oxidative environment whilst allowing continued production of bactericidal ROS.

It must be noted that ROS is not solely produced by the ETC. ROS are also produced at other sites by oxidase enzymes, including in peroxisomes and phagosomes (Snezhkina *et al.,* 2019). ROS is most notably synthesised by the NADPH oxidase (NOX) family. Astrocytes have been reported to express NOX2,

NOX4 and NOX5, expression of which are increased after controlled cortical impact, or exposure to LPS or pro-inflammatory cytokines (Cooney *et al.,* 2013; Sheng *et al.,* 2013). NF-κB itself upregulates expression of NOX (Anrathar *et al.,* 2006; González-Reyes *et al.,* 2017). Therefore, when considering ROS in the regulation of the immunometabolic response, whilst the ETC plays a role in ROS production, other sources cannot be overlooked.

Despite the important role of ROS in inflammation, there is evidence that excessive ROS production is a significant contributing factor to neurotoxicity and neurodegeneration (Angelova & Abramov, 2018). Uncoupling proteins (UCPs) uncouple OXPHOS from ATP production, allowing free movement of protons through ATP synthase with no need for oxygen (Bouillaud *et al.*, 2016). This allows the proton gradient to collapse. This can have a protective role, decreasing ROS production by increasing the $NAD^+$/NADH ratio and depolarising the mitochondrial membrane.

As previously mentioned, NF-κB signalling can inhibit OXPHOS through inhibiting transcription of ETC proteins coded for by mitochondrial DNA (**fig. 1.3.1.2**) (Albensi, 2019). NF-κB is transported into the mitochondria by binding to the mitochondrial transport protein mortalin (Flachbartová & Kovacech, 2013). However, in the presence of p53, which is upregulated by NF-κB signalling, the interaction between mortalin and NF-κB is disrupted, preventing NF-κB mediated inhibition of OXPHOS (Tornatore *et al.*, 2012). Therefore, NF-κB can regulate OXPHOS during inflammation.

In astrocytes there is evidence that OXPHOS is maintained during inflammation. In aging mice, increased inflammatory markers and NF-κB signalling in astrocytes correlates with elevated metabolic oxygen consumption (Jiang & Cadenas, 2014). This suggests that astrocytes are using oxidative metabolism during inflammation. Also, p53 expression is increased during pro-inflammatory simulation in rat astrocytes *in vitro* and gerbil astrocytes *in vivo* (Caito *et al.*, 2014; Panickar *et al.*, 2009; Tounai *et al.*, 2007). This suggests that OXPHOS may be maintained during inflammation through NF-κB-p53 signalling. However, this has never been directly examined, to our knowledge.

### 1.3.5 Mitochondrial dynamics in immunometabolism

Mitochondria form complex and dynamic networks within the cell. Two separate mitochondria can fuse together to form a single structure, or fragment to form daughter mitochondria. Mitochondrial dynamics are essential for mitochondrial maintenance, ensuring mitochondrial DNA replication, regulation of calcium signalling and redistributing mitochondrial ROS (Vafai & Mootha, 2012).

Mitochondrial dynamics also regulate OXPHOS rate, often in response to nutrient availability (Gomes *et al.*, 2011; Rambold *et al.*, 2011). Mitochondrial fusion promotes OXPHOS whilst mitochondrial fission limits OXPHOS (Rossignol *et al.*, 2004; Wai & Langer, 2016). These dynamics can be altered by inflammation. ROS, PI3K/Akt and MAPK signalling promote mitochondrial fission in some cell types (Rambold & Pearce, 2018; Wai & Langer, 2016). Furthermore, there is evidence that NF-κB signalling promotes mitochondrial fission in skeletal muscle cells (Nisr *et al.*, 2019). This also appears to be the case in astrocytes, with

increased mitochondrial fission observed after treatment with LPS and IFN-γ (Motori *et al.*, 2013). Treatment with the pro-inflammatory stimulus manganese reduces expression of mitofusin 2 (Mfn2), again suggesting reduced mitochondrial fusion and a shortening of mitochondria in astrocytes (Sarkar *et al.*, 2018). Hyperfusion of mitochondria in astrocytes has been shown to activate NF-κB signalling (Zemirli *et al.*, 2014). This suggests that NF-κB regulation of mitochondrial dynamics is bidirectional and designed to reduce hyperfusion of mitochondria. Fission allows mitochondria to move into the astrocytic processes (Genda *et al.*, 2011; Jackson *et al.*, 2014; Kolikova *et al.*, 2006; Reyes & Parpura, 2008). This allows local energy generation and regulation of $Ca^{2+}$ dynamics, which plays an important role in regulating astrocyte behaviour (Göbel *et al.*, 2018; Jackson & Robinson, 2015).

Although the previous data demonstrates that NF-κB signalling promotes mitochondrial fission, loss of NEMO or IKKβ does not affect mitochondrial dynamics in mouse fibroblasts. Conversely, loss of IKKα which activates the non-canonical NF-κB pathway in these cells reduced expression of Optic atrophy 1 (OPA1), a protein which promotes mitochondrial fusion, and increased mitochondrial fragmentation (Laforge *et al.*, 2016). This is supported by evidence that mTOR/NF-κB signalling increases OPA1 and fusion in cardiomyocytes in response to insulin (Parra *et al.*, 2014). Together these data suggest that canonical NF-κB promotes mitochondrial fission whilst non-canonical NF-κB promotes mitochondrial fusion.

### 1.3.6 Fatty acid oxidation in immunometabolism

Fats can also be used as a source of energy. Fatty acid oxidation (FAO), also known as β-oxidation, is the shortening of acyl-coA structures derived from fatty acids. This generates acetyl-coA which can be further metabolised by the TCA cycle. FAO occurs within bi-lipid bound structures, including peroxisomes and mitochondria. Four reactions make up the FAO cycle, with each cycle removing two carbon atoms from fatty acyl residues in the form of acetyl-CoA, generating NADH and $FADH_2$ (**fig 1.3.6**). The NADH and $FADH_2$ produced by FAO are used as reducing agents to drive OXPHOS. FAO is primarily regulated by availability of acyl-coA within the mitochondrion or peroxisome. Carnitine palmitoyl transferase I (CPT-1; see section 1.2.3.2 below) facilitates the transport of acyl-coA into the structure (mitochondrion or peroxisome; **fig. 1.3.6.1**) and thus acts as the rate-limiting step in FAO.

Astrocytes use FAO to obtain energy. Indeed, fatty acids appear to be the preferential fuel source for fuelling the TCA cycle (over glucose) in some astrocytes (Taïb *et al.*, 2013). Glucose dephosphorylates the metabolic regulator AMP activated protein kinase (AMPK) in hypothalamic neurons and astrocytes, reducing oxidation of the saturated long chain fatty acid palmitate (Taïb *et al.*, 2013). However, this is not the case in cortical astrocytes, where AMPK phosphorylation and fatty acid oxidation are maintained in the presence of glucose. This suggests that cortical astrocytes are using FAO to fuel the TCA cycle preferentially to glycolysis. Together this suggests brain region specific heterogeneity in astrocyte metabolism.

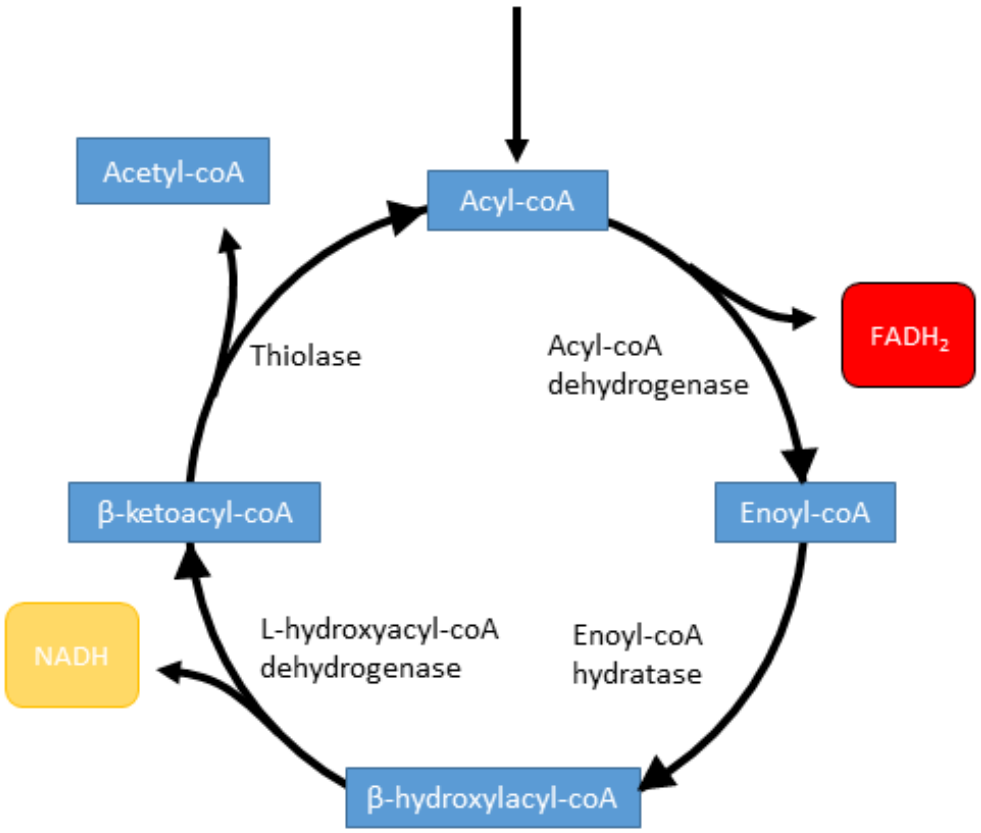


**Figure 1.3.6: A simplified schematic of the steps in fatty acid oxidation, including products and enzymes involved.** FAO uses acyl-coA derived from fatty acids to generate acetyl-coA and reducing agents flavin adenine dinucleotide (reduced, $FADH_2$) and nicotinamide adenine dinucleotide (reduced, NADH). Acetyl-coA is used as a substrate for the tricarboxylic acid (TCA) cycle, and the reducing agents generated are used in oxidative phosphorylation (OXPHOS). Each turn of the FAO cycle reduces the length of the acyl-coA by one carbon.

#### 1.3.6.1 Carnitine palmitoyl transferase I (CPT-1)

The main regulator of FAO is CPT-1A. CPT-1A is an enzyme which sits on the outer mitochondrial membrane and catalyses the reaction transferring an acyl group from coenzyme A to carnitine, allowing the acyl-carnitine to be transported into the intermembrane space through VDAC (Lee *et al.*, 2011). CPT-1A is exclusively expressed in astrocytes in the CNS, and inhibition of CPT-1A activity in brain tissue almost completely prevents FAO (Jernberg *et al.*, 2017). This suggests that in the CNS FAO is predominantly used by astrocytes to generate energy.

The main mechanism of regulation of CPT-1 activity is inhibition by malonyl co-A which is generated by acetyl-coA carboxylase 2 (ACC2) from acetyl-coA. AMPK is a major inhibitor of ACC2 activity (Herzig & Shaw, 2018). Activation of this kinase allows it to in turn phosphorylate downstream targets, including ACC2 to increase ATP production and decrease energy expenditure (Long & Zierath, 2006). As well as regulation by malonyl-coA, CPT-1A can be regulated at the transcriptional level with AMPK activation increasing the expression of CPT-1A (Kim *et al.*, 2011; Krämer *et al.*, 2007). Thus, through these combined modes of action, AMPK promotes acyl-CoA oxidation in the mitochondria.

Modulation of FAO has different effects on the inflammatory response depending on the cell type. In macrophages, limiting FAO through CPT-1A inhibition increases inflammation (Namgaladze *et al.*, 2014). However, in lymphocytes and epithelial cells inhibition of FAO reduces expression of inflammatory markers (Calle *et al.*, 2019; Mørkholt *et al.*, 2017). This suggests that in these cells FAO

is maintained during inflammation. It is important to note here that despite increasing energy production through FAO and glycolysis, activation of AMPK does not facilitate the pro-inflammatory response. Indeed, AMPK activation can lead to suppression of NF-κB phosphorylation, HIF-1α stabilisation and cytokine signalling, while pharmacological activation of AMPK in astrocytes replicated the anti-inflammatory effect of reduced glucose and/or pyruvate availability (Faubert *et al.*, 2013; Meares *et al.*, 2013; Salminen *et al.*, 2011). Therefore, during inflammation AMPK is often inactive with the pro-inflammatory stimulus LPS dephosphorylating AMPK (Fan *et al.*, 2018b). This means AMPK cannot be driving metabolic pathways in astrocytes during inflammation, so CPT-1A must be regulated through a different mechanism, if it is regulated at all during inflammation in astrocytes. To date, the effect of CPT-1A activity and expression on inflammation in astrocytes has not been explored, so I cannot comment on how FAO is regulated during inflammation in astrocytes.

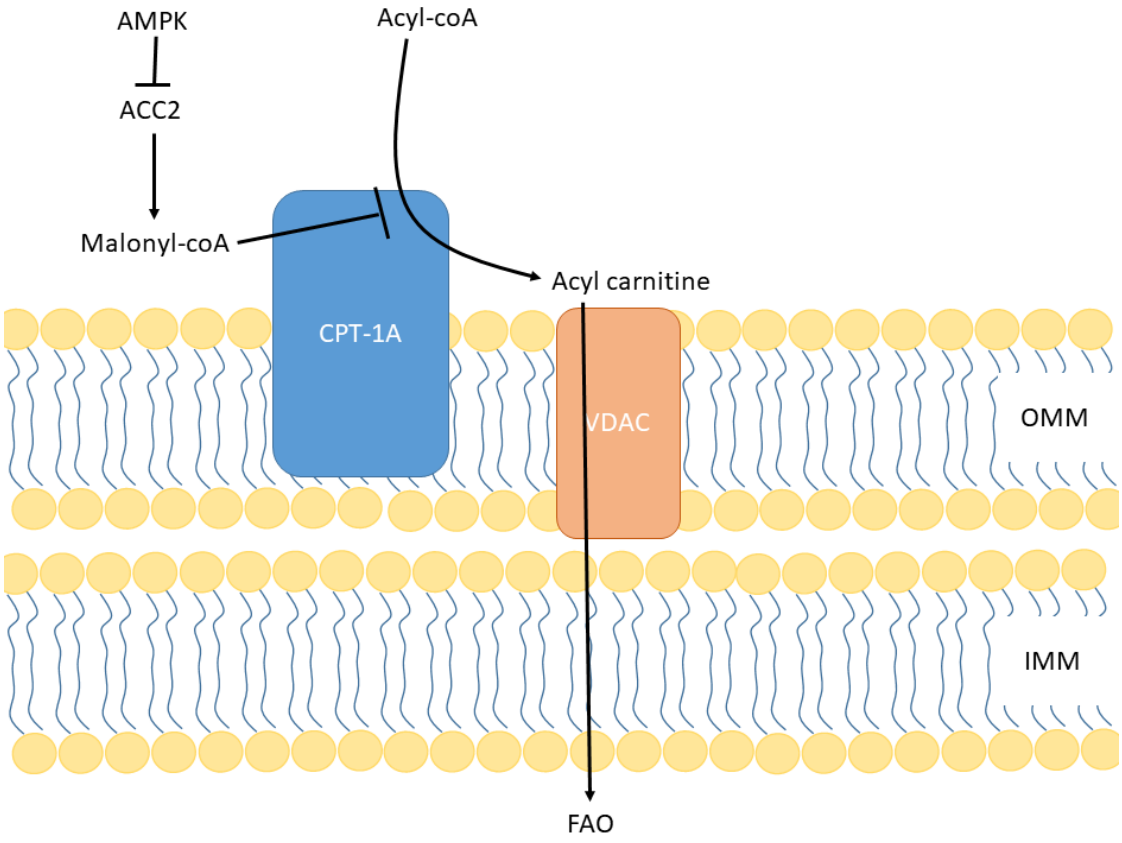


**Figure 1.3.6.1: The role and regulation of carnitine palmitoyl transferase 1A (CPT-1A).** CPT-1A catalyses the transfer of the acyl group from coA onto carnitine. This allows the transfer of the acyl group into the mitochondrion through the voltage dependent anion channel (VDAC). This provides acyl groups as a substrate for fatty acid oxidation (FAO). Activity of CPT-1A is inhibited by malonyl coA which is synthesised by acetyl-coA carboxylase 2 (ACC2). AMP activated protein kinase (AMPK) inhibits the production of malonyl coA by ACC2, resulting in increased CPT-1A activity.

## 1.4 Translocator protein 18 kDa (TSPO)

As discussed above, metabolism is a critical driver of the different stages of inflammation in most cell types examined thus far. There is currently significant interest in exploiting this intrinsic link between inflammation and metabolism to manage chronic inflammation and associated diseases (Norata *et al.*, 2015). One protein that is emerging as a potential therapeutic target in inflammation, particularly within the brain, is translocator protein 18 kDa (TSPO). Expression of TSPO is increased in the CNS in response to brain tumours and Alzheimer's disease (Bhoola *et al.*, 2018; Lagarde *et al.*, 2018). This has led to TSPO ligands being utilised to detect CNS inflammation in humans using Positron Emission Tomography (PET) (Dupont *et al.*, 2017; Werry *et al.*, 2019).

TSPO is upregulated in astrocytes during inflammation (Lavisse *et al.*, 2012). *In vitro* studies showing upregulation of TSPO in rodent microglia in response to pro-inflammatory stimuli led to the initial assumption that the increased CNS expression seen via PET imaging with TSPO ligands was predominantly microglial in origin. However, *in vitro* studies suggest that TSPO is not regulated in human macrophages or microglia (Narayan *et al.*, 2017; Owen *et al.*, 2017b). This indicates that in the human brain other cells in the CNS upregulate TSPO in response to inflammation. Indeed, Lavisse *et al*. provided evidence that in mice upregulation of TSPO in reactive astrocytes is at least in part responsible for the responses seen in PET imaging in response to CNS inflammation, using overexpression of the cytokine ciliary neurotrophic factor, which induces gliosis specifically in astrocytes (Lavisse *et al.*, 2012). This may suggest that in humans TSPO is upregulated in astrocytes during CNS disease.

### 1.4.1 Expression of TSPO

In humans the *Tspo* gene is located on the 22q13.31 chromosome and is composed of 891 nucleotides (Chang *et al.*, 1992; Riond *et al.*, 1991). The gene is arranged in four exons, with a large intron between the first and second exon (Casalotti *et al.*, 1992; Lin *et al.*, 1993). Only the third exon is completely translated, with partial translation of the other three exons, resulting in the gene encoding 169 amino acids (**fig. 1.4.1.1**; Casalotti *et al.*, 1992; Lin *et al.*, 1993). This gene is transcribed and translated into a protein composed of 5 transmembrane α-helices with a steroid binding site termed the Cholesterol Recognition/Interaction Amino Acid Consensus (CRAC) motif on the c-terminus (**fig. 1.4.2**) (Guo *et al.*, 2015; Korkhov *et al.*, 2010; Li *et al.*, 2015). Mechanisms behind the regulation of TSPO translation are still unclear. The *Tspo* gene is highly conserved between species, and prokaryotes express an ortholog of the protein known as tryptophan-rich sensory protein gene (*tspO)* (Chapalain *et al.*, 2009; Yeliseev & Kaplan, 1995; Yeliseev *et al.*, 1997).

Within the eukaryotic cell TSPO is expressed on the OMM, with the majority of literature reporting this as the only cellular location of TSPO (Anholt *et al.*, 1986; Basile & Skolnick, 1986; Bribes *et al.*, 2004). However it has also been reported on the Golgi apparatus, plasma membrane, lysosomes, peroxisomes, and the nuclear envelope of cancerous cells (Hardwick *et al.*, 1999; O'Beirne *et al.*, 1990; Oke *et al.*, 1992). Notably, the TSPO paralog TSPO2 is reported in mature erythrocytes, which are devoid of intracellular organelles including mitochondria and nuclei (Marginedas-Freixa *et al.*, 2016). A recent paper suggests that TSPO is strictly expressed on the OMM, whilst an isoform of TSPO termed PBR-S,

which is a truncated form of TSPO1 and not the same as TSPO2, is also localised to non-mitochondrial sites (Liu *et al.*, 2017a).

In humans, genetic variants of TSPO have been reported (Owen *et al.*, 2012). The most common polymorphisms are A147T and R162H (Owen *et al.*, 2012). These polymorphisms have been observed in 30% of the Caucasian population and 25% of the African American (Owen *et al.*, 2012), although reported at much lower rates in other human populations. Human polymorphisms have been associated with disrupted pregnenolone production and increased prevalence of neuropsychiatric disorders (Colasanti *et al.*, 2013; Costa *et al.*, 2009; Nakamura *et al.*, 2006). In the TSPO protein containing A147T polymorphism the area surrounding the CRAC motif is altered, which may result in a lower affinity for cholesterol, hence the phenotypes observed associated with the polymorphism (Li *et al.*, 2015; Milenkovic *et al.*, 2018). Similarly, the R162H polymorphism results in an amino acid substitution within the CRAC domain, induction of which leads to decreased circulating corticosteroids (Owen *et al.*, 2017a). This suggests that common polymorphisms within the TSPO gene alter steroidogenesis.

TSPO is expressed constitutively in many tissues (Gavish *et al.*, 1999). These tissues include the liver, kidney, brain, and steroidogenic tissues such as the adrenal gland and gonads. It has since been reported to be found in other tissues such as the spleen, lung, muscle, bone marrow, adipose tissue, and white blood cells including macrophages (Giatzakis & Papadopoulos, 2004). In healthy brain tissue TSPO is expressed at low levels in glial cells, including astrocytes and microglia, which are brain resident macrophages, and upregulated in response

to disease and inflammation (Gavish *et al.*, 1999; Karlstetter *et al.*, 2014; Lavisse *et al.*, 2012; Owen *et al.*, 2017b). Expression in human tissues is similar to that in murine tissues, suggesting that mouse-derived cells are a suitable model for studying this protein (Batarseh & Papadopoulos, 2010).

#### 1.4.1.1 Regulation of TSPO

As mentioned previously, TSPO is upregulated during inflammation (Lee *et al.*, 2016). This occurs through protein kinase C (PKC) mediated activation of MAPK signalling (**fig. 1.4.1.1**). Loss of PKCε and ERK1/2 from the mouse steroidogenic cell line MA-10, and fibroblasts results in suppression of TSPO expression, whereas overexpression of MAPK signalling pathway components in these cells increases TSPO expression (Batarseh *et al.*, 2008; Batarseh *et al.*, 2010).

This control of TSPO expression by MAPK signalling is mediated through the action of multiple transcription factors. For example, nuclear accumulation of the specificity protein 1 (Sp1), STAT3 and AP-1 transcription factors increase *Tspo* mRNA expression in fibroblasts, a mouse microglia cell line (BV-2) and MA-10 steroidogenic cells (Batarseh *et al.*, 2010; Giatzakis *et al.*, 2007; Giatzakis & Papadopoulos, 2004; Rashid *et al.*, 2018; Shimoyama *et al.*, 2019). Silencing of these transcription factors using RNA interference prevents increased TSPO expression after LPS stimulation of BV-2 microglia (Rashid *et al.*, 2018). Interestingly, there is evidence that PKC can also activate NF-κB signalling, suggesting a role for NF-κB in the regulation of TSPO expression (Garg *et al.*, 2012; Satoh *et al.*, 2004). However, the TSPO promotor is still active when NF-κB is inhibited (Batarseh *et al.*, 2010). This suggests that whilst TSPO expression

may be increased by NF-κB signalling, the activity of NF-κB is not essential for TSPO expression; therefore, NF-κB is not considered to be a major regulator of TSPO expression (Batarseh *et al.*, 2010). Regarding the current available evidence, the gene (*Tspo*) is thought to be primarily regulated by the PKCε-ERK1/2-AP1/Stat3 signalling transduction pathway (**fig. 1.4.1.1**) (Batarseh *et al.*, 2008; Batarseh *et al.*, 2010; Batarseh & Papadopoulos, 2010).

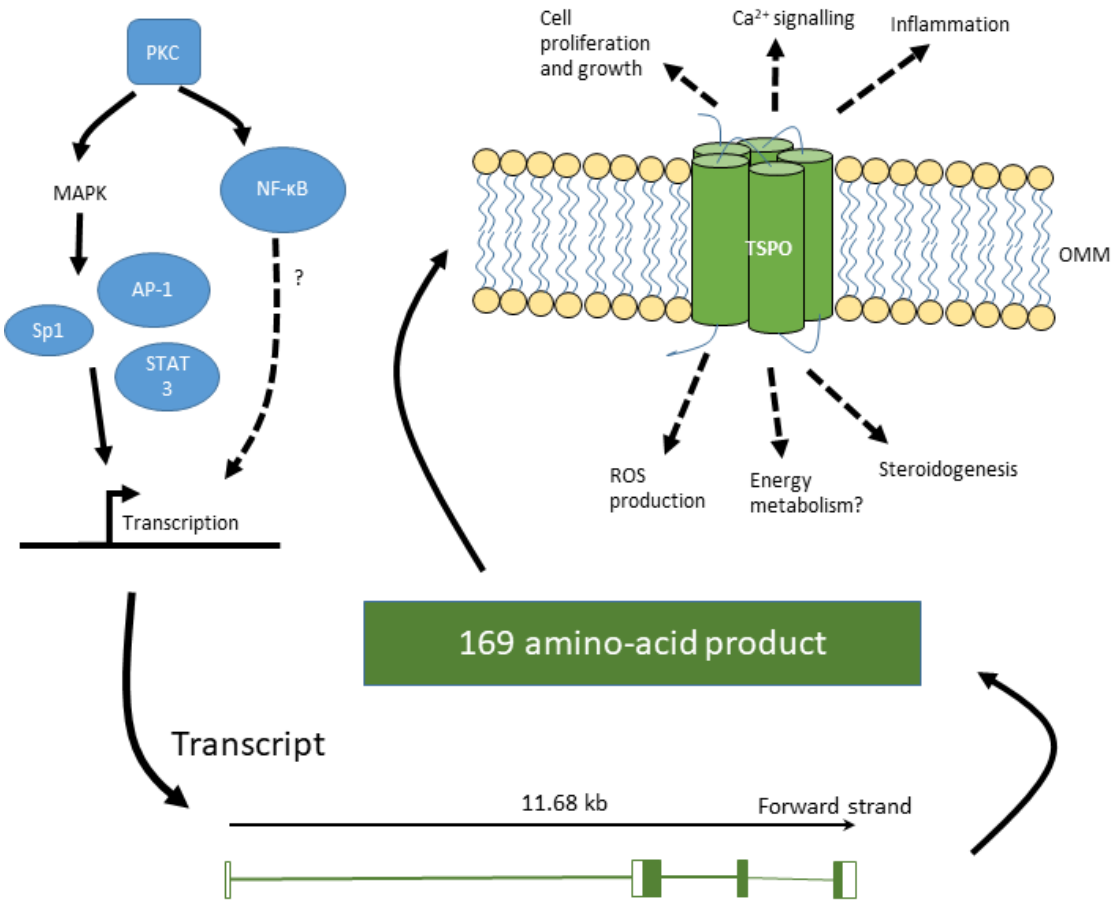


**Figure 1.4.1.1: Summary of the regulation and roles of translocator protein 18 kDa (TSPO).** TSPO expression has been implicated in multiple mechanisms. Expression of TSPO is regulated at the transcriptional level by activator protein 1 (AP-1), specificity protein 1 (Sp1), and signal transducer and activator of transcription 3 (STAT3). These are regulated by mitogen activated protein kinases (MAPKs), activated by protein kinase C (PKC). Nuclear factor κB (NF-κB), which is regulated by PKC may also regulate TSPO expression. When active, the promoter drives the synthesis of an 11.68 kb transcript (Exons depicted by boxes, introns by lines; adapted from Ensembl, 2020), of which the regions indicated in solid colour are transcribed into an 169 amino acid product.

### 1.4.2 Synthetic TSPO ligands

Activity of TSPO can be regulated by ligands binding to the protein. Endogenous ligands of TSPO include tetrapyrroles and acyl-coA binding protein (Guidotti *et al.*, 1983; Li *et al.*, 2015; Veenman *et al.*, 2016). Functions of these ligands include REDOX and metabolic regulation, although the extent through which this is mediated through TSPO in eukaryotes is currently unknown (Tonon *et al.*, 2019; Veenman *et al.*, 2016; Zhao *et al.*, 2016).

Several synthetic ligands against TSPO have been developed for use in humans (Michelle *et al.*, 2006). Some of the early ligands developed included PK11195, Ro5-4864 and XBD-173 (emapunil, AC-5261). Since then more specific ligands have been developed. These have been classified as either agonists or antagonists of TSPO based on their ability to displace PK11195 in radioligand binding assays and their impact on cholesterol transport (Campiani *et al.*, 1996; Katz *et al.*, 1992; Papadopoulos *et al.*, 1990). PK11195 is classified as a TSPO antagonist due to initial reports that PK11195 decreases steroidogenesis in MA-10 steroidogenic cells (Papadopoulos *et al.*, 1990). However, emerging evidence suggests that the effect of PK11195 on steroidogenesis is inconsistent, with some studies showing no change or increased steroidogenesis after PK11195 treatment (Selvaraj & Tu, 2016).

Ro5-4864 is classified as a TSPO agonist due to its ability to displace PK11195 and the finding that it consistently increases steroidogenesis (Le Fur *et al.*, 1983; Selvaraj & Tu, 2016). The ligand XBD-173 is also classified as a TSPO agonist due to increased steroidogenesis after treatment (Selvaraj & Tu, 2016). While

these synthetic ligands bind TSPO and clearly influence its purported function(s), caution needs to be used with respect to utilising the terms ‘agonist’ and ‘antagonist’, as TSPO is not a receptor. The terms ‘activator’ and ‘inhibitor’ may be more appropriate, but classification of these ligands remains challenging due to the currently poor definition of TSPO function.

TSPO ligands change the structure of TSPO. For example, PK11195 binds to multiple amino acids on separate cytoplasmic loops, resulting in a conformational change which obscures the channel formed by the 5 transmembrane alpha-helices (**fig. 1.4.2;** green squares) (Iatmanen-Harbi *et al.*, 2019; Jaremko *et al.*, 2014). This is thought to prevent transport of cholesterol into the mitochondria. Proposed ‘agonists’ probably modulate the activity of TSPO through a different mechanism as they increase steroidogenesis, but this is as yet unknown.

Recent studies have shown that PK11195 and Ro5-4864 bind to different amino acids in the TSPO structure (**fig. 1.4.2**) (Farges *et al.*, 1994; Jaremko *et al.*, 2014; Liu *et al.*, 2014b). This may suggest that Ro5-4864 causes a unique conformational change which promotes cholesterol transport. Interestingly, ligand displacement assays suggest that XBD-173 binds to a site more similar to PK11195 than Ro5-4864 (Zhang *et al.*, 2007). However, as XBD-173 has reported agonistic functions it must also promote channel opening, suggesting that while XBD-173 and PK11195 bind to similar sites on TSPO they cause different conformational changes (Biswas *et al.*, 2018; Zhang *et al.*, 2007).

As with many drugs, TSPO ligands have been shown to have off-target effects, with data from BV-2 microglial cells demonstrating that TSPO ligands can modulate metabolism in these cells in the absence of TSPO (Bader *et al.*, 2019). At micromolar concentrations, the TSPO ligand PK11195 inhibits ATP synthesis by isolated $F_1F_0$ATPase, directly mimicking inhibition of $F_1F_0$ATPase by benzodiazepine Bz-423 (Cleary *et al.*, 2007). This may result in some of the off-target effects of PK11195 and other TSPO ligands. This is something that must be considered when interpreting any ligand-based data as it is apparent that TSPO and the ATPase have some homologous domains (Cleary *et al.*, 2007).

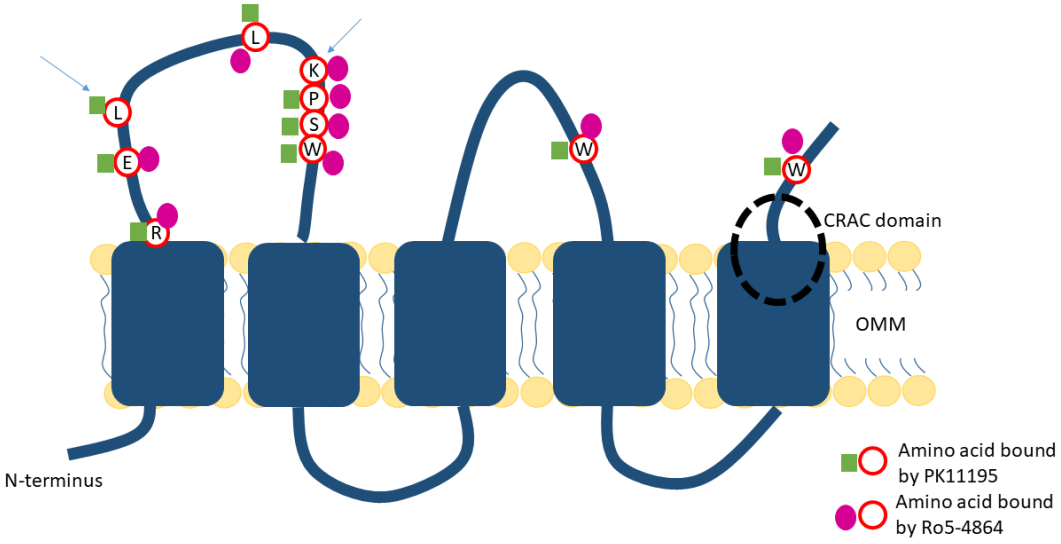


**Figure 1.4.2: A simplified structure of translocator protein 18 kDa (TSPO) showing the amino acids involved in binding TSPO ligands.** Differences in ligand binding indicated by arrows.

### 1.4.3 Functions of TSPO

In 1977, Braestrup and Squires identified TSPO in the kidney as an alternative binding site for the benzodiazepine diazepam (Braestrup & Squires, 1977). It was initially named peripheral benzodiazepine receptor (PBR) to distinguish it from the central benzodiazepine receptor found on the plasma membrane of some neurons (Braestrup *et al.*, 1979; Braestrup & Squires, 1977; Tallman *et al.*, 1978). In 2006 it was proposed that PBR should be renamed 'translocator protein (18kDa)' (TSPO) due to its apparent involvement in the translocation of cholesterol across the outer mitochondrial membrane (Papadopoulos *et al.*, 2006). After initial attempts to create a TSPO knockout mouse line failed it was assumed that loss of TSPO was embryonic lethal, but a viable global homozygous TSPO knockout mouse line was created in 2014 (Papadopoulos *et al.*, 1997; Tu *et al.*, 2014). This proved that functional TSPO expression is not essential for survival (Tu *et al.*, 2014) and is supported by findings that knockouts *in vivo* do not lead to an altered genetic profile, phenotype, or metabolic changes that are observed *in vitro* (Banati *et al.*, 2014).

#### 1.4.3.1 Steroidogenesis

TSPO transports cholesterol into the mitochondria for steroidogenesis. This has been shown in multiple studies from independent groups and in many cell types including in glial cells (Papadopoulos *et al.*, 2018). TSPO 'agonists' increase pregnenolone production in mitochondria purified from the brain (Papadopoulos *et al.*, 2018; Romeo *et al.*, 1993). This is inhibited by PK11195, suggesting that TSPO activity increases neurosteroid production, whilst 'antagonism' of TSPO reduces neurosteroid production.

In recent years as more data has emerged, whether TSPO plays a role in steroidogenesis has become a contentious issue and data has been published suggesting that TSPO is not essential for cholesterol transport into the mitochondria (Fan *et al.*, 2018a; Selvaraj & Stocco, 2018; Selvaraj *et al.*, 2016). Despite this on-going debate, TSPO is still believed to play a role in cholesterol transport as it contains a cholesterol binding domain, and there is significant supporting evidence from multiple publications and research groups (Jaipuria *et al.*, 2017; Jamin *et al.*, 2005; Lejri *et al.*, 2019; Li & Papadopoulos, 1998; Murail *et al.*, 2008; Musman *et al.*, 2017; Paradis *et al.*, 2013).

#### 1.4.3.2 Inflammation

TSPO ligands have been shown to be anti-inflammatory in many cell types (Horiguchi *et al.*, 2019; Pozzo *et al.*, 2019). However, the evidence for this in astrocytes is relatively sparse. TSPO ligands etifoxine, PK11195 and XBD-173 decrease TLR1/2 and TLR4 induced production of pro-inflammatory cytokines IL-6 and TNF-α in microglial cells (Lee *et al.*, 2016). This was also demonstrated in astrocytes, although XBD-173 did not affect TLR4 stimulated TNF-α release from astrocytes. However, in this study TSPO ligands were used at 50 µM regardless of their affinity, bioactivity and specificity, so there may be off-target effects at these relatively high concentrations. In C6 glioma cells PK11195 reduces production of the inflammatory mediator cyclooxygenase 2 (COX2), although again this was used at 10 µM, a concentration which has been shown to cause off-target effects (Cleary *et al.*, 2007; Santoro *et al.*, 2016).

Anti-inflammatory actions of TSPO ligands have also been reported *in vivo* in disease models. In mice, whilst Ro5-4864 and PK11195 reduce microglial reactive gliosis, these TSPO ligands did not reduce astrogliosis after LPS-induced inflammation (Veiga *et al.*, 2007). Intraperitoneal injection of the TSPO ligand etofoxine is neuroprotective in mouse models of multiple sclerosis, and PK11195 and Ro5-4864 reduce astrogliosis in hyper-phosphorylated tau expressing mouse models of Alzheimer's disease (Barron *et al.*, 2013; Daugherty *et al.*, 2013). These data suggest that *in vivo* TSPO ligands can reduce CNS disease severity, but it is unclear whether the primary mechanism is through microglia and/or astrocytes. Further to this, there is no data currently available from published literature exploring the effect of loss of TSPO on the *in vivo* response to infection. As such, there is clearly more to be understood about the role of TSPO in CNS inflammation.

#### 1.4.3.3 Regulation of reactive oxygen species production

The neuroprotective role of TSPO modulation may in part be due to regulation of ROS. TSPO expression is implicated in increasing ROS production, with its evolutionary role thought to be mainly related to ROS regulation in part due to TSPO acting as an oxygen sensor in bacteria (Batarseh & Papadopoulos, 2010; Gatliff *et al.*, 2014; Yeliseev *et al.*, 1997). In addition, colonic cells overexpressing *Tspo* have increased mitochondrial stability and resilience to ROS damage, as do cells treated with pharmacological TSPO 'agonists' (Issop *et al.*, 2016; Lejri *et al.*, 2019). This effect is proposed to be regulated through increased TSPO expression as a ratio compared to VDAC1 (Gatliff *et al.*, 2014; Issop *et al.*, 2016). However, loss of TSPO from MA-10 steroidogenic cells and treatment with TSPO 'antagonists' such as PK11195 also results in increased ROS production (Lejri *et*

*al.*, 2019; Tu *et al.*, 2016). Together these data suggest that TSPO plays a role in regulating ROS production; however, to what end is currently unclear as the data available appears to be contradictory.

#### 1.4.3.4 $Ca^{2+}$ signalling and interaction with VDAC

TSPO interacts with the VDAC, the principal $Ca^{2+}$ channel in the OMM (Gatliff *et al.*, 2014; Papadopoulos *et al.*, 1994; Shoshan-Barmatz *et al.*, 2019). Loss of TSPO results in elevated levels of mitochondrial $Ca^{2+}$ (Gatliff *et al.*, 2017). Furthermore, the interaction between VDAC and TSPO appears to reduce the ability of VDAC to transport cytosolic $Ca^{2+}$ into the mitochondria, leading to an accumulation of $Ca^{2+}$ in the cytosol (Gatliff *et al.*, 2017). This accumulation of $Ca^{2+}$ potentially influences multiple signalling pathways, affecting astrocyte behaviour (Bazargani & Attwell, 2016). For example, increases in cytosolic $Ca^{2+}$ can drive release of gliotransmitters such as ATP and glutamate; changes to cellular morphology, leading to the upregulation of GFAP associated with astrocyte activation; and synapse remodelling (Shigotomi *et al.,* 2019).

The interaction between TSPO and VDAC may play a role in the other functions attributed to TSPO. Downregulation of VDAC1 in astroglioma cells using small interfering RNA (siRNA) decreases TSPO expression, resulting in reduced cell growth and tumour volume (Arif *et al.*, 2016). However, this is not mediated through apoptosis, suggesting it is instead through a decrease in cell proliferation, which as previously discussed is a proposed role of TSPO (Arif *et al.*, 2016). However, it has not been shown what effect TSPO binding has on this role of VDAC.

#### 1.4.3.5 Cell maintenance and growth

In addition to regulating cellular inflammation, TSPO also seems to play a role in maintaining cell health through the regulation of autophagy. Autophagy is the degradation and metabolism of pre-existing cellular structures to generate energy or new precursors for biosynthesis (Ravanan *et al.*, 2017). This term is suffixed after the structure being degraded e.g. mitophagy is autophagy of the mitochondria, whereas lipophagy is autophagy of lipid droplets. Autophagy helps to maintain cell health through recycling and regenerating damaged cell structures, preventing the accumulation of cell death signals within the cell (Ravanan *et al.*, 2017).

In section **1.4.3.3** it was mentioned that TSPO overexpression increases ROS production in fibroblasts. Gatliff *et al.* showed that this overexpression of TSPO in fibroblasts also inhibits mitophagy due to excessive phosphorylation of VDAC1, resulting in reduced mitochondrial quality (Gatliff *et al.*, 2014). Conversely, in tanycytes, pharmacological inhibition or loss of TSPO activates lipophagy (Kim *et al.*, 2019). It is suggested that lipophagy is regulated through activation of AMPK, which in turn is activated by $Ca^{2+}$ signalling (Kim *et al.*, 2019). This provides evidence that expression of TSPO may restrict autophagy, possibly through interaction with VDAC.

TSPO was thought to play a role in apoptosis through regulating the mitochondrial permeability transition pore (MPTP) opening (Obame *et al.*, 2007). However, this has since been disputed, and the apparent role in apoptosis may instead be due

to the role of TSPO in autophagy allowing increased accumulation of pro-apoptotic proteins (Hurst *et al.*, 2017; Šileikytė *et al.*, 2014).

Data also suggests that TSPO regulates cell proliferation. In breast cancer cells TSPO ligands have been shown to decrease cell proliferation, and loss of TSPO decreases cell proliferation both *in vitro* and *in vivo* (Bader *et al.*, 2019; Mukherjee & Das, 2012). Conversely, TSPO overexpression increases cell proliferation and motility (Liu *et al.*, 2017b). However, in contrast to previous studies, loss of TSPO increased cell proliferation in glioblastoma cell lines and *in vivo* (Fu *et al.*, 2019). This may be related to the difference in the role of TSPO in inflammation in astrocytes compared to other cell types.

#### 1.4.3.6 Cell energy metabolism

There is increasing evidence that TSPO plays an important role in energy metabolism; however, its exact role remains unclear. The TSPO 'antagonist' PK11195 increases expression of metabolic genes including CPT-1A in zebra fish *in vivo* (Gut *et al.*, 2013). This suggests that TSPO acts to decrease fatty acid metabolism. This is supported by data that indicate that loss of TSPO increases fatty acid oxidation and expression of CPT-1A in MA-10 steroidogenic cells (Tu *et al.*, 2016).

There is also published data indicating that TSPO acts to increase mitochondrial energy production and OXPHOS rate. Loss of TSPO in mouse microglia significantly decreases mitochondrial ATP production and oxygen consumption

(Banati *et al.*, 2014). Similarly, TSPO 'agonists' including Ro5-4864 increase mitochondrial metabolism, mitochondrial membrane potential and glycolysis, resulting in increased ATP accumulation in SH-SY5Y cells (Grimm *et al.*, 2019; Lejri *et al.*, 2019). Overexpression of TSPO in Jurkat cells increases ETC gene expression, including ETC complex IV, which was abated by treatment with 100 nM PK11195 (Liu *et al.*, 2017b). This results in increased intracellular ATP accumulation (Liu *et al.*, 2017b). However, another paper suggests that TSPO knockdown in BV-2 cells has no effect on mitochondrial respiration, although it has been reported to increase proton leak and decrease coupling efficiency (Bader *et al.*, 2019).

Taken together, these data indicate that TSPO plays important regulatory roles within the cell. However, the exact role it is playing is yet to be fully elucidated. Interestingly it appears to be playing a role in both inflammatory and metabolic regulation. Although the underlying mechanism(s) by which this occurs are unclear, given the strong evidence for metabolic rate being a critical regulator of inflammation it is likely that these are related.

### 1.4.4 TSPO ligand safety and clinical use

Due to the variety and importance of possible roles for TSPO, it has become a promising drug target for neuropsychiatric disorders, inflammatory conditions and cancer (Rupprecht *et al.*, 2010). Some TSPO ligands are already approved for use in humans (Owen *et al.*, 2014; Rupprecht *et al.*, 2010; Sridharan *et al.*, 2019): etifoxine has been approved as an anxiolytic; XBD-173 has been used in pre-clinical human studies investigating anxiety and seizures; and radiolabelled

PK11195 has mainly been used for PET scanning (Choi & Kim, 2015; Hirvonen *et al.*, 2010). Indeed, the use of TSPO ligands in PET demonstrates their ability to cross the BBB, making them appropriate for potential treatment of CNS disease.

More data is emerging demonstrating the potential clinical applications of TSPO ligands. With studies in mice suggesting that TSPO ligands may be useful for the treatment of Alzheimer's disease, reducing β-amyloid plaques, and TSPO agonist etifoxine improving recovery from traumatic brain injury in mice, interest in TSPO as a drug target is increasing (Barron *et al.*, 2013; Shehadeh *et al.*, 2019). Novel ligands are currently being developed, which are more specific and able to bind TSPO regardless of the gene polymorphisms, which has been an issue with existing ligands (Alam *et al.*, 2017). An *in silico* approach is currently being used to develop TSPO inhibitors aimed at decreasing cancerous cell proliferation (Bhargavi *et al.*, 2017). TSPO ligands may be even more useful therapeutically once the function of TSPO has been fully elucidated.

## 1.5 Summary of introduction

The data discussed in sections **1.1-1.3** of this chapter demonstrate that astrocytes may undergo immunometabolic reprogramming. However, there are limited studies that have examined this directly. In many cell types the immunometabolic response is in part regulated by NF-κB signalling, and whilst NF-κB clearly plays a role in regulating metabolic responses during inflammation in astrocytes, to what extent NF-κB regulates the link between inflammation and metabolism in astrocytes needs further work. This work is of importance due to

the role of astrocytes and CNS inflammation in prevalent neurodegenerative diseases, such as Alzheimer's disease. TSPO, which is upregulated during inflammation and neurodegenerative diseases, is emerging as a player in metabolic regulation. As TSPO is primarily regulated during inflammation this protein has been explored as a therapeutic target for inflammatory disease, particularly in the CNS, due to the availability of safe ligands which can cross the BBB.

## 1.6 Aims of investigation

- Characterise the metabolic responses to inflammation in astrocytes.
- Establish the role of NF-κB signalling in immunometabolic responses in astrocytes.
- Investigate a potential role of TSPO in astrocyte metabolism.

# Chapter 2. Methods

## 2.1 Materials

### 2.1.1 Equipment

**Table 2.1.1** List of instruments and suppliers

| Instrument | Company |
|---|---|
| PHERAstar FS | BMG LABTECH |
| Seahorse XF$^{e}$96 Analyser | Agilent |
| DM4000B-M widefield microscope | Leica |
| DMi8 confocal microscope | Leica |
| BD Accuri C6 Plus Flow Cytometer | BD Biosciences |
| SimpliAmp Thermocycler | Applied Biosystems |
| Mini-PROTEAN tetra vertical handcast protein electrophoresis systems | Bio-Rad |
| Wide mini-sub cell GT cell nucleic acid electrophoresis system | Bio-Rad |
| GelMax Imager | UVP |
| TC20 Automated cell counter | Bio-Rad |
| Odyssey CLx imaging system | Li-Cor |

### 2.1.2 Reagents

Unless listed in **table 2.2**, all reagents were purchased from Sigma-Aldrich (part of Merck, UK) or ThermoFisher Scientific (UK).

**Table 2.1.2** List of reagents not sourced from ThermoFisher (UK) or Sigma-Aldrich (UK)

| Chemical | Supplier |
|---|---|
| Acrylamide | National diagnostics |
| ATPLite two step kit Luminescence assay system | Perkin Elmer |
| Bio-Rad Protein Assay Dye Reagent | BioRad |
| Bovine Serum Albumin, Fatty Acid Free (FAF-BSA) | Roche |
| DuoSet ELISAs | Bio-Techne |
| FCCP | Cambridge Bioscience |
| Fluoroshield mounting medium | Abcam |
| Foetal Bovine Serum (FBS) | Seralabs |
| GelRed | BIOTIUM |
| Glycolytic Stress Test | Agilent |
| Glucose Uptake-Glo | Promega |
| Hanks Balanced Salt Solution (HBSS) | Gibco |
| L-Glutamate | Gibco |
| Mitotracker CMXRos | Invitrogen |
| Mito Stress Test | Agilent |
| Odyssey blocking buffer | Li-Cor |
| Penicillin-Streptomycin | Gibco |

| | |
|---|---|
| Phosphate buffered saline | Oxoid |
| PK11195 | Tocris |
| Precision Plus Protein Dual Colour standards | BioRad |
| Primers | IDT |
| Protein G dynabeads | Invitrogen |
| Seahorse XF media | Agilent |
| Sucrose | Melford |
| Tetramethylrhodamine ethyl ester (TMRE) | Cambridge Bioscience |
| TPCA-1 | Tocris |
| Tris | Melford labs |
| Trypsin 0.05% | Gibco |
| Trypsin – phenol red free, 2.5% | Gibco |
| 11966 DMEM (No Glucose) | Gibco |

### 2.1.3 Animals and ethics

All animal studies were conducted in accordance with the UK Animals in Scientific Procedures Act 1986 (ASPA) and study plans were approved by the institutional Animal Welfare and Ethical Review Body at the University of Exeter. Mouse pups (postnatal day 1-5) were used to produce cultures of primary astrocytes from the cortex; offspring of both sexes were used. Pups from breeding pairs of C57BL6/J mice (Charles River, UK) were used for non-genetically modified (GM) astrocytes. Pups from breeding pairs of heterozygous C57BL/6NTac $Tspo^{tm1b(EUCOMM)Wtsi}$ (HMGU-EPD0803_2_H02-2-1; Infrafrontier, UK) mice were used for breeding. Homozygous TSPO knockout ($TSPO^{-/-}$) mice were used to culture TSPO-

deficient primary cortical astrocytes as described in **section 2.2.2**, with homozygous TSPO expressing littermates used as wildtype ($TSPO^{+/+}$) controls. Mice were group housed on a 12:12 light-dark cycle at 22 ± 2 °C, with unlimited access to standard laboratory rodent diet (EURodent diet [5LF2], LabDiet, UK) and water.

## 2.2 Methods

### 2.2.1 Genotyping

Genotypes of animals in the TSPO colony were determined using a polymerase chain reaction (PCR) and agarose gel electrophoresis. Tissue was biopsied from the tails of the pups immediately after euthanasia, or from the ear of living adult animals. Tissue was digested at 55 °C for 5 hours in PCR sample digestion buffer with non-ionic detergents (50 mM KCl, 10 mM Tris- HCl [pH 8.0], 2.5 mM $MgCl_2$-$6H_2O$, 0.1 mg/mL gelatine, 0.45% v/v Nonidet P40, 0.45% v/v Tween-20, 1% v/v proteinase K) prior to heating at 95 °C for 10 minutes. PCR reaction mix was made as detailed in **table 2.2.1.1** and PCR was run as detailed in **table 2.2.1.2**. A negative control reaction containing water instead of DNA digest was run with every PCR. 5 µL PCR product was run on agarose gel (1.5% w/v 1X TAE: 40 mM Tris Acetate [pH 6.8], 1 mM EDTA) with 0.05% GelRed (Biotum, UK; # 41003). GeneRuler 1 kb Plus DNA ladder (ThermoFisher, UK; # SM1333) was used to estimate size of bands. The presence of the higher band (~244 kb) only indicated a $TSPO^{-/-}$ mouse, the lower (~188 kb) band only indicated $TSPO^{+/+}$ mouse and the presence of both bands indicated $TSPO^{+/-}$ mouse (**fig. 2.2.1**). $TSPO^{+/-}$ mice were not used for this study.

**Table 2.2.1.1 Genotyping reaction composition**

| Component | Volume (µL) |
|---|---|
| 2X DreamTaq green PCR master mix (Thermo, UK; # K1081) | 10 |
| DNA-Free water | 6 |
| 5’ arm primer 5’>3’ [AGCAGAAGTAGGAAGAAGGTG] (10 pmol/µL) | 1 |
| 3’ arm primer 5’>3’ [GTCAACCCATCACTGCCTTCA] (10 pmol/µL) | 1 |
| LAR3 primer 5’>3’ [CAACGGGTTCTTCTGTTAGTCC] (10 pmol/µL) | 1 |
| DNA digest (50-100 ng) | 1 |
| Total volume | 20 |

**Table 2.2.1.2 Polymerase chain reaction cycling conditions**

| Temp (°C) | Time | # cycles |
|---|---|---|
| 95 | 5 minutes | 1 |
| 94 | 30 seconds | 39 |
| 65 | 45 seconds | |
| 72 | 45 seconds | |
| 72 | 10 minutes | 1 |
| 4 | Hold | 1 |

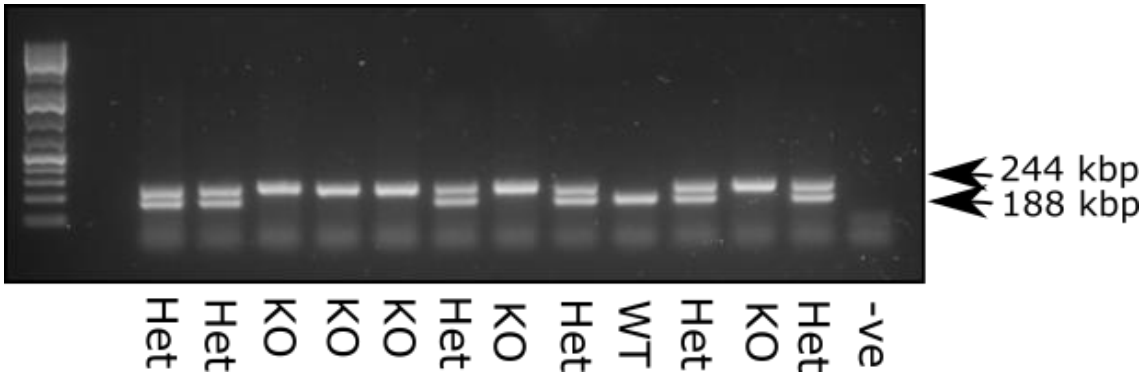


**Figure 2.2.1: An example electrophoresis gel of TSPO colony genotyping results.** DNA was extracted from ear or tail biopsies using PCR sample digestion buffer with non-ionic detergents and proteinase K. After PCR amplification the PCR product was separated and visualised using a 1.5% agarose electrophoresis gel with 0.05% GelRed. Band at 244 kb denotes TSPO $^{-/-}$ (KO) animals, 188 kb denotes TSPO $^{+/+}$ (WT) animals, and double bands denote TSPO $^{+/-}$ (Het) animals.

### 2.2.2 Primary astrocyte isolation and cell culture

Mouse primary cortical astrocytes were isolated using the method described by Schildge *et al.* (Schildge *et al.*, 2013). Briefly, pups (post-natal days 1-5) were decapitated in a regulated procedure and brains were removed from skulls. Forceps were used to blunt dissect brain to remove the cerebellum and hypothalamus. Cortical regions were chopped into smaller sections and digested in 0.5% w/v trypsin-EDTA in Hank's Balanced Salt Solution (HBSS) for 30 minutes at 37 °C with gentle agitation every 2-3 minutes. Trypsin was neutralised in supplemented Dulbecco's Modified Eagle's Media (DMEM; 25 mM glucose, 8 mM L-glutamate, 10% v/v foetal bovine serum (FBS), 200 U/mL penicillin-streptomycin) and cells were mechanically dislodged from cerebral membranes using repeated pipetting motions.

For culturing isolated cells, plastics were coated with poly-L-lysine (PLL; 4 µg/mL) by 30 minute incubation at room temperature and washed with PBS prior to seeding cell suspensions. Non-GM mouse primary astrocyte cultures were seeded at 2-3 brains in T75 flasks. GM mouse primary astrocytes were seeded at 1 brain per T25 flask. As previously described (Vlachaki Walker *et al.*, 2017), cultures were maintained in DMEM containing 25 mM glucose and supplemented with 10% v/v FBS (Seralabs), 200 U/mL penicillin-streptomycin and 8 mM L-glutamine. Media was replaced every 2-3 days. Cultures were maintained in a humidified incubator at 37 °C with 5% $CO_2$. Astrocytes were left to grow until 100% confluent.

Once confluent, cells were dissociated with trypsin (0.05% w/v) from culture flasks. After neutralisation of trypsin with media, cell suspensions were centrifuged at 100 x*g* for 5 minutes at room temperature and excess trypsin was removed. After this step non-GM cells were seeded for experimentation as described below. Once confluent, GM cells were frozen in 10% dimethylsulfoxide (DMSO) and 90% supplemented DMEM at -80 °C and stored in liquid nitrogen until use. For experimentation, homozygous cells of the same genotype were defrosted and centrifuged at 100 x*g* for 5 minutes at room temperature. Excess DMSO containing media was removed. Cells were combined to 3 cultures per T75 and allowed to grow to 100% confluence prior to dissociation with trypsin (0.05% w/v), centrifugation at 100 x*g* for 5 minutes and removal of trypsin and seeding for experiments as described below.

Prior to experimentation cells were seeded on PLL coated plasticware at an appropriate density as described for the experiment in the relevant section. The TC20 Automated Cell Counter (Bio-Rad, UK) was used to quantify cell numbers for seeding for experiments. 24 hours prior to experimentation cells were maintained in DMEM (Gibco) supplemented with 10% v/v FBS, 200 U/mL penicillin-streptomycin, 8 mM L-glutamine and 7.5 mM glucose. On the day of experimentation cells were cultured in serum free DMEM (Gibco) containing 2.5 mM glucose. Immunocytochemistry was used to confirmed that mature cultures contained >99% GFAP-immunoreactive glial cells, as described in **section 2.2.5** (**fig. 2.2.2**).

A

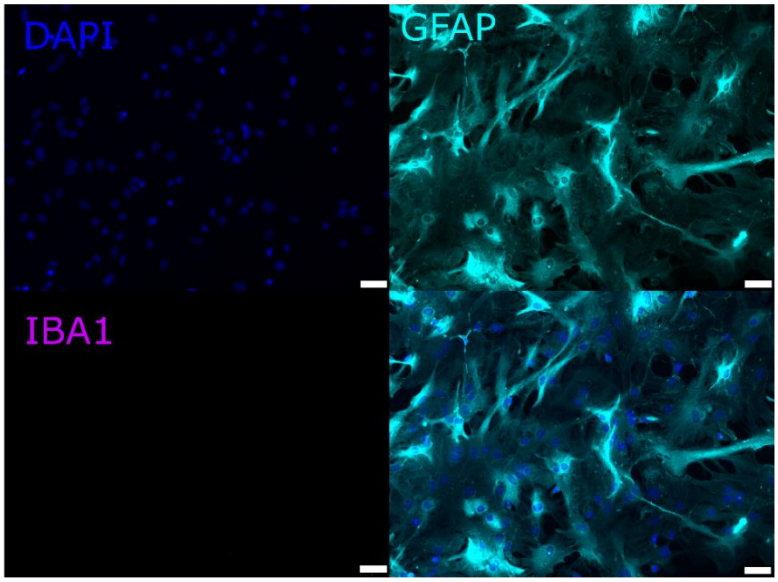


B

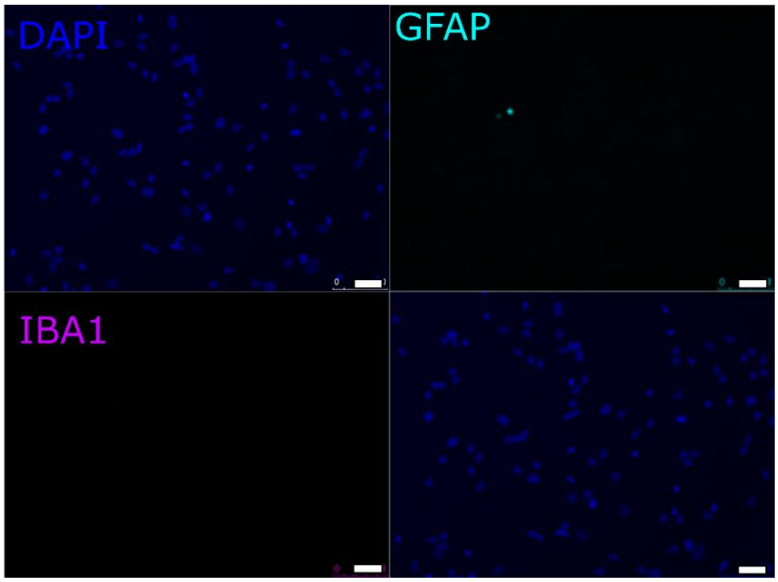


**Figure 2.2.2: Cultures taken from mouse brains were mainly GFAP expressing cells**. Glial cells were seeded at a density of 1 x $10^5$ cells per well on glass coverslips in 24 well plates prior to fixation with 4% paraformaldehyde and immunostaining. **A.** GFAP (Cyan) and IBA-1 (Magenta) immunostaining of primary glial culture. 99.7% of nuclei (DAPI; blue) were associated with GFAP-immunoreactivity (n=12; 3 images per coverslip across 4 coverslips). **B.** Example images of no first layer (primary antibody) negative control. Scale bars = 50 µm.

### 2.2.3 Human astroglioma cell line (U373) culture

Human astroglioma U373 cells were sourced from Sigma-Aldrich (UK). The U373 TSPO deficient cells were created by Daisy Stewart (a professional training year student) under the supervision of Dr Rosie Bamford and Dr Asami Oguro-Ando using CRISPR-Cas9 technology to knock out the TSPO gene through introduction of double strand breaks in exon 2. Non-genetically modified cells were continuously cultured in T75 sterile flasks up to p30 in stock DMEM to maintain passage equivalent controls which were transfected with a control empty vector. Genetically modified TSPO KO U373 line and the paired empty vector (EV) control line were used indefinitely, but for experiments presented in this work were p50-60. Although the high passage number generated is not ideal, due to the nature of CRISPR-Cas9 genetic modification this could not be avoided. However, a stable total knockout generated by CRISPR-Cas9 was preferable to a transient and partial knock down generated by siRNA, which would be an alternative method.

U373 cultures were maintained in DMEM containing 25 mM glucose and supplemented with 10% v/v FBS (Seralabs; UK), 200 U/mL penicillin-streptomycin and 8 mM L-glutamine. Cells were passaged when at approximately 70% confluence. During passage, cells were washed with 0.01 M PBS before being dissociated with trypsin (0.05% w/v) at 37 °C. Cells were centrifuged at 100 x*g* for 5 minutes at room temperature and excess trypsin was removed. 25-30% of the cell suspension was seeded into new T75 flasks to maintain the culture. Cells were seeded on plasticware at an appropriate density 24 hours prior to experimentation. The TC20 Automated Cell Counter (Bio-Rad, UK) was used to

quantify cell numbers for seeding. Cells were maintained after seeding for experimentation in DMEM (Gibco) supplemented with 10% v/v FBS, 200 U/mL penicillin-streptomycin, 8 mM L-glutamine and 7.5 mM glucose. On the day of experimentation cells were cultured in serum free DMEM (Gibco) containing 2.5 mM glucose.

### 2.2.4 Cell treatments

LPS (*E. coli* O26:B6) was conjugated to 0.17 mM fatty acid free bovine serum albumin [BSA (Roche, UK)] in 150 mM NaCl for 1 hour prior to treatment of cells. BSA was adjusted to pH 7.4 at 37 °C with 1 N NaOH. BSA conjugated LPS or BSA vehicle were diluted 1:10 into DMEM to give a final concentration of 1 µg/mL LPS and 0.017 mM BSA. Where used, TPCA-1 (1 µM; Tocris, UK; IKK-β inhibitor; $IC_{50}$ 17.9 nM) (Podolin *et al.*, 2005) was diluted in 0.1% v/v DMSO vehicle 2 hours prior to additional treatments. 2-deoxyglucose (2-DG; 10 mM) diluted in $ddH_2O$ was applied 1 hour prior to additional treatments, when used. Where TSPO ligands were used, cells were pre-treated with PK11195 (25 nM; Tocris, UK; $IC_{50}$ 2.2 – 5.65 nM) (Cleary *et al.*, 2007; James *et al.,* 2006; Kita *et al.*, 2004) or XBD-173 (25 µM; Sigma, UK; $IC_{50}$ 2.73-3.04 nM) (Kita *et al.*, 2004) made up in 0.1% v/v DMSO vehicle for 1 hour prior to additional treatment.

### 2.2.5 Immunocytochemistry and culture purity

For immunocytochemical staining, mouse primary astrocytes were plated on sterile PLL coated 13 mm diameter glass coverslips at a density of 1 x $10^5$ cells/coverslip. After treatment, cells were fixed with 4% w/v paraformaldehyde for 30 minutes at 37 °C and permeabilised for staining by treatment with lysine

block (0.01 M PBS, 0.02% v/v Triton-X100, 2% w/v lysine) for 15 minutes at room temperature. Purity of the mouse primary astrocyte culture was confirmed using mouse anti-GFAP (1:1000; Millipore; UK; #MAB360) and goat anti-IBA1 (1:1000; Abcam; UK; #ab5076) immunoreactivity. Both primary and secondary antibodies were diluted in lysine block. Fixed and permeabilised cells were incubated with each primary antibody overnight (~18 hours) at 4 °C, sequentially. After incubation with GFAP primary antibody, coverslips were incubated with fluorescent secondary donkey anti-mouse Alexafluor488 (1:500; Invitrogen; UK; #A-21202) for 1 hour at room temperature. After incubation with IBA1 antibody overnight, fixed cells were incubated with fluorescent secondary donkey anti-goat Alexafluor594 (1:500; Invitrogen; UK; #A-11058) for 1 hour at room temperature. Both between and after antibody incubations, fixed cells were washed three times for 5 minutes with 0.01 M PBS to remove unbound antibody. Nuclei were stained with DAPI at room temperature for 5 minutes (0.01 mg/mL, 0.01 M PBS). Coverslips were briefly washed in $H_2O$, mounted in Fluoroshield Mounting Medium (Abcam; UK) and allowed to dry prior to imaging using wide-field microscopy (DM4000B-M; 10x/0.30; Leica; UK). FIJI Cell Counter plugin (Fiji Is Just ImageJ; (Schneider *et al.*, 2012; Schindelin *et al.*, 2012) was used to manually count nuclei associated with GFAP or IBA-1 staining.

### 2.2.6 Mitochondrial network characterisation

Mitochondrial networks were visualised using mitochondrial dye Mitotracker Red CMXRos (Invitrogen; UK). Cells were seeded on 13 mm diameter glass coverslips at a density of 1 x $10^5$ cells/coverslip. Staining was carried out before treatment and fixation. Cells were stained with 100 nM Mitotracker Red CMXRos

in DMEM (serum free, 2.5 mM glucose) for 15 minutes at 37 °C. Cells were then washed with PBS and subjected to treatment conditions. After treatment, cells were fixed with 4% w/v paraformaldehyde for 30 minutes at 37 °C and permeabilised for staining by treatment with lysine block (0.01 M PBS, 0.02% v/v Triton-X100, 2% w/v lysine) for 15 minutes at room temperature. Nuclei were stained with DAPI (0.01 mg/mL, 0.01 M PBS) for 5 minutes at room temperature. Coverslips were briefly washed with $H_2O$, mounted in Fluoroshield Mounting Medium (Abcam; UK) and allowed to dry prior to imaging.

Cells were imaged individually by confocal microscopy (DMi8; Leica, UK) using the x64 oil immersion lens (1x magnification). The number and length of objects in the red channel of the processed images were quantified using a custom-written MatLab program (modified from root script provided by Dr John Chilton; **Appendix 1**). Data from this processing was analysed using Prism (v5).

### 2.2.7 Cell viability assay

Cells were seeded at a density of 3.5 x $10^5$ cells/well in 6 well plates. After 24 hours of treatment (described above in **section 2.2.4**) cells were dissociated with 0.05% w/v trypsin-EDTA and transferred to flow cytometry tubes where trypsin was neutralised with fluorescence activated cell sorting (FACS) buffer (2% v/v FBS in 0.01 M PBS). Cells were centrifuged at 100 *xg* for 5 minutes at room temperature and the supernatant was aspirated. Cells were resuspended in FACS buffer and stained with propidium iodide (2 µg/mL), which is taken into cells with disrupted membranes, for 10 minutes at 4°C. Uptake of dye was determined using flow cytometry (BD Accuri C6; BD Systems; UK). Data was collected with

the 488 nm wavelength laser with the 585/40 nm filter. Increased uptake representing dead or dying cells. The gating used to identify the number of alive vs dead cells is shown as part of the relevant figures. Cell sized objects were first defined using forward scatter (FSC) and side scatter (SSC), and any events too small to be cells were excluded from further analysis. A second region of interest on a second plot was defined using fluorescence, and events with high fluorescence relative to cell size as determined using the 488 nm laser combined with FSC were classified as dead cells.

### 2.2.8 Protein isolation

Cells were plated at a density of 4.5 x $10^5$ cells per 60 mm diameter dish. After treatment cells were washed with 0.01 M PBS to remove excess BSA (if appropriate). Cells were lysed and protein isolated using modified RIPA buffer and mechanical scraping on ice (**table 2.2.8**). Lipids were removed with centrifugation at 1.3 x $10^4$ *xg* at 4 °C for 20 minutes.

| **Table 2.2.8 Modified RIPA buffer** | |
|---|---|
| **Reagent** | **Concentration (mM)** |
| Tris HCL pH 7.4 | 25 |
| NaF | 50 |
| NaCl | 100 |
| EDTA pH 8 | 1 |
| EGTA pH 8 | 5 |
| Triton 100x | 1% |
| NaPPi | 10 |
| Sucrose | 270 |
| 2-Mercaptoethanol | 0.1% |
| Sodium orthovanadate | 1 |
| Benzamidine | 1 |
| Phenylmethylsulfonyl fluoride | 0.1 |

### 2.2.9 Protein estimation

Protein content was estimated using the Bradford method according to the manufacturer's instructions (BioRad; UK). Briefly, between 1 and 3 µg of sample protein were loaded per well in triplicate wells. This was usually between 0.3 and 1 µL of protein lysate from a 60 mm dish, or 10-30 µL of lysate from a seahorse plate well. Increasing protein concentrations in triplicate were used to create a standard curve of 0, 1, 2 and 3 µg BSA with the same volume of solution used to lyse cells as was present in the protein lysate loaded. 200 µL of Protein Assay Dye Reagent (20% v/v in water) was added per well and the plate was agitated for 5 minutes at 500 rpm in the PHERAstar FS (BMG LABTECH; UK) prior to measuring absorbance at 595 nm.

### 2.2.10 Immunoblotting

Lysates were diluted to 1 µg/µL in sample buffer (125 mM Tris/HCl [pH 6.8], 4% w/v sodium dodecyl sulphate, 20% v/v glycerol, bromophenol blue). Gels were hand cast within 5 days of immunoblotting (**table 2.2.10.1**). 10 µg protein was loaded per lane and proteins were separated on a 12% v/v resolving acrylamide gel with approximately 1 cm 4% v/v stacking acrylamide gel using SDS-PAGE (150 V, ~1 hour 20 minutes), and transferred to nitrocellulose membranes (0.45 nm pore; 100 V, 1 hour 10 minutes). 5 µL Precision Plus Protein Dual Colour standards (BioRad; UK) were run on all gels and used to estimate protein size.

For immunoblotting, membranes were blocked for 1 hour in Odyssey Blocking Buffer (TBS; Licor; UK). Primary antibodies against proteins of interest were made up in 2.5% w/v milk powder or 2.5% w/v BSA in 0.01 M Tris-buffered saline

with 0.1% v/v Tween-20 (TBS-T) as detailed in t**able 2.2.10.2** and incubated with the membranes overnight at 4 °C. The relative fluorescence of GAPDH was used as a loading control. Antibodies against GAPDH were incubated with membranes for 1 hour at room temperature (see **table 2.2.10.2** for further details). Between antibody binding steps, blots were washed three times for 5 minutes with TBS-T. Bound antibody was detected with species specific fluorescent antibodies, incubated with membranes for 1 hour at room temperature (see **table 2.2.10.2** for further details). Protein was visualised using the Li-Cor Odyssey CLx imaging system. Fluorescence from detected protein was estimated with Image Studio software (V5.2; Li-cor; UK). Data was normalised to GAPDH expression and again as a fold change from the mean of control groups. Full representative blots are shown in **Appendix 1**.

**Table 2.2.10.1 Immunoblotting gel formulation**

| **2 x Gels** | **4% v/v acrylamide** | **12% v/v acrylamide** |
|---|---|---|
| **$H_2O$** | 2.8 mL | 3.42 mL |
| **1.5 M Tris (lower buffer)** | | 3.15 mL |
| **0.5 M Tris (upper buffer)** | 1.25 mL | |
| **30% v/v Acrylamide** | 850 µL | 4.48 mL |
| **10% w/v SDS** | 50 µL | 110 µL |
| **20% w/v APS** | 50 µL | 55.4 µL |
| **TEMED** | 5.35 µL | 11 µL |

**Table 2.2.10.2 Antibodies used for immunoblotting**

| Antibody target | Species | Catalogue number | Supplier | Conc. | Vehicle (TBS-T 0.1%) |
|---|---|---|---|---|---|
| TSPO | Rabbit | ab109497 | Abcam | 1:1000 | 2.5% BSA |
| CPT-1A | Rabbit | 15184-1-AP | Protein Tech | 1:1000 | 2.5% Milk |
| GFAP | Mouse | mab360 | Millipore | 1:1000 | 2.5% Milk |
| GLUT1 | Rabbit | 07-1401 | Millipore | 1:1000 | 2.5% BSA |
| Phospho-NF-κB p65 (Ser 536) | Rabbit | 3033 | CST | 1:1000 | 2.5% BSA |
| NF-κB p65 | Rabbit | 8242 | CST | 1:1000 | 2.5% BSA |
| GAPDH | Mouse | 60004-1-IG | Protein Tech | 1:10,000 | 2.5% Milk |
| Mouse (Fluorescent secondary AlexaFluor 680) | Goat | A21057 | Invitrogen | 1:10,000 | 2.5% Milk |
| Rabbit (Fluorescent secondary Dylight 800) | Goat | 611-145-122 | Rockland | 1:10,000 | 2.5% Milk |

### 2.2.11 Cell culture media cytokine concentrations

Cells were plated at a density of 4.5 x $10^5$ cells per 60 mm diameter dish. Media was collected from cells after treatment and cytokine concentrations determined using DuoSet ELISAs (BioTechne; UK) against mouse TNF-α, IL-6 and IL-10 as per the manufacturer's instructions. Media taken from cells was undiluted for IL-6 and IL-10 ELISA and diluted 1:2 for TNF-α ELISA. Cytokine concentrations were normalised to protein concentration, collected and estimated using the Bradford method (BioRad; UK) as described in sections **2.2.8 - 2.2.9**.

### 2.2.12 Metabolic analyses

The metabolic rate of cells was determined by measuring extracellular acidification rate (ECAR) as a measure of glycolysis, and oxygen consumption rate (OCR) as a measure of mitochondrial function using the Seahorse Metabolic Bioanalyser $XF^e96$ (Agilent; UK). The day before treatment cells were plated in 96-well Agilent Seahorse Culture plates (Agilent; UK) at 4 x $10^4$ cells per well in supplemented DMEM (10% v/v FBS, 200 U/mL penicillin-streptomycin, 8 mM L-glutamine and 7.5 mM glucose). After treatment, and 1 hour prior to experimentation, media was replaced with Seahorse XF DMEM medium (pH 7.4; Agilent; UK) supplemented with either L-glutamine (2 mM; Glycolytic Stress Test) or L-glutamine (2 mM); glucose (2.5 mM); and sodium pyruvate (2.5 mM; Mito Stress Test). Cells were incubated for 1 hour at 37 °C in a humidified non-$CO_2$ incubator. Glycolysis and oxidative metabolism were determined using Glycolytic Stress Tests and Mito Stress Tests respectively, as per the manufacturer's instructions (Agilent, UK). Fatty acid oxidative metabolism was measured using

a modified Mito Stress Test following instructions provided by the manufacturer (Agilent, UK). Drugs were diluted in media as appropriate for the assay used.

#### 2.2.12.1 Glycolytic Stress Test

This assay measures the normal glycolytic rate of cells by introducing a surplus of glucose as a substrate. Glycolytic capacity is also measured in this assay by preventing oxidative phosphorylation through inhibiting ATP synthase with oligomycin, and so forcing the cells to use glycolysis as an alternative source of energy production. The difference between these two measures is the glycolytic reserve of the cell. Cells were treated sequentially with glucose (10 mM), oligomycin (1 µM), and 2-DG (50 mM). Glycolytic rate describes the highest ECAR measurement after addition of glucose (**fig. 2.2.12.1**). Glycolytic capacity describes the maximum ECAR measurement after addition of oligomycin (**fig. 2.2.12.1**). Glycolytic reserve was calculated as the difference between glycolytic capacity and glycolytic rate (**fig. 2.2.12.1**).

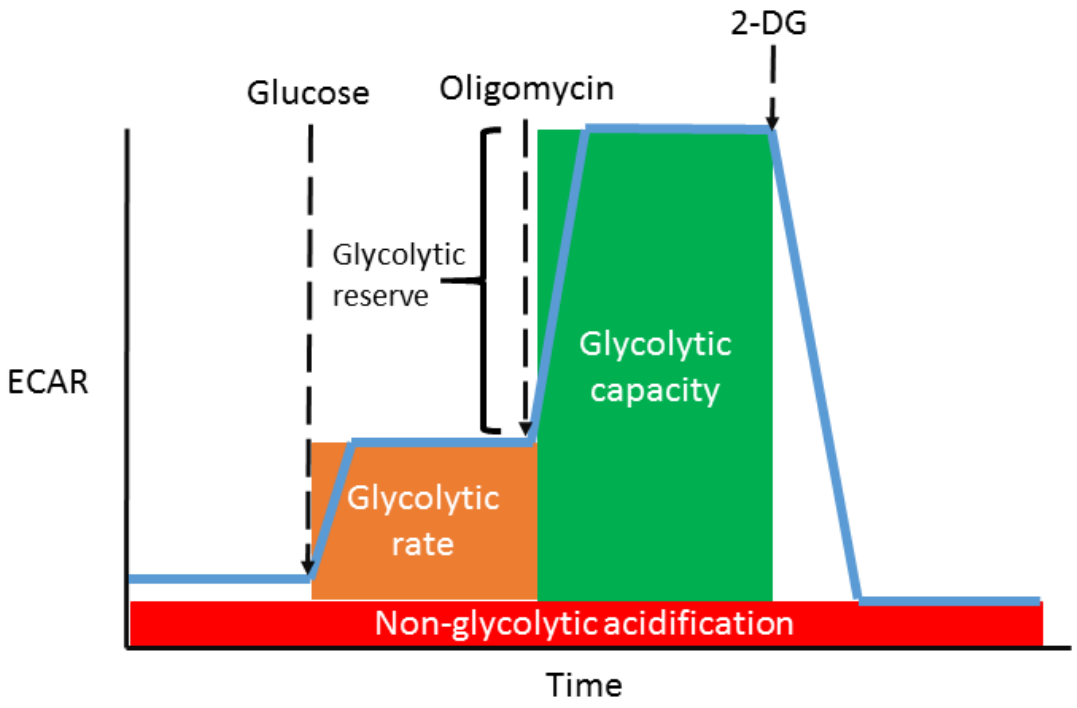


**Figure 2.2.12.1: Schematic of parameters used for metabolic calculations from the Glycolytic Stress Test.** Extracellular acidification rate (ECAR) was the output measure of this assay. Dotted lines indicate points of drug/substrate injection. 2-DG (2-deoxyglucose). Blue line represents example data.

#### 2.2.12.2 Mito Stress Test

This assay measures the capability of cells to use OXPHOS through measuring OCR. Cells were treated sequentially with oligomycin (0.5 µM; Complex V inhibitor), carbonyl cyanide-4 (trifluoromethoxy) phenylhydrazone (FCCP; 1 µM; OXPHOS uncoupler) and rotenone with antimycin A (R/A; 0.5 µM; Complex I and III inhibitors respectively). Basal respiration was calculated as OCR immediately prior to addition of oligomycin minus the lowest measurement after addition of R/A. ATP production was calculated as the difference between basal respiration and the lowest OCR measurement after addition of oligomycin. Proton leak was calculated as the difference between the lowest OCR measurement (after addition of oligomycin) and the lowest OCR measurement after addition of R/A. Maximal respiration was calculated as the maximum OCR measurement after FCCP addition, minus the lowest OCR measurement after R/A addition. Spare capacity was calculated as the difference between basal respiration and maximal respiration. Coupling efficiency was ATP production as a percentage of basal respiration (**fig. 2.2.12.2**).

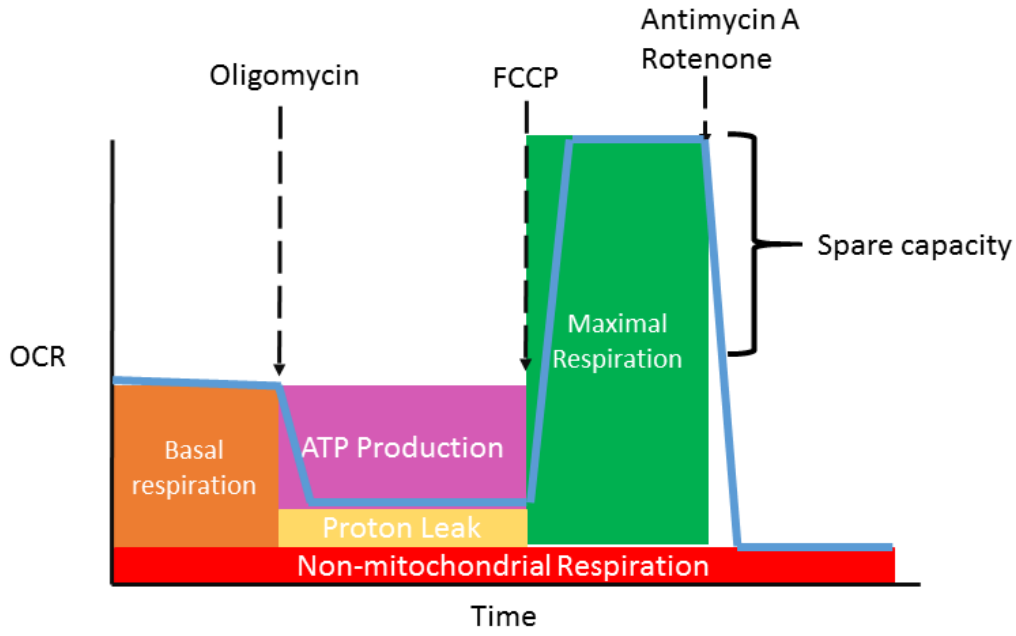


**Figure 2.2.12.2: Schematic of parameters used for metabolic calculations from the Mito Stress Test.** Oxygen consumption rate (OCR) was the output measure of this assay. Dotted lines indicate points of drug injection. Blue line represents example data.

#### 2.2.12.3 Baseline metabolism experiments

On the day of the experiment, treatment media was made up (2.5 mM glucose, 2.5 mM sodium pyruvate, 2 mM L-glutamine, in XF basal media) and pH was adjusted to 7.4 at 37 °C with NaOH and HCl. Cells were washed with 0.01 M PBS and 180 µL treatment media added per well. Cells were 'de-gassed' at 37 °C in a humidified non-$CO_2$ incubator for 1 hour prior to the start of the experiment. A cartridge was loaded with the appropriate amounts of treatment for injection (if used) and loaded for calibration at the start of the 1 hour de-gas. No commercial kits were used in these experiments.

#### 2.2.12.4 Fatty acid oxidation Mito Stress Test

This assay measures the ability of a cell to use fatty acids for respiration. Through depriving the cells of other metabolic substrates overnight and providing the cells with carnitine, the cells can use fatty acid oxidation and are prevented from using glucose and glucose stores to fuel OCR. Further to this, a control group is treated with etomoxir to inhibit transport of acyl-coA into the mitochondria by CPT-1 to give a negative control group. The respiration rate of this control group can be removed from the experimental group to give an OCR which is only driven by fatty acid oxidation (**fig. 2.2.12.4**).

Cells were plated at 4 x $10^4$ cells/well 48 hours prior to experimentation. 24 hours prior to experimentation media was replaced with substrate limited media (11966 DMEM, 0.5 mM glucose, 1 mM glutamate, 0.5 mM carnitine and 1% FBS). 45 minutes prior to experimentation the cell's media was replaced with fatty acid oxidation media (111 mM NaCl, 4.7 mM KCl, 1.25 mM $CaCl_2$, 2 mM $MgSO_4$, 1.2

mM $NaH_2PO_4$, 2.5 mM glucose, 0.5 mM carnitine and 5 mM HEPES; pH adjusted to 7.4 at 37 °C). 15 minutes prior to loading into the machine half of the cells were treated with CPT-1 inhibitor etomoxir (40 µM). Immediately prior to loading the plate into the machine, half of the etomoxir treated cells and half of the control cells were treated with palmitate (200 µM; 0.17 mM BSA). Cells were treated sequentially with oligomycin (0.5 µM), carbonyl cyanide-4 (trifluoromethoxy) phenylhydrazone (FCCP; 1 µM) and rotenone with antimycin A (R/A; 0.5 µM). Basal fatty acid oxidation was calculated as the difference between the [palmitate + etomoxir] group and the [palmitate – etomoxir] group immediately prior to oligomycin injection (**fig. 2.2.12.4**). Maximal fatty acid oxidation was calculated as the difference between the [palmitate + etomoxir] group and the [palmitate – etomoxir] group at the highest OCR rate after FCCP treatment (**fig. 2.2.12.4**).

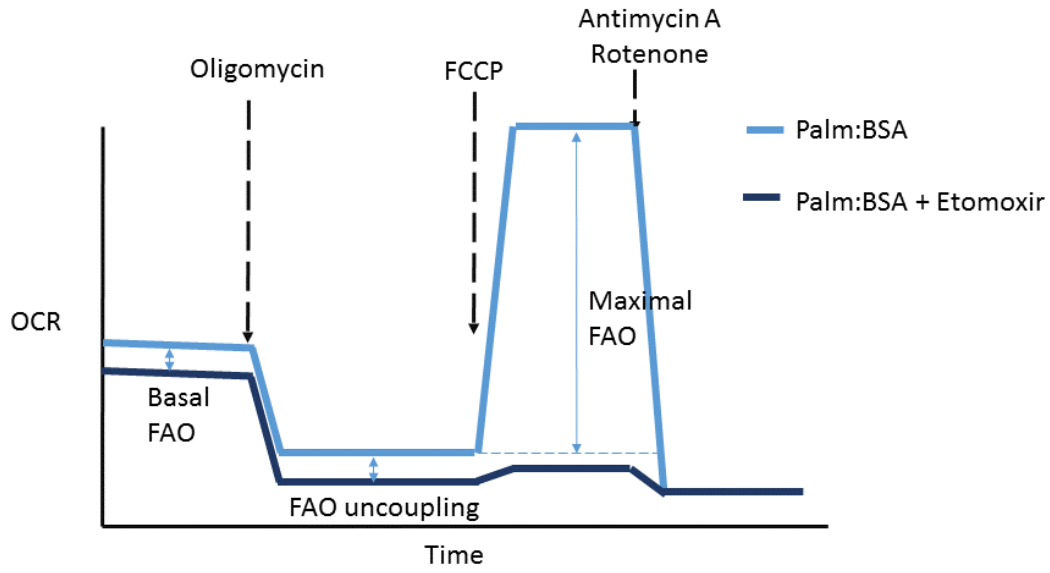


**Figure 2.2.12.4: Schematic of parameters used for metabolic calculations from the Fatty Acid Oxidation Mito Stress Test.** Oxygen consumption rate (OCR) was the output measure of this assay. Dotted lines indicate points of drug injection. Blue lines represent example data. Treatment groups were provided with palmitate conjugated to bovine serum albumin (Palm:BSA) as a substrate prior to the start of the assay.

### 2.2.13 Glucose uptake rate measurement

Cellular glucose uptake was determined using Glucose Uptake-Glo kit (Promega) following the manufacturer's instructions. Briefly, cells were plated at 4 x $10^4$ cells/well in 96-well plates. On the day of the experiment cells were treated as appropriate. After treatment cells were washed with 0.01 M PBS twice and PBS was removed. 10 µM 2-DG in 0.01 M PBS was added with omission of 2-DG used as a negative control. Reaction was stopped with stop buffer and neutralisation buffer prior to addition of detection reagent. Luminescence was measured after 30 minutes incubation in detection reagent using the PHERAstar plate reader (BMG LABTECH; UK). Data are shown as fold change from the mean of contemporaneous control groups.

### 2.2.14 Intracellular ATP measurements

Intracellular ATP concentrations (iATP) were quantified using the ATPLite Two Step kit (PerkinElmer; UK) following the manufacturer's instructions with modifications as previously described (Vlachaki Walker *et al.*, 2017). Briefly, cells were seeded at 4 x $10^3$ cells/well in a black 96-well plate. After treatment, cells were washed with 100 µL PBS. 40 µL DMEM was added to each well and cells were lysed with 40 µL mammalian lysis buffer and agitated at 500 rpm for 5 minutes on the PHERAstar plate reader. 80 µL ATPLite luciferase reagent was added to each well and the plate was dark adapted and agitated at 500 rpm on the PHERAstar for 10 minutes prior to measurement of luminescence. Data are shown as fold change from the mean of contemporaneous control groups.

### 2.2.15 Mitochondrial membrane potential

Mitochondrial membrane potential was determined using tetramethylrhodamine ethyl ester (TMRE) dye uptake. Cells were plated in 6-well plates at 3.5 x $10^5$ cells/well. After treatment (as appropriate), cells were dissociated using 0.05% w/v trypsin-EDTA. Cells were transferred to flow cytometry tubes, and trypsin was neutralised with FACS buffer (2% v/v FBS in 0.01M PBS). Cells were centrifuged at 100 *xg* for 5 minutes at room temperature and the supernatant was aspirated. Treatment for 15 minutes with the positive depolarisation control FCCP (10 µM; 0.04% v/v DMSO vehicle in FACS buffer) at 37 °C prior to TMRE dye uptake was used as an indicator of mitochondrial depolarisation. Cells were resuspended and incubated with TMRE (100 nM) in 0.04% v/v DMSO vehicle and FACS buffer for 30 minutes at 37 °C prior to centrifugation, aspiration of supernatant and resuspension in FACS buffer. Cellular fluorescence was determined using flow cytometry (BD Accuri C6; BD Systems; UK). Data was collected with the 488 nm wavelength laser with the 585/40 nm filter. Increased dye uptake correlates with increased mitochondrial polarisation. Example gating is shown in **Appendix 5**. Cell sized objects were first defined using FSC and SSC, and any events too small to be cells were excluded from further analysis. A second region of interest on a second plot was defined using fluorescence using the 488 nm laser. Cells treated with 0.04% v/v DMSO and no TMRE were used to define unstained cells. Region of interest M2 was determined as fluorescence intensity greater than the fluorescence intensity from the TMRE untreated control group. Mean fluorescence of events counted in M2 (Plot 2) was taken as fluorescence of treatment group. Data are shown as fold change from the contemporaneous mean of vehicle treated control groups.

## 2.2.16 Immunoprecipitation

Cells were seeded at 3 x $10^6$ cells/dish in 150 mm dishes and cultured for 24 hours prior to collection. Media was aspirated and cells washed with PBS. Cells were lysed with 500 µL ice cold immunoprecipitation lysis buffer (**table 2.2.16.1**) and homogenised using a Dounce glass homogeniser (30 turns). Supernatant was centrifuged at 1,000 *xg* for 10 minutes at 4 °C. Supernatant was kept, and the protein content quantified using the Bradford method according to the manufacturer's instructions (BioRad, UK) as described in **section 2.2.9**.

Protein G dynabeads (Invitrogen, UK) were washed with 0.02% v/v PBS-Tween and incubated with 200 µL primary antibody (at the appropriate concentrations; **table 2.2.16.2**) in 0.02% v/v Tween-20 (0.02% PBS-T: 0.01 M PBS) for 1 hour at room temperature on a rotary mixer. Supernatant was discarded and the dynabeads were washed 3 times with 0.02% PBS-T and transferred to a new tube. Dynabeads were incubated with 400 µg protein diluted in 0.01% v/v n-dodecyl-beta-maltoside (0.01% PBS-DBM: 0.01 M PBS) for 2 hours at 4 °C on a rotary mixer. Supernatant was removed to a fresh tube and 50 µL sample buffer (125 mM Tris/HCl [pH 6.8], 4% w/v sodium dodecyl sulphate, 20% v/v glycerol, bromophenol blue) added to the supernatant and incubated at 70 ºC for 5 minutes. Dynabeads were washed 3 times with 0.01% PBS-DBM and transferred to a fresh tube. Bound protein was eluted from the dynabeads by incubation at 70 °C for 5 minutes in 50 µL sample buffer (125 mM Tris/HCl [pH 6.8], 4% w/v sodium dodecyl sulphate, 20% v/v glycerol, bromophenol blue). Proteins in the samples were then identified using the immunoblotting method (described in **section 2.2.10**) to probe for presence of proteins of interest.

**Table 2.2.16.1 Immunoprecipitation lysis buffer**

| Compound | Concentration (mM) |
|---|---|
| Sucrose | 320 |
| EGTA | 1 |
| Tris-HCl (pH 7.8) | 10 |
| B-mercaptoethanol | 0.1% |
| Sodium orthovanadate | 1 |
| Benzamidine | 1 |
| Phenylmethylsulfonyl fluoride | 0.1 |

**Table 2.2.16.2 Antibodies used for immunoprecipitation**

| **Antibody target** | **Species** | **Catalogue number** | **Supplier** | **Conc.** |
|---|---|---|---|---|
| TSPO | Goat | NB100-41398 | Novus | 1:200 (2 µg/mL) |
| CPT-1A | Mouse | 66039-1-Ig | ProteinTech | 1:500 (4 µg/mL) |
| N/A | Goat (IgG) | I-5000 | Vector | 2 µg/mL |
| N/A | Mouse (IgG2A) | X0943 | Dako | 4 µg/mL |

## 2.3 Data presentation and statistics

Data were processed using Microsoft Excel 2013. GraphPad Prism 8 was used to present data and for statistical analyses. For comparisons between two groups, unpaired t-tests were used. For multiple comparisons, one-way ANOVA with post hoc Tukey's tests were used. For multiple comparisons between two independent variables, two-way ANOVA with post hoc Sidak's tests were used. A minimum of 3 independent replicates were used for each study. For studies using the Seahorse Metabolic Analyser 2-3 independent plates were used, and individual wells were used as separate experiments. Data are presented as mean ± standard error of the mean (SEM). Statistical significance was taken as $p<0.05$.

# Chapter 3. Metabolic changes due to inflammation are essential for cytokine release in mouse primary astrocytes

A modified version of this chapter is published as part of:

**The metabolic response to inflammation in astrocytes is regulated by nuclear factor-kappa B signalling.**

*Josephine L. Robb, Nadia A. Hammad, Paul G. Weightman Potter, John K. Chilton, Craig Beall, Kate L.J. Ellacott.* **Glia.** DOI:10.1002/glia.23835.

## 3.1 Introduction

In many immunocompetent cell types, including macrophages, dendritic cells and T-cells, it has been shown that during a pro-inflammatory response activity of the main metabolic pathways are altered, including glycolysis and oxidative phosphorylation (Dumitru *et al.*, 2018; O'Neill *et al.*, 2016; Thapa & Lee, 2019; Viola *et al.*, 2019). These metabolic changes are intrinsic to the inflammatory response and have been defined as 'immunometabolism' (Jung *et al.*, 2019; Loftus & Finlay, 2016). Immunometabolic changes can vary greatly in magnitude and timescale depending on cell type. Although immunometabolic changes have been explored in depth in peripheral immune cells, there is comparatively little data available investigating an intrinsic link between metabolism and inflammation in astrocytes.

In most cell types the initial response to pro-inflammatory stimulation requires an increase in glycolytic rate (Loftus & Finlay, 2016; O'Neill *et al.*, 2016; Wang *et al.*, 2017). There is some data available suggesting that this is also the case in astrocytes. For example, in aging mice, increased nuclear NF-κB activity in astrocytes correlates with elevated aerobic metabolism (Jiang & Cadenas, 2014). Furthermore, *in vitro* studies in mouse primary astrocytes demonstrate that treatment with pro-inflammatory cytokines increases their glucose uptake, reduces intracellular glycogen stores, and increases flux through the tricarboxylic acid (TCA) cycle and pentose phosphate pathway (Bélanger *et al.*, 2011b; Gavillet *et al.*, 2008). Exposure to nitric oxide, which can be an inflammatory factor in high concentrations (Sharma *et al.*, 2007), also enhances the activity of hypoxia inducible factor 1α (HIF1α) and the cellular energy sensor AMP-activated protein kinase (AMPK) (Almeida *et al.*, 2004; Brix *et al.*, 2012). These signalling pathways regulate glycolysis in astrocytes. This suggests that astrocytes rely on glucose metabolism during inflammation. In a related study, Meares *et al.* showed that decreasing substrate availability to astrocytes *in vitro,* by limiting glucose and pyruvate, reduces interferon-gamma (IFN-γ) induced inflammatory responses (Meares *et al.*, 2013). The anti-inflammatory effect of reduced glucose and/or pyruvate availability was replicated by pharmacological activation of AMPK (Meares *et al.*, 2013). Together these data suggest that there is a glycolytic component to the response to pro-inflammatory stimulation in astrocytes. However, the link between glycolysis and inflammation has not been directly studied.

In cells such as pro-inflammatory macrophages and dendritic cells the increase in glycolysis is coupled with a decrease in OXPHOS and changes in enzyme activity in the TCA cycle, leading to accumulation of TCA intermediates such as citrate and succinate (Kelly & O'Neill, 2015; Krawczyk *et al.*, 2010). Intermediates generated by the TCA cycle are scavenged and used to synthesise new proteins and fats required for growth and inflammatory molecule production. In addition, accumulation of succinate drives the pro-inflammatory phenotype through inhibition of anti-inflammatory immunomodulators (Mills *et al.*, 2016). The concomitant decrease in OXPHOS activity is essential for macrophages to enter a pro-inflammatory state as OXPHOS suppresses inflammation in macrophages through preventing modification of the electron transport chain for reactive oxygen species generation (Maranzana *et al.*, 2013; Sag *et al.*, 2008; Vats *et al.*, 2006). However, OXPHOS is not suppressed during inflammation in all immunomodulatory cell types. In T cells and alternatively activated macrophages OXPHOS is maintained during inflammation whereas in memory T cells OXPHOS is increased during an infection, promoting long term survival (Sena *et al.*, 2013; van der Windt *et al.*, 2012; Wang *et al.*, 2011). The relative dependence on OXPHOS and the TCA cycle during inflammation is clearly different in different cell types. However, the role of mitochondrial energy production in astrocytes during inflammation has not been extensively explored.

*In vivo*, astrocytes are highly glycolytic compared to neurons (Fernández-Moncada *et al.*, 2018; Pellerin & Magistretti, 1994; Vardjan *et al.*, 2018; Yellen, 2018). This increases lactate production by astrocytes, which can be used as a fuel by neurons and also reduces oxygen consumption by astrocytes. Whilst OXPHOS in astrocytes does not appear to be essential for astrocyte survival,

disruption reduces neuronal viability and astrocyte proliferation after traumatic brain injury (Fiebig *et al.*, 2019; Supplie *et al.*, 2017). Indeed, loss of mitochondria in astrocytes through prevention of mitochondrial DNA replication leads to neuronal death and spongiotic encephalopathy (Ignatenko *et al.*, 2018). This suggests that mitochondrial metabolism/OXPHOS capability in astrocytes is essential for maintenance of the extracellular environment during times of stress. Supporting this, disruption of OXPHOS in astrocytes increases reactive gliosis in mice (Fiebig *et al.*, 2019). This demonstrates that OXPHOS may play a role in resolving inflammation in astrocytes. In many cell types OXPHOS can be regulated through changes to mitochondrial networks, known as mitochondrial dynamics (Wai & Langer, 2016). OXPHOS is increased by mitochondrial fusion, and limited by mitochondrial fission. Motori *et al.* have demonstrated that mitochondrial networks become more fragmented in astrocytes during inflammation resulting from trauma (Motori *et al.*, 2013). This suggests that OXPHOS is reduced in astrocytes during inflammation.

Together these published data may suggest that, in common with other immune competent cells, astrocytes increase glycolysis and reduce OXPHOS during pro-inflammatory stimulation. In many cell types it has been shown that preventing glycolysis reduces the ability of the cell to become inflamed (Abboud *et al.*, 2018; Lee *et al.*, 2019). This has led to the repurposing of some metabolic drugs as therapies for disease, including cancers (Singer *et al.*, 2018), Alzheimer's disease (Campbell *et al.*, 2018; Koenig *et al.*, 2017), and autoimmune diseases such as multiple sclerosis and lupus (Norata *et al.*, 2015). If astrocytes have immunometobolic responses this may open opportunities for new therapies for neuroinflammatory conditions.

## 3.2 Hypothesis

In this chapter I tested the overarching hypothesis that metabolic changes during inflammation are essential for cytokine release in astrocytes. I further hypothesised that glycolytic rate will be increased but OXPHOS will be reduced during pro-inflammatory stimulation.

## 3.3 Results

### 3.3.1 Lipopolysaccharide (LPS) stimulated NF-κB signalling in mouse primary astrocytes

LPS was used as a pro-inflammatory stimulus in this model. This molecule activates toll like receptor 4 (TLR4) signalling, activating signalling pathways which include NF-κB signalling, an important pro-inflammatory transcription factor. To confirm LPS-induced NF-κB signalling in mouse primary astrocytes, cells were treated with LPS for 3 hours or 24 hours. NF-κB (p65) phosphorylation (Ser536) and total NF-κB expression were quantified using immunoblotting. Phosphorylation of Ser536 was used as a measure of NF-κB activity, as phosphorylation at this site has been demonstrated to be essential for canonical NF-κB signalling and nuclear translocation both *in vitro* and *in vivo* (Hu *et al.,* 2004; Jiang *et al.,* 2003; Sakuri *et al.,* 1999). NF-κB phosphorylation was increased 3 hours and 24 hours after LPS treatment compared to untreated controls (83% and 87.6% respectively, $p<0.0001$ at both time points (**fig. 3.3.1.1A-B**). Total expression of NF-κB was not altered by LPS treatment after 3 hours or 24 hours (**fig. 3.3.1.2A-B)**.

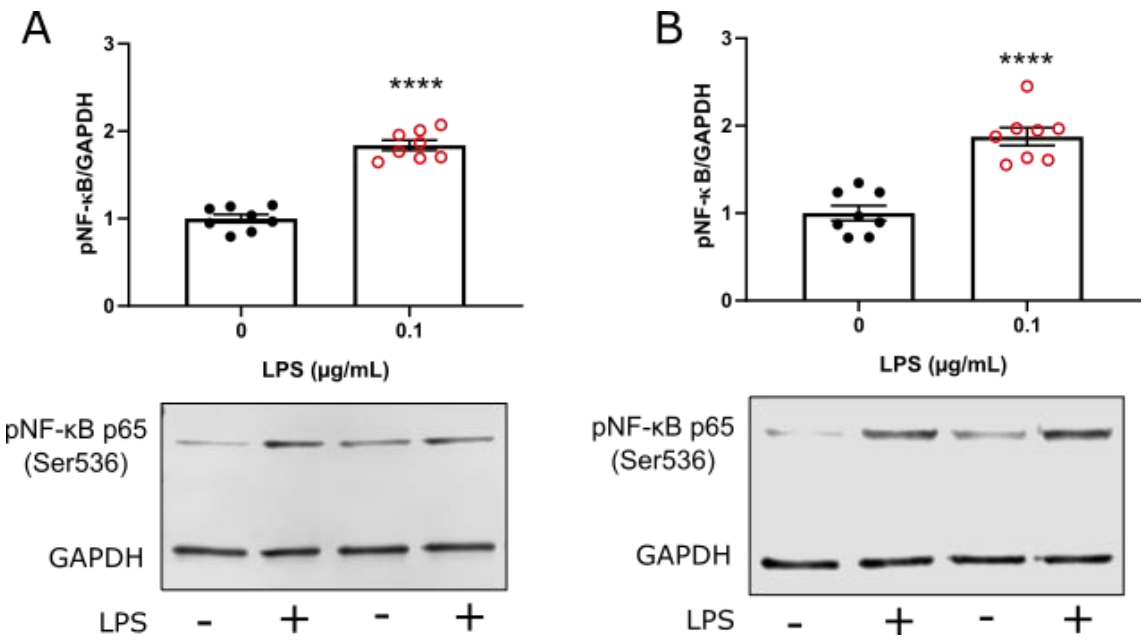


**Figure 3.3.1.1: LPS increased phosphorylation of p65 NF-κB.** Mouse primary astrocytes were seeded at a density of 4.5 x $10^5$ cells per dish in 60 mm dishes prior to treatment with lipopolysaccharide (LPS; 0.1 μg/mL) or vehicle. Cells were lysed and protein collected for immunoblotting. **A-B.** Anti-phospho-NF-κB p65 (Ser536) immunoblot after 3 hours (**A**) or 24 hours (**B**) treatment with anti-GAPDH loading control. **Top:** Densitometric analysis of anti-phospho-NF-κB p65 (Ser536) fluorescence normalised to anti-GAPDH fluorescence and represented as fold change in fluorescence from the mean of vehicle treated controls (n=8). Unpaired t-test, **** $p<0.0001$. Data are presented as mean ± standard error of mean. **Bottom:** Representative immunoblot of phospho-NF-κB p65 (Ser536) with GAPDH loading control.

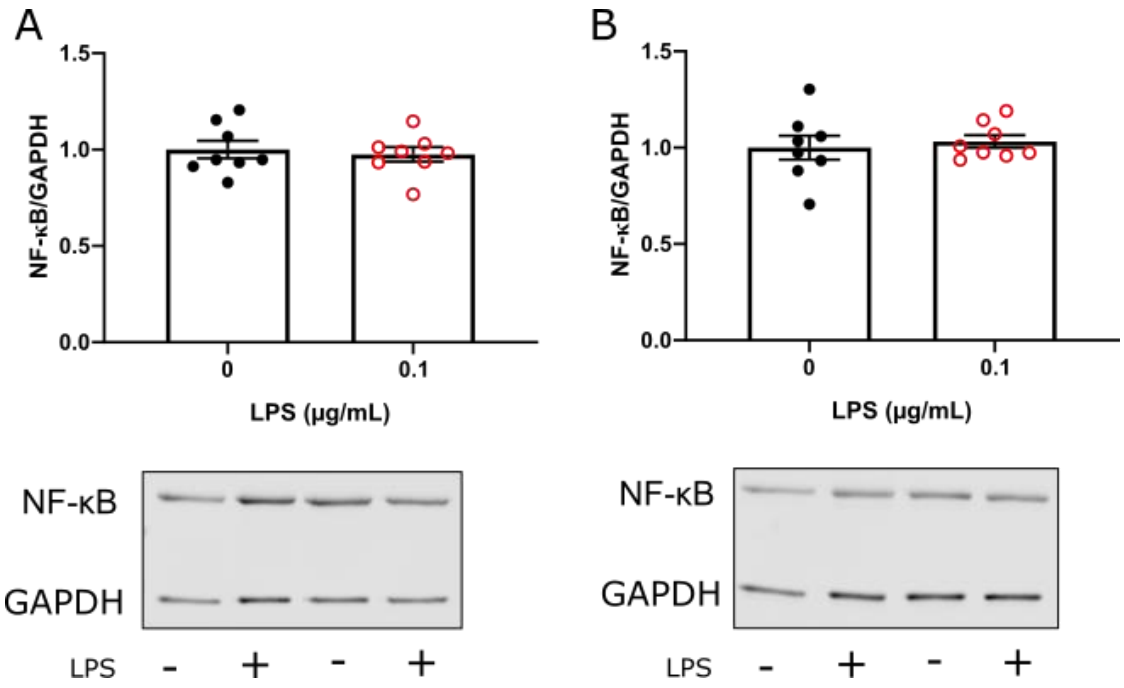


**Figure 3.3.1.2: LPS did not regulate total expression of NF-κB.** Mouse primary astrocytes were seeded at a density of 4.5 x $10^5$ cells per dish in 60 mm dishes prior to treatment with lipopolysaccharide (LPS; 0.1 µg/mL) or vehicle. Cells were lysed and protein collected for immunoblotting. **A-B.** Anti-NF-κB p65 immunoblot after 3 hours (**A**) or 24 hours (**B**) treatment with anti-GAPDH loading control. **Top:** Densitometric analysis of anti-NF-κB p65 fluorescence normalised to anti-GAPDH fluorescence and represented as fold change in fluorescence from the mean of vehicle treated controls (n=8). Unpaired t-test. Data are presented as mean ± standard error of mean. **Bottom:** Representative immunoblot of NF-κB p65 with GAPDH loading control.

### 3.3.2 LPS increased cytokine secretion from mouse primary astrocytes

TNF-α release was increased in comparison to vehicle-treated controls (0.017 mM BSA) after 3 hours treatment with LPS (**fig. 3.3.2A**; $p<0.0001$). Neither IL-6 (**fig. 3.3.2C**) nor IL-10 (**fig. 3.3.2E**) release were increased after 3 hours treatment with LPS. After 24 hours of LPS treatment release of TNF-α, IL-6 and IL-10 ($p<0.01$) were all increased compared to vehicle-treated controls (**fig. 3.3.2B, D & F;** $p<0.0001$, $p=0.0002$, and $p=0.0028$ respectively).

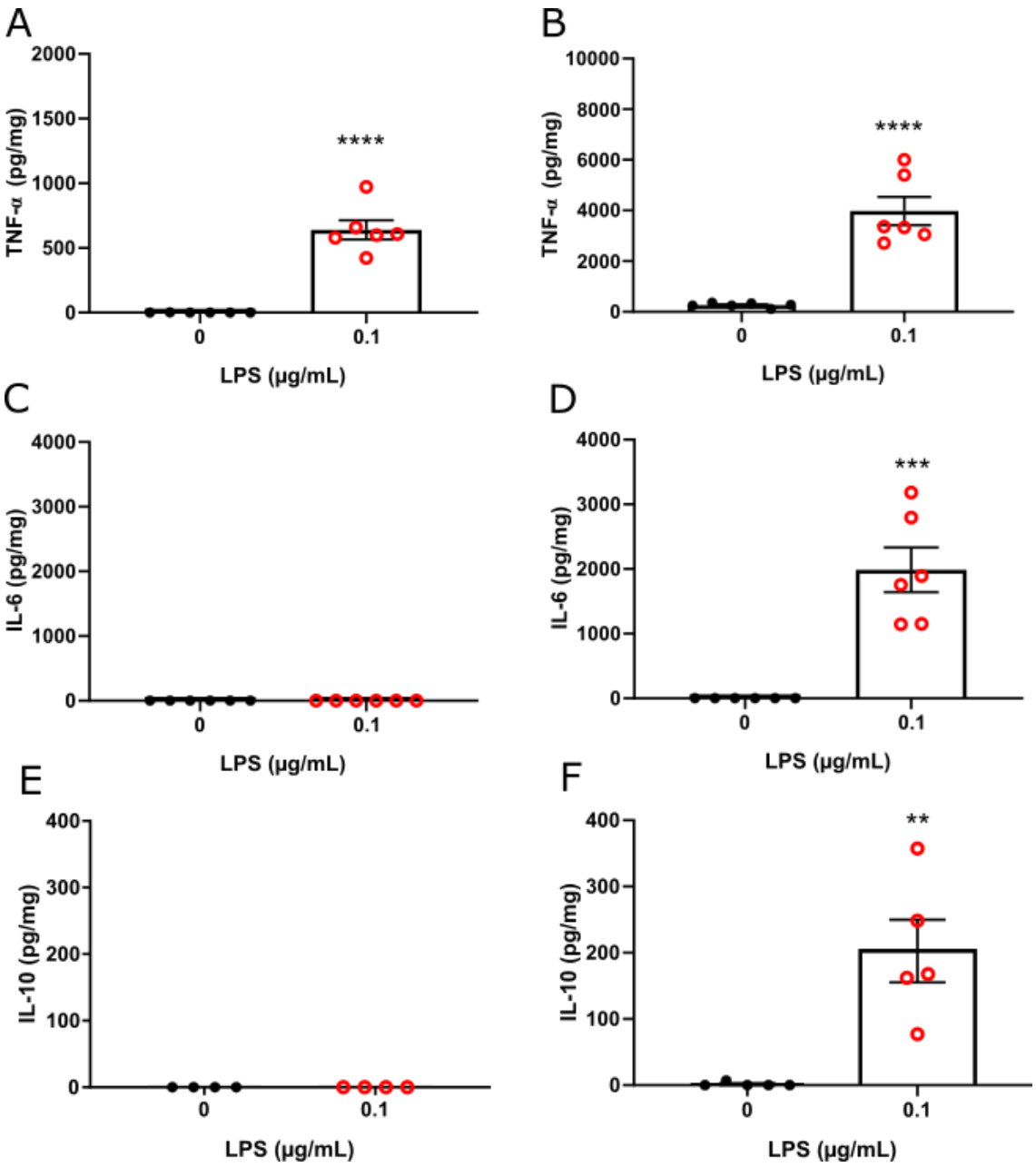
A
TNF-α (pg/mg)
2000
1500
1000
500
0
****
0
0.1
LPS (µg/mL)
B
TNF-α (pg/mg)
10000
8000
6000
4000
2000
0
****
0
0.1
LPS (µg/mL)
C
IL-6 (pg/mg)
4000
3000
2000
1000
0
0
0.1
LPS (µg/mL)
D
IL-6 (pg/mg)
4000
3000
2000
1000
0
***
0
0.1
LPS (µg/mL)
E
IL-10 (pg/mg)
400
300
200
100
0
0
0.1
LPS (µg/mL)
F
IL-10 (pg/mg)
400
300
200
100
0
**
0
0.1
LPS (µg/mL)

**Figure 3.3.2: LPS increased cytokine release from mouse primary astrocytes.** Mouse primary astrocytes were seeded at a density of 4.5 x $10^5$ cells per dish in 60 mm dishes prior to treatment with lipopolysaccharide (LPS; 0.1 µg/mL) or vehicle. Conditioned media was collected and used for estimation of extracellular cytokine concentrations using DuoSet ELISAs (BioTechne, UK). **A-B.** Extracellular TNF-α concentration 3 hours **(A)** or 24 hours **(B)** after LPS treatment (n=6). **C-D.** Extracellular IL-6 concentration 3 hours **(C)** or 24 hours **(D)** after LPS treatment (n=6). **E-F.** Extracellular IL-10 concentration 3 hours **(E;** n=4**)** or 24 hours **(F;** n=5**)** after LPS treatment. Unpaired t-test, ** p<0.01, *** p<0.001, **** p<0.0001. Data are expressed as mean ± standard error of the mean.

### 3.3.3 Lipopolysaccharide did not decrease viability of mouse primary astrocytes

To ensure that cell viability was not decreased by the concentration of LPS used in this study, cell viability was measured using propridium iodide exclusion. Cell viability was not affected by treatment with LPS after 24 hours, with >90% cell viability, in both LPS and vehicle-treated control groups (**fig 3.3.3**).

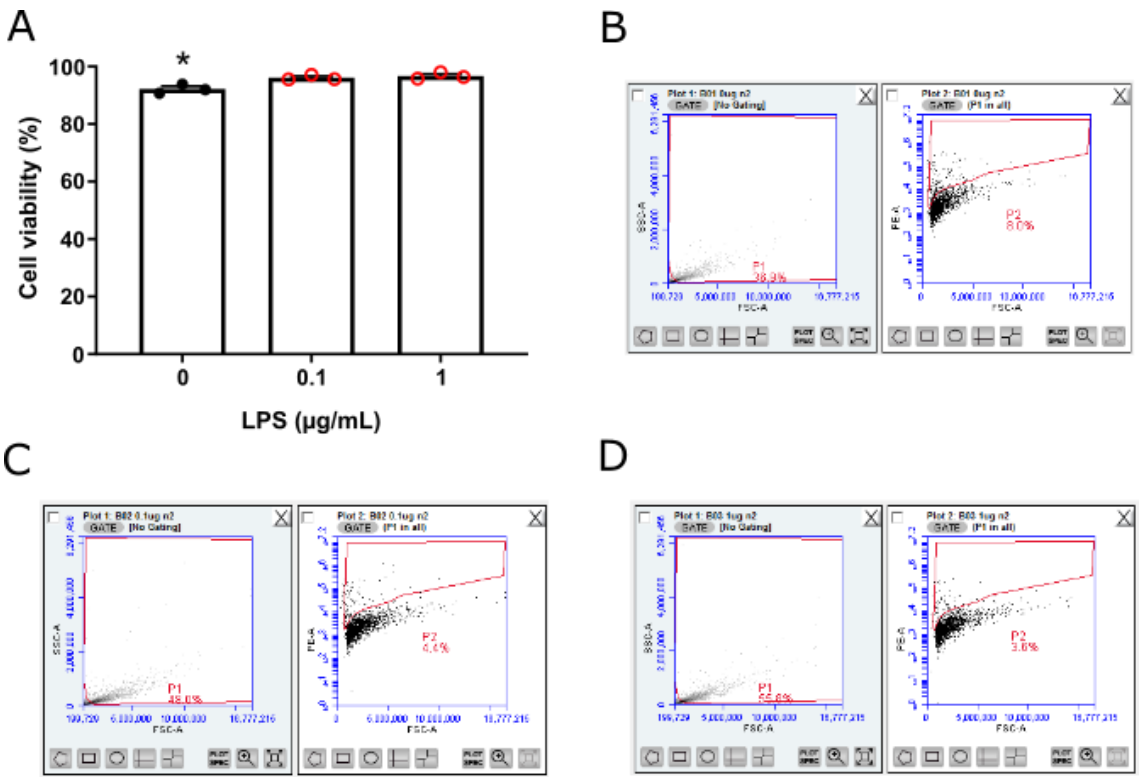


**Figure 3.3.3: LPS did not affect cell viability of mouse primary astrocytes.** Propidium iodide staining and flow cytometry of cells 24 hours after treatment with lipopolysaccharide (LPS). Cells were seeded at a density of 3.5 x $10^5$ cells per well in a 6 well plate. After treatment with LPS, cells were trypsinised and stained with 2 µg/mL propidium iodide prior to analysis with the BD Accuri C6 Plus flow cytometer**. A**. Percentage cell viability. One-way ANOVA with post hoc Tukey; * $p<0.05$; n=3. Data are presented as mean ± standard error of the mean. **B-D.** Gating used to define events. Plot 2 region of interest and P1 defined non-viable cells. Example data from 0 µg/mL **(B)**, 0.1 µg/mL **(C)**, and 1 µg/mL **(D)** LPS treated cells.

### 3.3.4 LPS induced an acute increase in glycolytic rate in mouse primary astrocytes

The acute metabolic consequences of LPS stimulation of mouse primary astrocytes were measured using the Seahorse Bioanalyzer XF$^{e}$96. Following a baseline period, the cells were treated with LPS or vehicle (0.017 mM BSA). Oxygen consumption rate (OCR) (**fig. 3.3.4.1A-B**) and extracellular acidification rate (ECAR) (**fig. 3.3.4.1C-D**) were measured for 1 hour every 6 minutes. No change in OCR was observed after treatment with LPS compared to vehicle, indicating that oxidative phosphorylation (OXPHOS) was not altered after LPS treatment (**fig. 3.3.4.1A-B**). However, there was a 20% increase in ECAR indicating an increase in glycolytic rate (**fig. 3.3.4.1C-D**, $p<0.0001$). There was a 25% increase in glucose uptake rate after 15 minutes treatment with LPS in comparison to vehicle treated controls, however this did not reach statistical significance (**fig. 3.3.4.2;** $p=0.24$).

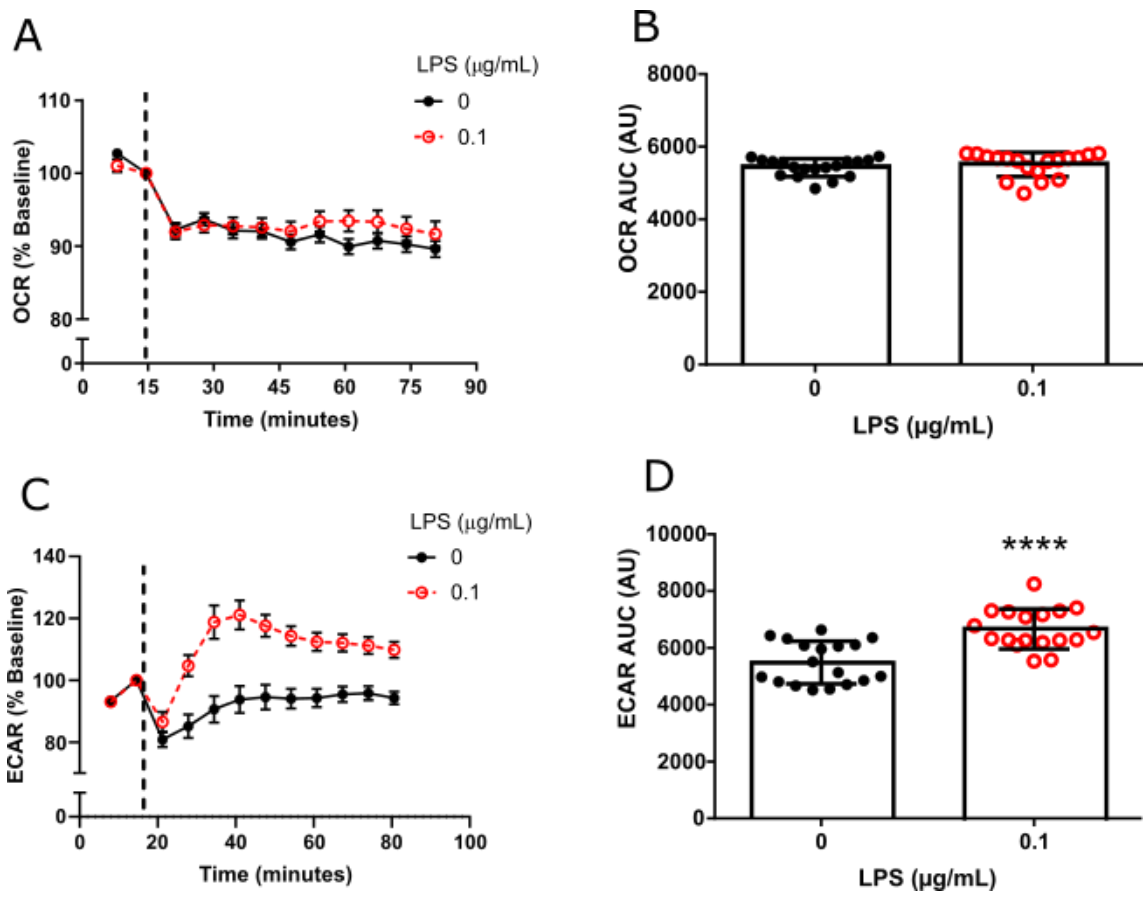


**Figure 3.3.4.1: LPS increased glycolysis in mouse primary astrocytes.** Cells were seeded at a density of 4 x $10^4$ cells per well in Seahorse XF96 cell culture microplates. Oxidative phosphorylation rate, represented as oxygen consumption rate (OCR) and glycolysis represented as extracellular acidification rate (ECAR) of the cells were measured using the Seahorse BioAnalyzer XFe96. **A**. OCR over time of cortical primary mouse astrocytes (CRTAS). Treatment point indicated by dotted line. Lipopolysaccharide (LPS; 0.1 µg/mL) treatment compared with vehicle treated control (0.017 mM fatty acid free bovine serum albumin). **B.** Area under the curve (AUC) of OCR after treatment with LPS. **C.** ECAR over time of CRTAS after treatment with LPS. **D.** AUC of ECAR after treatment with LPS. Unpaired t-test, **** $p<0.0001$; n=18, from two independent plates. Data are expressed as mean ± standard error of the mean.

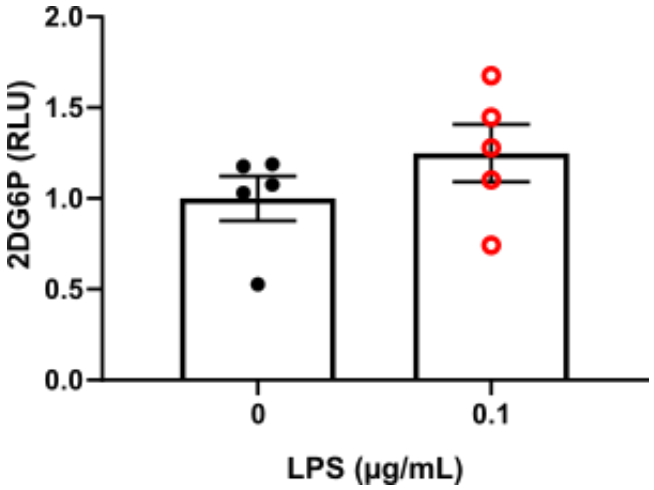


**Figure 3.3.4.2: Glucose uptake rate was not significantly altered within 15 minutes LPS treatment.** Mouse primary astrocytes were seeded at a density of 4 x $10^4$ cells per well in 96 well plates. Glucose uptake rate after treatment with lipopolysaccharide (LPS) was estimated using the Glucose Uptake-Glo kit (Promega, UK). Glucose uptake was represented as fold change in 2-deoxyglucose-6-phosphate (2DG6P) luminescence compared to the mean of vehicle treated controls after 15 minutes treatment with LPS. Unpaired t-test, $p>0.05$; n=5. Data are expressed as mean ± standard error of the mean.

### 3.3.5 Changes to glycolytic metabolism were maintained 3 hours after treatment with LPS in mouse primary astrocytes

To further interrogate the changes in cellular metabolism related to inflammation, mouse primary astrocytes were treated with LPS for 3 hours and subjected to a Glycolytic Stress Test to assess glycolytic rate, capacity and reserve. After 3 hours treatment with LPS, glycolytic rate and capacity were both significantly increased by 26% (p=0.0138) and 20% (p=0.025) respectively (**fig. 3.3.5.1A-C**). However, glucose uptake rate was not significantly increased in cells treated with LPS for 3 hours compared to vehicle-treated controls (**fig. 3.3.5.2;** p=0.46). The glycolytic reserve was unchanged between LPS treated astrocytes and vehicle treated controls (**fig. 3.3.5.1D**).

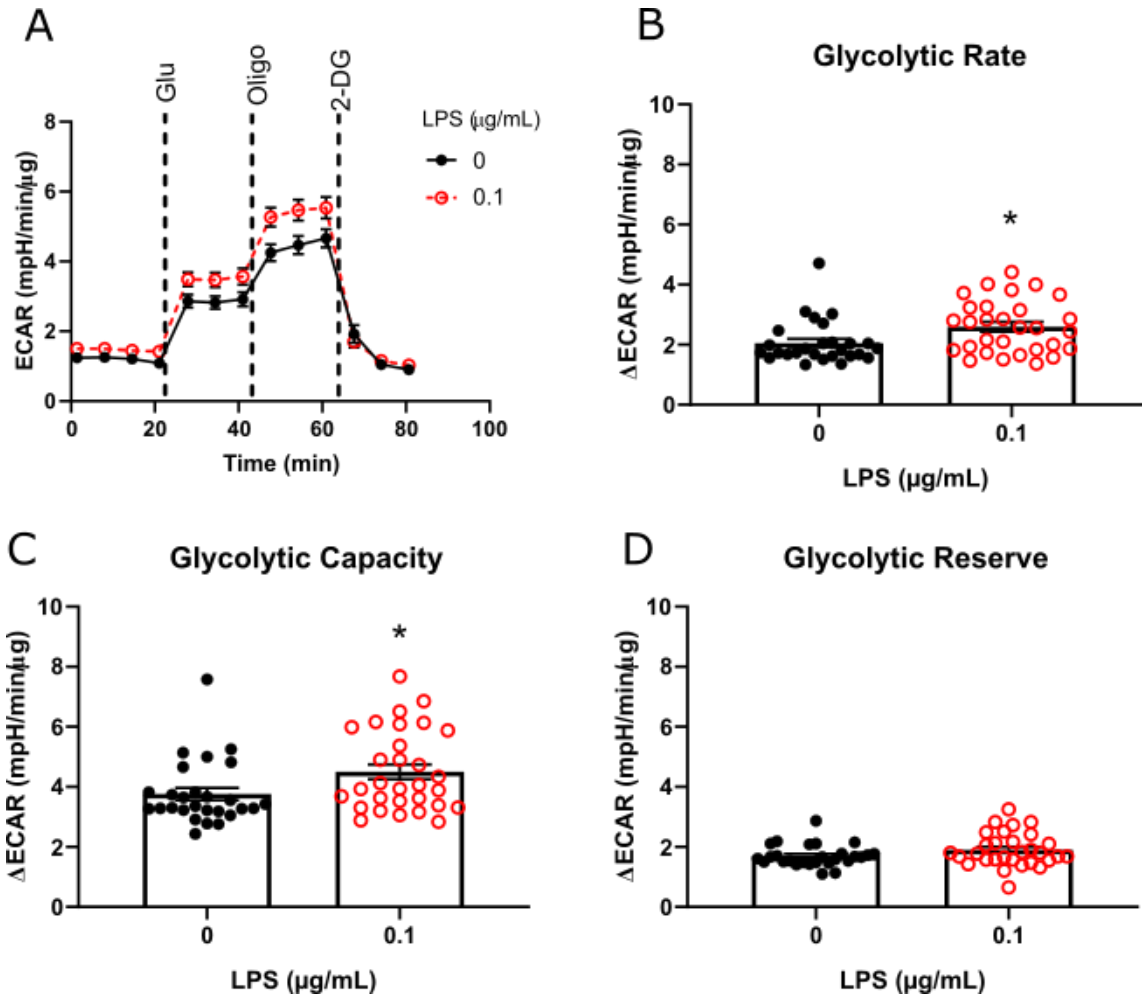
A
Glu
Oligo
2-DG
LPS (µg/mL)
0
0.1
ECAR (mpH/min/µg)
Time (min)
B
Glycolytic Rate
ΔECAR (mpH/min/µg)
LPS (µg/mL)
C
Glycolytic Capacity
ΔECAR (mpH/min/µg)
LPS (µg/mL)
D
Glycolytic Reserve
ΔECAR (mpH/min/µg)
LPS (µg/mL)

**Figure 3.3.5.1: 3 hours LPS treatment increased glycolysis in mouse primary astrocytes.** Cells were seeded at a density of 4 x $10^4$ cells per well in Seahorse XF96 cell culture microplates. Glycolysis, represented as extracellular acidification rate (ECAR) of the cells was measured using the Seahorse BioAnalyzer XFe96 in conjunction with a Glycolytic Stress Test (Agilent, UK). **A.** ECAR of mouse primary cortical astrocytes during a Glycolytic Stress Test 3 hours after treatment with LPS compared with vehicle treated control (0.017 mM fatty acid free bovine serum albumin; Glu = 10 mM glucose; Oligo = 1 µM oligomycin; 2-DG = 50 mM 2-deoxyglucose). **B.** Glycolytic rate: change in ECAR after treatment with glucose. **C.** Glycolytic capacity: change in ECAR after treatment with oligomycin. **D.** Glycolytic reserve: difference between glycolytic rate and glycolytic capacity. Unpaired t-test, * $p<0.05$; n=30, 2 independent plates. Data are expressed as mean ± standard error of the mean.

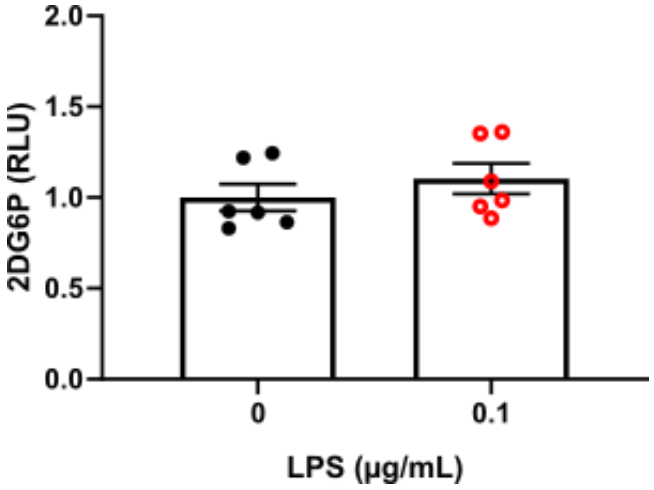


**Figure 3.3.5.2: Glucose uptake rate in mouse primary astrocytes was not altered by 3 hours LPS treatment.** Mouse primary astrocytes were seeded at a density of 4 x $10^4$ cells per well in 96 well plates. Glucose uptake rate after treatment with lipopolysaccharide (LPS) was estimated using the Glucose Uptake-Glo kit (Promega, UK). Glucose uptake was represented as fold change in 2-deoxyglucose-6-phosphate (2DG6P) luminescence from the mean of vehicle treated controls after 3 hours treatment with lipopolysaccharide (LPS). Unpaired t-test, $p>0.05$; n=6. Data are expressed as mean ± standard error of the mean.

### 3.3.6 Mitochondrial metabolism was not altered after 3 hours treatment with LPS

Mouse primary astrocytes were exposed to LPS for 3 hours and studied using a Mito Stress Test, to assess OXPHOS (**fig. 3.3.6A**). There was no change in basal or maximal OXPHOS compared to vehicle treated controls (**fig. 3.3.6B-C**). This resulted in no change in spare mitochondrial capacity (**fig. 3.3.6D**). In addition to mitochondrial function being unchanged, 3 hours LPS treatment did not change mitochondrial efficiency, with no change in proton leak or oxygen associated ATP production (**fig. 3.3.6E-G**).

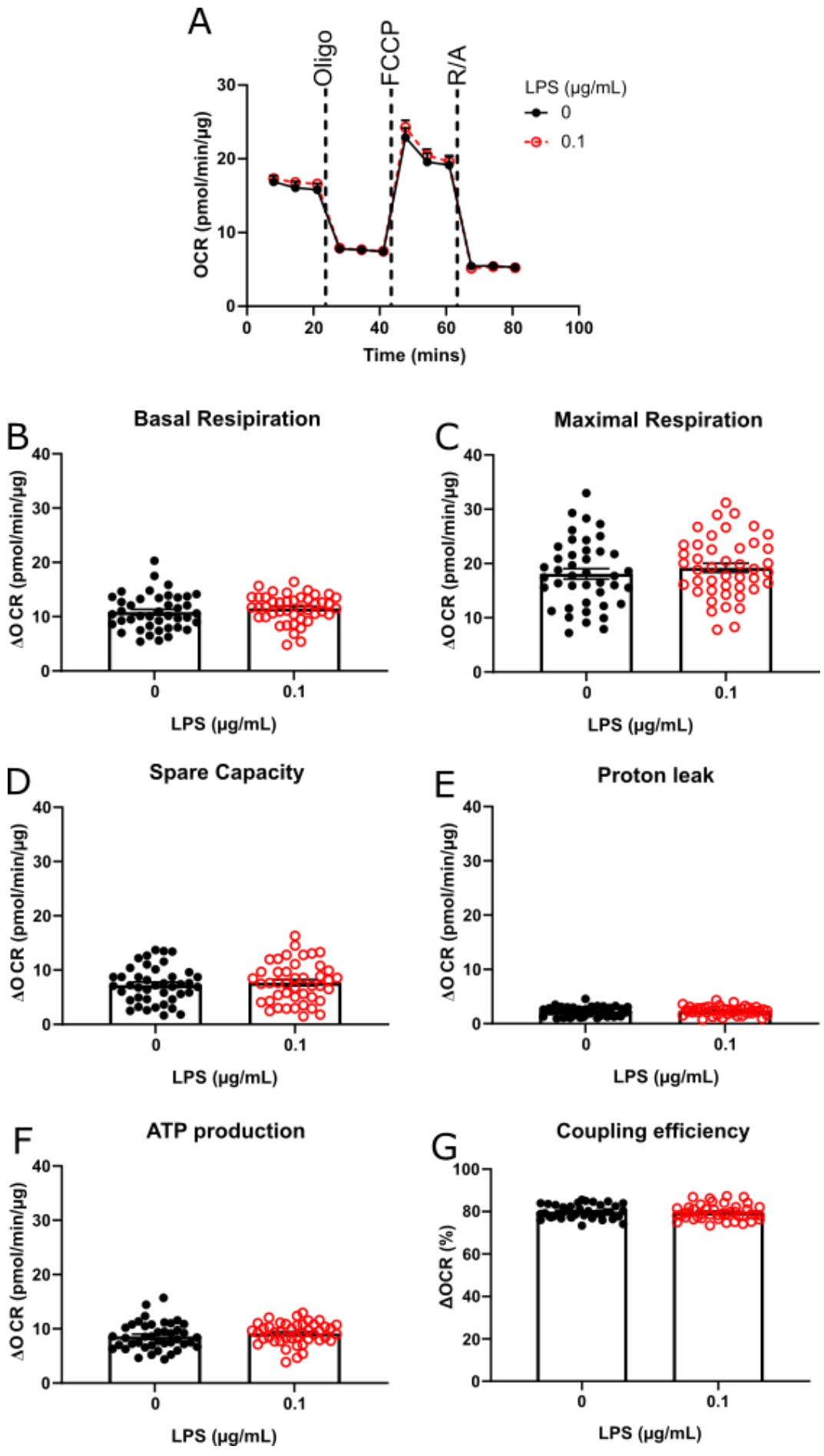
A
Oligo
FCCP
R/A
LPS (µg/mL)
0
0.1
OCR (pmol/min/µg)
Time (mins)
B
Basal Resipiration
C
Maximal Respiration
D
Spare Capacity
E
Proton leak
F
ATP production
G
Coupling efficiency
ΔO CR (pmol/min/µg)
ΔOCR (%)
LPS (µg/mL)

**Figure 3.3.6: Mitochondrial metabolism was not altered by 3 hours of LPS treatment.** Cells were seeded at a density of 4 x $10^4$ cells per well in Seahorse XF96 cell culture microplates. Oxidative phosphorylation, represented as oxygen consumption rate (OCR) of the cells was measured using the Seahorse BioAnalyzer XFe96 in conjunction with a Mito Stress Test (Agilent, UK). **A.** OCR of mouse primary cortical astrocytes during a Mito Stress Test 3 hours after treatment with lipopolysaccharide (LPS; 0.1 µg/mL) compared with vehicle treated control (0.017 mM fatty acid free bovine serum albumin). Oligo = 0.5 µM oligomycin; FCCP = 1 µM; R/A = 0.5 µM rotenone/antimycin. **B.** Basal Respiration: difference in OCR prior to oligomycin injection and after rotenone/antimycin injection. **C**. Maximal respiration: difference in OCR after injection of FCCP and after rotenone/antimycin injection. **D.** Spare capacity: difference in OCR between basal respiration (**B**) and maximal respiration (**C**). **E.** Proton leak: difference in OCR after oligomycin injection and after rotenone/antimycin injection. **F.** ATP production: difference in OCR prior to oligomycin injection and after oligomycin injection. **G.** Coupling efficiency: percentage of basal respiration (**B**) used for ATP production (**F**). Unpaired t-test, $p>0.05$; n=42-44, 3 independent plates. Data are presented as mean ± standard error of the mean.

### 3.3.7 The glycolytic capacity of mouse primary astrocytes was greatly reduced after 24 hour treatment with LPS

Mouse primary astrocytes were treated with LPS for 24 hours prior to study with a Glycolytic Stress Test. In contrast to the acute (3 hours) treatment, after 24 hours LPS treatment there was no significant difference in glycolytic rate between LPS and vehicle treated groups (**fig. 3.3.7.1A-B**; p=0.29). However, glycolytic capacity was reduced by 47% in the LPS group in comparison to vehicle treated controls (**fig. 3.3.7.1C**; p=0.0002), resulting in a 97% decrease in glycolytic reserve (**fig. 3.3.7.1D**; p<0.0001). This reduced capacity could be partly due to the 37% reduction in the rate of glucose uptake seen in the 24 hour LPS-treated group, compared to a vehicle treated control (**fig. 3.3.7.2**; p=0.0091). These data show that after 24 hours of exposure to LPS, mouse primary astrocytes undergo pronounced changes in their cellular metabolism, characterised by a reduction in both the glucose uptake and glycolytic capacity of the cells.

Due to the inherit instability of the assay used, variation in baseline between assays was high. To account for this, data were represented as a fold change from the mean of the contemporaneous controls. However, this resulted in the loss of the ability to compare between the controls. Additionally, as the assays were not run simultaneously, this comparison would not be appropriate due to various confounding factors including the circadian rhythms of the cells and variations in environmental conditions. Therefore I cannot comment on whether there was any change in glucose uptake by the control group between the 3 hour and 24 hour time points. To investigate this further a direct assay comparing these two time points would be required.

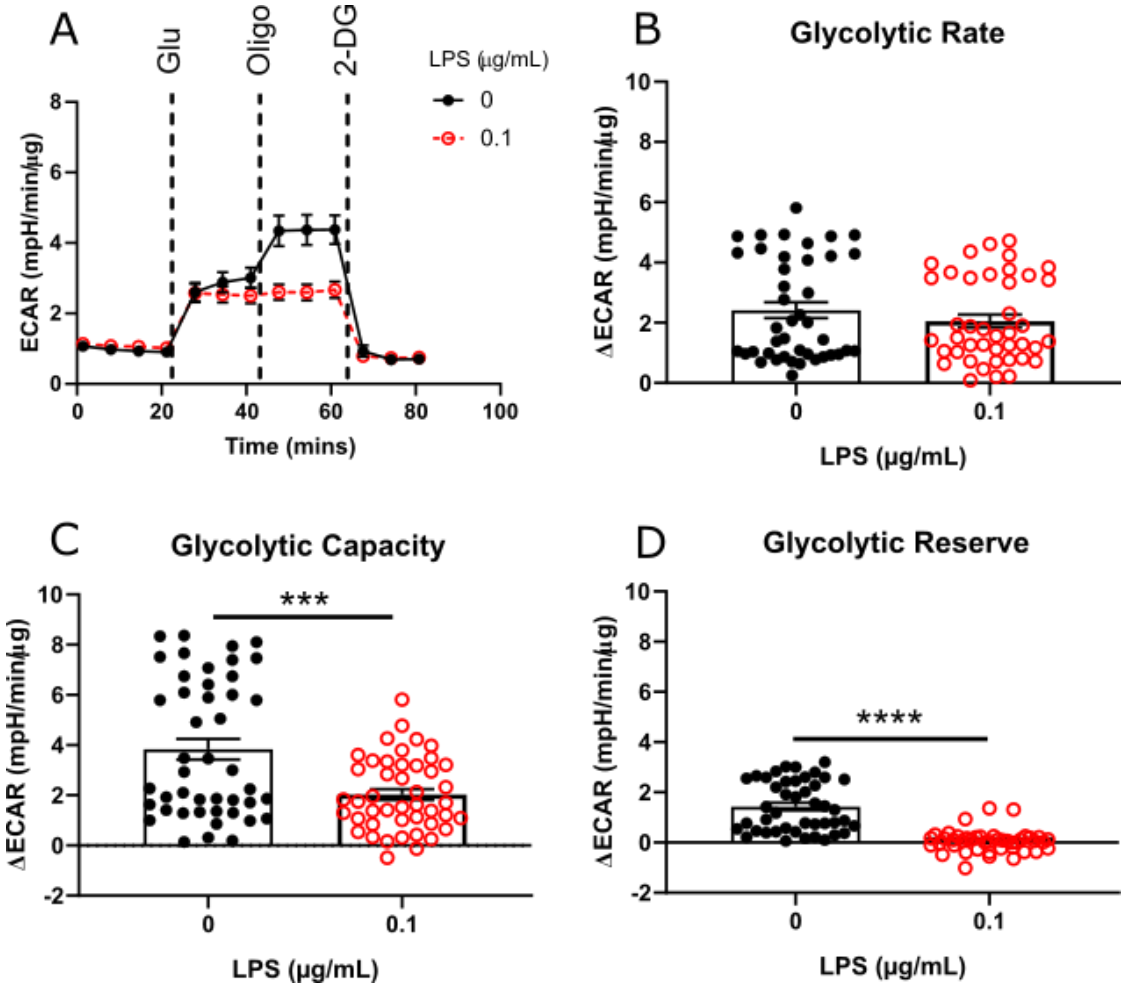
A
Glu
Oligo
2-DG
LPS (µg/mL)
0
0.1
ECAR (mpH/min/µg)
Time (mins)
B
Glycolytic Rate
ΔECAR (mpH/min/µg)
LPS (µg/mL)
C
Glycolytic Capacity
***
ΔECAR (mpH/min/µg)
LPS (µg/mL)
D
Glycolytic Reserve
****
ΔECAR (mpH/min/µg)
LPS (µg/mL)

**Figure 3.3.7.1: 24 hours LPS treatment suppressed glycolytic capacity in mouse primary astrocytes.** Cells were seeded at a density of 4 x $10^4$ cells per well in Seahorse XF96 cell culture microplates. Glycolysis, represented as extracellular acidification rate (ECAR) of the cells was measured using the Seahorse BioAnalyzer XFe96 in conjunction with a Glycolytic Stress Test (Agilent, UK). **A.** ECAR of mouse primary cortical astrocytes during a Glycolytic Stress Test 24 hours after treatment with LPS compared with vehicle treated control (0.017 mM fatty acid free bovine serum albumin; Glu = 10 mM glucose; Oligo = 1 µM oligomycin; 2-DG = 50 mM 2-deoxyglucose). **B.** Glycolytic rate: change in ECAR after treatment with glucose compared to post-2-deoxyglucose treatment. **C.** Glycolytic capacity: change in ECAR after treatment with oligomycin compared to post-2-DG treatment. **D.** Glycolytic reserve: difference between glycolytic rate and glycolytic capacity. Unpaired t-test, **** $p<0.0001$, *** $p<0.001$; n=30, 2 independent plates. Data are expressed as mean ± standard error of the mean.

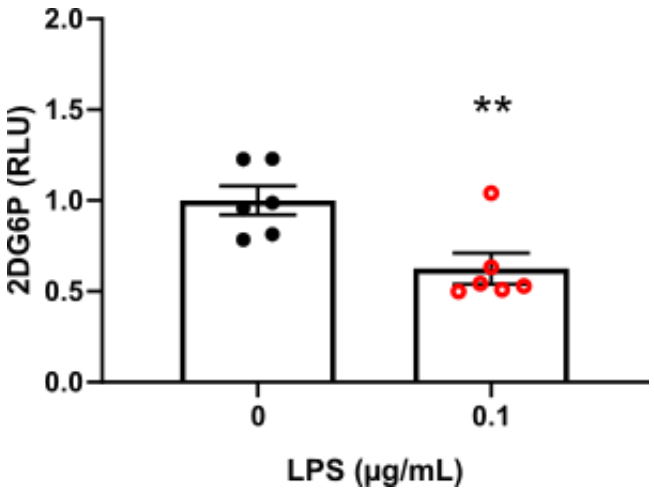


**Figure 3.3.7.2: Glucose uptake was repressed by 24 hours LPS treatment.** Mouse primary astrocytes were seeded at a density of 4 x $10^4$ cells per well in 96 well plates. Glucose uptake rate after treatment with lipopolysaccharide (LPS) was estimated using the Glucose Uptake-Glo kit (Promega, UK). Glucose uptake was represented as fold change in 2-deoxyglucose-6-phosphate (2DG6P) luminescence compared to the mean of vehicle treated controls after 24 hours treatment with lipopolysaccharide (LPS). Unpaired t-test, ** $p<0.01$; n=6. Data are expressed as mean ± standard error of the mean.

### 3.3.8 GLUT1 expression was reduced by 24 hour LPS treatment in mouse primary astrocytes

GLUT1 is a glucose transporter expressed in astrocytes that has previously been reported to be regulated during inflammation (Wieman *et al.*, 2007). To investigate potential causes of the reduced glycolytic capacity observed after 24 hours LPS treatment, GLUT1 expression was quantified using immunoblotting. Bands of multiple molecular weights were detected around the 55 kDa mark, ranging from ~45-55 kDa in weight. All bands detected were quantified as GLUT1, and the variation in weight was likely due to varying levels of glycosylation and/or phosphorylation, as has previously been reported (Devraj *et al.,* 2011; Kumagai *et al.,* 1994). After 3 hours of LPS treatment astrocyte GLUT1 expression was not altered compared to vehicle treated controls (**fig. 3.3.8A**; p=0.96). In line with the alterations in glycolytic rate and capacity seen after 24 hours LPS treatment (**fig. 3.3.7.1**A-D) and in concordance with the glucose uptake data (**fig. 3.3.7.2**), 24 hour treatment with LPS significantly reduced astrocyte GLUT1 expression compared to vehicle treated controls (**fig. 3.3.8B**; p=0.0044).

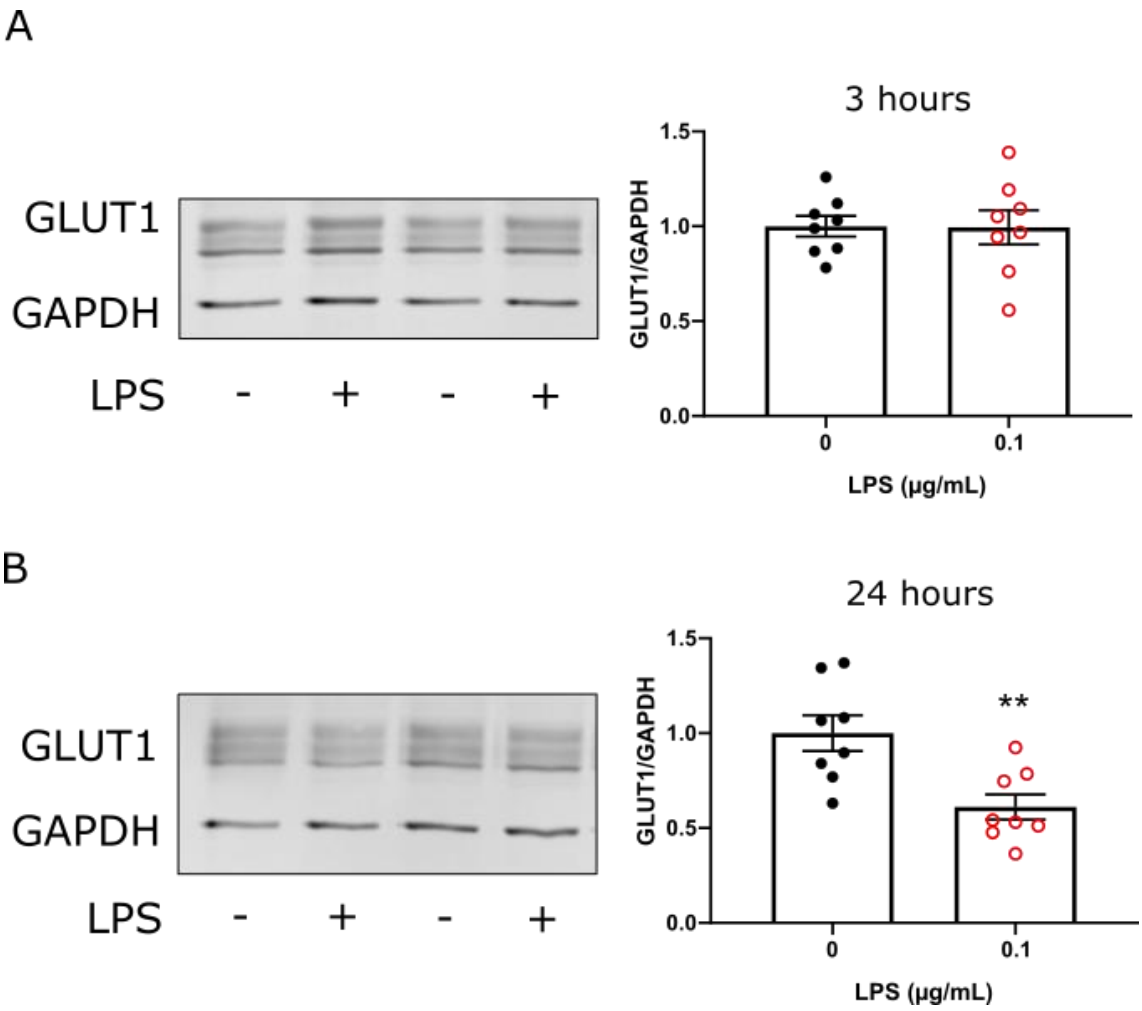


**Figure 3.3.8: GLUT1 expression was suppressed by 24 hours LPS treatment.** Mouse primary astrocytes were seeded at a density of 4.5 x $10^5$ cells per dish in 60 mm dishes prior to treatment with lipopolysaccharide (LPS; 0.1 µg/mL) or vehicle. Cells were lysed and protein collected for immunoblotting. **A-B.** GLUT1 expression quantified by immunoblotting with anti-GLUT1 (Millipore) after 3 hours (**A**; n=7) or 24 hours (**B**; n=6) treatment with lipopolysaccharide (LPS; 0.1 µg/mL). **Left**: Representative blot. **Right**: Densitometric analysis normalised to GAPDH (Protein Tech) and as fold change compared to mean of vehicle treated controls. Unpaired t-test, ** $p<0.01$. Data are expressed as mean ± standard error of the mean.

### 3.3.9 Basal mitochondrial respiration in mouse primary astrocytes was increased after 24 hours LPS treatment

The impact of chronic exposure to an inflammatory stimulus on mitochondrial metabolism was investigated. Mouse primary astrocytes were exposed to LPS for 24 hours prior to study with a Mito Stress Test. Basal mitochondrial respiration was increased by 53% in comparison to vehicle treated controls (**fig. 3.3.9A & B**; $p<0.0001$). Conversely, maximal mitochondrial respiration was reduced by 27% (**fig. 3.3.9C**; $p=0.0003$), resulting in a 79% reduction in spare capacity (**fig. 3.3.9D**; $p<0.00001$). Proton leak was significantly increased by 54% (**fig. 3.3.9E**; $p=0.0019$). Mitochondrial ATP production was increased by 52% (**fig. 3.3.9F**; $p<0.0001$). The mitochondrial coupling efficiency was unchanged (**fig. 3.3.9G**). Together these data suggest after 24 hours of LPS treatment basal mitochondrial activity of mouse primary astrocytes is increased, despite reduced mitochondrial capacity.

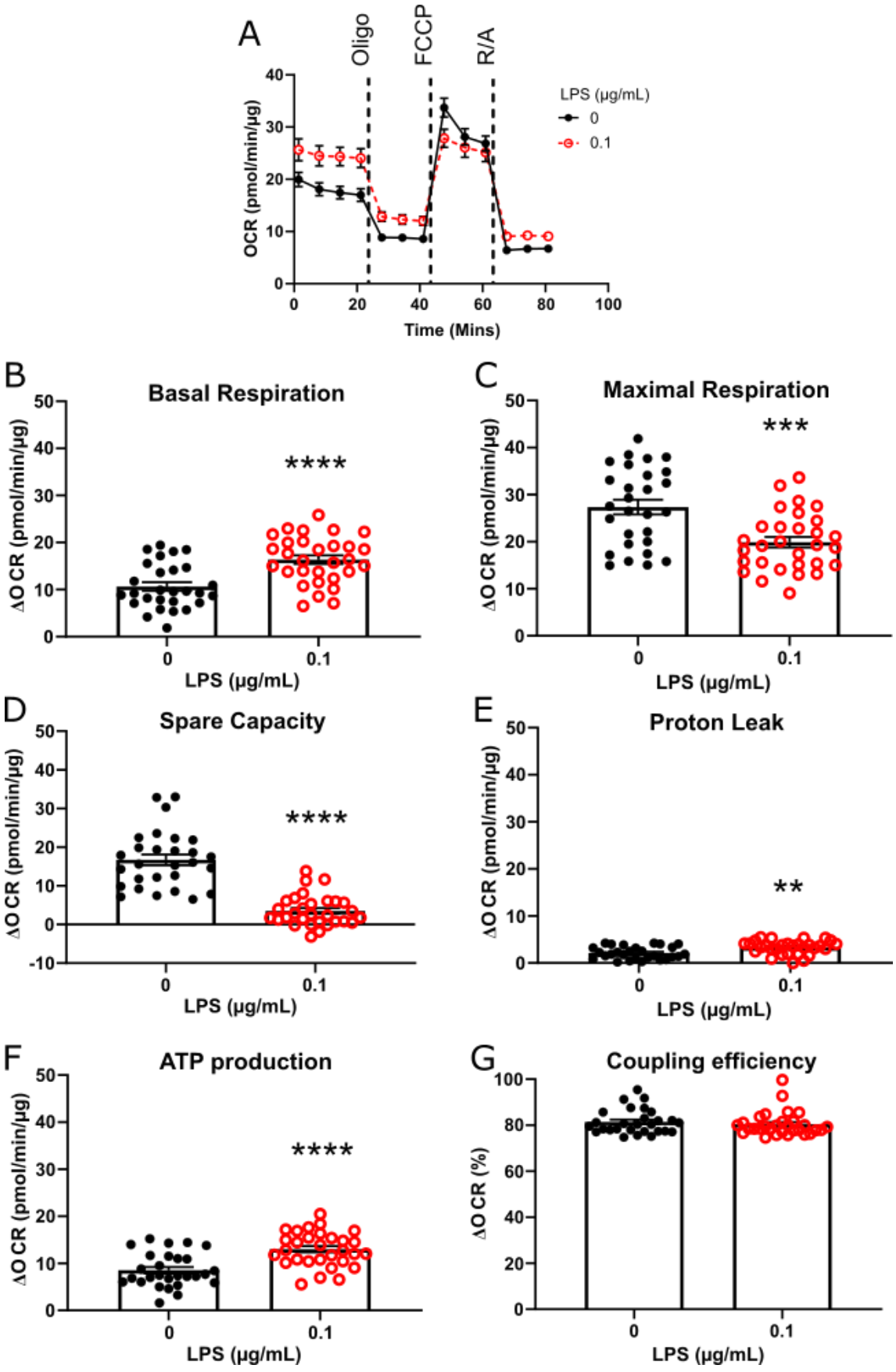
A
Oligo
FCCP
R/A
LPS (µg/mL)
0
0.1
OCR (pmol/min/µg)
Time (Mins)
B
Basal Respiration
****
ΔO CR (pmol/min/µg)
LPS (µg/mL)
C
Maximal Respiration
***
D
Spare Capacity
****
E
Proton Leak
**
F
ATP production
****
G
Coupling efficiency
ΔO CR (%)

**Figure 3.3.9: Basal mitochondrial metabolism was increased by 24 hours LPS.** Cells were seeded at a density of 4 x $10^4$ cells per well in Seahorse XF96 cell culture microplates. Oxidative phosphorylation, represented as oxygen consumption rate (OCR) of the cells was measured using the Seahorse BioAnalyzer XFe96 in conjunction with a Mito Stress Test (Agilent, UK). **A.** OCR of mouse primary cortical astrocytes during a Mito Stress Test 24 hours after treatment with lipopolysaccharide (LPS; 0.1 µg/mL) compared with vehicle treated control (0.017 mM fatty acid free bovine serum albumin). Oligo = 0.5 µM oligomycin; FCCP = 1 µM; R/A = 0.5 µM rotenone/antimycin. **B.** Basal Respiration: difference in OCR prior to Oligo injection and after R/A injection. **C**. Maximal respiration: difference in OCR after injection of FCCP and after R/A injection. **D.** Spare capacity: difference in OCR between basal respiration (**B**) and maximal respiration (**C**). **E.** Proton leak: difference in OCR after Oligo injection and after R/A injection. **F.** ATP production: difference in OCR prior to Oligo injection and after Oligo injection. **G.** Coupling efficiency: percentage of basal respiration (**B**) used for ATP production (**F**). Unpaired t-test, **** $p<0.0001$, *** $p<0.001$, ** $p<0.01$; n=42-44, 3 independent plates. Data are presented as mean ± standard error of the mean.

### 3.3.10 LPS did not alter mitochondrial potential

As a complementary measure of mitochondrial activity, mitochondrial membrane potential was assessed using TMRE dye uptake. 15 minutes after treatment with LPS there was no change in mitochondrial membrane potential in LPS treated astrocytes compared to vehicle treated controls (**fig. 3.3.10A;** p=0.58), while the positive control, the mitochondrial oxidative phosphorylation uncoupler FCCP, significantly reduced TMRE uptake by 72% (**fig. 3.3.10A;** p<0.0001). Mouse primary astrocytes treated for 3 hours with LPS did not have different TMRE uptake compared to vehicle treated controls (**fig. 3.3.10B**), in contrast to the FCCP treated positive controls which showed a 70% reduction in TMRE uptake (**fig. 3.3.10B;** p<0.0001). There is no difference in TMRE dye uptake in cells treated with LPS for 24 hours compared to vehicle treated controls (**fig. 3.3.10C**) although FCCP positive controls reduced TMRE uptake by 67% **(**p<0.0001). This suggests that the integrity of the mitochondrial membrane was not immediately altered by LPS treatment, and rate of proton flow across the membrane was not altered. This corroborates the observed absence of change in coupling efficiency.

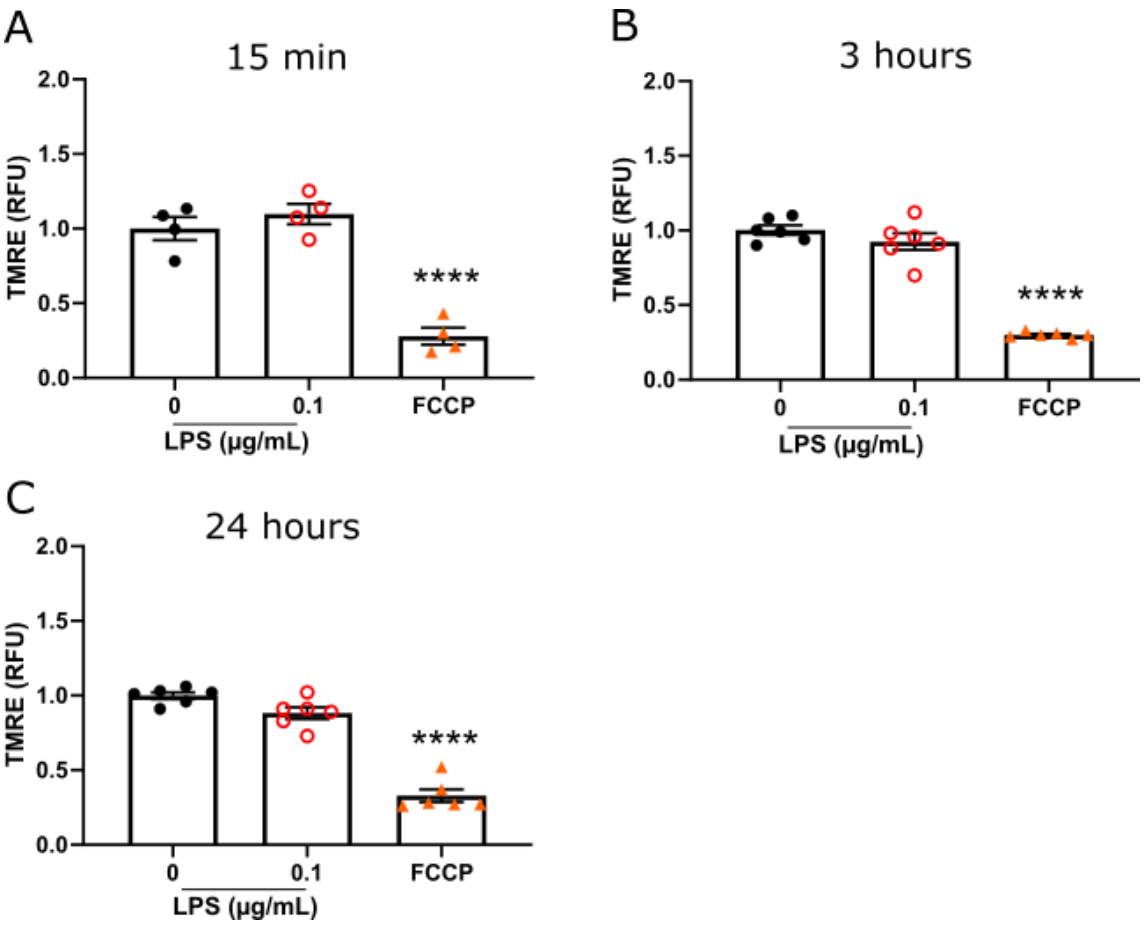


**Figure 3.3.10: Mitochondrial membrane potential was not altered by LPS.** TMRE dye uptake as a fold change from controls after 15 minutes (**A**; n=4), 3 hours (**B**; n=6), or 24 hours (**C**; n=6) treatment with lipopolysaccharide (LPS; 0.1 µg/mL). FCCP (10 µM) was used as a positive depolarisation control. Cells were seeded at a density of 3.5 x $10^5$ cells per well in a 6 well plate. After treatment with LPS, cells were dissociated and incubated with FCCP prior to incubation with TMRE (100 nM) and analysis with the BD Accuri C6 Plus flow cytometer. One-way ANOVA with post hoc Tukey, **** $p<0.0001$. Data are presented as mean ± standard error of the mean.

### 3.3.11 The number of individual mitochondria were reduced after 3 hours LPS treatment

Although there was no measurable change in mitochondrial potential in the LPS-treated astrocytes, some cell types alter their mitochondrial dynamics to regulate energy metabolism in response to LPS treatment (Nair *et al.*, 2019; Park *et al.*, 2013). Mitochondrial network connectivity was assessed using immuno-cytochemistry and confocal microscopy. No change was found in mitochondrial networks after 15 minutes (**fig. 3.3.11.1**) or 24 hours treatment (**fig. 3.3.11.3**) in LPS- compared to vehicle-treated controls. However, after 3 hours treatment with LPS there was a 39% reduction in the number of mitochondria (**fig. 3.3.11.2C;** p=0.0003), seemingly due to there being less mitochondria under 2 µm in length (**fig. 3.3.11.2B**). This may suggest increased mitochondrial fusion 3 hours after LPS treatment, or alternatively increased mitophagy of fragmented mitochondria.

The total number of mitochondria in the control group was lower in after 24 hours compared to the earlier time points. This may be reflective of increased mitochondrial fusion, resulting in a reduced number of mitochondria without reducing mitochondrial biomass, due to changes in the cell cycle stage. It has previously been reported that the $G_1$-S phase of the cell cycle results in mitochondrial fusion compared to the $G_0$ phase which is characterised by mitochondrial fission and more punctate mitochondria (Antico Arciuch *et al.,* 2012).

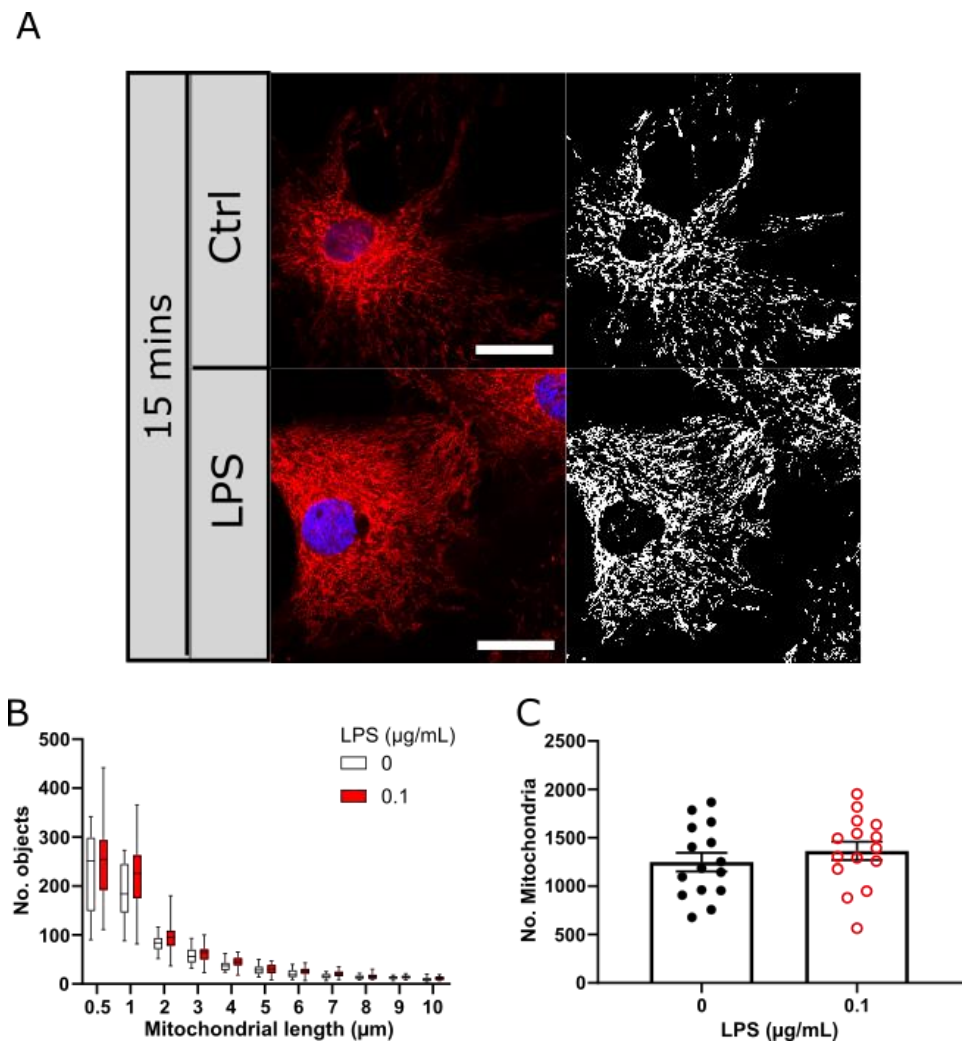


**Figure 3.3.11.1: Mitochondrial networks were not altered by 15 minutes LPS treatment.** Cells were seeded at a density of 1 x $10^5$ cells per well on glass coverslips in 24 well plates. Prior to treatment, cells were stained MitoTracker Red CMXRos (100 nM). After treatment cells were fixated with 4% paraformaldehyde prior to DAPI staining and imaging. **A**. Representative images of the mitochondrial networks of mouse primary astrocytes treated with vehicle or lipopolysaccharide (LPS; 0.1 µg/mL) for 15 minutes, with example processed images for analysis. **B**. Mitochondrial length distribution (two-way ANOVA with post hoc Tukey). **C.** Number of mitochondria per cell (unpaired t-test). n=16; 4 independent coverslips with 4 cells per coverslip. Scale bar = 20 µm. Data are presented as mean ± standard error of the mean.

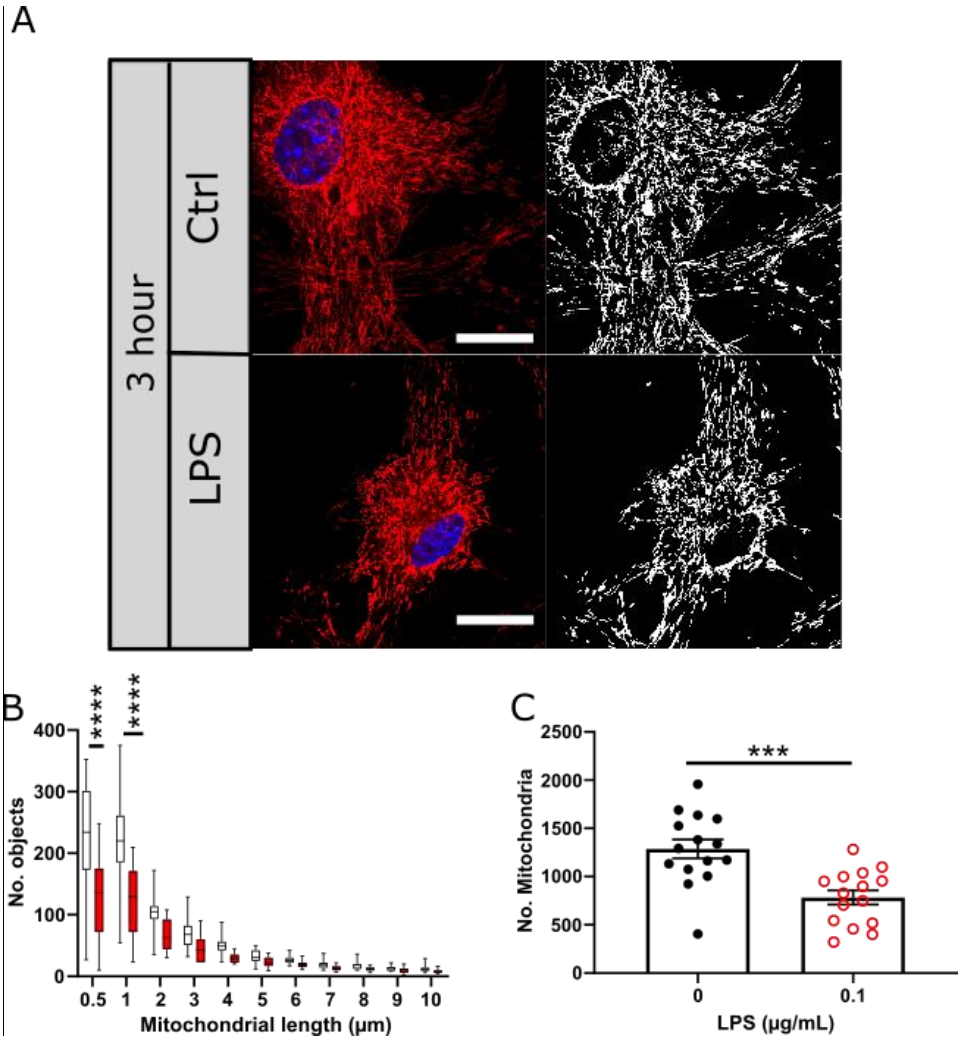


**Figure 3.3.11.2: The number of mitochondria were decreased 3 hours after treatment with LPS**. Cells were seeded at a density of 1 x $10^5$ cells per well on glass coverslips in 24 well plates. Prior to treatment, cells were stained MitoTracker Red CMXRos (100 nM). After treatment cells were fixated with 4% paraformaldehyde prior to DAPI staining and imaging. **A**. Representative images of the mitochondrial networks of mouse primary astrocytes treated with vehicle or lipopolysaccharide (LPS; 0.1 µg/mL) for 3 hours, with example processed images for analysis. **B**. Mitochondrial length distribution (two-way ANOVA with post hoc Sidak; **** $p<0.0001$). **C.** Number of mitochondria per cell (unpaired t-test; *** $p<0.001$). n=15; 3 independent coverslips with 5 cells per coverslip. Scale bar = 20 µm. Data are presented as mean ± standard error of the mean.

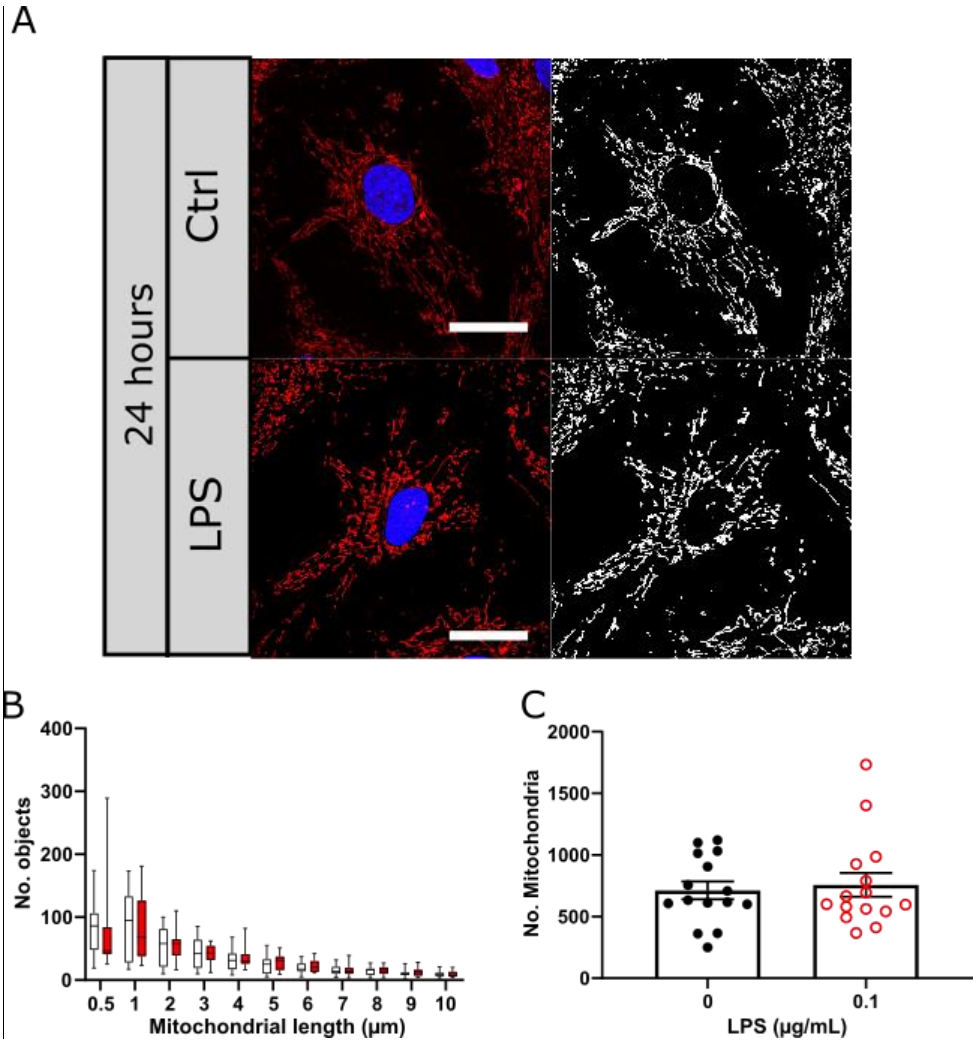


**Figure 3.3.11.3: Mitochondrial networks were not altered by 24 hours LPS treatment.** Cells were seeded at a density of 1 x $10^5$ cells per well on glass coverslips in 24 well plates. Prior to treatment, cells were stained MitoTracker Red CMXRos (100 nM). After treatment cells were fixated with 4% paraformaldehyde prior to DAPI staining and imaging. **A**. Representative images of the mitochondrial networks of mouse primary astrocytes treated with vehicle or lipopolysaccharide (LPS; 0.1 µg/mL) for 24 hours, with example processed images for analysis. **B**. Mitochondrial length distribution (two-way ANOVA with post hoc Tukey). **C.** Number of mitochondria per cell (unpaired t-test). n=15; 3 independent coverslips with 5 cells per coverslip. Scale bar = 20 µm. Data are presented as mean ± standard error of the mean.

### 3.3.12 Intracellular ATP was not altered by LPS

ATP is the key unit of cellular energy. As oxidative phosphorylation is more efficient at generating ATP than glycolysis, any change in metabolic pathways used may affect intracellular ATP (iATP) content. iATP concentrations were not altered after 15 minutes of treatment with LPS in comparison to vehicle treated controls (**fig. 3.3.12A**; p=0.31) despite increased glycolytic rate. iATP concentrations were also unchanged 3 hours (**fig. 3.3.12B;** p=0.78) and 24 hours after treatment with LPS compared to vehicle treated controls (**fig. 3.3.12C**; p=0.48) despite the metabolic adaptations observed. This suggests that in the face of pro-inflammatory stimulation astrocytes can maintain their intracellular energy levels, at least in part, through altered substrate utilisation.

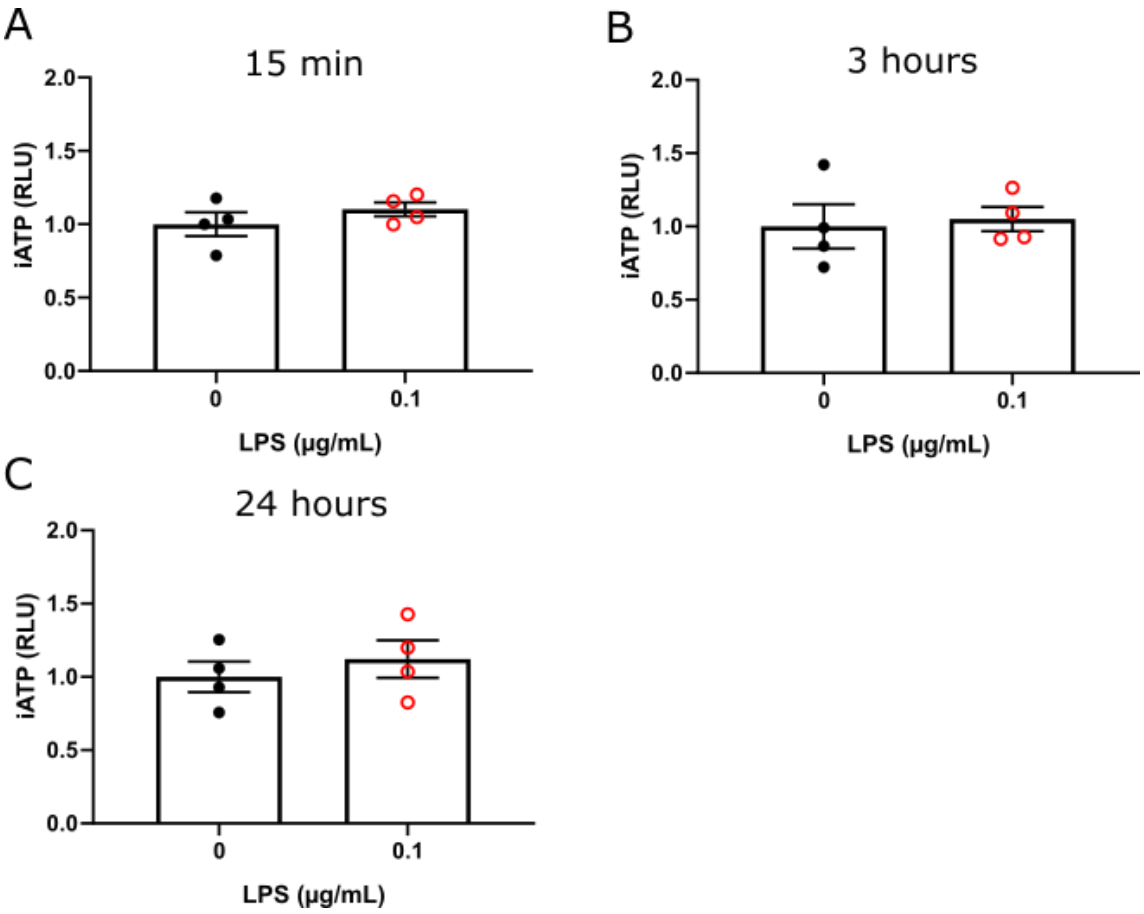


**Figure 3.3.12: Intracellular ATP is not altered by LPS treatment.** Fold change in intracellular ATP (iATP) in mouse primary astrocytes 15 minutes (**A**), 3 hours (**B**) and 24 hours (**C**) after lipopolysaccharide (LPS; 0.1 µg/mL) treatment compared to mean of vehicle treated controls. Mouse primary astrocytes were seeded at a density of 4 x $10^3$ cells per well in black 96 well plates. iATP after treatment with lipopolysaccharide (LPS) was estimated using the ATPLite TwoStep kit (PerkinElmer, UK). Unpaired t-test, $p>0.05$; n=4. Data are presented as mean ± standard error of the mean.

### 3.3.13 2-deoxyglucose inhibited glycolysis but not mitochondrial metabolism in mouse primary astrocytes

In many cell types which display an increase in glycolytic rate during pro-inflammatory stimulation, access to glycolysis is essential for inflammation (Hamilton *et al.*, 1986; Kawauchi *et al.*, 2008b; Lee *et al.*, 2019; Liu *et al.*, 2016; Michl *et al.*, 1976; Tannahill *et al.*, 2013). To ensure Icould selectively inhibit glycolysis in these cells, mouse primary astrocytes were treated with the non-metabolisable glucose analogue 2-deoxyglucose (2-DG; 10 mM), a glycolytic inhibitor, and their metabolism measured. Mouse primary astrocytes showed a 36% reduction in glycolytic rate after addition of 2-DG (**fig. 3.3.13A-B**; $p<0.0001$). No significant change in OCR was measured, suggesting that astrocyte mitochondrial metabolism was unaffected by this intervention (**fig. 3.3.13C-D**).

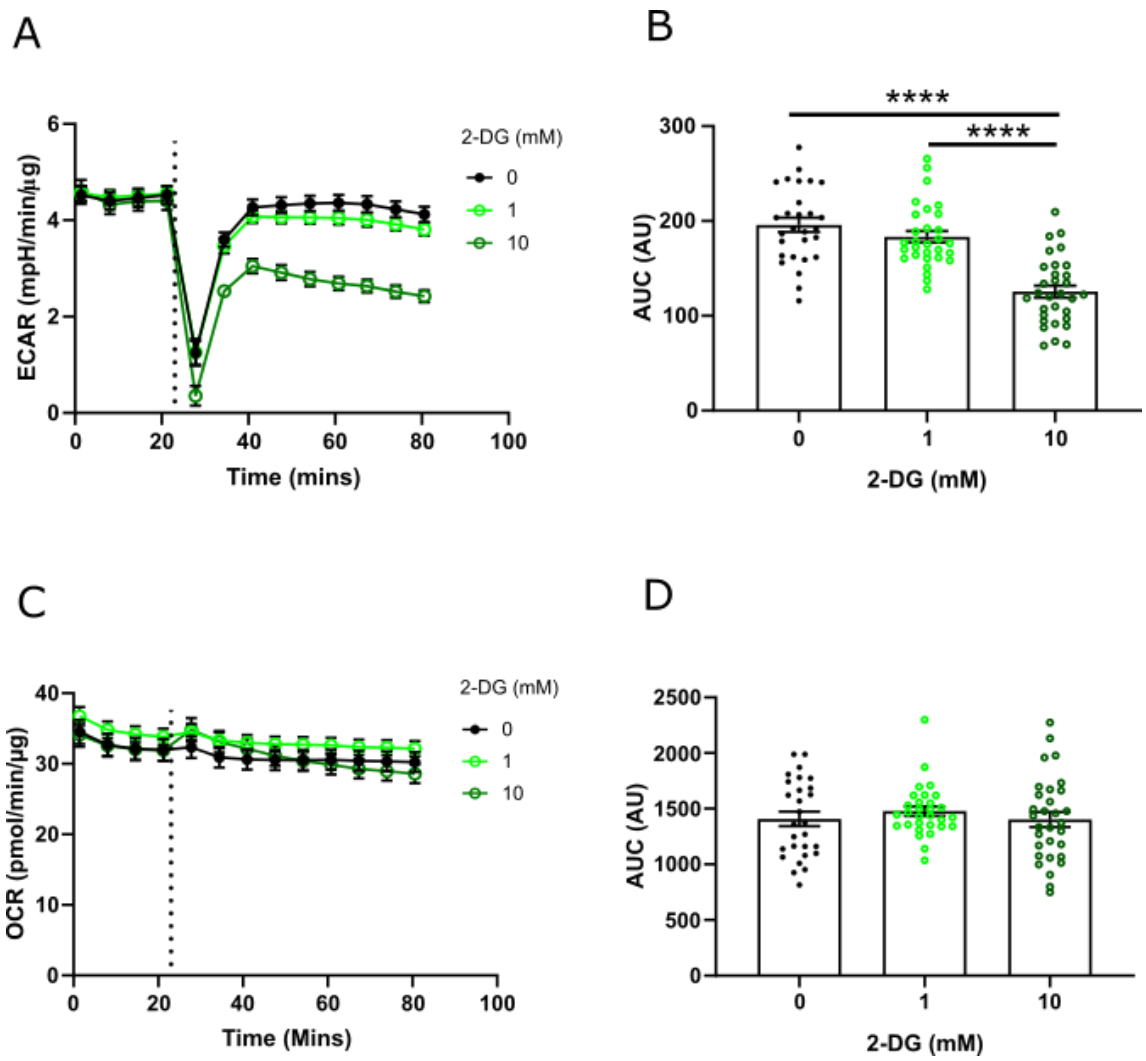


**Figure 3.3.13: 2-DG inhibited glycolysis in mouse primary astrocytes.** Cells were seeded at a density of 4 x $10^4$ cells per well in Seahorse XF96 cell culture microplates. Oxidative phosphorylation rate, represented as oxygen consumption rate (OCR) and glycolysis represented as extracellular acidification rate (ECAR) of the cells were measured using the Seahorse BioAnalyzer XFe96. **A.** ECAR of primary mouse astrocytes over time after treatment with 2-deoxyglucose (2-DG) as indicated by dotted line. **B.** Area under the curve (AUC) of ECAR after treatment with 2-DG. **C.** OCR of mouse primary astrocytes over time after treatment with 2-DG. **D.** AUC of OCR after treatment with 2-DG. One-way ANOVA with post hoc Tukey, **** $p<0.0001$; n=28-32, 2 independent plates. Data are expressed as mean ± standard error of the mean.

### 3.3.14 2-DG caused minimal cell death

Astrocytes are a highly glycolytic cell type (Bélanger *et al.*, 2011a; Fernández-Moncada *et al.*, 2018; Pellerin & Magistretti, 1994; Vardjan *et al.*, 2018; Yellen, 2018). Therefore, blocking glycolysis using 2-DG may result in cell death, which could have caused the results reported here. To assess this, cell viability after 2-DG treatment was measured using propidium iodide exclusion. 24 hours treatment with 2-DG caused a 2% decrease in cell viability which, while statistically significant (**fig. 3.3.14A;** $p<0.0001$), was unlikely to explain the observed changes in metabolism (**fig. 3.3.13**), cytokine release (**fig. 3.3.15**), and NF-κB phosphorylation (**fig. 3.3.16**).

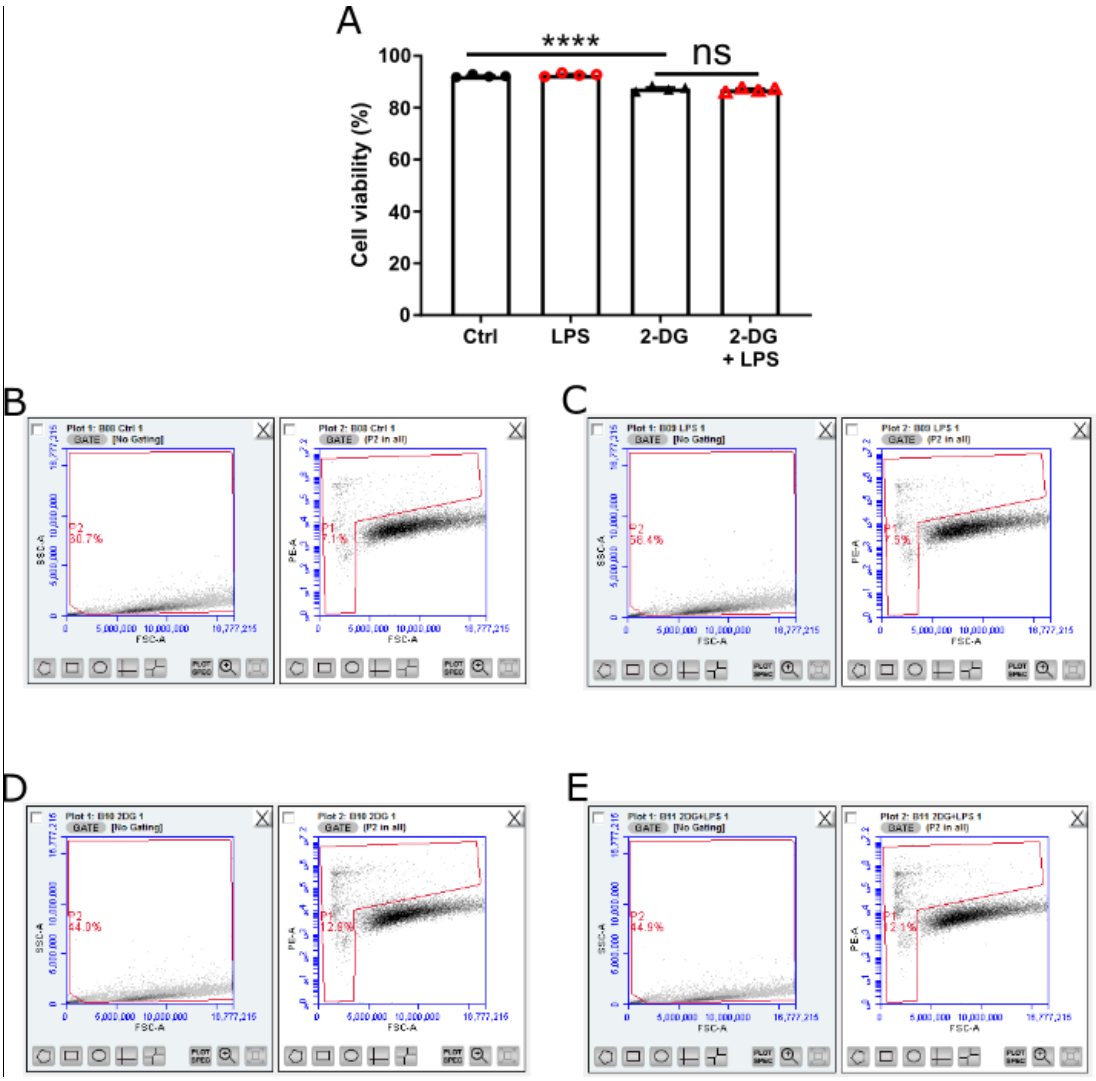


**Figure 3.3.14: 2-DG caused cell death in mouse primary astrocytes.** Propidium iodide staining and flow cytometry of cells 24 hours after treatment. Cells were seeded at a density of 3.5 x $10^5$ cells per well in a 6 well plate. After treatment with LPS, cells were dissociated and stained with 2 µg/mL propidium iodide prior to analysis with the BD Accuri C6 Plus flow cytometer**.** **A**. 2 hour pre-treatment with 2-deoxyglucose (2-DG; 10 mM) ± lipopolysaccharide (LPS; 0.1 µg/mL; **** $p<0.0001$, ns $p>0.05$; n=4). One-way ANOVA with post hoc Tukey. Data are presented as mean ± standard error of the mean. **B-E.** Gating used to define events. Plot 2 region of interest and P1 defined non-viable cells. Example collection plots with data from Ctrl **(B),** LPS **(C)**, 2-DG **(D)** 2-DG+LPS treated cells.

### 3.3.15 Inhibition of the glycolytic response to LPS attenuated cytokine release from mouse primary astrocytes

To investigate the importance of glycolytic metabolism for the inflammatory response in astrocytes, glycolysis was inhibited by 2 hours treatment with 2-DG (10 mM) prior to stimulation with LPS. 2-DG significantly reduced TNF-α and IL-6 release at both 3 hours and 24 hours (**fig. 3.3.15A-B**; 3 hours $p=0.03$, 24 hours $p=0.0118$; **fig. 3.3.15C-D**, $p<0.0001$) and completely abolished IL-10 release at both time points (**fig. 3.3.15E-F**; $p<0.0001$).

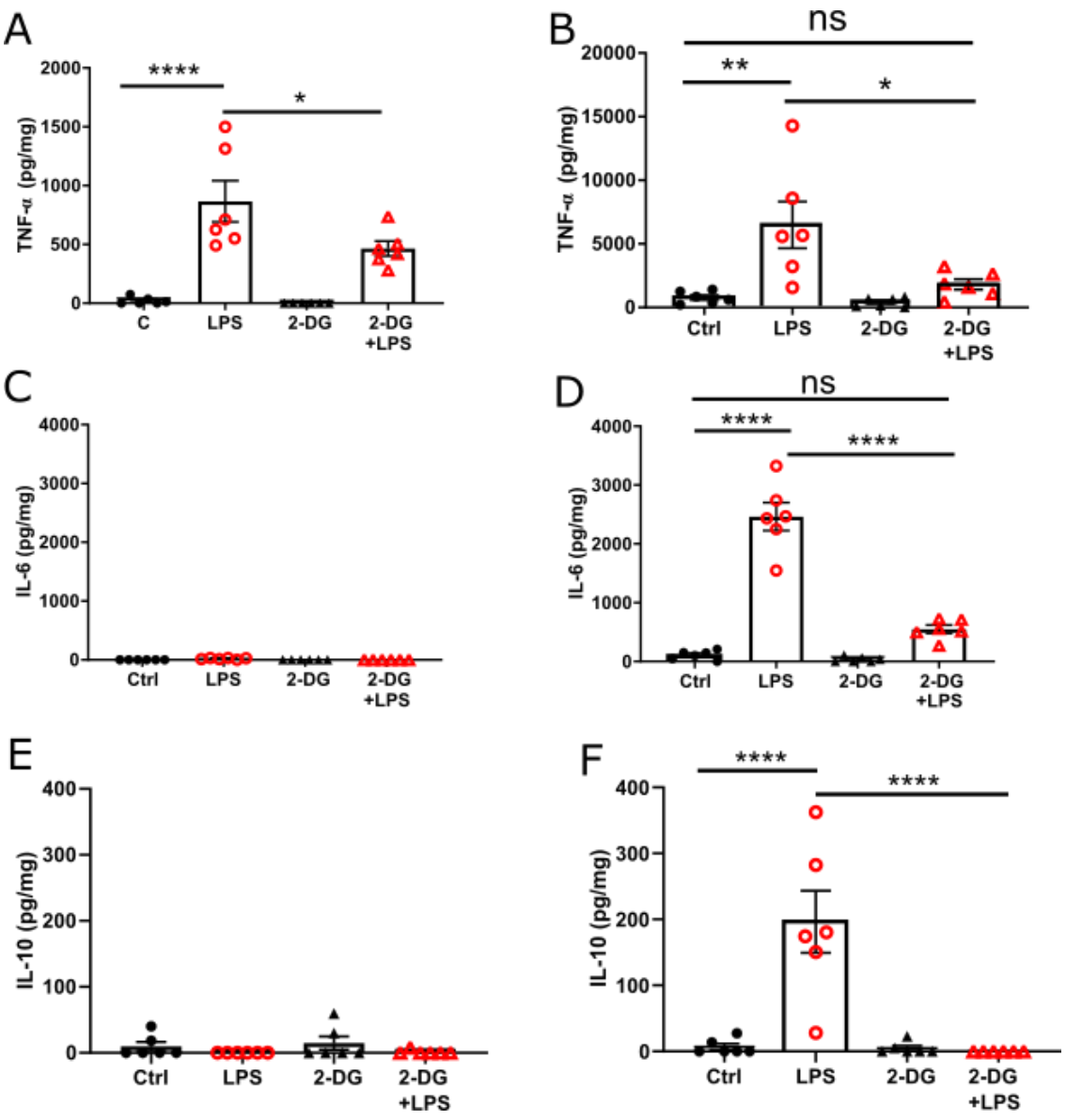
A
TNF-α (pg/mg)
2000
1500
1000
500
0
****
*
C
LPS
2-DG
2-DG +LPS
B
ns
**
*
20000
15000
10000
5000
0
Ctrl
LPS
2-DG
2-DG +LPS
C
IL-6 (pg/mg)
4000
3000
2000
1000
0
Ctrl
LPS
2-DG
2-DG +LPS
D
ns
****
****
4000
3000
2000
1000
0
Ctrl
LPS
2-DG
2-DG +LPS
E
IL-10 (pg/mg)
400
300
200
100
0
Ctrl
LPS
2-DG
2-DG +LPS
F
****
****
400
300
200
100
0
Ctrl
LPS
2-DG
2-DG +LPS

**Figure 3.3.15: 2-DG decreased cytokine release after LPS treatment.** Mouse primary astrocytes were seeded at a density of 4.5 x $10^5$ cells per dish in 60 mm dishes prior to treatment or vehicle. Conditioned media was collected and used for estimation of extracellular cytokine concentrations using DuoSet ELISAs (BioTechne, UK). **A-B.** Extracellular TNF-α concentration 3 hours **(A)** or 24 hours **(B)** after lipopolysaccharide (LPS; 0.1 µg/mL) treatment ± 2-deoxyglucose (2-DG; 10 mM) 2 hours pre-treatment (n=6). **C-D.** Extracellular IL-6 concentration 3 hours **(C)** or 24 hours **(D)** after LPS treatment ± 2-DG 2 hours pre-treatment (n=6). **E-F.** Extracellular IL-10 concentration 3 hours **(E)** or 24 hours **(F)** after LPS treatment ± 2-DG 2 hours pre-treatment (n=6). One-way ANOVA with post-hoc Tukey, ns $p>0.05$, * $p<0.05$, ** $p<0.01$, **** $p<0.0001$. Data are expressed as mean ± standard error of the mean.

### 3.3.16 Inhibition of glycolysis attenuated NF-κB phosphorylation after 24 hours

Although reduced cytokine release was measured, this may have been due to multiple factors including reduced substrate availability for synthesis of new molecules (Menk *et al.*, 2018; Williams & O'Neill, 2018). To investigate whether intact glycolysis was required for initiation of NF-κB signalling, mouse primary astrocytes were pre-treated with 2-DG for 2 hours prior to treatment with LPS or vehicle. 2-DG pre-treatment abolished the LPS-induced increase in NF-κB phosphorylation (Ser536) at 24 hours post-treatment (**fig. 3.3.16.1B**; $p<0.0001$) but not 3 hours after LPS treatment (**fig. 3.3.16.1A**; $p=0.80$). Total expression of NF-κB was not affected by treatment with 2-DG at either time point (**fig. 3.3.16.2**).

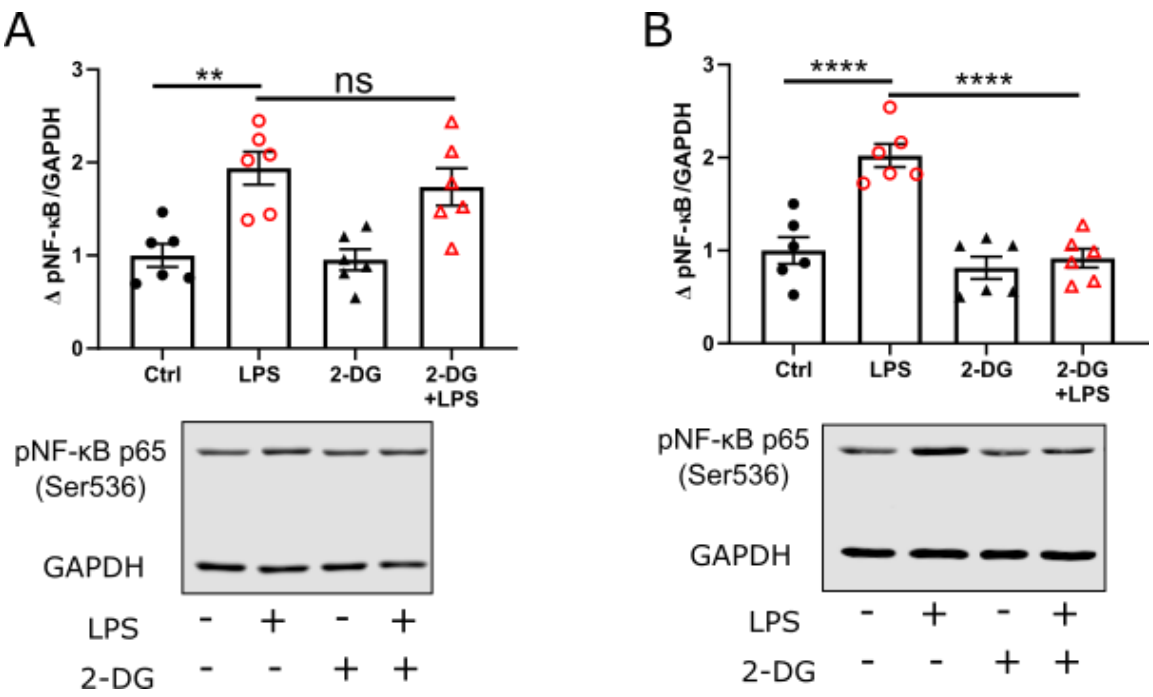


**Figure 3.3.16.1: 2-DG reduced LPS induced p65 NF-κB phosphorylation after 24 hours.** Mouse primary astrocytes were seeded at a density of 4.5 x $10^5$ cells per dish in 60 mm dishes prior to treatment or vehicle. Cells were lysed and protein collected for immunoblotting. **A-B.** Anti-phospho-NF-κB p65 (Ser536) immunoblot after 2 hours pre-treatment with 2-deoxyglucose (2-DG; 10 mM) ± 3 hours (**A**) or 24 hours (**B**) treatment with lipopolysaccharide (LPS; 0.1 µg/mL) with anti-GAPDH loading control. **Top:** Densitometric analysis of anti-phospho-NF-κB p65 (Ser536) fluorescence normalised to anti-GAPDH fluorescence and represented as fold change from mean of vehicle treated controls (n=6). **Bottom:** representative immunoblot of phospho-NF-κB p65 (Ser536) with GAPDH loading control. One-way ANOVA with post-hoc Tukey, ns $p>0.05$, ** $p<0.01$, **** $p<0.0001$. Data are expressed as mean ± standard error of the mean.

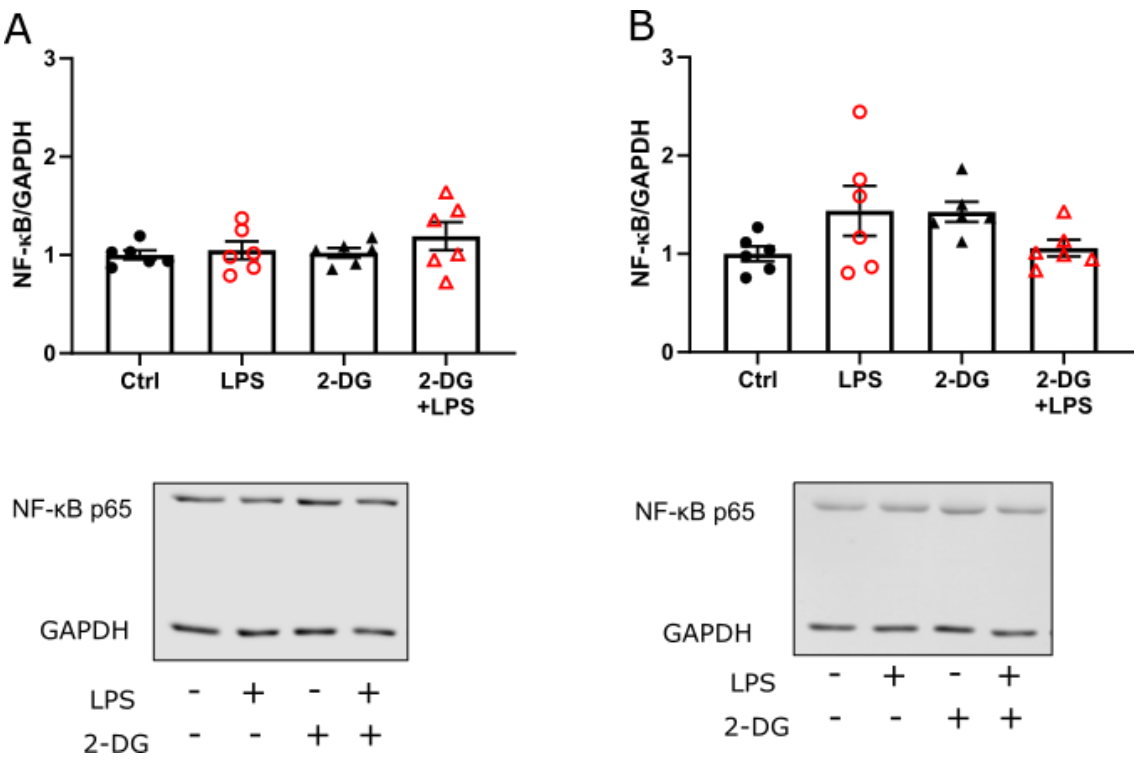


**Figure 3.3.16.2: 2-DG did not affect total p65 NF-κB expression.** Mouse primary astrocytes were seeded at a density of 4.5 x $10^5$ cells per dish in 60 mm dishes prior to treatment or vehicle. Cells were lysed and protein collected for immunoblotting. **A-B.** Anti-NF-κB p65 immunoblot after 2 hours pre-treatment with 2-deoxyglucose (2-DG; 10 mM) ± 3 hours (**A**) or 24 hours (**B**) treatment with lipopolysaccharide (LPS; 0.1 µg/mL) with anti-GAPDH loading control. **Top:** Densitometric analysis of anti-NF-κB p65 fluorescence normalised to anti-GAPDH fluorescence and represented as fold change from mean of vehicle treated controls (n=6). **Bottom:** representative immunoblot of NF-κB p65 with GAPDH loading control. One-way ANOVA with post-hoc Tukey. Data are expressed as mean ± standard error of the mean.

## 3.4 Discussion

In this chapter I have shown that astrocytes have a dynamic metabolic response to inflammation. In support of our hypothesis, I have shown that astrocytes increase glycolytic rate in response to LPS, which is necessary for cytokine release. However, contrary to the initial hypothesis I have shown that mitochondrial metabolism is maintained, or even increased, during a pro-inflammatory stimulus in astrocytes.

**Table 3.4 Summary of the astrocytic metabolic response to LPS**

| | Experimental measure | 3 hours | 24 hours |
|---|---|---|---|
| **Glycolysis** | Glucose uptake | Unchanged | Down |
| | GLUT1 expression | Unchanged | Down |
| | Rate | Up | Unchanged |
| | Capacity | Up | Down |
| | Reserve | Unchanged | Down |
| **Mitochondrial metabolism** | Basal respiration | Unchanged | Up |
| | Maximal respiration | Unchanged | Down |
| | Spare capacity | Unchanged | Down |
| | ATP production | Unchanged | Up |
| | Proton leak | Unchanged | Up |
| | Coupling efficiency | Unchanged | Unchanged |
| | Membrane potential | Unchanged | Unchanged |
| | Mitochondrial fission | Decrease | Unchanged |

### 3.4.1 Astrocytes release cytokines in response to pro-inflammatory signalling

The data shown in this chapter confirms that in this model LPS induces a pro-inflammatory state in mouse primary astrocytes, as has been previously published, both *in vitro* and *in vivo* (Chistyakov *et al.*, 2018; Li *et al.*, 2016; Rosciszewski *et al.*, 2018). This includes release of pro-inflammatory cytokines TNF-α and IL-6 over a 24 hour time frame. These molecules are transcriptionally regulated by NF-κB signalling, and as the research question regarded this signalling pathway other pro-inflammatory molecules regulated primarily by other pathways were not measured. It is likely that other inflammatory pathways are also activated, as the main receptor of LPS, TLR4, also activates MAPK signalling.

### 3.4.2 Astrocytes have a metabolic response to inflammation

The data presented here indicate that glycolytic metabolism in astrocytes increases rapidly after a pro-inflammatory stimulation. Within 40 minutes of LPS treatment glycolytic metabolism was significantly increased and 3 hours after pro-inflammatory stimulation, astrocytes showed an increased rate of glycolysis and glycolytic capacity. Due to the speed of this response (<40 minutes; see **fig. 3.3.4.1C**), this initial increase in glucose uptake and glycolysis is likely to be driven by increased activity of key rate limiting glycolytic enzymes, such as hexokinase II. Although no change in total GLUT1 expression was seen at 3 hours after LPS treatment, our studies did not assess sub-cellular localisation of GLUT1; therefore, increased localisation of GLUT1 at the plasma membrane at this time point cannot be ruled out. The increase in glycolytic rate observed after

3 hours of LPS treatment may be due to NF-κB mediated increase in expression of c-Myc – a transcription factor which regulates expression of many glycolytic genes (Goetzman & Prochownik, 2018), and increases transcription of hexokinase II (Londhe *et al.*, 2018). The use of intracellular glycogen stores may also enable the rapid increase in glycolytic rate in the absence of changes in glucose uptake, but this would need to be directly measured in order to confirm this statement. Astrocyte glycogen depletion has previously been observed following cytokine treatment (Gavillet *et al.*, 2008). It is likely that a combination of these mechanisms contribute to the increased rate of glycolysis observed.

As OXPHOS is still intact, HIF is unlikely to be regulating glycolysis as HIF-1α can be regulated by reverse electron transport through Complex I (Movafagh *et al.*, 2015; Wang *et al.*, 2019). However, in this model Complex I still appears to be being used for OXPHOS. Motori *et al.* showed increased mitochondrial fragmentation during inflammation in astrocytes (Motori *et al.*, 2013). However, in addition to regulating OXPHOS, mitochondrial fragmentation plays an essential role in allowing removal of dysfunctional mitochondria through mitophagy. Mitophagy in astrocytes is essential during inflammation to maintain mitochondria (Huenchuguala *et al.*, 2017). This prevents cytochrome c release from the mitochondria, preventing initiation of apoptosis. I have shown that mitochondrial number decreases 3 hours after pro-inflammatory stimuli. Taken together with the data presented by Motori, mitochondrial fragmentation may be promoting mitochondrial health through allowing mitophagy.

Chronic LPS exposure (24 hours) resulted in metabolic adaptations in astrocytes, probably to maintain ATP production in the face of prolonged insult: glycolytic capacity and reserve were reduced but were accompanied by increased mitochondrial metabolism. It has previously been shown that astrocytes increase TCA cycle rate after 48 hours treatment with IL-1β or TNF-α (Gavillet *et al.*, 2008). Therefore, the increase in mitochondrial metabolism was probably driven by increased TCA cycling to enable utilisation of alternate fuel sources. This change from glycolysis to TCA cycling may suggest that the astrocytes have depleted intracellular glycogen stores, so have limited access to substrates for glycolysis. This is further supported by the data shown here that expression of the glucose transporter GLUT1 is suppressed after 24 hours inflammation, leading to a decrease in glucose uptake. Reduced GLUT1 expression may explain the attenuated glycolytic capacity and glucose uptake I observed in astrocytes exposed to LPS for 24 hours. It is possible that restricting glucose uptake, through downregulating GLUT1 expression, may be a mechanism through which astrocytes attempt to reduce and/or resolve glycolytic activity to limit the inflammatory response. This conclusion is further supported by the increased concentrations of the anti-inflammatory cytokine IL-10 measured at 24 hours, demonstrating that astrocytes are mitigating the pro-inflammatory environment by this time point.

### 3.4.3 The glycolytic response to LPS is essential for inflammation in astrocytes

Not only is glycolytic rate increased during inflammation, it appears that glycolysis is essential for cytokine release from mouse primary astrocytes during LPS

stimulation. Blocking glycolytic function with the non-metabolisable glucose analogue 2-DG reduced cytokine release and NF-κB phosphorylation, suggesting reduced activity of the NF-κB pathway. As NF-κB phosphorylation was still evident 3 hours after glycolytic inhibition, this may suggest a role for paracrine and autocrine actions of astrocyte-derived cytokines in perpetuating the inflammatory response. The initial production of cytokines may be reduced due to 2-DG associated suppression of other inflammatory pathways. Glycolytic enzyme pyruvate kinase isoenzyme M2 acts as a kinase for STAT3 (Gao *et al.*, 2012). Reduced glycolytic flux may lead to lower expression of this enzyme, reducing STAT3 signalling. This would lead to a reduced inflammatory response. Alternatively, the reduced glycolytic rate may prevent the production of carbon intermediates required for cytokine production, through limiting the repurposing of TCA cycle enzymes (Menk *et al.*, 2018; Williams & O'Neill, 2018). This would result in a negative feedback loop reducing the inflammatory response (Caslin *et al.*, 2018; McGettrick & O'Neill, 2013). Although 2-DG treatment caused statistically significant levels of cell death in the primary astrocytes, this represented a less than 2% decrease in cell viability. Therefore, it is unlikely to be cell death causing the reductions in cytokine release and NF-κB phosphorylation observed. It has been reported that in macrophages 2-DG reduces mitochondrial function independently from glycolytic function (Wang *et al.*, 2018). However, in our data there was no change in oxidative rate as a result of 2-DG treatment. This suggests that the changes in inflammatory state were probably a result of glycolytic inhibition rather than mitochondrial modulation. However, I did not measure the effect of 2-DG on the cells after 24 hours, therefore the suppressed inflammatory response may be driven through limited mitochondrial function rather than restricted glycolysis.

## 3.5 Conclusion

In conclusion, astrocytes have a dynamic metabolic response to pro-inflammatory stimulation, which is essential for a cellular pro-inflammatory response. Inhibition of the early glycolytic response is sufficient to inhibit cytokine release and NF-κB mediated signalling in astrocytes. Additionally, glucose transporter GLUT1 is downregulated after extended periods of inflammation, resulting in reduced glucose uptake and glycolytic capacity.

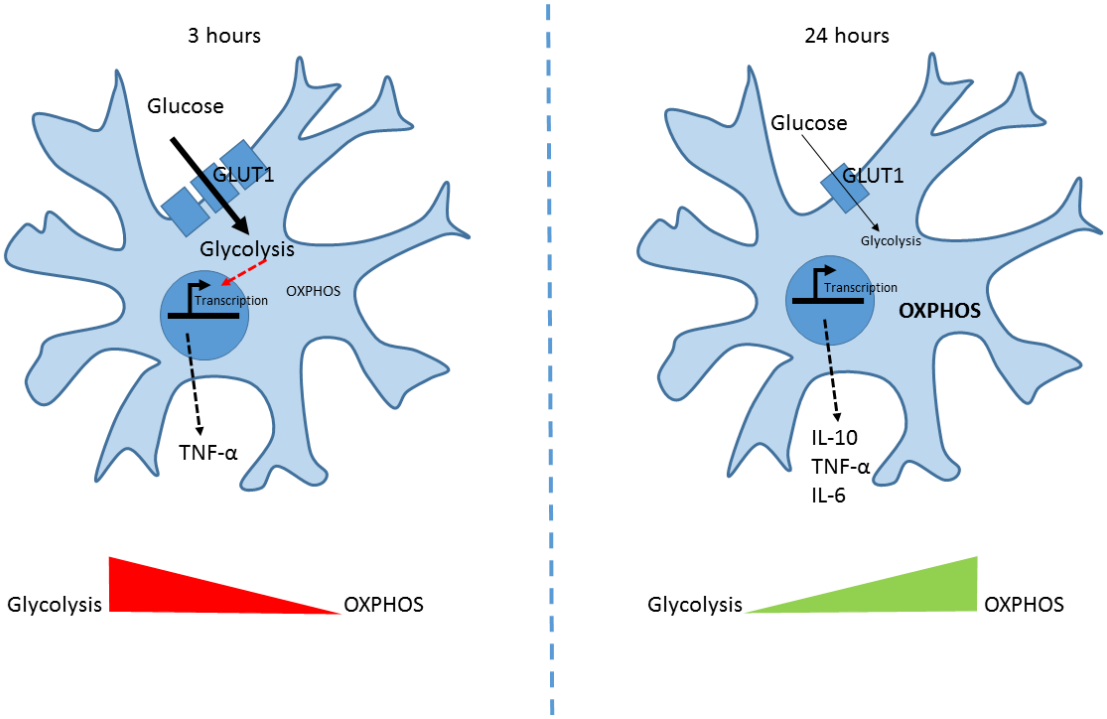


**Figure 3.5: Summary of chapter.** 3 hours after pro-inflammatory stimulus, astrocytes increased their use of glycolytic metabolism to allow synthesis of cytokines. 24 hours after pro-inflammatory stimulus, glycolytic rate is reduced through downregulation of GLUT1, and oxidative phosphorylation is increased.

# Chapter 4. NF-κB regulates the metabolic response to inflammation in mouse primary astrocytes

A modified version of this chapter is published as part of:

**The metabolic response to inflammation in astrocytes is regulated by nuclear factor-kappa B signalling.**

*Josephine L. Robb, Nadia A. Hammad, Paul G. Weightman Potter, John K. Chilton, Craig Beall, Kate L.J. Ellacott.* **Glia.** DOI:10.1002/glia.23835.

## 4.1 Introduction

During inflammation NF-κB signalling is activated in astrocytes (Lukasiuk *et al.*, 1995; Migheli *et al.*, 1997). This has been reported in multiple models with NF-κB increasing release of IL-6, TNF-α and IL-10, among other immunomodulatory agents (Cao *et al.*, 2006; Choi *et al.*, 2014; Collart *et al.*, 1990; Son *et al.*, 2008; Sparacio *et al.*, 1992). Preventing inflammation in astrocytes through inhibition of the NF-κB signaling pathway can alter the pathophysiological response to disease. For example, inhibition of NF-κB activity in glial-fibrillary acidic protein (GFAP) expressing astrocytes promotes functional recovery of spinal cord injury in mice, resulting in reduced glial scarring and increased locomotor activity (Brambilla *et al.*, 2005). It has also been reported that NF-κB signalling in astrocytes can regulate systemic energy homeostasis and food intake in mice

(Buckman *et al.*, 2014; Douglass *et al.*, 2017). Inhibition of astrocyte NF-κB signaling in the mouse hypothalamus, by deleting IKKβ from GFAP expressing cells, improves glucose tolerance and reduces obesity by promoting energy expenditure (Douglass *et al.*, 2017). These data demonstrate that in astrocytes NF-κB signalling plays an integral role in managing energy homeostasis and the cellular response to disease.

Multiple PPRs can initiate NF-κB signalling. Whilst astrocytes do express multiple PPRs, including TNFR, IL-1 receptor, CD-40L and other TLRs, such as TLR -1, -2 and -9, only TLR-4 is sensitive to PAMPs from gram-negative bacteria, and thus can detect LPS (Kaltschmidt *et al.*, 2005; Kielian, 2006; Lu *et al.*, 2008; Rosciszewski *et al.*, 2018). Decreased TLR-4 expression through siRNA or activity through anti-TLR-4 antibodies, or loss of the co-receptor CD-14 almost completely ablates both human and mouse astrocyte activation and cytokine release induced by LPS, suggesting in these cells TLR-4 is the dominant LPS sensor (Park *et al.,* 2017; Tarassishin *et al.,* 2014; Li *et al.,* 2016). Therefore, whilst other receptors may be capable of activating NF-κB signalling, in response to LPS this is predominantly mediated through the TLR-4.

Activation of TLR-4 leads to recruitment of intracellular kinases. These kinases initiate multiple intracellular signalling cascades, including canonical NF-κB signalling, culminating in increased transcription of many genes associated with inflammation (**fig. 1.2.5.2**) (Gorina *et al.*, 2011; Lu *et al.*, 2008; Rosciszewski *et al.*, 2018). Inhibition of TLR4 activation by LPS in astrocytes prevents NF-κB signalling. This is neuroprotective, reducing inflammation and improving memory

dysfunction *in vitro* and *in vivo* (Gong *et al.*, 2014; Li *et al.*, 2018; Muhammad *et al.*, 2019; Zhou *et al.*, 2015). This demonstrates that TLR-4 stimulation by LPS is an activator of NF-κB in astrocytes and that NF-κB plays a role in pathology.

In other cell types it has been demonstrated that NF-κB signalling can regulate glycolysis during inflammation through multiple mechanisms. These include direct regulation of glucose transporter (eg. GLUT1) expression and insertion into the membrane, and hexokinase II expression (Kawauchi *et al.*, 2008b; Londhe *et al.*, 2018; Sommermann *et al.*, 2011). NF-κB may also indirectly regulate glycolysis by impacting the activity of other transcription factors including HIF-1α which can regulate expression of glycolytic enzymes (D'Ignazio *et al.*, 2016; van Uden *et al.*, 2008). This may suggest that the changes to glycolytic metabolism in astrocytes observed in the previous chapter are modulated by NF-κB signalling.

Together this evidence may suggest that NF-kB plays a role in driving metabolic changes in astrocytes during inflammation. To our knowledge this mechanism of metabolic regulation has not been explored in astrocytes.

## 4.2 Hypothesis

In this chapter I hypothesised that the metabolic response to inflammation in astrocytes is regulated by NF-κB signalling.

## 4.3 Results

### 4.3.1 NF-κB inhibitor TPCA-1 reduced LPS-induced NF-κB Ser536 phosphorlyation

TPCA-1 was developed as a specific inhibitor of IKK-β and is used in this study to inhibit canonical NF-κB signalling (Podolin *et al.*, 2005). To confirm that the concentration of TPCA-1 used was sufficient to inhibit NF-κB activation in mouse primary astrocytes, NF-κB phosphorylation (Ser536) was quantified using immunoblotting in lysates of cells treated with TPCA-1 and/or LPS for 3 hours and 24 hours. NF-κB phosphorylation (Ser536) was significantly increased by LPS treatment (3 hours, 71%, p=0.021; 24 hours, 84%, p=0.0208) but attenuated by TPCA-1 pre-treatment. This was evident to a greater extent after 24 hours (**fig. 4.3.1.1B;** 20% increase from control, p=0.87) than after 3 hours (**fig. 4.3.1.1A;** 41% increase from control, p=0.28). Total NF-κB expression was not altered by treatments after 3 hours or 24 hours (**fig. 4.3.1.2A-B**).

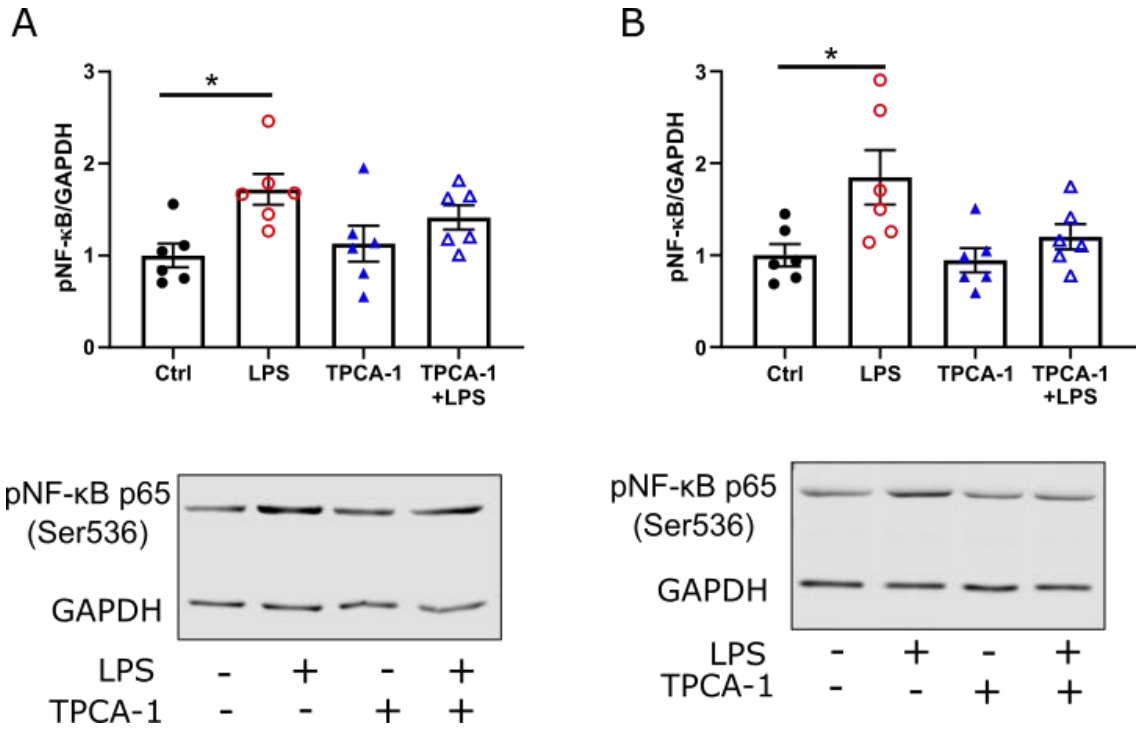


**Figure 4.3.1.1: Pharmacological compound TPCA-1 inhibited NF-κB p65 phosphorylation by LPS in mouse primary astrocytes.** Mouse primary astrocytes were seeded at a density of 4.5 x $10^5$ cells per dish in 60 mm dishes prior to treatment or vehicle. Cells were lysed and protein collected for immunoblotting. **A-B.** Immunoblot of NF-κB p65 phosphorylation (Ser536) with GAPDH loading control after 2 hours pre-treatment with NF-κB inhibitor TPCA-1 (1 µM) ± 3 hours **(A)** or 24 hours **(B)** treatment with lipopolysaccharide (LPS; 0.1 µg/mL). **Top:** Densitometric analysis of NF-κB p65 phosphorylation as a fold change from the mean of vehicle treated controls. **Bottom:** Representative blot. One-way ANOVA with post hoc Tukey, * $p<0.05$. n=6. Data are expressed as mean ± standard error of the mean.

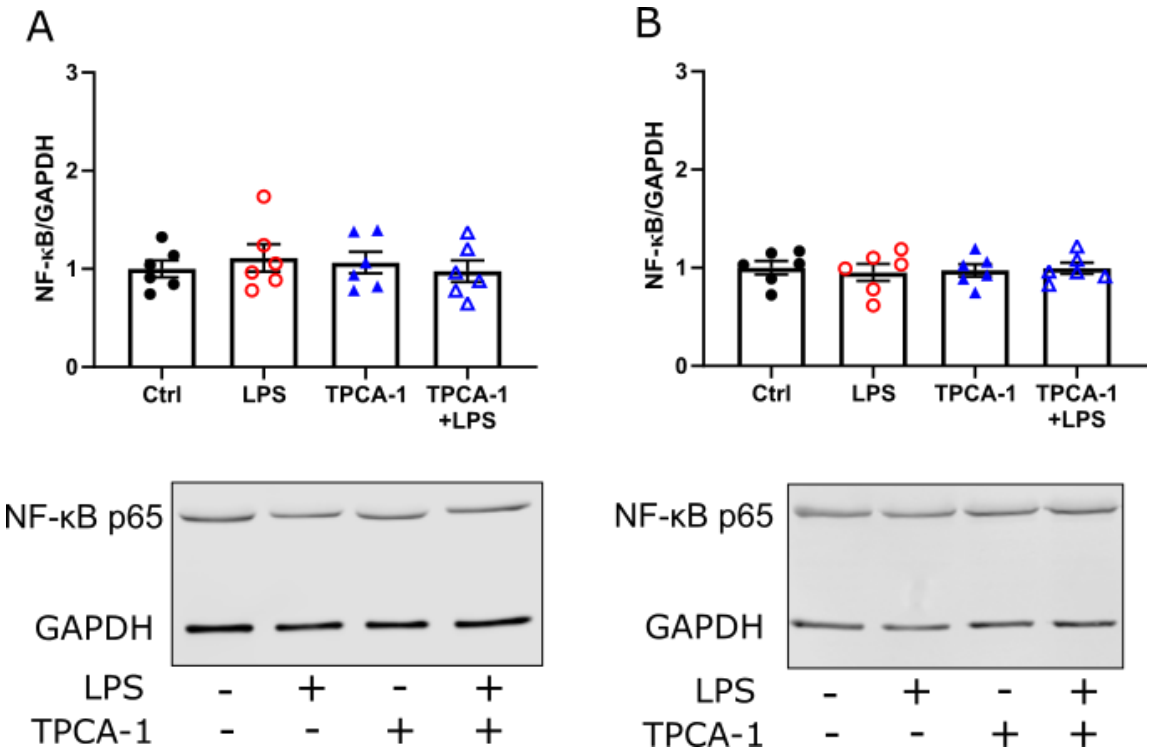


**Figure 4.3.1.2: TPCA-1 did not modulate NF-κB p65 expression in mouse primary astrocytes.** Mouse primary astrocytes were seeded at a density of 4.5 x $10^5$ cells per dish in 60 mm dishes prior to treatment or vehicle. Cells were lysed and protein collected for immunoblotting. **A-B.** Immunoblot of NF-κB p65 with GAPDH loading control after 2 hours pre-treatment with NF-κB inhibitor TPCA-1 (1 µM) and 3 hours **(A)** or 24 hours **(B)** treatment with lipopolysaccharide (LPS; 0.1 µg/mL). **Top:** Densitometric analysis of NF-κB p65 as a fold change from the mean of vehicle treated controls. **Bottom:** Representative blot. One-way ANOVA with post hoc Tukey, n=6. Data are expressed as mean ± standard error of the mean.

### 4.3.2 TPCA-1 did not reduce cell viability

At micromolar concentrations TPCA-1 has been reported to decrease cell viability in macrophages, dendritic cells and T-cells (Tilstra *et al.*, 2014). To make sure inhibition of NF-κB signalling had no effect on cell viability which could affect our data, cell viability was measured using propidium iodide exclusion. TPCA-1 treatment had no impact on cell viability (**fig. 4.3.2**; p=0.95). This indicates that any reduction in reported measures after inhibition with TPCA-1 are not attributable to reduced cell viability.

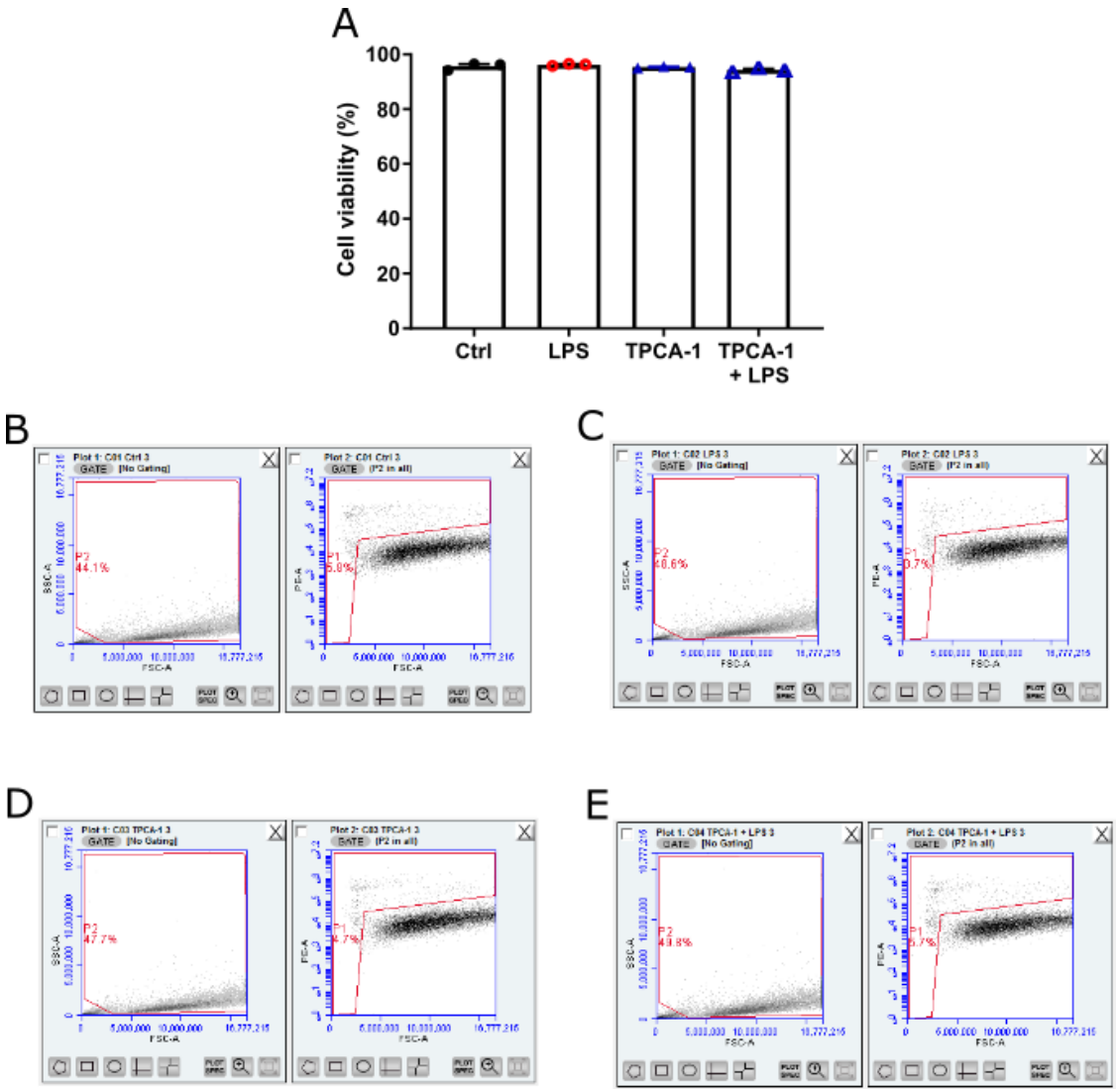


**Figure 4.3.2: TPCA-1 did not affect cell viability in mouse primary astrocytes.** Propidium iodide staining and flow cytometry of cells 24 hours after treatment. Cells were seeded at a density of 3.5 x $10^5$ cells per well in a 6 well plate. After treatment with LPS, cells were trypsinised and stained with 2 µg/mL propidium iodide prior to analysis with the BD Accuri C6 Plus flow cytometer**. A**. 2 hours pre-treatment with NF-κB inhibitor TPCA-1 (1 µM) ± lipopolysaccharide (LPS; 0.1 µg/mL; n=3). One-way ANOVA with post hoc Tukey. Data are presented as mean ± standard error of the mean. **B-E.** Gating used to define events. Plot 2 region of interest and P1 defined non-viable cells. Example collection plots with data from Ctrl **(B),** LPS **(C)**, TPCA-1 **(D)** TPCA-1+LPS treated cells.

### 4.3.3 NF-κB inhibitor TPCA-1 reduced LPS induced cytokine release

To confirm that NF-κB played a role in inflammatory signalling in mouse primary astrocytes, and regulated the cytokines measured in the study, TPCA-1 was used to inhibit NF-κB signalling. 2 hours of pre-treatment with TPCA-1 inhibited the inflammatory response to LPS after 3 hours and 24 hours of treatment. TNF-α and IL-6 release were significantly reduced by TPCA-1 (**fig. 4.3.3A-D**; $p<0.0001$).

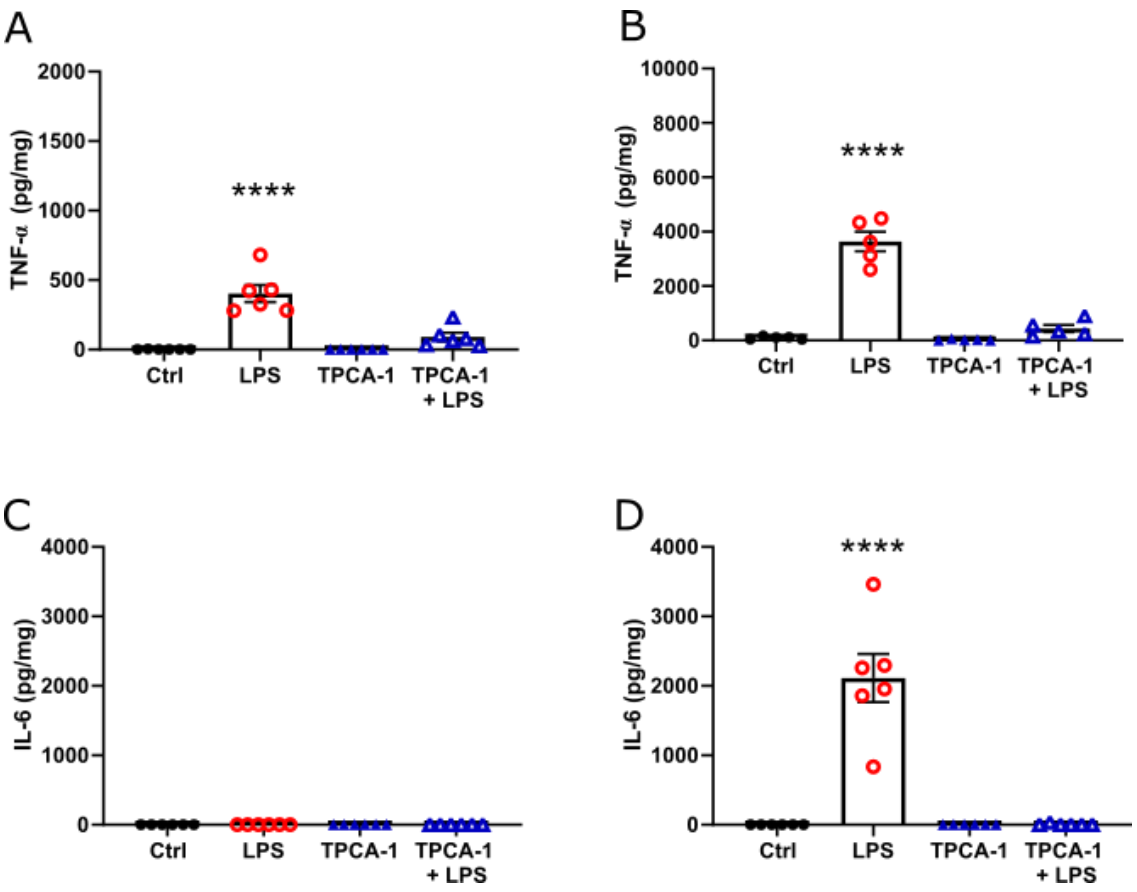


**Figure 4.3.3: NF-κB inhibition reduced LPS induced release of pro-inflammatory cytokines in mouse primary astrocytes.** Mouse primary astrocytes were seeded at a density of 4.5 x $10^5$ cells per dish in 60 mm dishes prior to treatment or vehicle. Conditioned media was collected and used for estimation of extracellular cytokine concentrations using DuoSet ELISAs (BioTechne, UK). **A-B.** Extracellular TNF-α concentration after 2 hours pre-treatment with NF-κB inhibitor TPCA-1 (1 µM) ± 3 hours (**A;** n=5) or 24 hours (**B;** n=4) lipopolysaccharide (LPS; 0.1 µg/mL) treatment. **C-D.** Extracellular IL-6 concentration after 2 hours pre-treatment with TPCA-1 (1 µM) ± 3 hours (**C**) or 24 hours (**D**) LPS treatment (n=6). One-way ANOVA with post hoc Tukey, **** $p<0.0001$ relative to all other data sets on the graph. Data are expressed as mean ± standard error of the mean.

### 4.3.4 NF-κB inhibition reduced baseline glycolytic metabolism and prevented LPS induced increases in glycolytic rate

Previously published work on other cell types has implicated NF-κB signalling in the regulation of cellular metabolism (Goetzman & Prochownik, 2018; Sommermann *et al.*, 2011). To investigate the effect of inhibiting NF-κB signalling on glycolytic metabolism in mouse primary astrocytes during inflammation, astrocytes were exposed to TPCA-1 (1 μM) for 2 hours prior to treating with LPS for 3 hours, after which a Glycolytic Stress Test was performed. Cells treated with TPCA-1 and LPS displayed a 27% reduction in glycolytic rate compared to cells treated with LPS alone (**fig. 4.3.4A-B**; $p<0.0001$). This suggests that NF-κB signalling plays an instrumental role in the glycolytic response to LPS. Importantly, treatment with TPCA-1 alone reduced glycolytic rate by 28% compared to vehicle treated astrocytes (**fig. 4.3.4A-B**; $p<0.0001$). This suggests that NF-κB signalling plays an important role in regulating basal metabolism in astrocytes independently from pro-inflammatory signalling. Glycolytic capacity was also significantly reduced in TPCA-1 groups (in the presence (29%; $p<0.0001$) or absence (36%; $p<0.0001$) of LPS) compared to controls (**fig. 4.3.4C-D**). This resulted in a reduction of glycolytic reserve in TPCA-1 groups of 45% without LPS ($p<0.0001$) and 32% with LPS treatment ($p<0.0001$).

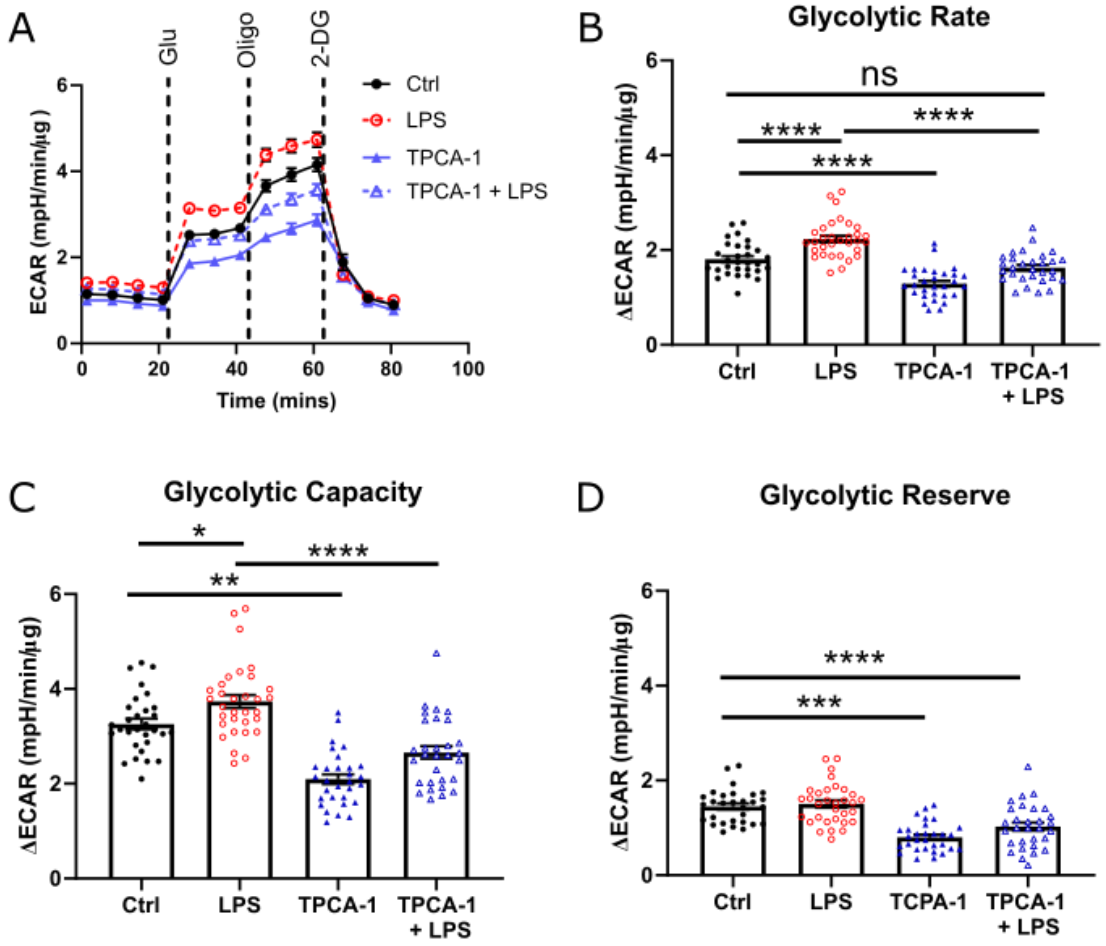
A
Glu
Oligo
2-DG
Ctrl
LPS
TPCA-1
TPCA-1 + LPS
ECAR (mpH/min/µg)
Time (mins)
B
Glycolytic Rate
ns
****
****
****
ΔECAR (mpH/min/µg)
Ctrl
LPS
TPCA-1
TPCA-1 + LPS
C
Glycolytic Capacity
*
****
**
ΔECAR (mpH/min/µg)
Ctrl
LPS
TPCA-1
TPCA-1 + LPS
D
Glycolytic Reserve
****
***
ΔECAR (mpH/min/µg)
Ctrl
LPS
TCPA-1
TPCA-1 + LPS

**Figure 4.3.4: NF-κB inhibition reduced glycolytic metabolism in mouse primary astrocytes after 3 hours treatment with LPS.** Cells were seeded at a density of 4 x $10^4$ cells per well in Seahorse XF96 cell culture microplates. Glycolysis, represented as extracellular acidification rate (ECAR) of the cells was measured using the Seahorse BioAnalyzer XFe96 in conjunction with a Glycolytic Stress Test (Agilent, UK). **A.** ECAR of mouse primary cortical astrocytes during a Glycolytic Stress Test after 2 hour pre-treatment with NF-κB inhibitor, TPCA-1 (1 µM) ± 3 hours lipopolysaccharide (LPS; 0.1 µg/mL) compared with vehicle treated control (0.017 mM fatty acid free bovine serum albumin/0.01% v/v DMSO). Glu= 10 mM glucose, Oligo = 1 µM oligomycin, 2-DG = 10 mM 2-deoxyglucose. **B.** Glycolytic rate: change in ECAR after Glu treatment. **C.** Glycolytic capacity: change in ECAR after Oligo treatment. **D.** Glycolytic reserve: difference between glycolytic rate and glycolytic capacity. One-way ANOVA with post hoc Tukey; ns $p>0.05$, * $p<0.05$, ** $p<0.01$, **** $p>0.0001$; n=32, 2 independent plates. Data are expressed as mean ± standard error of the mean.

### 4.3.5 Inhibition of NF-κB did not have a regulatory effect on mitochondrial metabolism independently of LPS after 3 hours of treatment

To investigate whether NF-κB signalling plays a role in normal mitochondrial function, Mito Stress Tests were conducted on mouse primary astrocytes pre-treated with TPCA-1 for 2 hours prior to treatment with LPS for 3 hours. TPCA-1 pre-treatment did not change mitochondrial maximal respiration, proton leak or spare capacity with or without treatment with LPS compared to vehicle treated controls (**fig. 4.3.5.1C, D & F** respectively). TPCA-1 pre-treatment prior to LPS significantly increased basal respiration by 18% (**fig. 4.3.5.1B**; p=0.01), increasing mitochondrial ATP production by 21% (**fig. 4.3.5.1E**; p=0.002), due to a 2% increase in coupling efficiency (**fig. 4.3.5.1G**; p=0.028). Despite increased mitochondrial ATP production, there was no change in intracellular ATP content after TPCA-1 treatment compared to vehicle treated controls (**fig. 4.3.5.2**).

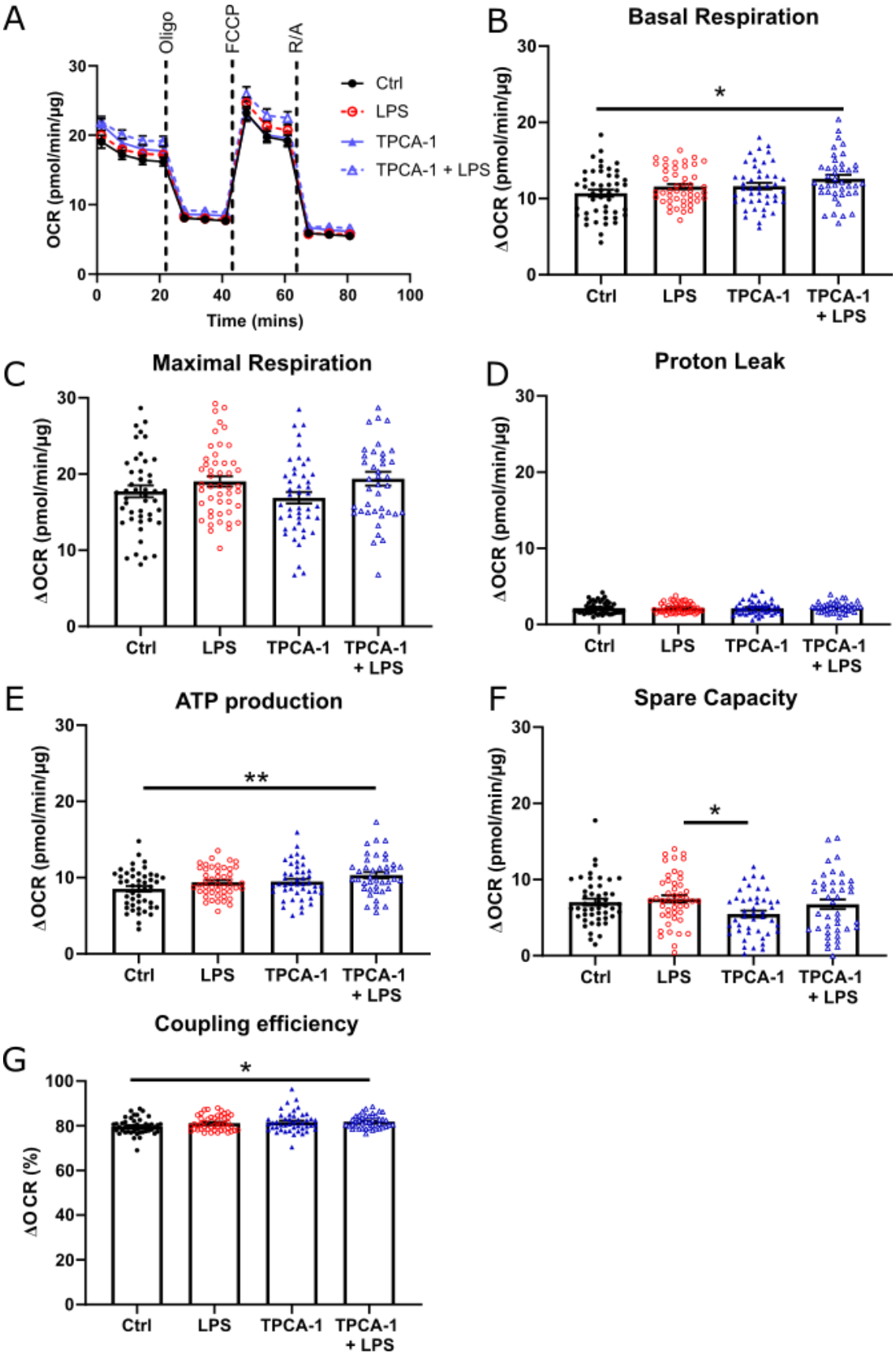
A
Oligo
FCCP
R/A
Ctrl
LPS
TPCA-1
TPCA-1 + LPS
OCR (pmol/min/µg)
Time (mins)
B
Basal Respiration
ΔOCR (pmol/min/µg)
C
Maximal Respiration
D
Proton Leak
E
ATP production
F
Spare Capacity
G
Coupling efficiency
ΔO CR (%)

**Figure 4.3.5.1: NF-κB inhibition did not alter mitochondrial function in astrocytes 3 hours after LPS treatment.** Cells were seeded at a density of 4 x $10^4$ cells per well in Seahorse XF96 cell culture microplates. Oxidative phosphorylation, represented as oxygen consumption rate (OCR) of the cells was measured using the Seahorse BioAnalyzer XFe96 in conjunction with a Mito Stress Test (Agilent, UK). **A.** OCR of mouse primary cortical astrocytes during a Mito Stress Test after 2 hours pre-treatment with NF-κB inhibitor, TPCA-1 (1 µM) ± 3 hours lipopolysaccharide (LPS; 0.1 µg/mL) compared with vehicle treated control (0.017 mM fatty acid free bovine serum albumin/0.01% v/v DMSO). Oligo = 0.5 µM oligomycin, FCCP = 1 µM, R/A = 0.5 µM rotenone/antimycin. **B.** Basal respiration: difference in OCR prior to Oligo injection and after R/A injection. **C.** Maximal respiration: difference in OCR after injection of FCCP and after R/A injection. **D.** Proton leak: difference in OCR after Oligo injection and after R/A injection. **E.** ATP production: difference in OCR prior to Oligo injection and after Oligo injection. **F.** Spare capacity: difference in OCR between basal respiration (**B**) and maximal respiration (**C**). **G.** Coupling efficiency: percentage of basal respiration (**B**) used for ATP production (**E**). One-way ANOVA with post-hoc Tukey, * $p<0.05$, ** $p<0.01$; n=45, 3 independent plates. Data are presented as mean ± standard error of the mean.

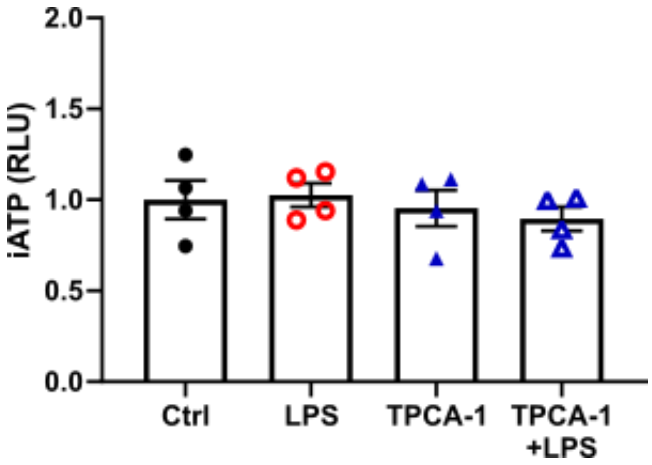


**Figure 4.3.5.2: NF-κB inhibition did not affect intracellular ATP in mouse primary astrocytes.** Mouse primary astrocytes were seeded at a density of 4 x $10^3$ cells per well in black 96 well plates. Intracellular ATP (iATP) after treatment was estimated using the ATPLite TwoStep kit (PerkinElmer, UK). iATP represented as a fold change from the mean of vehicle treated controls (one-way ANOVA with post-hoc Tukey, $p>0.05$; n=4). Data are presented as mean ± standard error of the mean.

### 4.3.6 Glycolytic consequences of prolonged exposure to LPS were abolished through inhibition of NF-κB signalling

To establish whether the longer-term effects of LPS on metabolism were impacted by inhibition of NF-κB, mouse primary astrocytes were cultured with TPCA-1 for 2 hours prior to addition of LPS for 24 hours. TPCA-1 treatment did not alter the astrocyte glycolytic rate after 24 hours in the presence or absence of LPS (**fig. 4.3.6A-B**). Treatment with TPCA-1 prevented the 24 hour LPS induced decrease in glycolytic capacity (**fig. 4.3.6C;** 37%; $p=0.0003$) and reserve (**fig. 4.3.6D;** 72% $p<0.0001$), but TPCA-1 alone did not alter glycolytic capacity or reserve when compared to vehicle treated astrocytes.

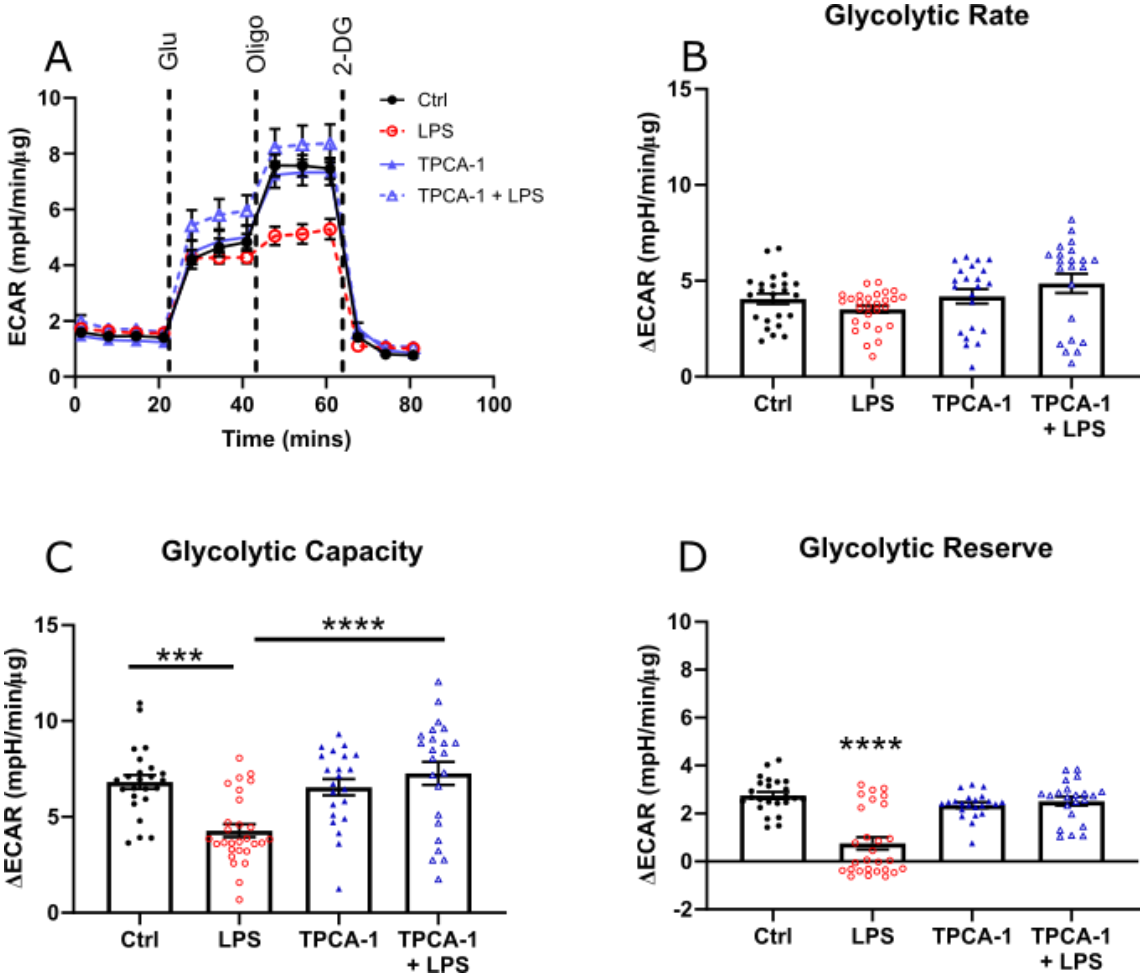
A
Glu
Oligo
2-DG
Ctrl
LPS
TPCA-1
TPCA-1 + LPS
ECAR (mpH/min/µg)
Time (mins)
B
Glycolytic Rate
ΔECAR (mpH/min/µg)
Ctrl
LPS
TPCA-1
TPCA-1 + LPS
C
Glycolytic Capacity
***
****
ΔECAR (mpH/min/µg)
Ctrl
LPS
TPCA-1
TPCA-1 + LPS
D
Glycolytic Reserve
****
ΔECAR (mpH/min/µg)
Ctrl
LPS
TPCA-1
TPCA-1 + LPS

**Figure 4.3.6: Inhibition of NF-κB signalling prevented the reduction in glycolytic capacity induced by 24 hours LPS treatment in mouse primary astrocytes.** Cells were seeded at a density of 4 x $10^4$ cells per well in Seahorse XF96 cell culture microplates. Glycolysis, represented as extracellular acidification rate (ECAR) of the cells was measured using the Seahorse BioAnalyzer XFe96 in conjunction with a Glycolytic Stress Test (Agilent, UK). **A.** ECAR of mouse primary cortical astrocytes during a Glycolytic Stress Test 24 hours after 2 hour pre-treatment with NF-κB inhibitor, TPCA-1 (1 µM) ± lipopolysaccharide (LPS; 0.1 µg/mL) compared with vehicle treated control (0.017 mM fatty acid free bovine serum albumin/0.01% v/v DMSO). Glu = 10 mM glucose, Oligo = 1 µM oligomycin, 2-DG = 10 mM 2-deoxyglucose **B.** Glycolytic rate: change in ECAR after treatment with Glu. **C.** Glycolytic capacity: change in ECAR after treatment with Oligo. **D.** Glycolytic

### 4.3.7 GLUT1 expression was reduced by 24 hour LPS treatment in mouse primary astrocytes through NF-κB signalling

To determine whether the LPS-induced decrease in GLUT1 was NF-κB dependent, lysates from mouse primary astrocytes cultured for 2 hours with TCPA-1 prior to treatment with LPS for 24 hours were immunoblotted with anti-GLUT1. The LPS-induced reduction in GLUT-1 expression (47%; $p<0.0001$) was partially attenuated by TPCA-1 pre-treatment (**fig. 4.3.7**; $p=0.081$).

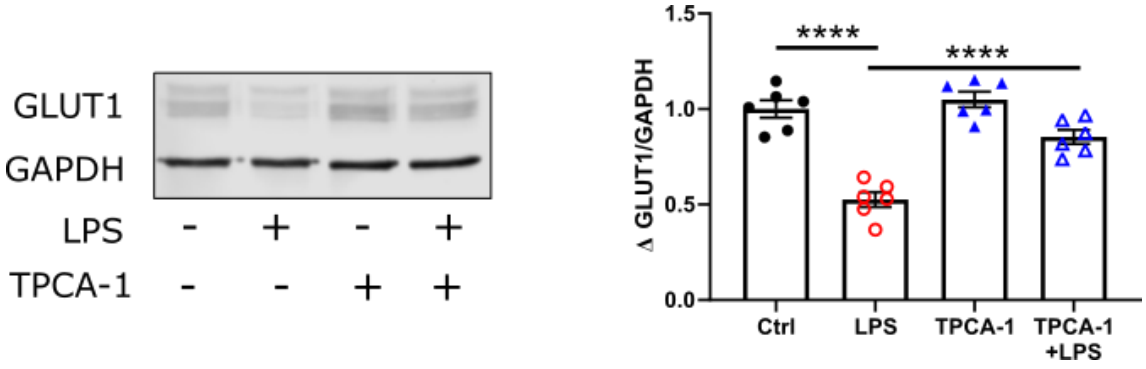


**Figure 4.3.7: Inhibition of NF-κB prevented the suppression of GLUT1 expression induced by 24 hours LPS treatment in mouse primary astrocytes.** Mouse primary astrocytes were seeded at a density of 4.5 x $10^5$ cells per dish in 60 mm dishes prior to treatment or vehicle. Cells were lysed and protein collected for immunoblotting. **A.** Representative immunoblot of GLUT1 expression with GAPDH loading control after 2 hour pre-treatment with NF-κB inhibitor TPCA-1 (1 μM) ± 24 hour treatment with lipopolysaccharide (LPS; 0.1 μg/mL). **B.** Densitometric analysis of **A** as a fold change from means of vehicle treated controls. One-way ANOVA with post hoc Tukey, **** p<0.0001, *** p<0.001; n=6. Data are expressed as mean ± standard error of the mean.

### 4.3.8 Inhibition of NF-κB altered mitochondrial respiration independently from LPS treatment after 24 hours

To investigate the role of NF-κB in the previously observed mitochondrial response to a chronic inflammatory stimulus (**fig. 3.3.14**), astrocytes were pre-treated with TPCA-1 for 2 hours prior to treatment for 24 hours with LPS. LPS-induced increases in basal respiration (65%; $p<0.0001$), proton leak (84%; $p<0.0001$) and mitochondrial ATP production (61%; $p<0.0001$) were reduced by TPCA-1 pre-treatment (**fig. 4.3.8.1A, B, D, & E**). Maximal respiration was reduced by TPCA-1 pre-treatment with LPS treatment by 35% ($p<0.0001$). This was greater than the reduction induced by LPS-alone (-18%; $p=0.013$; **fig. 4.3.8.1C**). Treatment with TPCA-1 alone reduced basal respiration and ATP production by 25% ($p=0.013$) and 24% ($p=0.011$) respectively, independently from LPS treatment (**fig. 4.3.8.1B & F**). Despite this change in mitochondrial ATP production, intracellular ATP levels were not altered (**fig. 4.3.8.2**). TPCA-1 reduced maximal respiration by 33% (**fig. 4.3.8.1C**; $p<0.0001$), independently of LPS treatment, suggesting that NF-κB signalling may play a role in normal mitochondrial metabolism, which was attenuated by TPCA-1. TPCA-1 pre-treatment attenuated the LPS induced 78% reduction in spare capacity to 55% (**fig. 4.3.8.1F**; $p<0.0001$). No significant change was seen in coupling efficiency after pre-treatment with TPCA-1 (**fig. 4.3.8.1G**).

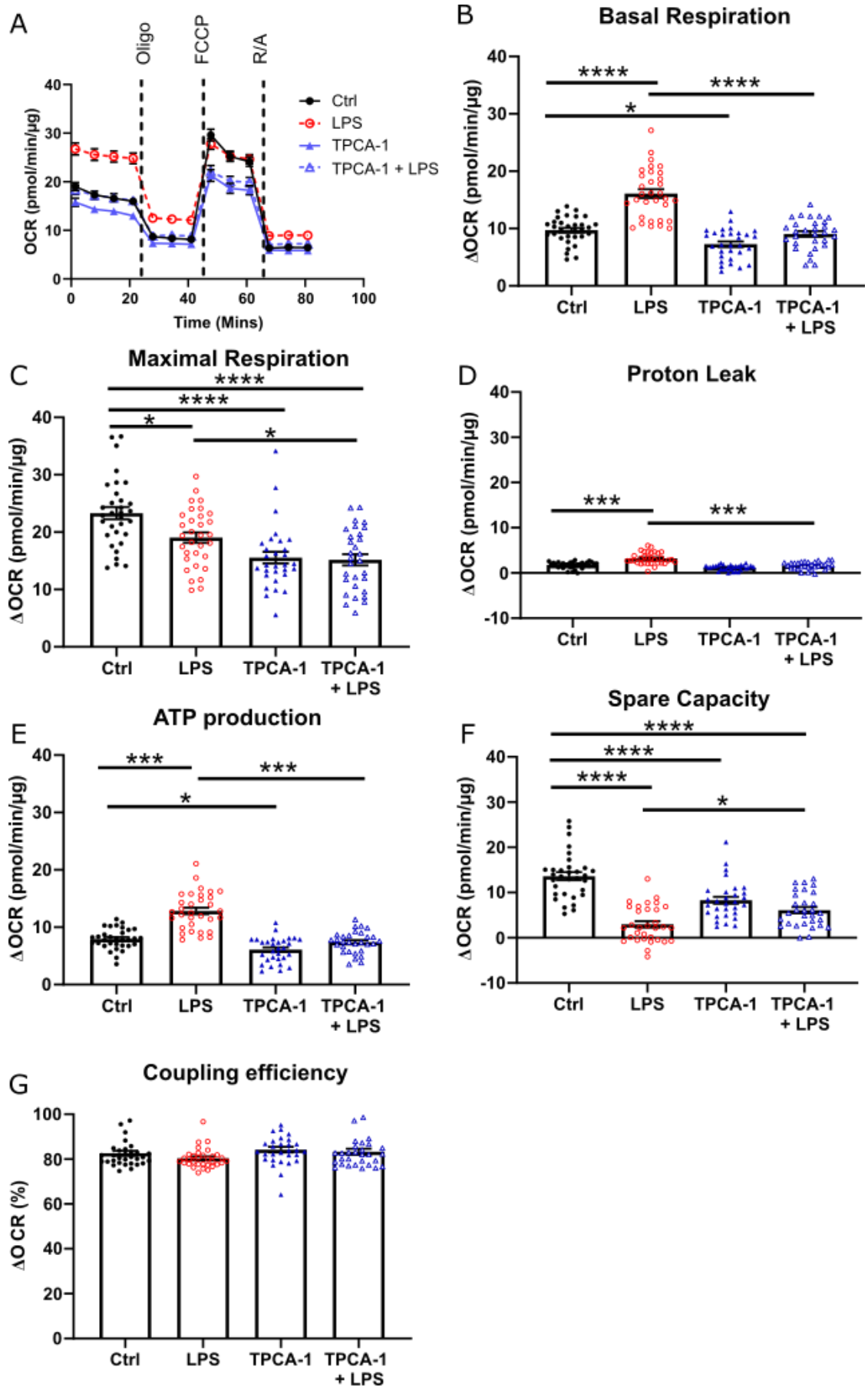
A
Oligo
FCCP
R/A
OCR (pmol/min/µg)
Time (Mins)
Ctrl
LPS
TPCA-1
TPCA-1 + LPS
B
Basal Respiration
ΔOCR (pmol/min/µg)
C
Maximal Respiration
D
Proton Leak
E
ATP production
F
Spare Capacity
G
Coupling efficiency
ΔO CR (%)

**Figure 4.3.8.1: NF-κB inhibition prevented LPS induced changes to mitochondrial metabolism in mouse primary astrocytes 24 hours after treatment.** Cells were seeded at a density of 4 x $10^4$ cells per well in Seahorse XF96 cell culture microplates. Oxidative phosphorylation, represented as oxygen consumption rate (OCR) of the cells was measured using the Seahorse BioAnalyzer XFe96 in conjunction with a Mito Stress Test (Agilent, UK). **A.** OCR of mouse primary cortical astrocytes during a Mito Stress Test 24 hours after 2 hour pre-treatment with NF-κB inhibitor, TPCA-1 (1 μM) ± lipopolysaccharide (LPS; 0.1 μg/mL) compared with vehicle treated control (0.017 mM fatty acid free bovine serum albumin/0.01% v/v DMSO). Oligo = 0.5 μM oligomycin, FCCP = 1 μM, R/A = 0.5 μM rotenone/antimycin. **B.** Basal respiration: difference in OCR prior to Oligo injection and after R/A injection. **C**. Maximal respiration: difference in OCR after injection of FCCP and after R/A injection. **D.** Proton leak: difference in OCR after Oligo injection and after R/A injection. **E.** ATP production: difference in OCR prior to Oligo injection and after Oligo injection. **F.** Spare capacity: difference in OCR between basal respiration (**B**) and maximal respiration (**C**). **G.** Coupling efficiency: percentage of basal respiration (**B**) used for ATP production (**E**). One-way ANOVA with post-hoc Tukey; **** $p<0.0001$, *** $p<0.001$, * $p<0.05$; n=30, 2 independent plates. Data are presented as mean ± standard error of the mean.

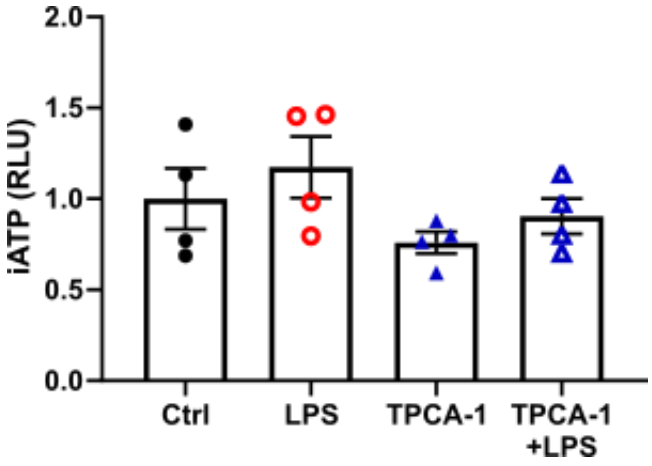


**Figure 4.3.8.2: Inhibition of NF-κB did not alter intracellular energy balance after 24 hours in mouse primary astrocytes.** Mouse primary astrocytes were seeded at a density of 4 x $10^3$ cells per well in black 96 well plates. Intracellular ATP (iATP) after treatment was estimated using the ATPLite TwoStep kit (PerkinElmer, UK). iATP represented as fold change in luminescence from the mean of vehicle treated controls (one-way ANOVA with post-hoc Tukey, $p>0.05$; $n=4$). Data are presented as mean ± standard error of the mean.

## 4.4 Discussion

In this chapter I have demonstrated that NF-κB signalling regulates metabolism in mouse primary astrocytes both during inflammation and independently from a pro-inflammatory stimulus. This data supports our hypothesis.

**Table 4.4.1 Summary of the astrocytic metabolic response to 3 hours LPS treatment after inhibiting NF-κB signalling**

| | Experimental measure | 3 hours | | |
|---|---|---|---|---|
| | | LPS | TPCA-1 + LPS | TPCA-1 |
| Glycolysis | Rate | Up | Restored | Down |
| | Capacity | Up | Restored | Down |
| | Reserve | Unchanged | Down | Down |
| Mitochondrial metabolism | Basal respiration | Unchanged | Up | Unchanged |
| | Maximal respiration | Unchanged | Unchanged | Unchanged |
| | Spare capacity | Unchanged | Unchanged | Unchanged |
| | ATP production | Unchanged | Up | Unchanged |
| | Proton leak | Unchanged | Unchanged | Unchanged |
| | Coupling efficiency | Unchanged | Up | Unchanged |

| | Table 4.4.2 Summary of the astrocytic metabolic response to 24 hours treatment with LPS after inhibiting NF-κB signalling | | | |
|---|---|---|---|---|
| | **Experimental measure** | **24 hours** | | |
| | | **LPS** | **TPCA-1 + LPS** | **TPCA-1** |
| **Glycolysis** | GLUT1 expression | Down | Restored | Unchanged |
| | Rate | Unchanged | Unchanged | Unchanged |
| | Capacity | Down | Restored | Unchanged |
| | Reserve | Down | Restored | Unchanged |
| **Mitochondrial metabolism** | Basal respiration | Up | Restored | Unchanged |
| | Maximal respiration | Down | Down | Down |
| | Spare capacity | Down | Partially restored | Down |
| | ATP production | Up | Restored | Down |
| | Proton leak | Up | Restored | Down |
| | Coupling efficiency | Unchanged | Unchanged | Unchanged |

### 4.4.1 NF-κB signalling regulates release of pro-inflammatory agents in astrocytes

The main receptor for LPS in astrocytes is TLR-4 (Gorina *et al.*, 2011; Lu *et al.*, 2008). This receptor activates multiple intracellular pro-inflammatory signalling pathways, including MAPKs, Akt and NF-κB (Lu *et al.*, 2008). NF-κB is activated through multiple mechanisms and an important regulatory mechanism is phosphorylation of Ser536 by IKK-β. Once phosphorylated NF-κB can translocate into the nucleus where it initiates transcription of target genes. In the model used here, the pro-inflammatory state caused by LPS was at least in part contributed

to by NF-κB signalling. Phosphorylation of NF-κB was induced by LPS at both 3 hours and 24 hours. Pharmacological inhibition of IKK-β with TPCA-1 reduced both NF-κB phosphorylation and release of TNF-α and IL-6, which are transcriptionally regulated by NF-κB (Collart *et al.*, 1990; Son *et al.*, 2008; Sparacio *et al.*, 1992). This has previously be demonstrated (Birrell *et al.*, 2005; Podolin *et al.*, 2005). However, it is worth noting that TPCA-1 has also been shown to inhibit STAT3, a transcription factor expressed in mouse primary astrocytes which plays a role in inflammatory signalling in other cell types (Nan *et al.*, 2014). Therefore a role for STAT3 in the mechanisms explored here cannot be ruled out. Additionally, TLR-4 acts through multiple signalling pathways which were not explored in this body of work. These may play an integral role in astrocyte immunometabolism, which may be reflected through reduced autocrine/paracrine signalling. To investigate the role of these pathways would require data that is not currently available.

### 4.4.2 NF-κB signalling regulates the metabolic response to inflammation in astrocytes

Inhibition of NF-κB signalling abolished the metabolic changes induced by pro-inflammatory stimuli. NF-κB signalling has been shown to increase translocation of GLUT transporters into the plasma membrane (Sommermann *et al.*, 2011). GLUT transporters are important regulators of glycolytic rate (Macheda *et al.*, 2005). As inhibition of NF-κB signalling with TPCA-1 abolished LPS-induced increases in glycolytic rate and capacity 3 hours after treatment, NF-κB-regulated changes to GLUT localisation may be the mechanism through which mouse primary astrocytes increase glycolysis during pro-inflammatory stimulation. To

confirm this, further investigation looking at subcellular localisation of GLUT1 and other glucose transporters after pro-inflammatory stimulation in these cells is required.

24 hours of LPS exposure significantly reduced glycolytic capacity and reserve, whilst basal mitochondrial metabolism was increased. These changes were attenuated by TPCA-1 pre-treatment, suggesting they were driven by NF-κB signalling. In other cell types, NF-κB promotes expression and stabilisation of p53 (Aleyasin *et al.*, 2004; Fujioka *et al.*, 2004; Mauro *et al.*, 2011). p53 expression reduces transcription of the glucose transporter GLUT1 (Johnson & Perkins, 2012; Mauro *et al.*, 2011; Schwartzenberg-Bar-Yoseph *et al.*, 2004; Wang *et al.*, 2018). Glucose uptake and GLUT1 expression were significantly reduced by 24 hours LPS treatment. This reduction in GLUT1 expression was abolished by TPCA-1 pre-incubation, suggesting glycolytic rate and capacity is reduced due to restricted glucose uptake due to NF-κB signalling increasing p53 activity and the subsequent suppression of GLUT1 expression. A restriction in glucose uptake through reduced GLUT1 expression may be a mechanism by which astrocytes attempt to reduce and/or resolve their inflammatory response via limiting glycolytic activity. The restoration of glycolytic capacity and rate after pre-incubation with TPCA-1 may also be in part due to intracellular glycogen stores being maintained as the cells have not experienced a period of increased glycolysis.

In the presence of p53, NF-κB promotes mitochondrial metabolism (Mauro *et al.*, 2011). p53 upregulates cytochrome oxidase II, a subunit of OXPHOS complex IV

(Matoba *et al.*, 2006). As the increase in basal mitochondrial metabolism was attenuated by TPCA-1, together these data may suggest that p53 is upregulated by NF-κB 24 hours after a pro-inflammatory stimulus. However, I did not directly measure p53 expression. This would be an interesting line of investigation to follow up, particularly in light of the role of p53 mutations in cancer, a disease which is well documented to have immunometabolic changes.

Although the evidence presented in this chapter suggests it is likely that p53 is the driving mechanism of the immunometabolic changes reported here, there are multiple other pathways by which NF-κB could be acting that should be considered. NF-κB has been shown to promote mitochondrial health. The NF-κB subunit p62, which has not been investigated in this body of work, mediates mitophagy in response to LPS stimulation (Zhong *et al.*, 2016). Mitophagy is the removal of damaged mitochondria through autophagy. Damaged mitochondria can recruit proteins that initiate apoptosis. Therefore, NF-κB driven mitophagy prevents apoptosis in response to mitochondrial damage. The work by Motori *et al.* and our previous data presented in Chapter 3 suggest that mitophagy may be important in astrocytes during inflammation (**fig 3.3.11**) (Motori *et al.*, 2013). NF-κB can also regulate mitochondrial dynamics in other cell types. Knock out of NF-κB regulators IKKα, IKKβ and NEMO from a mouse endothelial fibroblast cell line significantly reduced expression of OPA1, a major regulator of inner mitochondrial membrane fusion. Additionally, TNF receptors were shown to maintain mitochondrial fusion through OPA1 driven by NF-κB and STAT3 signalling in cardiomyocytes (Nan *et al.*, 2017). Together, this suggests that NF-κB signalling is important for mitochondrial fusion. However, I did not directly

explore the role of NF-κB on mitophagy and regulators of mitochondrial dynamics in these cells. This would be an interesting avenue for further study.

Beyond the regulation of mitochondrial dynamics, NF-κB signalling has been shown to regulate mitochondrial respiration through altering gene expression (Albensi, 2019). NF-κB binds the c-Myc promoter to increase expression of c-Myc (Ji *et al.*, 1994). C-myc is an important transcription factor which is essential for the expression of mitochondrial proteins such as components of electron transfer chain complexes I, II and IV, and therefore normal OXPHOS function (Agarwal *et al.*, 2019; Goetzman & Prochownik, 2018; Graves *et al.*, 2012; Li *et al.*, 2005; Wang *et al.*, 2015). However, as c-Myc activity and expression was not measured in this body of work I cannot confirm the involvement of this transcription factor in astrocyte immunometabolism.

### 4.4.3 NF-κB signalling maintains normal astrocyte metabolism in the absence of inflammatory stimulation

In the absence of a pro-inflammatory stimulus, I demonstrate here that there is still a low level of NF-κB p65 phosphorylation in mouse primary astrocytes. Although in our model this may be an artefact of low levels of stress induced by *in vitro* culture, there are studies suggesting that there is also a low level of NF-κB signalling present in astrocytes *in vivo* (Dresselhaus & Meffert, 2019). Interestingly, the data presented in this chapter suggests that NF-κB signalling is important for maintenance of normal metabolic function in the absence of a pro-inflammatory stimulus. TPCA-1 treatment in the absence of a pro-inflammatory stimulus reduced glycolytic rate compared to vehicle treated controls. This

suggests that NF-κB plays a role in glycolysis during normal metabolic function. As this decrease in rate was only evident after the addition of glucose, it may indicate that inhibition of NF-κB signalling in astrocytes reduces the ability of the cell to take up exogenous glucose, rather than reflecting an altered ability to utilise internal glycogen stores. This may suggest that inhibition of NF-κB reduces GLUT1, and other glucose transporters, insertion into the cellular membrane. This would support the previous speculation that the increase in glycolytic rate driven by NF-κB is due to GLUT1 insertion into the membrane. Again, this would need to be verified through investigating the subcellular localisation of GLUT transporters. However, the decrease in glycolytic rate after NF-κB inhibition is transient, as the glycolytic profile is restored to control levels after 24 hours. This suggests that astrocytes have compensatory mechanisms to ensure normal cellular function can be maintained. Therefore, although NF-κB is important for normal glycolytic flux, it does not appear to be essential.

After 24 hours inhibition of NF-κB signalling, mitochondrial metabolism is significantly decreased even in the absence of a pro-inflammatory stimulus. However, this is not evident 3 hours after NF-κB inhibition. This suggests that the role NF-κB plays in the maintenance of normal metabolic metabolism is in regulating transcription. Therefore, the absence of NF-κB signalling would not be evident until after autophagy of pre-existing proteins. However, the expression of many mitochondrial proteins is driven by promoters targeted by the transcription factor c-Myc during normal metabolism. As NF-κB promotes c-Myc transcription and expression, this may be the mechanism through which NF-κB maintains normal mitochondrial function (Ji *et al.*, 1994). No later time points were

investigated, so I cannot comment on whether there may be redundancy mechanisms for maintaining mitochondrial function, although it is highly probable.

Alternatively to translocating to the nucleus, the p65 NF-κB subunit can localise in the mitochondria after pro-inflammatory stimulation in the absence of tumour suppressor p53 (Cogswell *et al.*, 2003; Johnson *et al.*, 2011). This suppresses the transcription of mitochondrial genes and oxygen consumption through decreased cytochrome oxidase III expression. This is therefore a secondary mechanism through which NF-κB can regulate OXPHOS. To investigate whether this mechanism is playing a role in basal metabolism in these cells, employing methods to investigate subcellular localisation of p65 would be informative. Together, these data suggest that the low level of NF-κB phosphorylation plays a role in normal astrocyte metabolism.

## 4.5 Conclusion

This chapter demonstrates that the rapid and flexible glycolytic response to inflammatory insults in astrocytes was abolished through inhibition of canonical NF-κB signalling using the pharmacological inhibitor TPCA-1, implicating this pathway as a major regulator of inflammatory metabolism in astrocytes. Furthermore, pharmacological inhibition of NF-κB signalling was sufficient to impact basal glycolytic metabolism in astrocytes, independent of inflammation, suggesting an integral role for NF-κB in astrocyte resting metabolism. In support of the hypothesis, inhibition of glycolysis prevented cytokine release from astrocytes, and resulted in inhibition of NF-kB phosphorylation, suggesting that glycolysis in astrocytes is essential for maintaining an inflammatory response.

Together these data indicate that in astrocytes metabolic adaptations are necessary for the full inflammatory response to LPS and, in turn, inhibiting NF-κB signalling is sufficient to impact basal metabolism.

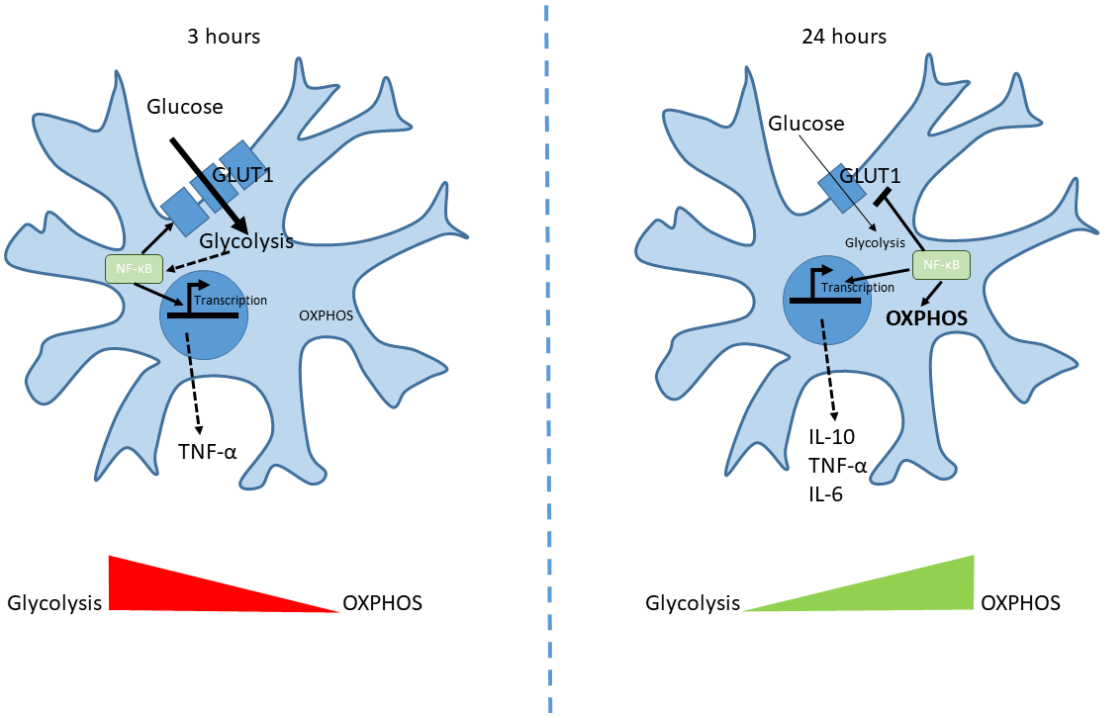


**Figure 4.5: Summary of chapter.** 3 hours after pro-inflammatory stimulus, astrocytes increase their use of glycolytic metabolism through NF-κB mediated mechanisms to allow the synthesis of cytokines. 24 hours after pro-inflammatory stimulus, NF-κB driven mechanisms decrease glycolytic rate through downregulation of GLUT1 expression, and NF-κB signalling increases oxidative phosphorylation.

# Chapter 5. TSPO as a regulator of astrocyte metabolism

## 5.1 Introduction

Translocator protein 18 kDa (TSPO) is an outer mitochondrial membrane (OMM) protein expressed in tissues throughout the body and highly conserved across kingdoms and phyla (Fan *et al.*, 2012). In mammals TSPO expression is significantly upregulated during pro-inflammatory conditions including within the brain, most notably in glial cells, including astrocytes (McNeela *et al.*, 2018). TSPO is also upregulated in many cancerous cells, including in gliomas (brain tumours) (Galiègue *et al.*, 2004; Janczar *et al.*, 2015; Miyazawa *et al.*, 1998). This has led to TSPO being used as a radioligand target for positron emission tomography (PET) imaging for neuroinflammatory conditions such as Alzheimer's disease (Edison *et al.*, 2018; Largeau *et al.*, 2017).

Interest in the function of TSPO increased when evidence began to emerge demonstrating anti-inflammatory and protective properties of some TSPO ligands. This suggested therapeutic potential in targeting TSPO (Arbo *et al.*, 2015). In cells in culture, TSPO ligands derived from a natural TSPO antagonist called quinazoline, such as PK11195, reduce LPS-induced microglial activation, reducing release of pro-inflammatory cytokines including TNF-α, IL-1β and IL-6 (Bae *et al.*, 2014; Biswas *et al.*, 2018). *In vivo* TSPO agonists have protective effects. Etifoxine reduces oedema after intracerebral haemorrhage in rodents,

promoting healing and reducing inflammation through an action on microglia, and reduces neuronal loss after traumatic brain injury in rats (Li *et al.*, 2017; Shehadeh *et al.*, 2019). TSPO agonist XBD-173 (emapunil, AC-5216) protects against neurodegeneration in a mouse model of Parkinson's disease, and retinal ischemia (Gong *et al.*, 2019; Mages *et al.*, 2019). Quinazoline-derived tricyclic compounds which modulate TSPO have also been reported to have protective effects on glioblastoma cells, preventing cell death from glutamate toxicity (Vainshtein *et al.*, 2015). Together these data suggest that modulation of TSPO activity is protective in neurological disease or after CNS injury.

For many years the primary function of TSPO was thought to be as a regulator of steroidogenesis due to its proposed role in transporting cholesterol into mitochondria (Papadopoulos *et al.*, 2018). As such, the CNS protective effects of TSPO ligands have been partially attributed to increased neurosteroid production (Dhir & Rogawski, 2012). However, recently the importance of TSPO in steroidogenesis *in vivo* has been called into question because, on the cellular and whole organism level, steroid production is maintained even in the absence of TSPO (Tu *et al.*, 2014). This suggests that the role of TSPO in regulating inflammation is probably partially independent of any contribution to steroidogenesis.

Emerging evidence from multiple independent research teams suggests that TSPO plays a role in regulating mitochondrial metabolism. For example, deletion of TSPO from MA-10 steroidogenic cells increases fatty acid oxidation (FAO) and the expression of genes associated with its regulation, including carnitine

palmitoyl transferase 1A (CPT-1A), the rate-limiting enzyme in this process (Tu *et al.*, 2016). Additionally, complementary independent data shows that systemic treatment with the TSPO antagonist PK11195 increases gene expression of CPT-1A in mice and zebrafish (Gut *et al.*, 2013). CPT-1A, like TSPO, is localised to the outer mitochondrial membrane where it is critical for mediating the transport of fatty acids into the mitochondrion for oxidation. As yet, the regulatory role of TSPO in astrocyte metabolism is unclear.

As further support of a potential role in regulating cellular metabolism, TSPO expression is upregulated in cancerous cells. In many cancers, cells undergo a metabolic shift termed the 'Warburg effect' characterised by increased aerobic glycolysis and lactate production, and a decrease in mitochondrial respiration (Vander Heiden *et al.*, 2009). I postulate that in this context the decrease in mitochondrial respiration may potentially be modulated through increased expression of TSPO.

Taken together these studies support an important regulatory role for TSPO in suppressing fatty acid metabolism potentially by regulating CPT-1A activity. These data may suggest that the anti-inflammatory and protective action of TSPO ligands observed by others may be driven through TSPO-mediated regulation of cellular metabolism, which may be a promising therapeutic target for reducing inflammation in astrocytes.

## 5.2 Hypothesis

I hypothesise that the anti-inflammatory actions of TSPO ligands are driven by modulation of cellular metabolism via an interaction with CPT-1A. By understanding the role of TSPO in astrocyte metabolism I hope to further development of therapies for CNS disease.

## 5.3 Results

### 5.3.1 TSPO expression was upregulated after 24 hours in LPS treated mouse primary astrocytes

TSPO expression has been reported to be upregulated in response to inflammation in many cell types, both *in vivo* and *in vitro* (McNeela *et al.*, 2018). To confirm that TSPO expression was regulated during inflammation in mouse primary astrocytes, the cells were exposed to LPS for 3 hours or 24 hours, and protein lysates were immunoblotted to quantify relative expression of TSPO. 3 hours after LPS treatment there was no significant change in TSPO expression compared with vehicle treated cells (**fig. 5.3.1A & B**). However, TSPO expression was significantly increased (40% increase; **fig. 5.3.1C & D;** p=0.0396) after 24 hours of exposure to LPS.

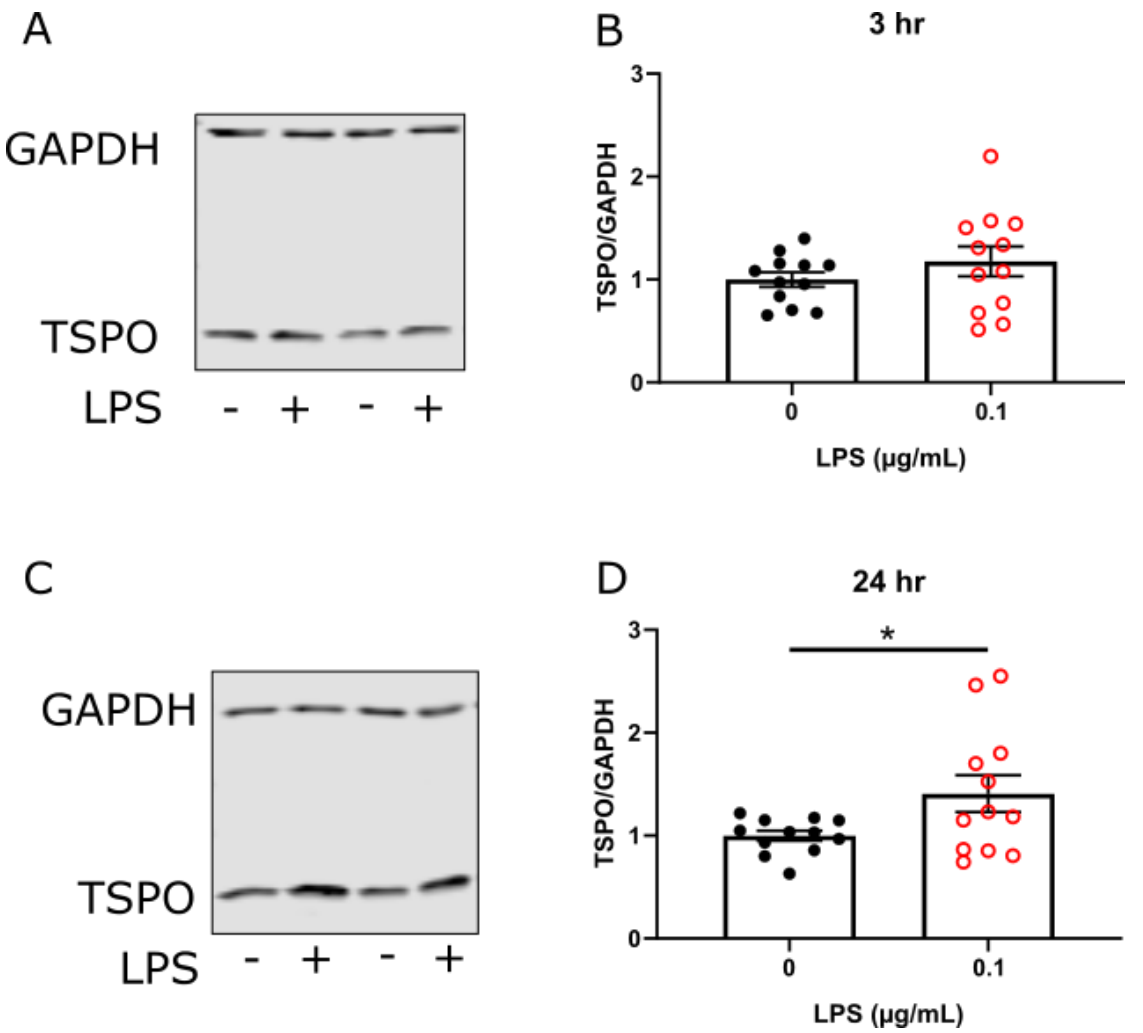


**Figure 5.3.1: TSPO expression in mouse primary astrocytes was increased after 24 hours of LPS treatment.** Mouse primary astrocytes were seeded at a density of 4.5 x $10^5$ cells per dish in 60 mm dishes prior to treatment with lipopolysaccharide (LPS; 0.1 µg/mL) or vehicle. Cells were lysed and protein collected for immunoblotting. **A.** Representative immunoblot of TSPO expression with GAPDH loading control after 3 hours treatment with LPS. **B.** Densitometric analysis of **A** as fold change from mean of vehicle treated controls. **C.** Representative immunoblot of TSPO expression with GAPDH loading control after 24 hours LPS treatment. **D.** Densitometric analysis of **C** as fold change from mean of vehicle treated controls. Unpaired t-test, * p>0.05; n=12. Data are expressed as mean ± standard error of the mean.

### 5.3.2 TSPO expression in mouse primary astrocytes was decreased following inhibition of glycolysis with 2-DG

As demonstrated in Chapters 3 and 4 of this thesis, mouse primary astrocytes have a metabolic response to LPS-induced inflammation. As TSPO is regulated during inflammation, I investigated whether TSPO expression could be regulated by metabolic fluctuations independent of inflammatory activation. After 24 hours of treatment, TSPO expression was decreased significantly by the glycolytic inhibitor 2-DG (50% reduction; p=0.0016), but was not modulated by the AMP kinase (AMPK) activator AICAR (**fig. 5.3.2**). Treatment with 0.1 µg/mL LPS was used as a positive control (50% increase; p=0.0013).

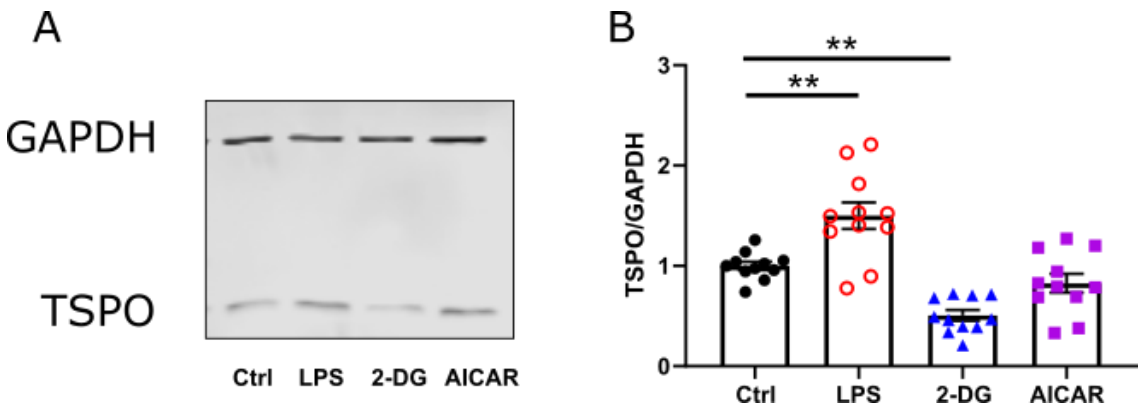


**Figure 5.3.2: TSPO expression was reduced following inhibition of glycolysis with 2-DG but unchanged by activation of the major metabolic regulator AMPK.** Mouse primary astrocytes were seeded at a density of 4.5 x $10^5$ cells per dish in 60 mm dishes prior to treatment or vehicle. Cells were lysed and protein collected for immunoblotting. **A.** Representative immunoblot of TSPO expression with GAPDH loading control after 24 hours treatment with lipopolysaccharide (LPS; 0.1 µg/mL), 2-deoxyglucose (2-DG; 10 mM), or AMPK activator AICAR (1 µM). **B.** Densitometric analysis of **A** as fold change from mean of vehicle treated controls. One-way ANOVA with post-hoc Tukey, ** $p<0.01$; n=11. Data are expressed as mean ± standard error of the mean.

### 5.3.3 TSPO ligands did not cause cell death after 24 hours

To ensure the concentrations of TSPO ligands used in the forthcoming studies were not causing cell death, cell viability was measured after 24 hours of treatment by measuring propridium iodide exclusion using flow cytometry. The TSPO antagonist PK11195 (**fig. 5.3.3.1;** 50 nM) did not cause significant cell death. The TSPO agonist XBD-173 (**fig. 5.3.3.2;** 50 µM) decreased cell viability by 3.4% after 24 hours of treatment compared to DMSO vehicle treated controls ($p=0.02$). However, while statistically significant, this low percentage of cell death is unlikely to be responsible for the magnitude of change seen in other experiments using this ligand.

Further studies in this chapter used 25 nM PK11195, as the $K_D$ (equilibrium dissociation constant) of the compound is reported as 7.4 ± 3 nM, reported as and concentrations greater than 1 µM of PK11195 are reported to have off-target effects, including inhibiting ATP synthesis (Hatty *et al.*, 2014; Cleary *et al.*, 2007; James *et al.,* 2006; Kita *et al.*, 2004; Lacapère *et al.*, 2001). Although the $K_i$ (inhibitory constant) of XBD-173 is reported as 0.297 ± 0.009 nM (when displacing [$^3$H]-PK11195), XBD-173 was used at 25 µM to enable comparison with previously published literature while minimising cell death (Biswas *et al.*, 2018; Karlstetter *et al.*, 2014; Kita *et al.*, 2004; Ravikumar *et al.*, 2016).

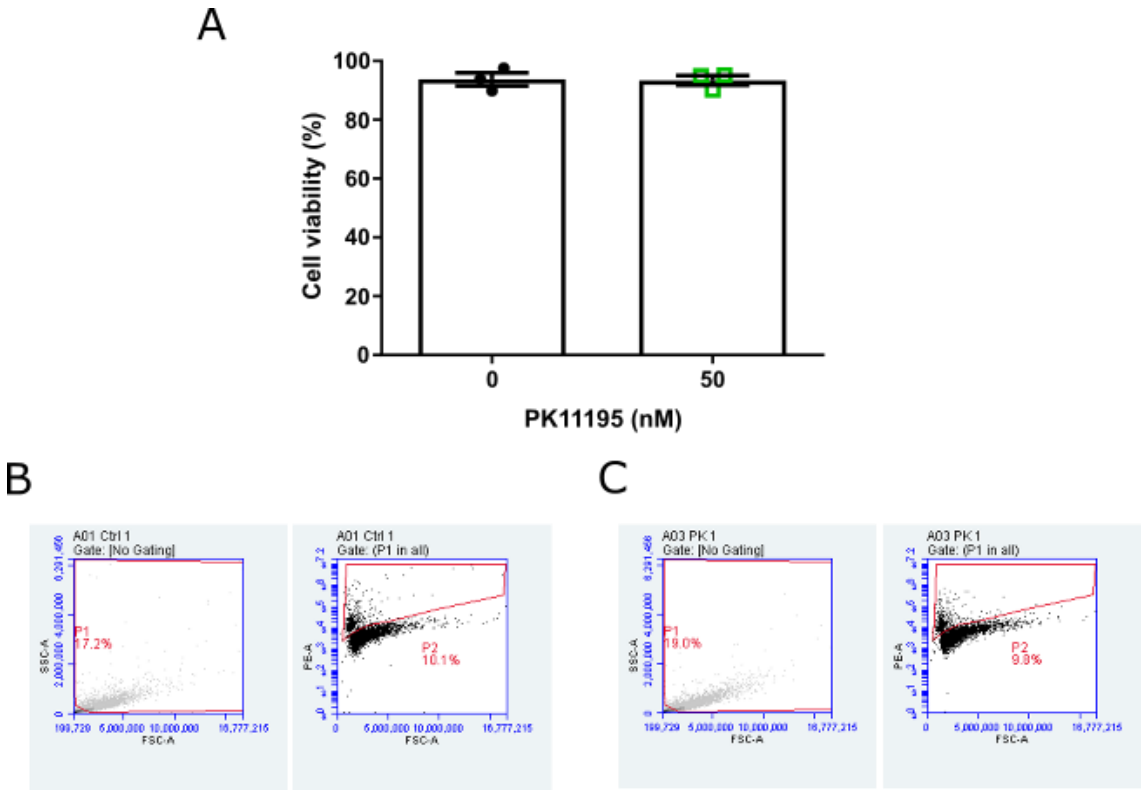


**Figure 5.3.3.1: The TSPO ligand PK11195 did not decrease viability of mouse primary astrocytes after 24 hours of treatment.** Cells were seeded at a density of 3.5 x $10^5$ cells per well in a 6 well plate. After treatment with LPS, cells were dissociated and stained with 2 µg/mL propidium iodide prior to analysis with the BD Accuri C6 Plus flow cytometer. **A.** Percentage of cells excluding propidium iodide 24 hours after treatment with PK11195 (50 nM). Unpaired t-test; n=3. Data are expressed as mean ± standard error of the mean. **B-C.** Gating used to define events. Plot 2 region of interest P2 defined non-viable cells from plot 1 region of interest P1. Example collection plots contain data from control (**B**) and PK11195 (**C**; 50 nM) treated cells.

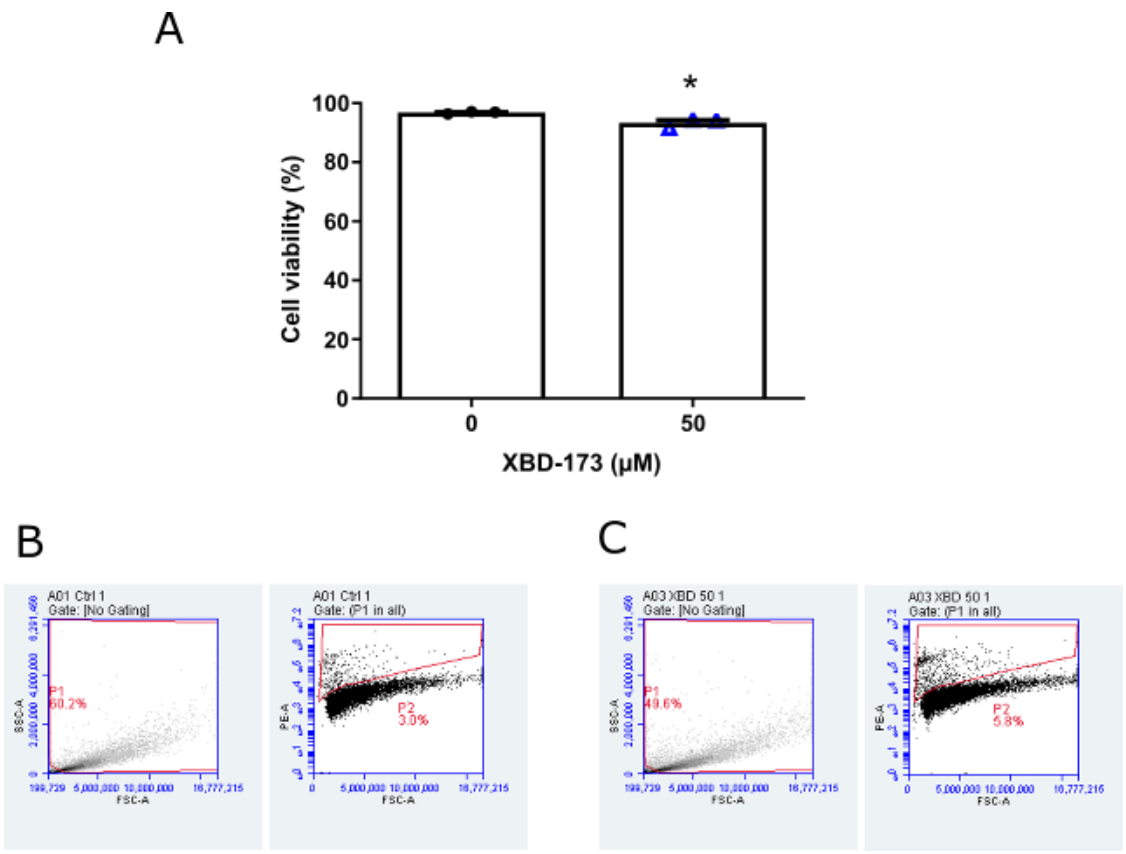


**Figure 5.3.3.2: The TSPO ligand XBD-173 did not have a major impact on viability of mouse primary astrocytes after 24 hours of treatment.** Cells were seeded at a density of 3.5 x $10^5$ cells per well in a 6 well plate. After treatment with LPS, cells were dissociated and stained with 2 µg/mL propidium iodide prior to analysis with the BD Accuri C6 Plus flow cytometer. **A.** Percentage of cells excluding propidium iodide 24 hours after treatment with XBD-173 (50 µM). Unpaired t-test, * $p<0.05$; n=3. Data are expressed as mean ± standard error of the mean. **B-C.** Gating used to define events. Plot 2 region of interest P2 defined non-viable cells from plot 1 region of interest P1. Example collection plots contain data from control (**B**) and XBD-173 (**C;** 50 µM) treated cells.

### 5.3.4 TSPO ligands did not reduce inflammation in mouse primary astrocytes

There have been several reports from *in vivo* models that TSPO ligands reduce inflammation, including in the CNS (Bae *et al.*, 2014; Biswas *et al.*, 2018; Daugherty *et al.*, 2013). ELISAs against TNF-α and IL-10 were used to measure cytokine release from astrocytes after LPS treatment in the presence or absence of TSPO ligands. LPS increased astrocyte TNF-α release after 3 hours ($p<0.0001$). However, neither PK11195 (**fig. 5.3.4.1A;** 25 nM) nor XBD-173 (**fig. 5.3.4.1B;** 25 μM) reduced this LPS-induced TNF-α release. LPS increased IL-10 release after 24 hours ($p<0.0001$). While PK11195 had no impact (**fig. 5.3.4.2A**), XBD-173 significantly reduced LPS-induced IL-10 from astrocytes by 85.3% (**fig. 5.3.4.2B;** $p<0.0001$).

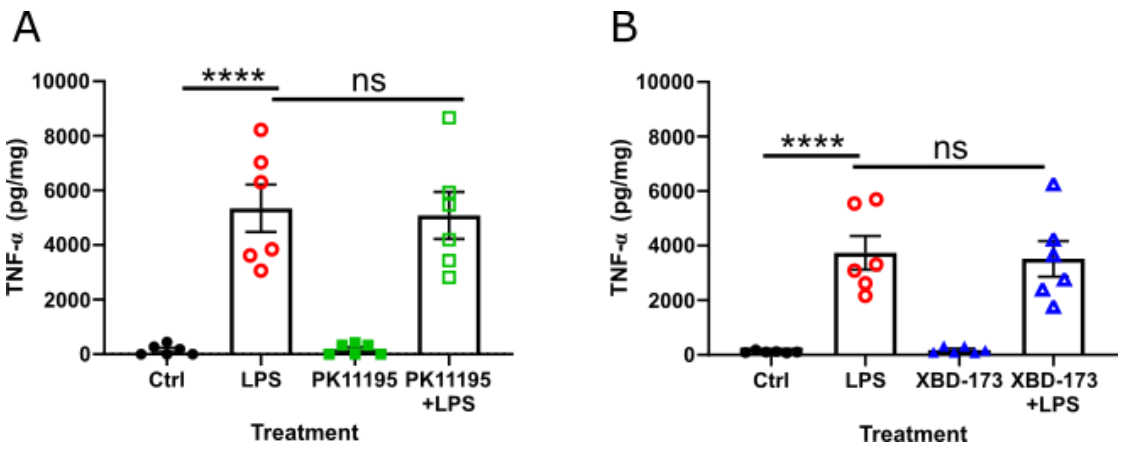


**Figure 5.3.4.1: TSPO ligands did not change LPS-induced TNF-α release from mouse primary astrocytes.** Mouse primary astrocytes were seeded at a density of 4.5 x $10^5$ cells per dish in 60 mm dishes prior to treatment or vehicle. Conditioned media was collected and used for estimation of extracellular cytokine concentrations using DuoSet ELISAs (BioTechne, UK). **A.** TNF-α release from mouse primary astrocytes after 1 hour PK11195 (25 nM) pre-treatment and 3 hours lipopolysaccharide (LPS; 0.1 µg/mL) treatment (n=6). **B.** TNF-α release from mouse primary astrocytes after 1 hour XBD-173 (25 µM) pre-treatment and 3 hours LPS treatment (n=6). One-way ANOVA with post-hoc Tukey, *** $p<0.001$, ns $p>0.05$. Data are presented as mean ± standard error of the mean.

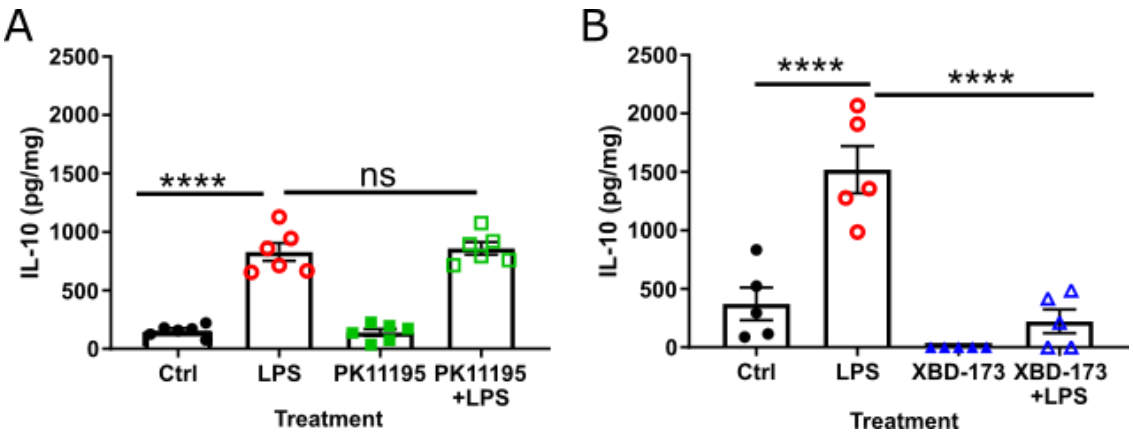


**Figure 5.3.4.2: TSPO ligands had differential effects on LPS-induced IL-10 release from mouse primary astrocytes.** Mouse primary astrocytes were seeded at a density of 4.5 x $10^5$ cells per dish in 60 mm dishes prior to treatment or vehicle. Conditioned media was collected and used for estimation of extracellular cytokine concentrations using DuoSet ELISAs (BioTechne, UK). **A.** IL-10 release from mouse primary astrocytes after 1 hour PK11195 (25 nM) pre-treatment and 24 hours lipopolysaccharide (LPS; 0.1 µg/mL) treatment (n=6). **B.** IL-10 release from mouse primary astrocytes after 1 hour XBD-173 (25 µM) pre-treatment and 24 hours LPS treatment (n=5). One-way ANOVA with post-hoc Tukey, **** $p<0.0001$, ns $p>0.05$. Data are presented as mean ± standard error of the mean.

### 5.3.5 TSPO ligands altered basal metabolism in mouse primary astrocytes

Mouse primary astrocytes were treated with TSPO ligands for 1 hour prior to measuring basal extracellular acidification rate (ECAR) as a measure of glycolysis and basal oxygen consumption rate (OCR) as a measure of mitochondrial metabolic function. TSPO antagonist PK11195 (25 nM) significantly increased ECAR by 52% (**fig. 5.3.5.1C-D;** p=0.0052), and OCR by 62% (**fig. 5.3.5.1A-B;** p=0.0133). Conversely TSPO agonist XBD-173 (50 µM) significantly decreased ECAR by 35% (**fig. 5.3.5.2C-D;** p=0.001). XBD-173 (50 µM) significantly reduced OCR by 57% compared to control (**fig. 5.3.5.2A-B;** p=0.0001). However, lower concentrations of XBD-173 (25 µM) did not alter either OCR or ECAR after 1 hour of treatment (**fig. 5.3.5.2C-D**). Although basal metabolism was altered within an hour, mitochondrial membrane potential, measured by TMRE uptake, was not altered 1 hour after treatment with TSPO ligands (**fig. 5.3.5.3**), in contrast to the positive control FCCP which caused a 71% reduction (P<0.0001). Glucose uptake was also unaltered 1 hour after treatment with TSPO ligands (**fig. 5.3.5.4**).

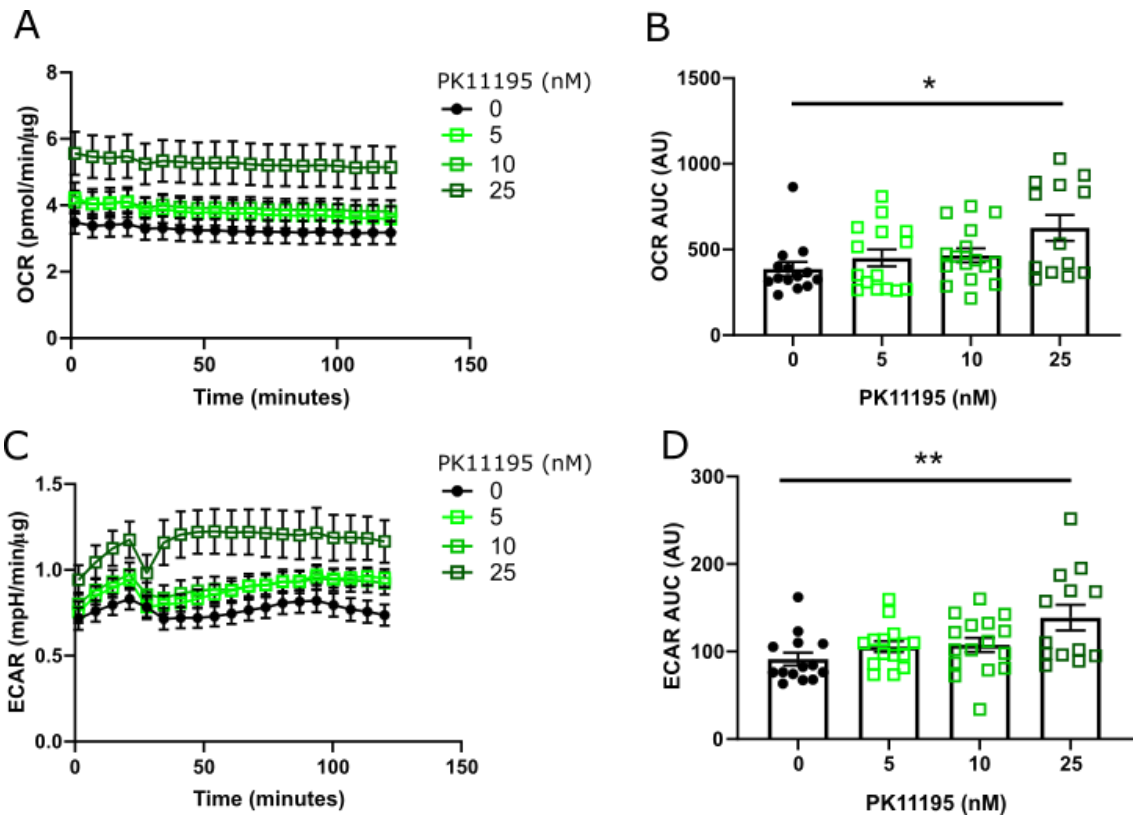


**Figure 5.3.5.1: TSPO ligands altered basal metabolic rate in mouse primary astrocytes.** Cells were seeded at a density of 4 x $10^4$ cells per well in Seahorse XF96 cell culture microplates. After 1 hour pre-treatment, oxidative phosphorylation rate, represented as oxygen consumption rate (OCR) and glycolysis represented as extracellular acidification rate (ECAR) of the cells were measured using the Seahorse BioAnalyzer XFe96. **A.** OCR after 1 hour pre-treatment with PK11195 (n=14-16). **B.** Area under the curve (AUC) of A. **C.** ECAR after 1 hour pre-treatment with PK11195 (n=14-16). **D.** AUC of C. One-way ANOVA with post-hoc Tukey, ** $p<0.01$, * $p<0.05$. Data are presented as mean ± standard error of the mean.

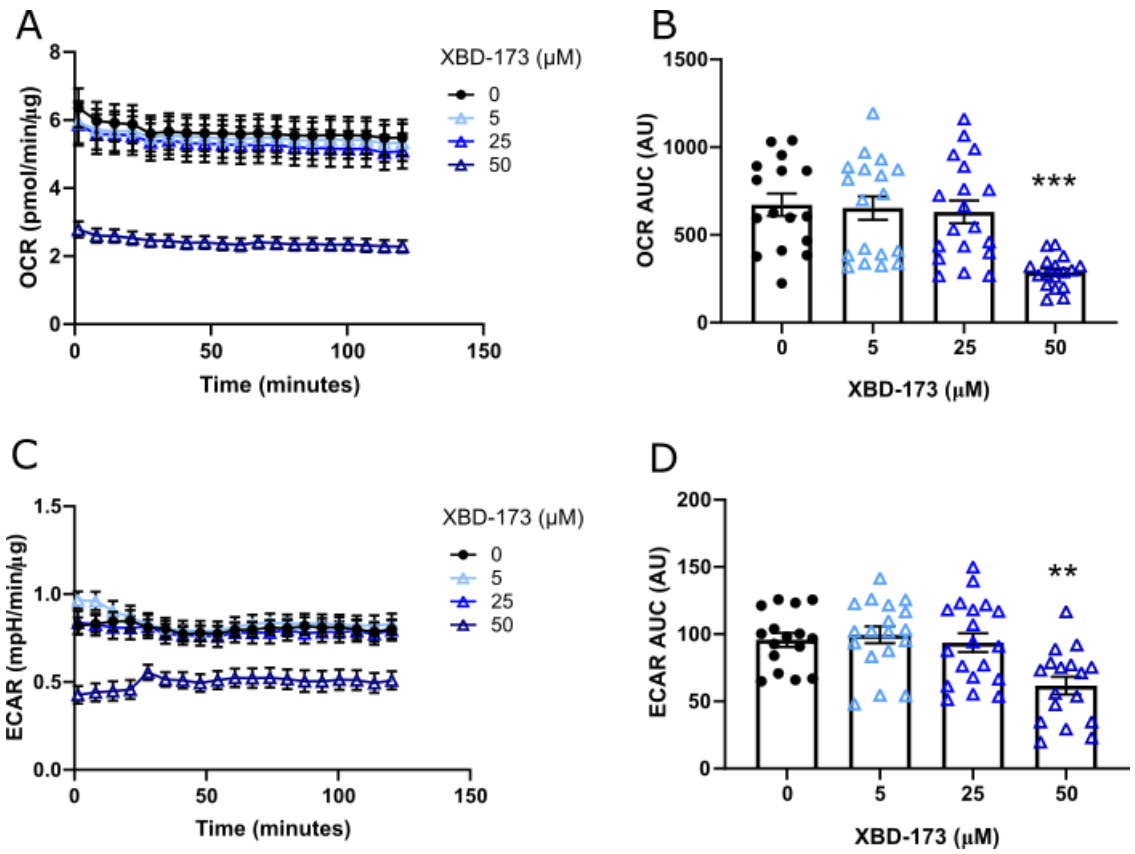


**Figure 5.3.5.2: TSPO ligands altered basal metabolic rate in mouse primary astrocytes.** Cells were seeded at a density of 4 x $10^4$ cells per well in Seahorse XF96 cell culture microplates. After 1 hour pre-treatment, oxidative phosphorylation rate, represented as oxygen consumption rate (OCR) and glycolysis represented as extracellular acidification rate (ECAR) of the cells were measured using the Seahorse BioAnalyzer XFe96. **A.** Mitochondrial metabolic rate represented by oxygen consumption rate (OCR) after 1 hour pre-treatment with XBD-173 (n=16-18). **B.** Area under the curve (AUC) of A. **C.** Glycolytic rate represented by the extracellular acidification rate (ECAR) after 1 hour pre-treatment with XBD-173 (n=16-18). **D.** AUC of C. One-way ANOVA with post-hoc Tukey, *** $p<0.001$, ** $p<0.01$. Data are presented as mean ± standard error of the mean.

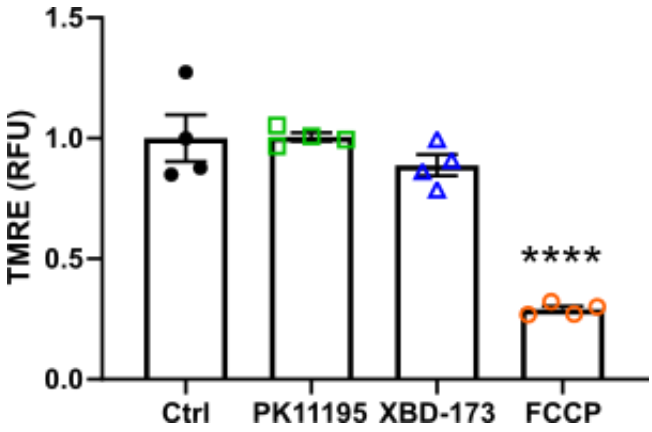


**Figure 5.3.5.3: TSPO ligands did not alter mitochondrial membrane potential.** TMRE uptake by mouse primary astrocytes after 1 hour incubation with PK11195 (25 nM) or XBD-173 (25 µM), relative to DMSO vehicle treated control. FCCP (1 µM) used as positive depolarisation control. Cells were seeded at a density of 3.5 x $10^5$ cells per well in a 6 well plate. After treatment with LPS, cells were dissociated and incubated with FCCP prior to incubation with TMRE (100 nM) and analysis with the BD Accuri C6 Plus flow cytometer. One-way ANOVA with post hoc Tukey, **** $p<0.0001$; n=4. Data are presented as mean ± standard error of the mean.

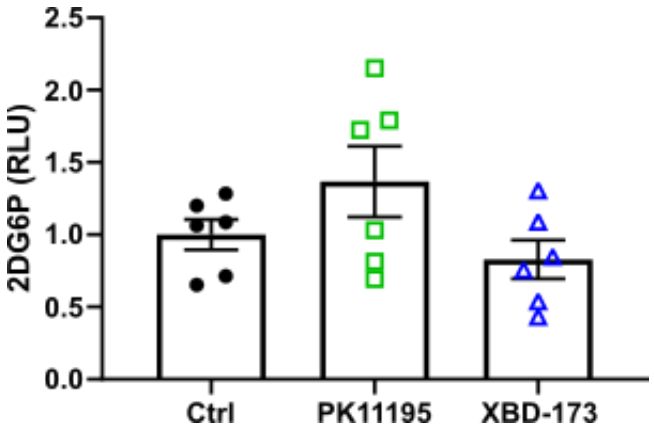


**Figure 5.3.5.4: TSPO ligands did not alter glucose uptake rate.** Mouse primary astrocytes were seeded at a density of 4 x $10^4$ cells per well in 96 well plates. Glucose uptake rate after treatment with lipopolysaccharide (LPS) was estimated using the Glucose Uptake-Glo kit (Promega, UK). Glucose uptake by mouse primary astrocytes was represented as fold change 2-deoxyglucose-6-phosphate (2DG6P) luminescence after 1 hour incubation with PK11195 (25 nM) or XBD-173 (25 µM), relative to mean of contemporaneous DMSO vehicle treated controls. One-way ANOVA with post hoc Tukey; n=6. Data are presented as mean ± standard error of the mean.

### 5.3.6 The TSPO ligand XBD-173 increased fatty acid oxidation

Modulation of TSPO activity impacts fatty acid metabolism in other cell types (Gut *et al.*, 2013; Kim *et al.*, 2019; Tu *et al.*, 2016). To explore this in astrocytes, mouse primary astrocytes treated for 1 hour with TSPO ligands were evaluated in the Seahorse bioanalyser using a fatty acid oxidation (FAO) Mito Stress Test, as described in the methods. By limiting access to glucose and pyruvate overnight, and providing carnitine and exogenous fatty acids in the form of palmitate (C16), the cells decrease glucose metabolism and increase dependency on fatty acid metabolism. By blocking fatty acid transport into the mitochondria in some of the cells using CPT-1 inhibitor etomoxir (40 μM), this assay allows quantification of oxygen consumption specifically attributable to oxidation of fatty acids (see **fig. 2.2.12.4**). Treatment with PK11195 did not alter the basal or maximal rate of FAO compared to vehicle treated controls (**fig. 5.3.6A, C & D**). However, treatment with XBD-173 increased basal FAO rate by 219.6% (**fig. 5.3.6B & C;** p=0.005) and maximal respiration by 152.8% (**fig. 5.3.6B & D;** p=0.0019) compared to vehicle treated controls.

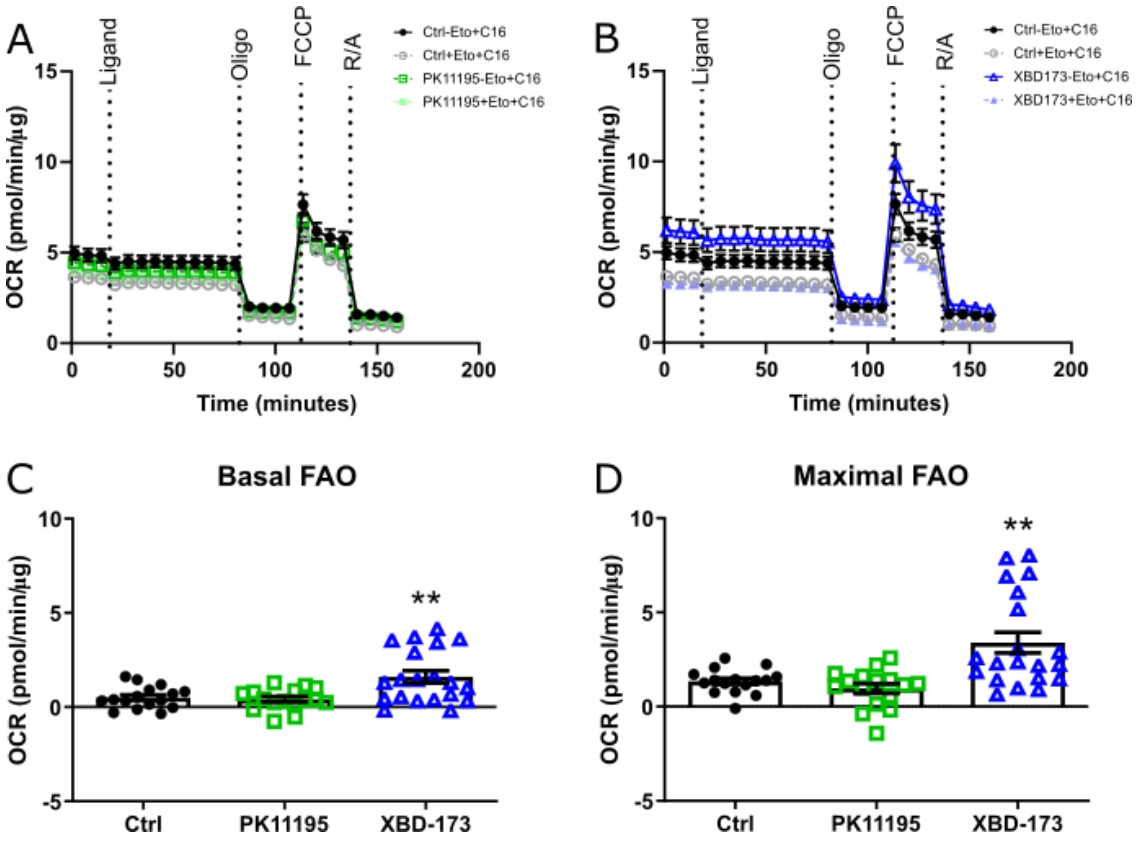
A
Ligand
Oligo
FCCP
R/A
Ctrl-Eto+C16
Ctrl+Eto+C16
PK11195-Eto+C16
PK11195+Eto+C16
OCR (pmol/min/µg)
Time (minutes)
B
Ligand
Oligo
FCCP
R/A
Ctrl-Eto+C16
Ctrl+Eto+C16
XBD173-Eto+C16
XBD173+Eto+C16
OCR (pmol/min/µg)
Time (minutes)
C
Basal FAO
OCR (pmol/min/µg)
**
Ctrl
PK11195
XBD-173
D
Maximal FAO
OCR (pmol/min/µg)
**
Ctrl
PK11195
XBD-173

**Figure 5.3.6: TSPO ligand XBD-173 increased fatty acid oxidation rate in mouse primary astrocytes.** Cells were seeded at a density of 4 x $10^4$ cells per well in Seahorse XF96 cell culture microplates. Oxidative phosphorylation, represented as oxygen consumption rate (OCR) of the cells was measured using the Seahorse BioAnalyzer XFe96 in conjunction with a fatty acid oxidation (FAO) Mito Stress Test (Agilent, UK). **A.** Time course of FAO Mito Stress test in PK11195 treated mouse primary astrocytes. **B.** Time course of FAO Mito Stress test in XBD-173 treated mouse primary astrocytes. Ligands [PK11195 (25 nM) or XBD-173 (25 µM)], oligomycin (oligo; 0.5 µM), FCCP (1 µM), and rotenone/antimycin (R/A; 0.5 µM) were added as indicated by vertical dotted lines. Palmitate (200µM; C16) was added at time = 0. **C.** Basal FAO rate calculated as the difference in OCR between etomoxir treated negative controls (eto; 40 µM) and the comparable treatment group immediately prior to addition of oligo. **D.** Maximal FAO rate calculated as the difference in OCR between etomoxir treated negative controls (eto; 4 µM) and the comparable treatment group after addition of FCCP. One-way ANOVA with post hoc Tukey, ** $p<0.01$. n=19-21. Data are presented as mean ± standard error of the mean.

### 5.3.7 TSPO knock out astrocytes did not express TSPO

Due to concerns about potential off-target effects of TSPO ligands, TSPO knock out models were employed to further explore the role of the protein in cellular metabolism and verify the specificity of the TSPO ligands (Bader *et al.*, 2019; Cleary *et al.*, 2007). Two different models were used: primary astrocytes derived from mice with germline knock out of TSPO ($TSPO^{-/-}$) and a CRISPR/Cas9 gene edited TSPO-deficient human astroglioma cell line (U373).

Mouse $TSPO^{-/-}$ astrocytes were used to more directly compare with the data collected in mouse primary astrocytes using ligands. These cells were untransformed so were less likely to display phenotypic drift than frequently passaged immortalised cell lines. This means the cells may behave more closely to how they would behave *in vivo*. Additionally, to complement the data collected with mouse primary astrocytes and TSPO ligands it was important to use astrocytes from the same species, particularly as has been shown that human astrocytes behave differently to mouse astrocytes (Oberheim *et al.*, 2009). The transformed U373 cell line was also used as there is evidence in the literature that TSPO is highly expressed in cancer cells, such as astrogliomas. Therefore, studying the function of TSPO in the human astroglioma U373 cell line was an interesting model for studying TSPO in the context of a cancer cell.

Germline heterozygous ($TSPO^{+/-}$) mice were imported from MRC Harwell from mice re-derived from sperm obtained from the Infrafrontier European Mutant Mouse Archive and used to establish a breeding colony in Exeter. Astrocytes from $TSPO^{-/-}$ animals of both sex were used and compared to wild-type ($TSPO^{+/+}$)

littermates. TSPO expression was verified in $TSPO^{+/+}$ and $TSPO^{-/-}$ mouse primary astrocytes using immunoblotting (**fig. 5.3.7A**). GFAP expression was used to confirm the lysates were from astrocytes (**fig. 5.3.7B**).

The U373 CRISPR/Cas9 TSPO deficient cell line was created by Daisy Stewart as part of her professional training year project in the Ellacott lab under the guidance of Dr Rosie Bamford and Dr Asami Oguro-Ando. TSPO expression was verified in the unmodified control (WT), empty vector (EV) and TSPO deficient (KO) cells using immunoblotting by Daisy Stewart under my guidance (**fig. 5.3.7C**).

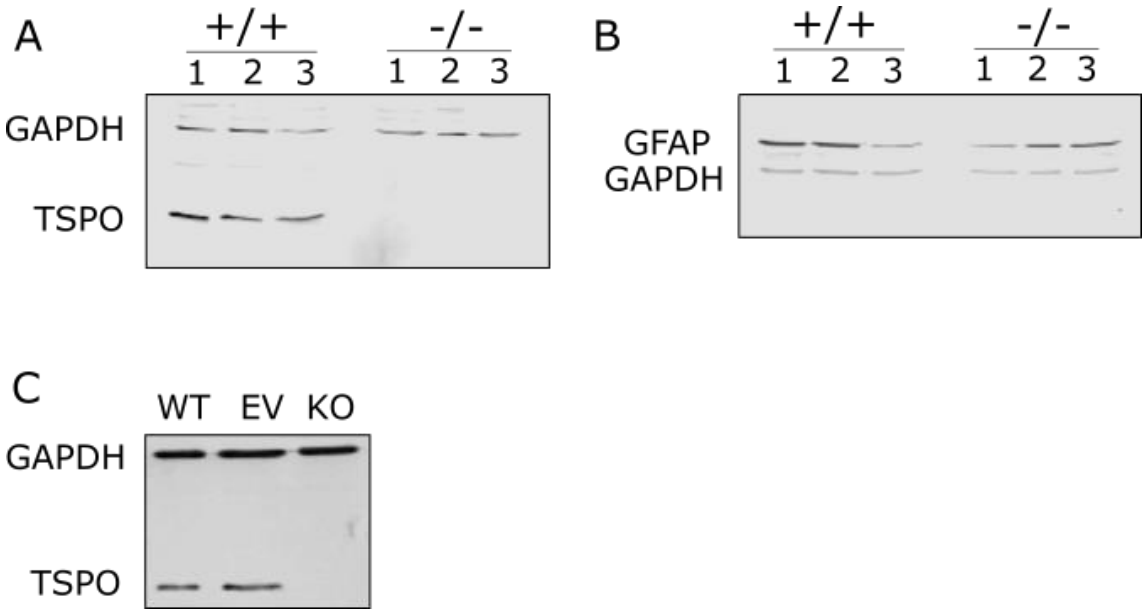


**Figure 5.3.7: The genetically modified cells used did not express TSPO**

Mouse primary astrocytes or U373 astroglioma cells were seeded at a density of 4.5 x $10^5$ cells per dish in 60 mm dishes prior to lysis. Protein collected for immunoblotting. **A.** Immunoblot of TSPO expression in mouse primary astrocytes from $TSPO^{+/+}$ and $TSPO^{-/-}$ mice. GAPDH was used as a loading control. **B.** Immunoblot of GFAP expression in mouse primary astrocytes from $TSPO^{+/+}$ and $TSPO^{-/-}$ mice. GAPDH was used as a loading control. Columns (1-3) indicate independent samples from different animals (same samples used in panels A and B). **C.** Immunoblot of TSPO expression in U373 lysates from untransfected cells (WT), cells transfected with an empty CRISPR/Cas9 vector (EV), and transfected with a CRISPR/Cas9 vector containing guide RNA (KO). GAPDH was used as a loading control.

### 5.3.8 TSPO expression was higher in U373 astrocytoma cells than in mouse primary astrocytes

To assess baseline differences between the two models used, TSPO expression was compared in 10 µg of lysate from a number of different glial cell types in culture. Subjectively, TSPO expression appeared to be higher in U373 astroglioma cells compared to mouse primary astrocytes (CRT). Although equal quantities of protein were loaded TSPO expression could not be accurately quantified due to the significant variation in GAPDH expression between cell types (**fig. 5.3.8;** immunoblot performed by Daisy Stewart under my supervision). Whilst this difference in TSPO expression is interesting, and something to bear in mind when considering the other data sets collected in these cell types this experiment would need further repeats, including an appropriate loading control of total protein to be able to draw conclusions from it. Out of interest, human primary astrocytes (HPA) and mouse microglia (BV-2) cell lines were also compared, and found to express TSPO; however, these are not explored further in this thesis.

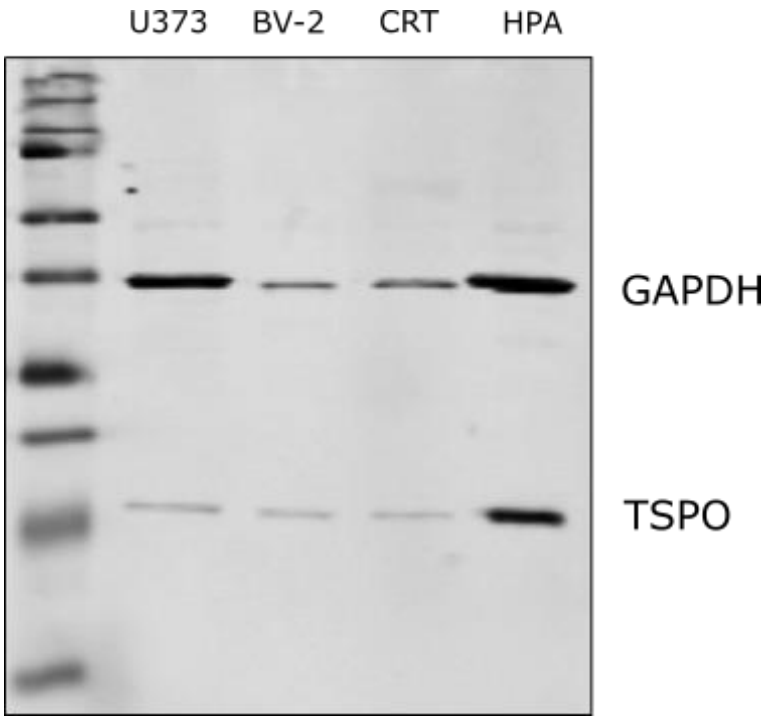


**Figure 5.3.8: TSPO was differentially expressed in different glial cell types.** Immunoblot of TSPO expression in 10 µg protein lysate from human astroglioma (U373), mouse microglia (BV-2), mouse primary astrocytes (CRT), and human primary astrocytes (HPA). GAPDH was used as a loading control. Cells were seeded at a density of 4.5 x $10^5$ cells per dish in 60 mm dishes prior to lysis and protein collection for immunoblotting.

### 5.3.9 Basal metabolic parameters were different in U373 and mouse primary astrocytes

To assess whether U373 human astrocytoma and mouse primary astrocytes had different basal metabolic phenotypes they were directly compared using the Seahorse metabolic analyser by Daisy Stewart under my supervision. Compared with mouse primary astrocytes, U373 cells had 40.7% lower mitochondrial respiration (**fig. 5.3.9A;** $p<0.0001$) but 56.3% higher glycolytic rate (**fig. 5.3.9B;** $p=0.0003$). This suggests that in line with what is reported in many cancer cell types, U373 cells are more reliant on glycolysis than mouse primary astrocytes, which showed comparatively higher OXPHOS (DeBerardinis & Chandel, 2016).

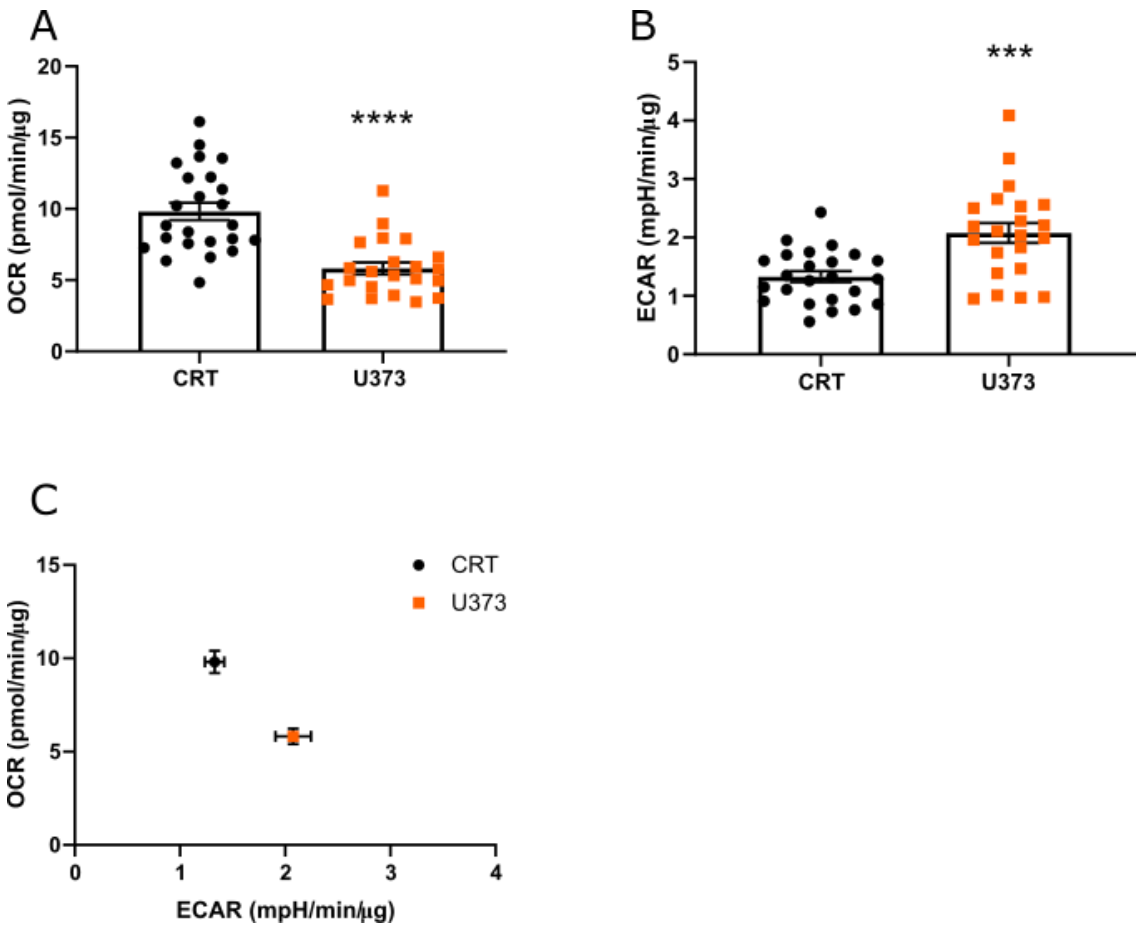


**Figure 5.3.9: U373 astroglioma cells and mouse primary astrocytes had different metabolic phenotypes.** Cells were seeded at a density of 4 x $10^4$ cells per well in Seahorse XF96 cell culture microplates. Oxidative phosphorylation rate, represented as oxygen consumption rate (OCR) and glycolysis represented as extracellular acidification rate (ECAR) of the cells were measured using the Seahorse BioAnalyzer XFe96. **A.** OCR in U373 and mouse primary astrocytes. **B.** ECAR in U373 and mouse primary astrocytes. **C.** OCR compared to ECAR of mouse primary astrocytes and U373 cells. Unpaired t-test, **** $p<0.0001$, *** $p<0.001$; n=22-24. Data are presented as mean ± standard error of the mean.

### 5.3.10 Metabolic effects of TSPO ligands were absent in TSPO-KO U373 astroglioma cells

To verify that PK11195 did not have off-target effects at the concentrations used in these studies, TSPO-KO U373 cells were treated with PK11195 (25 nM) and XBD-173 (25 μM) for 1 hour prior to metabolic analysis. Whilst PK11195 increased ECAR by 63% in WT U373 cells (**fig. 5.3.10B**; $p<0.0001$), this effect was completely attenuated by loss of TSPO ($p=0.95$). XBD-173 did not alter ECAR or OCR after 1 hour treatment in WT or TSPO-KO U373 cells (**fig. 5.3.10A & B**); however, based on the earlier studies with mouse primary astrocytes (**fig. 5.3.5**) this was not unexpected at the concentration used in this experiment. Contrary to studies in mouse primary astrocytes (**fig. 5.3.5.1**) OCR was not significantly increased after treatment with PK11195 (**fig. 5.3.10A**). Interestingly, loss of TSPO in U373 cells reduced basal OCR by 24% (**fig. 5.3.10A**; $p=0.0131$) and ECAR by 47% (**fig. 5.3.10B**; $p=0.0052$) compared to WT controls. This is further evidence that TSPO modulates astrocyte metabolism.

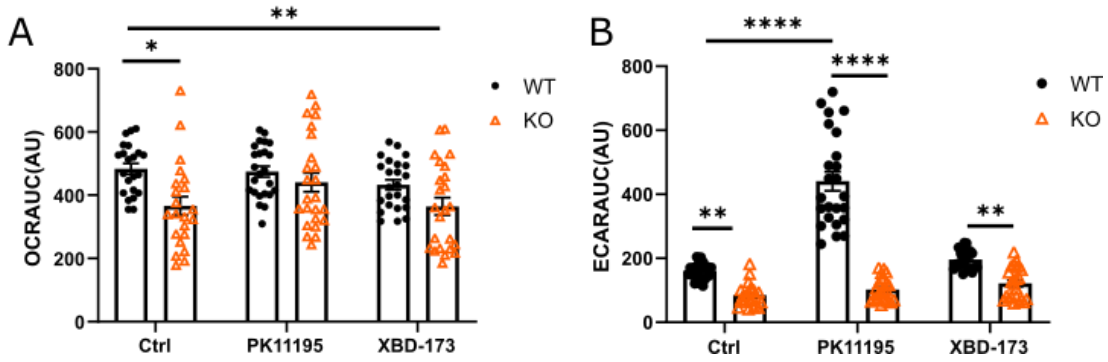


**Figure 5.3.10: Loss of TSPO prevented TSPO ligand induced changes to U373 astroglioma metabolism.** Cells were seeded at a density of 4 x $10^4$ cells per well in Seahorse XF96 cell culture microplates. After 1 hour pre-treatment, oxidative phosphorylation rate, represented as oxygen consumption rate (OCR) and glycolysis represented as extracellular acidification rate (ECAR) of the cells were measured using the Seahorse BioAnalyzer XFe96. **A.** Area under the curve (AUC) of the OCR of U373 cells expressing TSPO (WT) or not expressing TSPO (KO) 1 hour after treatment with PK11195 (25 nM) or XBD-173 (25 µM). Two-way ANOVA: Genotype $p$=0.0002, $F_{(1,134)}$=14.39; Ligand $p$=0.044, $F_{(2,134)}$=3.19; Interaction $p$=0.22, $F_{(2,134)}$=1.53 **B**. AUC of the ECAR of TSPO-WT or TSPO-KO 1 hour after treatment with PK11195 or XBD-173. Two-way ANOVA: Genotype, $p$<0.0001, $F_{(1,134)}$=194.0; Ligand, $p$<0.0001, $F_{(2,134)}$=58.51; Interaction, $p$<0.0001, $F_{(2,134)}$=56.95. Multiple comparisons by post-hoc Tukey's, * p<0.05, ** p<0.01, **** p<0.0001; n=22-26. Data are presented as mean ± standard error of the mean.

### 5.3.11 Loss of TSPO reduced mitochondrial respiration in mouse primary astrocytes

Metabolism in TSPO-deficient mouse primary astrocytes was measured using a Mito Stress Test in the Seahorse bioanalyser. $TSPO^{-/-}$ astrocytes had 37.1% reduction in basal mitochondrial metabolism compared to $TSPO^{+/+}$ astrocytes (**fig. 5.3.11.1A & B;** p=0.0006). Loss of TSPO also reduced maximal mitochondrial metabolism by 40.2% (**fig. 5.3.11.1A & C;** p=0.0012). Proton leak and ATP production were also reduced in $TSPO^{-/-}$ in astrocytes by 46% and 35.8% respectively (**fig. 5.3.11.1D,** p<0.0001; **fig. 5.3.11.1E,** p=0.0009). However, spare capacity and coupling efficiency were unaltered (**fig. 5.3.11.1F & G**). ECAR prior to addition of oligomycin was reduced by 52.6% in $TSPO^{-/-}$ cells (**fig. 5.3.11.2;** p=0.0001). This suggests $TSPO^{-/-}$ reduced glycolytic rate in mouse primary astrocytes.

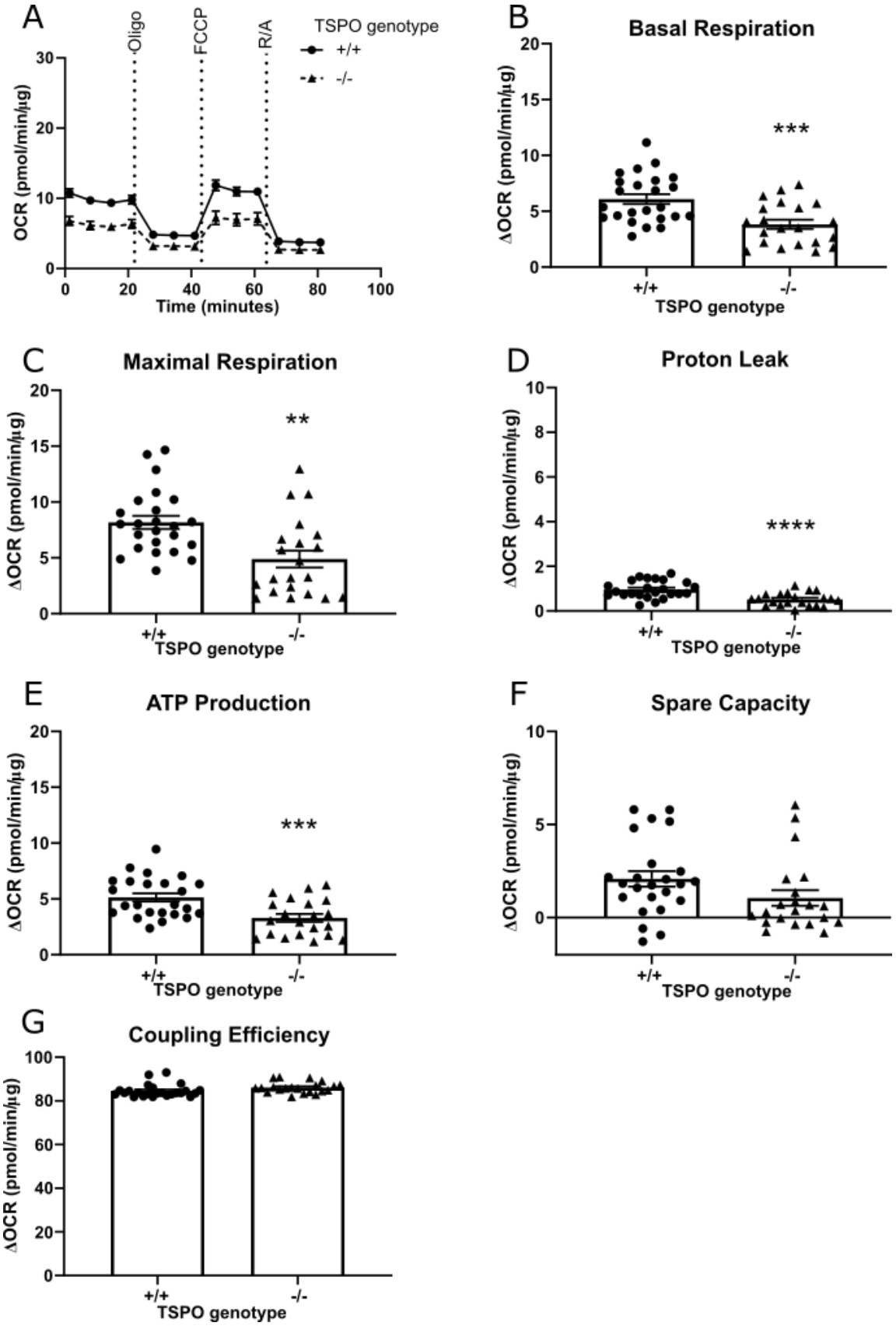
A
Oligo
FCCP
R/A
TSPO genotype
+/+
-/-
OCR (pmol/min/µg)
Time (minutes)
B
Basal Respiration
ΔOCR (pmol/min/µg)
***
TSPO genotype
C
Maximal Respiration
**
D
Proton Leak
****
E
ATP Production
***
F
Spare Capacity
G
Coupling Efficiency

**Figure 5.3.11.1: Loss of TSPO reduced mitochondrial metabolism in mouse primary astrocytes**. Cells were seeded at a density of 4 x $10^4$ cells per well in Seahorse XF96 cell culture microplates. Oxidative phosphorylation, represented as oxygen consumption rate (OCR) of the cells was measured using the Seahorse BioAnalyzer XFe96 in conjunction with a Mito Stress Test (Agilent, UK). **A.** OCR of mouse primary cortical astrocytes during a Mito Stress Test expressing (+/+) and not expressing TSPO (-/-). Oligomycin (Oligo; 0.5 µM), FCCP (1 µM), and rotenone/antimycin (R/A; 0.5 µM) were added as indicated by vertical dotted line. **B.** Basal mitochondrial respiration in TSPO +/+ and -/- mouse primary astrocytes, calculated as the difference in OCR before addition of Oligo and after addition of R/A. **C.** Maximal mitochondrial respiration, calculated as the difference in OCR after addition of FCCP and after addition of R/A. **D.** Proton leak, calculated as the difference between OCR after Oligo addition and after addition of R/A. **E.** Mitochondrial ATP production, calculated as the difference in OCR before and after addition of Oligo. **F.** Spare capacity, calculated as the difference in OCR between basal and maximal mitochondrial metabolism. **G.** Coupling efficiency, the percentage of basal metabolism used for ATP production. Unpaired t-test, **** $p<0.0001$, *** $p<0.001$, ** $p<0.01$. n=22-24. Data are presented as mean ± standard error of the mean.

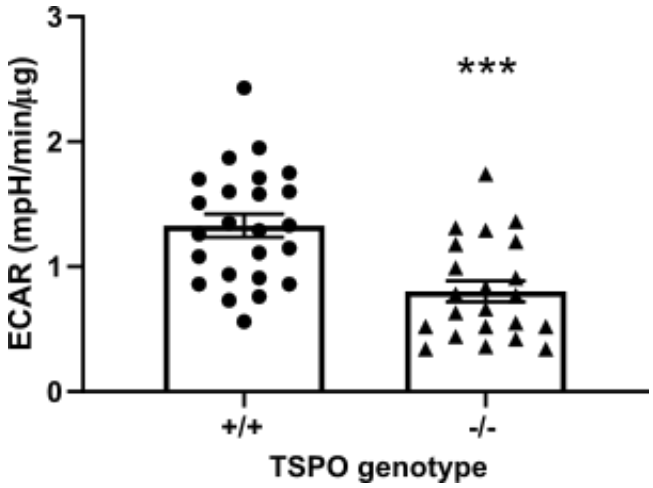


**Figure 5.3.11.2: Loss of TSPO reduced glycolytic metabolism in mouse primary astrocytes**. Extracellular acidification rate (ECAR) data from Mito Stress Test in **fig. 5.3.11.1** prior to injection of oligomycin (0.5 µM) in mouse primary astrocytes expression (+/+) and not expressing TSPO (-/-). Unpaired t-test, *** $p<0.001$. n=22-24. Data are presented as mean ± standard error of the mean.

### 5.3.12 Loss of TSPO from U373 astroglioma cells decreased mitochondrial function

To investigate whether loss of TSPO from human astroglioma cells resulted in a similar response as was seen in mouse primary astrocytes, TSPO-KO U373 cells were subjected to a Mito Stress Test (**fig. 5.3.12.1A**). Basal respiration was reduced in cells not expressing TSPO by 26% (**fig. 5.3.12.1B**; $p<0.0002$), leading to a 26% reduction in mitochondrial ATP production (**fig. 5.3.12.1E**; $p<0.0004$) compared to empty vector controls (EV). Maximal respiration was reduced by 27% (**fig. 5.3.12.1C**; $p<0.001$). Proton leak was reduced by 19% (**fig. 5.3.12.1D**; $p<0.0011$). Spare capacity was reduced by 27% (**fig. 5.3.12.1F**; $p<0.0025$). However, coupling efficiency was unchanged (**fig. 5.3.12.1G**). ECAR was also significantly reduced by 46% (**fig. 5.3.12.2**; $p<0.0001$).

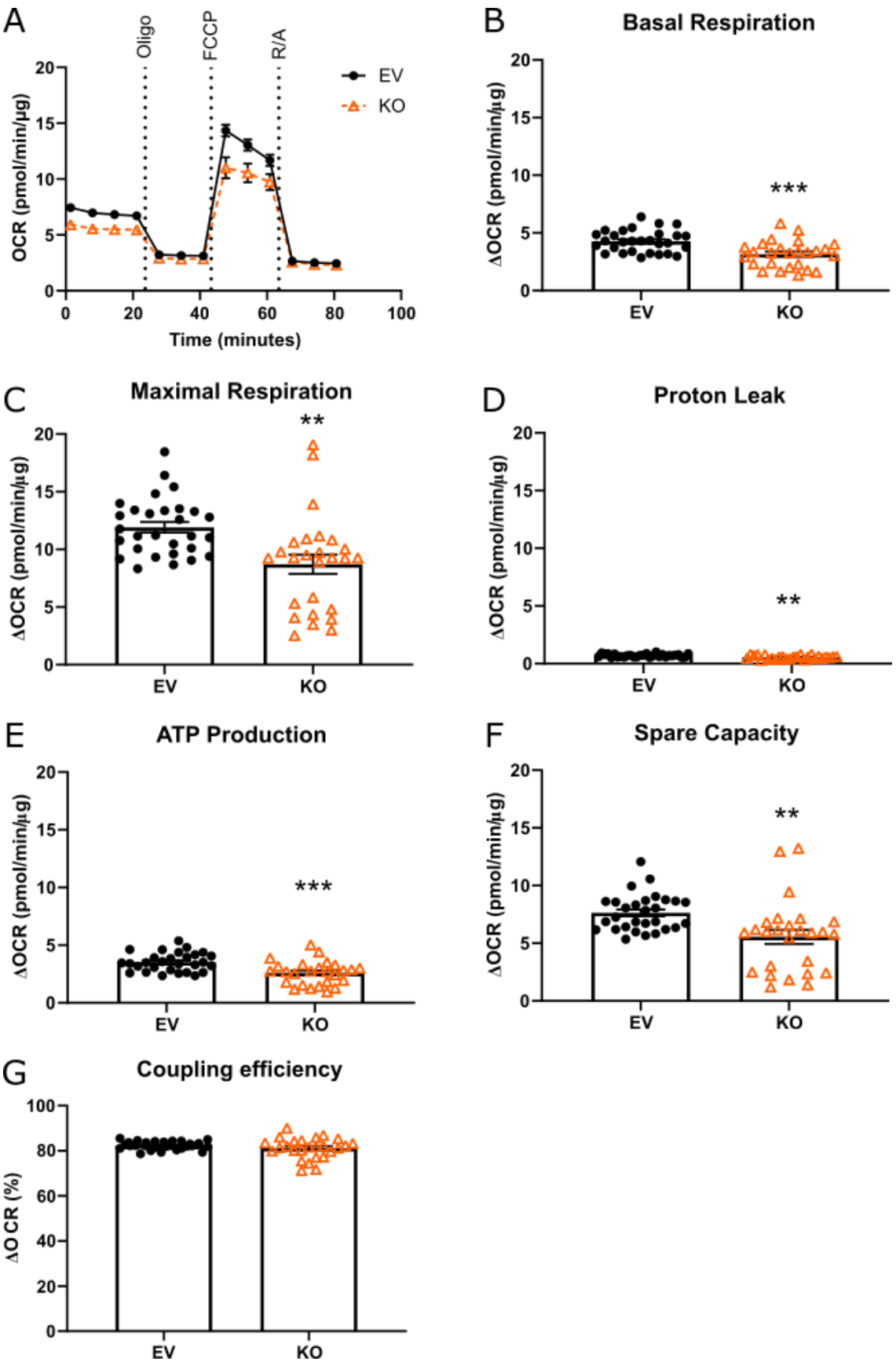
A
Oligo
FCCP
R/A
EV
KO
OCR (pmol/min/µg)
Time (minutes)
B
Basal Respiration
ΔOCR (pmol/min/µg)
***
EV
KO
C
Maximal Respiration
**
D
Proton Leak
E
ATP Production
F
Spare Capacity
G
Coupling efficiency
ΔO CR (%)

**Figure 5.3.12.1: Loss of TSPO reduced mitochondrial metabolism in U373 astroglioma cells.** Cells were seeded at a density of 4 x $10^4$ cells per well in Seahorse XF96 cell culture microplates. Oxidative phosphorylation, represented as oxygen consumption rate (OCR) of the cells was measured using the Seahorse BioAnalyzer XFe96 in conjunction with a Mito Stress Test (Agilent, UK). **A.** OCR of U373 cells during a Mito Stress Test expressing (EV) and not expressing (KO) TSPO. Oligomycin (Oligo; 0.5 µM), FCCP (1 µM), and rotenone/antimycin (R/A; 0.5 µM) were added as indicated by the vertical dotted line. **B.** Basal mitochondrial respiration in TSPO EV and KO U373 cells, calculated as the difference in OCR before addition of Oligo and after addition of R/A. **C.** Maximal mitochondrial respiration, calculated as the difference in OCR after addition of FCCP and after addition of R/A. **D.** Proton leak, calculated as the difference between OCR after Oligo addition and after addition of R/A. **E.** Mitochondrial ATP production, calculated as the difference in OCR before and after addition of Oligo. **F.** Spare capacity, calculated as the difference in OCR between basal and maximal mitochondrial metabolism. **G.** Coupling efficiency, the percentage of basal metabolism used for ATP production. Unpaired t-test, *** $p<0.001$, ** $p<0.01$; n=22-24. Data are presented as mean ± standard error of the mean.

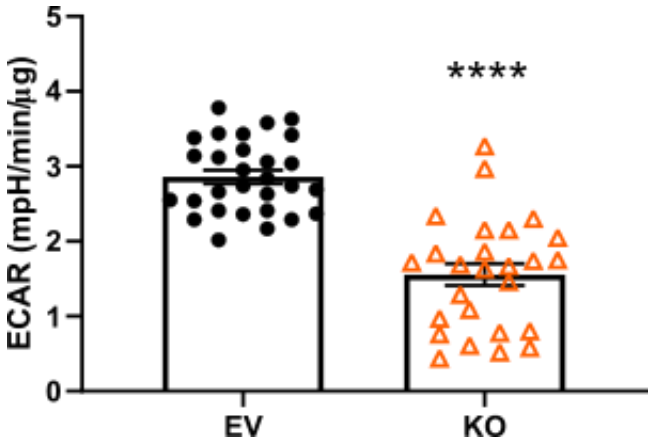


**Figure 5.3.12.2: Loss of TSPO reduced glycolytic metabolism in U373 astroglioma cells**. Extracellular acidification rate (ECAR) data from Mito Stress Test (**fig. 5.3.12.1**) of human U373 astroglioma cells expressing (EV) and not expressing (KO) TSPO prior to injection of oligomycin. Unpaired t-test, **** $p<0.001$; n=22-24. Data are presented as mean ± standard error of the mean.

### 5.3.13 Loss of TSPO from U373 astroglioma cells increased fatty acid oxidation

To investigate the role of TSPO in U373 metabolism, the FAO Mito Stress Test was used (as described above in **section 5.3.6**). In U373 cells, loss of TSPO increased maximal rate of FAO by 145.5% compared to EV controls (**fig 5.3.13C;** p=0.0025). However, basal FAO was not altered in TSPO-KO cells compared to EV controls (**fig 5.3.13B**).

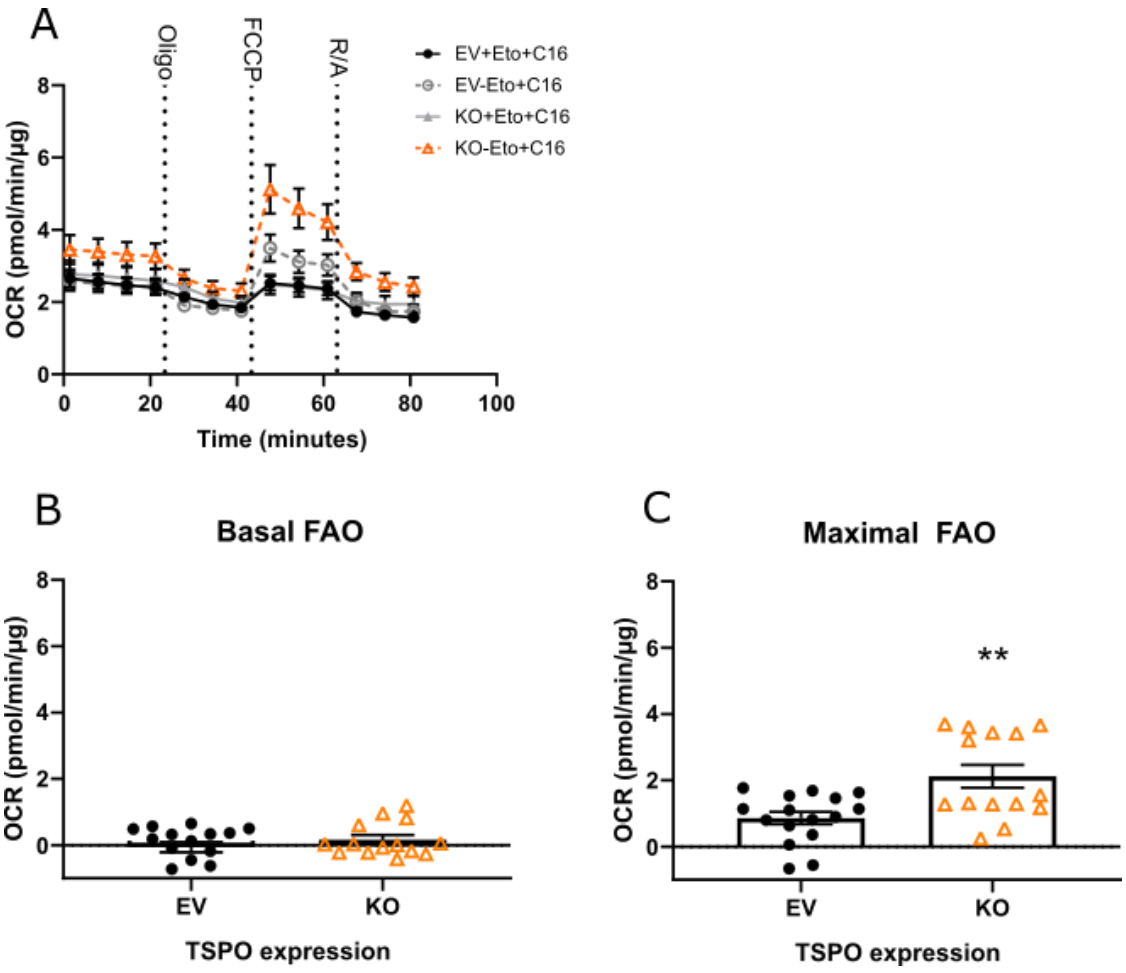
A
Oligo
FCCP
R/A
EV+Eto+C16
EV-Eto+C16
KO+Eto+C16
KO-Eto+C16
OCR (pmol/min/µg)
Time (minutes)
B
Basal FAO
OCR (pmol/min/µg)
EV
KO
TSPO expression
C
Maximal FAO
**
OCR (pmol/min/µg)
EV
KO
TSPO expression

**Figure 5.3.13: Loss of TSPO increased rate of fatty acid oxidation in human U373 astroglioma cells.** Cells were seeded at a density of 4 x $10^4$ cells per well in Seahorse XF96 cell culture microplates. Oxidative phosphorylation, represented as oxygen consumption rate (OCR) of the cells was measured using the Seahorse BioAnalyzer XFe96 in conjunction with a fatty acid oxidation (FAO) Mito Stress Test (Agilent, UK). **A.** Time course of FAO Mito Stress Test in U373 astroglioma cells expressing (EV) and not expressing (KO) TSPO. Oligomycin (Oligo; 0.5 µM), FCCP (1 µM), and rotenone/antimycin (R/A; 0.5 µM) were added as indicated by vertical dotted lines. Palmitate (200 µM; C16) was provided as a substrate. **B.** Basal FAO rate calculated as the difference in oxygen consumption rate (OCR) between etomoxir treated negative controls (eto; 40 µM) and the comparable treatment group immediately prior to addition of Oligo. **C.** Maximal FAO rate calculated as the difference in OCR between etomoxir-treated negative controls and the comparable treatment group after addition of FCCP. One-way ANOVA with post hoc Tukey, ** $p<0.01$. n=16-20. Data are presented as mean ± standard error of the mean.

### 5.3.14 Loss of TSPO did not alter intracellular energy balance in U373 astroglioma cells

Although loss of TSPO increased FAO in U373 cells, TSPO-KO cells did not have altered mitochondrial membrane potential compared to EV controls (**fig 5.3.14.1**). TSPO-KO cells also maintained intracellular ATP levels (iATP) compared to EV controls (**fig 5.3.14.2**). Although glucose uptake rate was reduced by 25.3%, this decrease was not statistically significant (**fig 5.3.14.3;** p=0.11).

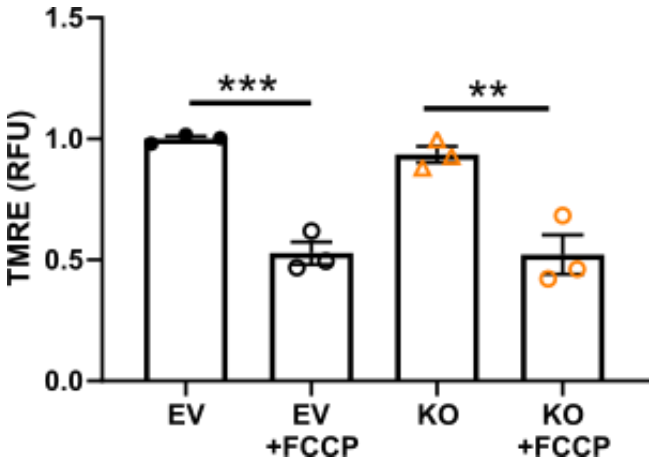


**Figure 5.3.14.1: Mitochondrial membrane potential was not altered by loss of TSPO in human astroglioma cells.** TMRE uptake by U373 astroglioma cells not expressing TSPO (KO), relative to mean of TSPO expressing U373 empty vector (EV) controls. FCCP (1 µM) was used as positive depolarisation control. Cells were seeded at a density of 3.5 x $10^5$ cells per well in a 6 well plate. After treatment with LPS, cells were dissociated and incubated with FCCP prior to incubation with TMRE (100 nM) and analysis with the BD Accuri C6 Plus flow cytometer. One-way ANOVA with post hoc Tukey, *** $p<0.001$, ** $p<0.01$; n=3. Data are expressed as mean ± standard error of the mean.

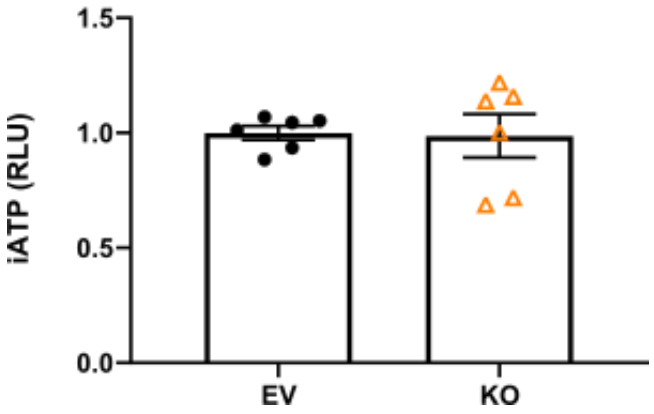


**Figure 5.3.14.2: Intracellular ATP levels were not altered by loss of TSPO in human astroglioma cells.** Intracellular ATP (iATP) measurement in U373 astroglioma cells not expressing TSPO (KO), relative to mean of TSPO expressing U373 empty vector (EV) controls. U373 cells were seeded at a density of 4 x $10^3$ cells per well in black 96 well plates. iATP after loss of TSPO was estimated using the ATPLite TwoStep kit (PerkinElmer, UK). Unpaired t-test, n=6. Data are represented as mean ± standard error of the mean.

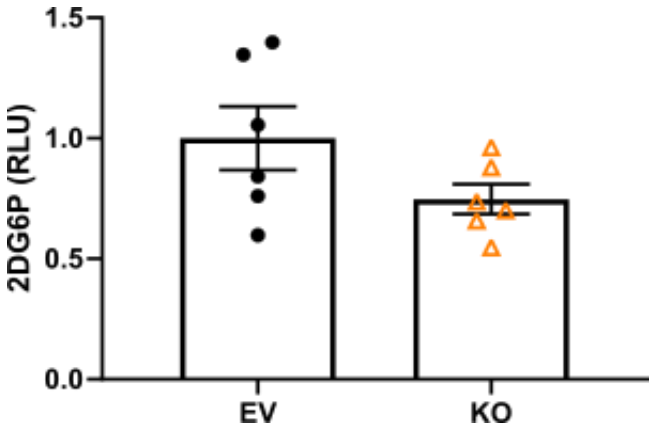


**Figure 5.3.14.3: Glucose uptake rate was not altered by TSPO KO in human astroglioma cells.** U373 cells were seeded at a density of 4 x $10^4$ cells per well in 96 well plates. Glucose uptake rate after loss of TSPO was estimated using the Glucose Uptake-Glo kit (Promega, UK). Glucose uptake was represented as fold change in 2-deoxyglucose-6-phosphate (2DG6P) luminescence by U373 astroglioma cells not expressing TSPO (KO), relative to mean of TSPO expressing U373 empty vector (EV) controls. Unpaired t-test, n=6. Data are represented as mean ± standard error of the mean.

### 5.3.15 TSPO is part of a protein complex with CPT1a

To investigate how TSPO may be regulating FAO in these cells, I explored possible protein-protein interactions. TSPO has been shown to interact with many mitochondrial proteins, both directly, and indirectly through forming complexes (Ilkan & Akar, 2018; Milenkovic *et al.*, 2015; Shoshan-Barmatz *et al.*, 2019). Carnitine palmitoyl transferase-1A (CPT-1A) is the rate-limiting step of fatty acid oxidation. Co-immunoprecipitation was used to investigate a possible interaction between CPT-1A and TSPO in human astroglioma cells. Antibodies were used to pull down TSPO (and any associated proteins) from U373 lysate. Non-specific IgG antibodies were used as negative controls in the pull down. Immunoblotting was then used to confirm that CPT-1A was present in the protein pulled down using the anti-TSPO antibody (**fig 5.3.15.1**). This demonstrated the TSPO was in a protein complex with CPT-1A in these cells. In a separate confirmatory experiment, an antibody was used to pull down CPT-1A and any associated proteins. Immunoblotting was used to detect TSPO in the protein pulled down with this antibody, and negative controls confirmed that the CPT-1A antibody was specific for CPT-1A in these cells (**fig 5.3.15.2**). The antibodies used to immunoprecipitate and immunoblot for proteins were raised in different species to reduce cross-reactivity and increase specificity (TSPO: rabbit, goat; CPT-1A: mouse, rabbit respectively). A second band ~65-70 kDa in size was detected in the non-immunoprecipitated lysate lanes after CPT-1A immunoblotting. This may be a fragment of CPT-1A or a non-specific band. However, it did not appear in either the CPT-1A immunoprecipitate or the TSPO immunoprecipitate. As the higher band, closer to 88 kDa in size was detected by both CPT-1A antibodies, this was taken to be the CPT-1A band.

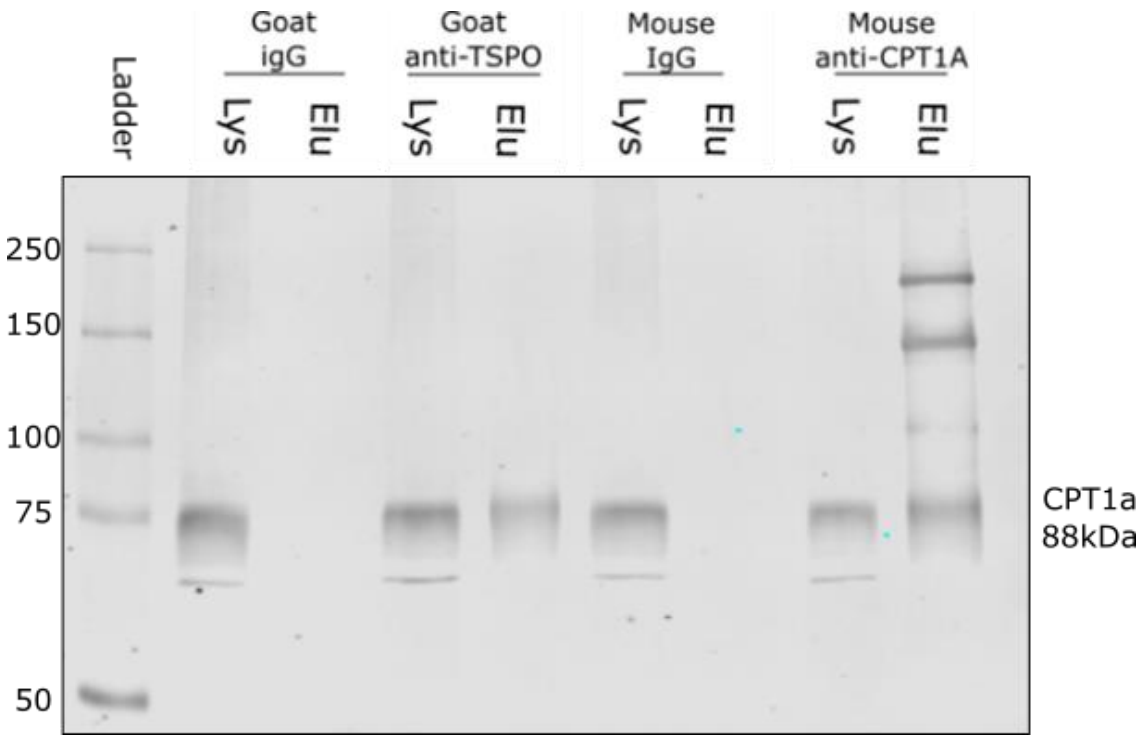


**Figure 5.3.15.1: CPT-1A is in a protein complex with TSPO in U373 astrocytoma cells.** Immunoblot against CPT-1A of total protein lysates (lys) and immunoprecipitated protein (Elu). U373 cells were seeded at a density of 3 x $10^6$ cells per plate in a 150 mm plate prior to lysis and protein quantification. Immunoprecipitations were performed with Protein G Dynabeads (Invitrogen, UK), and CPT-1A was detected in the lysate at the expected weight of 88 kDa using immunoblotting. Goat IgG used as a negative control for TSPO immunoprecipitation. Goat anti-TSPO used to co-immunoprecipitate TSPO and interacting proteins. Mouse IgG used as negative control for CPT-1A immunoprecipitation. Mouse anti-CPT-1A used as positive control for CPT-1A antibody and immunoprecipitation technique.

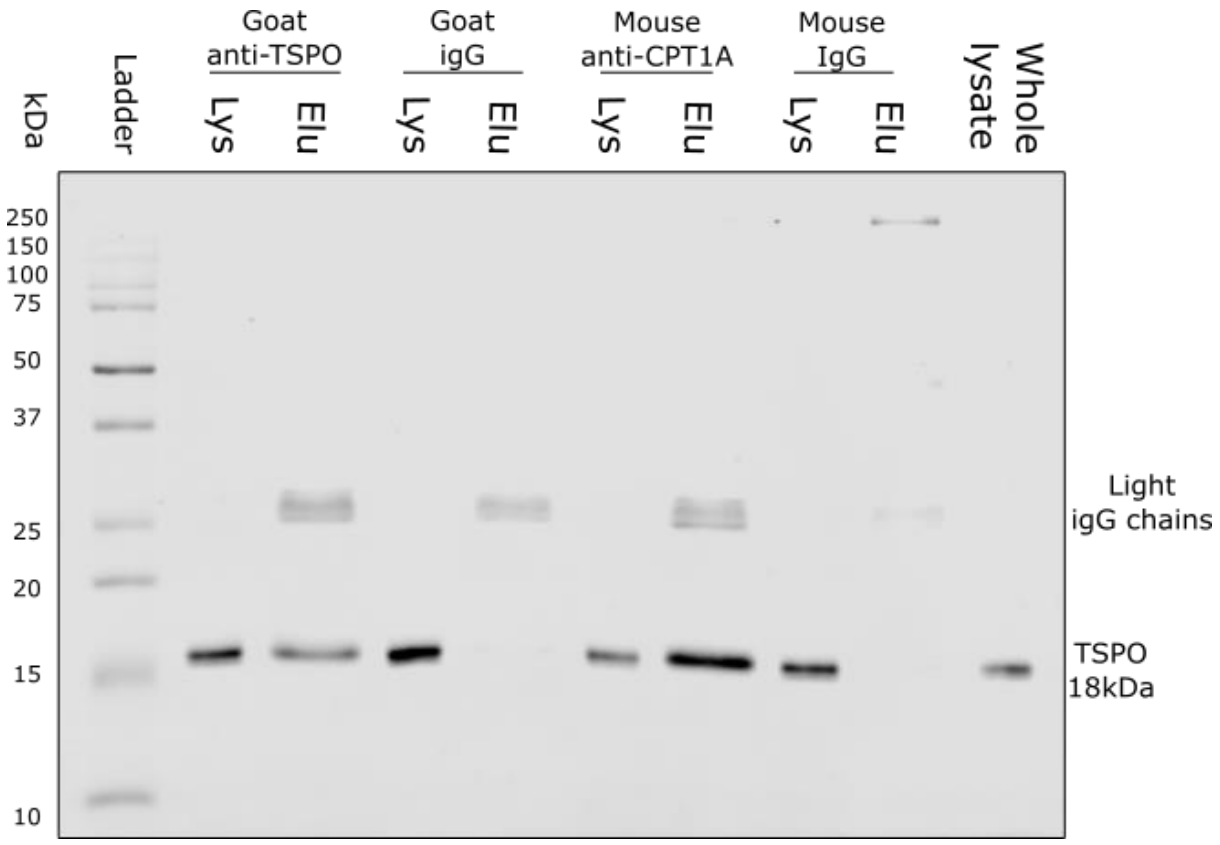


**Figure 5.3.15.2: TSPO is in a protein complex with CPT-1A in U373 astrocytoma cells.** Immunoblot against TSPO (antibody raised in rabbit) of total protein lysates (lys) and immunoprecipitated protein (Elu). U373 cells were seeded at a density of 3 x $10^6$ cells per plate in a 150 mm plate prior to lysis and protein quantification. Immunoprecipitations were performed with Protein G Dynabeads (Invitrogen, UK), and TSPO was detected in the lysate at the expected weight of 18 kDa using immunoblotting. Goat anti-TSPO used as positive control for TSPO antibody and immunoprecipitation technique. Goat IgG used as a negative control for TSPO immunoprecipitation. Mouse anti-CPT-1A to co-immunoprecipitate CPT-1A and interacting proteins. Mouse IgG used as negative control for CPT-1A immunoprecipitation. Whole cell lysate used as positive control for TSPO expression in these cells.

## 5.4 Discussion

I have shown here that loss of TSPO increases FAO in astrocytes, whilst decreasing overall OXPHOS and glycolysis. Furthermore, TSPO was found to be in a protein complex with CPT-1A, the rate-limiting step of fatty acid oxidation. This may represent a functional mechanism by which TSPO impacts fatty acid metabolism.

**Table 5.4 Summary of the regulation of metabolism in astrocytes following manipulation of TSPO signalling.**
NDA=No data available.

| Model | Species | FAO | Glycolysis | Oxidative phosphorylation |
|---|---|---|---|---|
| Primary astrocytes + XBD-173 (25 μM) | Mouse | Up | Unchanged | Unchanged |
| Primary astrocytes + PK11195 (25 nM) | Mouse | Unchanged | Up | Up?<br>*Data inconsistent* |
| Primary astrocytes TSPO$^{-/-}$ | Mouse | NDA | Down | Down |
| U373 TSPO-KO | Human | Up | Down | Down |
| U373 + XBD-173 (25 μM) | Human | NDA | Unchanged | Unchanged |
| U373 + PK11195 (25 nM) | Human | NDA | Up | Unchanged |
| U373 TSPO-KO + XBD-173 (25 μM) | Human | NDA | Unchanged | Unchanged |
| U373 TSPO-KO + PK11195 (25 nM) | Human | NDA | Unchanged | Unchanged |

### 5.4.1 TSPO may be regulated by OXPHOS

As has been previously shown in other cell types and *in vivo*, I have demonstrated that TSPO is upregulated in astrocytes in response to pro-inflammatory stimulation with LPS (Beckers *et al.*, 2018; Bonsack & Sukumari-Ramesh, 2018; Lavisse *et al.*, 2012). This increase was only seen after 24 hours, not after 3 hours, of LPS treatment. At the 24 hour time point I previously observed adaptations in both mitochondrial and glycolytic metabolism in mouse primary astrocytes in response to inflammatory stimulation (**Chapter 3**). However, as I saw no change in TSPO expression after 3 hours of LPS treatment, when astrocytes show changes in ECAR but not OCR (**Chapter 3**), this may suggest that TSPO is upregulated during increased OXPHOS as opposed to being regulated by changes in glycolysis.

To explore this further I treated cells with the glycolysis inhibitor 2-DG for 24 hours. In contrast to upregulation by LPS, TSPO expression was downregulated by 2-DG. Data shown in **Chapter 3** suggests that 2-DG does not regulate OXPHOS within the first hour of treatment in mouse primary astrocytes. However, I did not examine whether any adaptation in cellular metabolism occurred after 24 hours treatment with 2-DG and published data from macrophages suggests that treatment with 2-DG decreases both glycolysis and OXPHOS after 1 hour of treatment (Wang *et al.*, 2018). If 2-DG induces a similar decrease in OXPHOS in astrocytes, as is seen in macrophages, this would support the supposition that TSPO is regulated by OXPHOS, with increased TSPO expression during states of increased OXPHOS and decreased TSPO expression during low OXPHOS states. To support this, future studies measuring cellular metabolism after 24

hours of 2-DG treatment would be important. Additionally, measuring TSPO expression after systematically modulating different aspects of cellular metabolism could be informative: directly inhibiting OXPHOS using rotenone or oligomycin to inhibit the ETC; using etomoxir to inhibit FAO; and treating with UK5099 to inhibit the TCA cycle (O'Neill *et al.*, 2016). These experiments may shed more light on the regulation of TSPO levels by metabolic function.

### 5.4.2 Treatment with an AMPK activator does not regulate TSPO expression

Although it appears that metabolic cues such as increased OXPHOS may play a role in regulating TSPO expression, in our study TSPO was not regulated by pharmacological activation of the major metabolic regulator AMPK. It is well established that AMPK increases OXPHOS through promoting glucose transport into the cell and fatty acid transport into the mitochondria by CPT-1A; thus increasing both glucose metabolism and FAO (Herzig & Shaw, 2018; Long & Zierath, 2006). Therefore, if TSPO expression is regulated by overall mitochondrial metabolism it is somewhat surprising that TSPO expression was not regulated following pharmacological AMPK activation with AICAR. This may suggest that TSPO is upstream of AMPK, and not directly regulated by AMPK activity.

This conclusion is supported by recently published data. It has been demonstrated that PK11195 treatment and loss of TSPO in a glial cell type called tanycytes leads to phosphorylation of AMPK through $Ca^{2+}$ signalling (Kim *et al.*, 2019). TSPO has been shown to interact with VDAC, a major $Ca^{2+}$ channel in the

OMM. Disruption of this interaction through loss or modulation of TSPO may increase $Ca^{2+}$ signalling, promoting AMPK activation through calcium-calmodulin-dependent protein kinase kinase (CaMKK). In work from a separate group, loss of TSPO increases expression of the AMPKα subunit in glioma cells (Fu *et al.*, 2019). These data suggest TSPO can regulate AMPK activity, rather than AMPK activity regulating TSPO.

However, AMPK is activated by low cellular energy state, and as I have shown that modulation or loss of TSPO alters metabolic function in the cell the changes to AMPK activation may be a response to these changes to maintain metabolic homeostasis rather than through direct regulation by TSPO. However, our data shows that iATP levels are not decreased by modulation of TSPO expression or activity, so are unlikely to be activating AMPK. Important experiments are needed to further investigate this data. It would be important to measure metabolic changes and AMPK phosphorylation by AICAR at 24 hours in mouse primary astrocytes, to ensure the AICAR was active. Additionally, to more rigorously investigate the mechanism through which AMPK activation is related to TSPO modulation, measurements of AMPK phosphorylation and ADP:ATP ratios in the cell after loss or pharmaceutical modulation of TSPO in our model would be needed.

### 5.4.3 Pharmacological modulation of TSPO did not alter pro-inflammatory cytokine release

Contrary to published data from *in vivo* models and microglia in culture indicating anti-inflammatory actions, treatment with TSPO ligands did not alter the profile of

LPS-induced astrocyte pro-inflammatory cytokine release measured in this study (Azrad *et al.*, 2019; Mages *et al.*, 2019). However, this is not completely unprecedented, as Klee *et al*. showed in a recent study that loss of TSPO did not alter microglial activation and retinal degradation after light damage (Klee *et al.*, 2019). While it is feasible that TSPO ligands had no anti-inflammatory effect, this is not certain as only limited cytokines and time points were measured. Therefore, use of a cytokine array, or RT-qPCR at multiple time points may reveal changes in the inflammatory profile that were not evident in this study.

Interestingly, after 24 hours a decrease in LPS-induced IL-10 release was observed after treatment with XBD-173, but not PK11195. This may suggest that XBD-173 acts through a different mechanism to PK11195, and this is supported by the finding that the drugs have different effects on steroidogenesis (Selvaraj & Tu, 2016). It is important to reiterate that TSPO ligands are classified as agonists based on their ability to displace PK11195 or their activity in promoting steroid production, a function of TSPO that has recently become controversial (Selvaraj & Tu, 2016; Zhang *et al.*, 2007). Therefore their nomenclature as agonists or antagonists may not accurately reflect their action on TSPO as an inflammatory or metabolic mediator. Considering the differential effects of the two ligands used in this study, and the uncertainty regarding their effect on TSPO activity, it would be pertinent to also examine inflammation in TSPO-deficient astrocytes after treatment with LPS.

As the metabolic effect of TSPO ligands were measured an hour after treatment, whereas inflammation was measured after 24 hours, I do not know if the

metabolic changes persisted. Therefore I cannot comment on the effect of the metabolic change on inflammation in these cells. It would be appropriate to investigate the metabolic function of these cells at 24 hours after ligand exposure to investigate the anti-inflammatory response of these cells, or alternatively, in a more clinically relevant study to expose cells to LPS for 3 and 24 hours prior to a 1 hour treatment with TSPO ligands to mimic treatment with TSPO ligands after the onset of an inflammatory disease.

### 5.4.4 Modulation of TSPO signalling impacts astrocyte metabolism

#### Glucose metabolism

Studies have suggested that TSPO regulates glucose metabolism, as increased TSPO expression correlates with increased glucose metabolism in many cell types (Ferrarese *et al.*, 1994). Consistent with this evidence, U373 astroglioma cells — which expressed higher levels of TSPO — had higher rates of glycolysis, but reduced OCR and FAO rate compared to mouse primary astrocytes. Our data showed loss of TSPO from mouse primary astrocytes and U373 astroglioma cells decreased glycolysis (ECAR) in both cell types. However, whilst glucose uptake was reduced after loss of TSPO from human astroglioma cells, this was not statistically significant.

Recent published work shows that in glioblastoma cells loss of TSPO increases aerobic glycolysis (Fu *et al.*, 2019). This may well be driven by an increase in expression of genes associated with aerobic glycolysis. Proteins upregulated include GLUT1, hexokinase II and lactate dehydrogenase (LDH), suggesting a shift towards aerobic glycolysis after loss of TSPO (Fu *et al.*, 2019). This is

contrary to our data presented here. It is possible that TSPO promotes glycolysis coupled to oxidative metabolism and restrains aerobic glycolysis. This would limit total glycolytic rate to that needed for supplying the TCA cycle and OXPHOS. Loss of TSPO would therefore increase aerobic glycolysis if the enzymes required for aerobic glycolysis were present. Radio isotope labelling of glucose and mass spectrometry in combination with TSPO ligands or loss of TSPO may be used to assess this change in glucose fate. However, it is important to note that our evidence comparing mouse primary astrocytes to U373 cells is circumstantial, and as U373 cells are derived from a malignant astrocytoma glioblastoma the increased glycolytic rate may be attributable in part to aerobic glycolysis and not be a result of increased TSPO expression.

In line with the findings in this study, adipocytes have been shown to increase glucose uptake after treatment with TSPO ligands including PK11195 (Li & Papadopoulos, 2015). Our data shows that PK11195 increased glycolysis within 1 hour of treatment. However, the increase in glucose uptake seen after treatment with PK11195 was not statistically significant. XBD-173 did not alter glycolytic rate or glucose uptake. PK11195 reduces glucose metabolism in activated microglia, and as our data was not statistically significant, I cannot confidently draw conclusions (Amitani *et al.*, 2008). Additionally, this appears to be contradictory to our own data which has shown that TSPO modulation or loss decreases glycolysis. This again may suggest that PK11195 is acting through a different mechanism to loss of TSPO and XBD-173. To investigate this more robustly, a Glycolytic Stress Test could be used after treatment with PK11195 to show whether the changes in glucose uptake and ECAR changes are directly driven by glycolytic rate.

Importantly, the TSPO ligands used had no effects on metabolism in the TSPO-deficient U373 cells at the concentrations used, thus confirming the specificity of their effects. For consistency and increased robustness, these studies should be repeated in the primary astrocytes from TSPO-deficient mice, particularly as PK11195 did not induce the same increase in OCR in U373 cells as was observed in mouse primary astrocytes.

**OXPHOS**

Recent publications have shown that loss of TSPO from human primary microglia, mouse microglia, mouse GL261 glioma cells, and glioblastoma cells reduces OXPHOS, whilst over-expression of TSPO in T-cells (Jurkat) which normally do not express TSPO at all increases expression of genes related to OXPHOS (Banati *et al.*, 2014; Fu *et al.*, 2019; Milenkovic *et al.*, 2018). TSPO ligands PK11195 and Ro5-4864 also suppress mitochondrial metabolism in GL251 glioma cells (Fu *et al.*, 2019). In agreement with this, our data shows that astrocytes cultured from mice with germline deletion of TSPO and U373 astroglioma cells lacking TSPO have significantly decreased OXPHOS rates compared to TSPO-expressing controls.

Previously published work suggests that this decrease in OXPHOS may be driven by mitochondrial dysfunction through increased mitochondrial fragmentation (Fu *et al.*, 2019). However, in our studies no decrease in mitochondrial coupling efficiency or change in mitochondrial membrane potential was observed following loss of TSPO. I would have expected both of these parameters to have been

decreased if the mitochondria were dysfunctional, fragmenting and/or undergoing mitophagy (Twig & Shirihai, 2011). This may instead suggest that OXPHOS is limited by substrate supply in the absence of TSPO, rather than mitochondrial dysfunction, and may imply that the decrease in glycolytic flux and the decrease in OXPHOS after loss of TSPO are linked.

**FAO**

I have presented data here showing that FAO was significantly increased by loss of TSPO from U373 human astroglioma cells. FAO was also similarly increased following treatment with the TSPO ligand XBD-173. This suggests XBD-173, which has previously been classified as a TSPO agonist based on is activity in PK11195 displacement and steroidogenesis assays, impacts FAO in a similar manner to loss of TSPO (Selvaraj & Tu, 2016). The findings in the TSPO-deficient U373 cells are supported by multiple published studies in other cell types. Work presented by Tu *et al.* using the mouse testicular Leydig cell line MA-10 shows that TSPO deficiency increases FAO and expression of related proteins including CPT-1A (Tu *et al.*, 2016). Additionally, *in vivo* the TSPO agonist etifoxine reduces intracellular lipid accumulation in hepatocellular carcinoma cells, whilst in mouse tanycytes *in vitro* both PK11195 and loss of TSPO also reduce intracellular lipid accumulation (Kim *et al.*, 2019; Lin *et al.*, 2019). This is attributed by the authors to increased lipophagy, which could provide substrate for increased FAO (Schulze *et al.*, 2017). Together, these data suggest that treatment with TSPO ligands or loss of TSPO increase FAO.

In our studies the TSPO ligand PK11195 did not alter FAO in mouse primary astrocytes. This is surprising as published data from other groups show that PK11195 upregulates the expression of mRNA of proteins associated with FAO, including CPT-1A in zebra fish, and increases lipophagy (Gut *et al.*, 2013; Kim *et al.*, 2019). This is consistent with the change in CPT-1A protein expression seen after loss of TSPO from Leydig cells (Tu *et al.*, 2016). This may suggest that TSPO has multiple functions relating to increasing lipid mobilisation and PK11195 increases these genes independently from the role of TSPO in regulating FAO. CPT1-A gene expression and lipophagy are known to be regulated by activation of AMPK and this may be the mechanism through which PK11195 is acting: PK11195 and loss of TSPO have previously been demonstrated to activate AMPK (Kim *et al.*, 2011; Kim *et al.*, 2019; Krämer *et al.*, 2007). To further explore this, data on AMPK expression and phosphorylation after treatment with TSPO ligands or loss of TSPO would be important.

### 5.4.5 TSPO as a metabolic substrate integrator and switch

Together data from the literature and metabolic data presented in this chapter suggest that increased TSPO expression decreases FAO but promotes overall OXPHOS during inflammation through increasing glucose metabolism. This suggests that TSPO may play a role in regulating the substrate switching during metabolism. I have demonstrated a novel interaction between CPT-1A and TSPO, shown for the first time here. This is supported by evidence in the literature that VDAC and CPT-1A are found in a protein complex (Gatliff *et al.*, 2014; Papadopoulos *et al.*, 1994). This interaction between TSPO and CPT-1A may be part of the molecular mechanism by which TSPO regulates FAO.

The reported interaction between TSPO and VDAC may mediate the increase in glycolysis and OXPHOS attributed to TSPO (Milenkovic *et al.*, 2015; Veenman *et al.*, 2008). VDAC has previously been shown to couple the glycolytic regulator hexokinase II with the mitochondria to increase glycolytic rate (Camara *et al.*, 2017; McEnery *et al.*, 1993; Pastorino & Hoek, 2008). This is facilitated through an interaction between VDAC and adenosine nucleotide transporter (ANT) (Camara *et al.*, 2017; Pastorino & Hoek, 2008). When hexokinase II is coupled to the mitochondria, glycolytic rate increases due to increased provision of ATP through the VDAC-ANT complex, allowing faster phosphorylation of glucose into glucose-6-phosphate (Colombini, 2012; John *et al.*, 2011; Mathupala *et al.*, 2006; Rostovtseva & Colombini, 1996). This increases production of pyruvate, allowing increased transport and metabolism of pyruvate within the mitochondria.

Hexokinase targeting to the mitochondria also increases ADP turnover and return to the ETC through the VDAC-ANT complex for re-phosphorylation into ATP, allowing maintenance of OXPHOS (Gumaa & McLean, 1969; Robey & Hay, 2006; Wilson, 2003). Additionally, it has been reported that VDAC imports pyruvate into the mitochondrial intermembrane space, prior to transport into the mitochondrial matrix by pyruvate translocase for further metabolism, and this appears to be generally accepted (Fang & Maldonado, 2018; Lee, 2014). However, to our knowledge there is no data available that directly demonstrates this role of VDAC. Therefore, whilst there is strong evidence that VDAC links glycolytic rate and OXPHOS, whether pyruvate trafficking by VDAC plays a role in this must be regarded with caution without further investigation. An interaction

between TSPO and VDAC in this complex may explain why rates of OXPHOS and glycolysis both appear to be regulated by modulation of TSPO activity. Taken together these data suggest that TSPO may form a complex with CPT-1A, VDAC, and hexokinase II enabling it to increase glycolysis and OXPHOS through promoting glucose phosphorylation by hexokinase II, and possibly pyruvate trafficking into the mitochondria by VDAC, while potentially inhibiting supply of acyl-coA to the β-oxidation cycle through reducing CPT-1A activity (see **fig. 5.5.1**).

This potential model must be approached with caution at this stage as CPT-1A, VDAC and TSPO existing in a complex together at the same time has not yet been demonstrated. This could be investigated using immunoprecipitation, mass spectrometry and immunoblotting techniques. Additionally, whilst existence of this complex would be interesting, the functional relevance of the complex would need to be verified by using CPT-1A and hexokinase activity assays to directly evaluate the activity of these enzymes following modulation of TSPO activity with ligands and/or genetic manipulation.

In our studies I did not observe any alterations in iATP, suggesting that astrocytes are capable of defending ATP levels in the absence of TSPO. This indicates that although TSPO appears to play a role in fuel selection during metabolism, it does not maintain energy supply or regulate demand. However other groups have shown that over-expression of TSPO in T-cells increases iATP after addition of ADP (Liu *et al.*, 2017b). This suggests that TSPO acts to ensure ATP is rapidly produced during perceived energy deficit, making cells preferentially use glucose

to produce energy. Interestingly, TSPO ligand Ro5-4864 prevents astrocyte cell death during glucose deprivation, suggesting that astrocytes can make use of an alternative fuel source when TSPO is modulated (Baez *et al.*, 2017). As modulation or loss of TSPO has been shown to increase AMPK phosphorylation, I suggest that this is potentially through increased AMPK activity and increased FAO capability (Kim *et al.*, 2019).

## 5.5 Conclusion

In conclusion, I have shown in this chapter that loss of TSPO increases FAO but decreases overall oxidative metabolism. This suggests that TSPO expression restricts FAO in astrocytes. This suppression of FAO could potentially be mediated through the interaction between TSPO and CPT-1A shown here. Additionally, TSPO expression appears to promote mitochondrial metabolism of substrates other that fatty acids. This may indicate that TSPO plays a role in regulating substrate use through promoting glucose use and pyruvate trafficking into the mitochondria, and restricting FAO to allow inflammation.

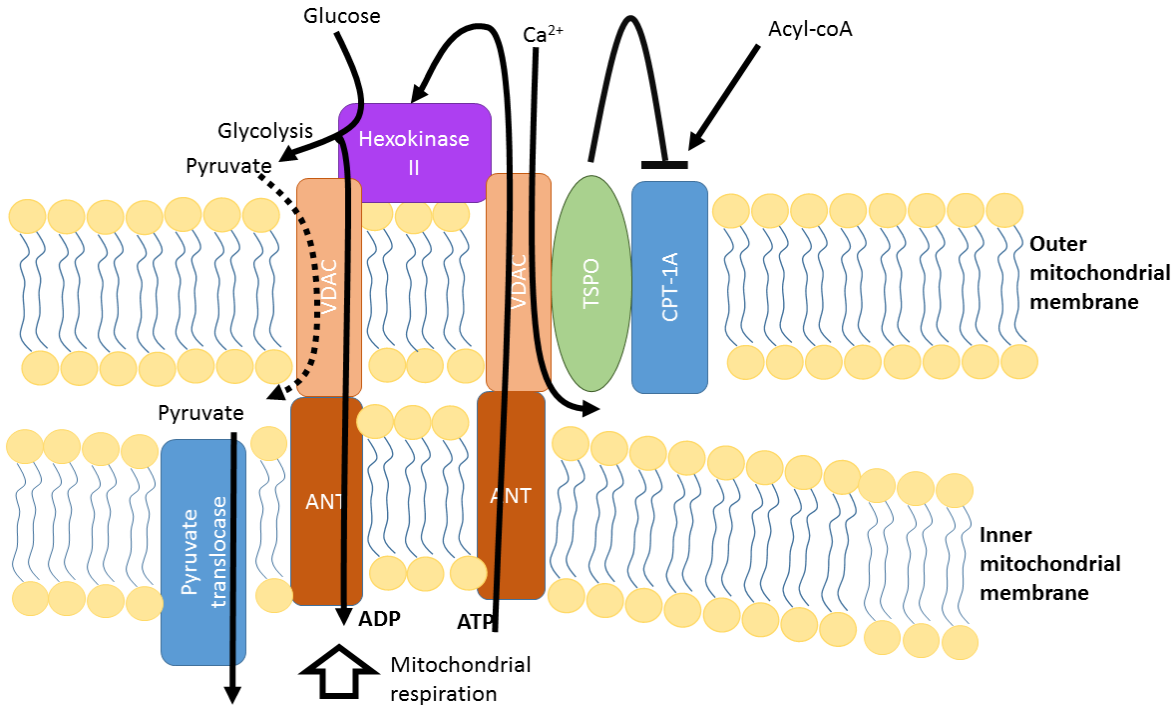


**Figure 5.5.1: Hypothetical model by which TSPO regulates metabolism.** Translocator protein 18 kDa (TSPO) interacts with carnitine palmitoyl transferase 1A (CPT-1A) to inhibit fatty acid transport into the mitochondria. Voltage dependent anion channel (VDAC) associated with hexokinase II binds the TSPO/CPT-1A complex to 'dock' to mitochondria and adenosine nucleotide transporter (ANT). This increases ATP/ADP exchange between the mitochondrial matrix and hexokinase II, increases calcium ($Ca^{2+}$) transport into the mitochondria, and possibly pyruvate transport. This increases OXPHOS rate and decreases cytoplasmic $Ca^{2+}$, restricting $Ca^{2+}$ mediated activation of AMP activated protein kinase (AMPK).

# Chapter 6. Discussion and Limitations

This chapter will summarise the key findings of this body of work and bring together the themes covered. It will also highlight limitations of the studies imposed by the methods used and propose further studies which would help address any questions raised by this thesis.

## 6.1 Summary of findings

### 6.1.1 NF-κB regulates astrocyte immunometabolism

This thesis aimed to characterise immunometabolic behaviour in astrocytes and examine the role of NF-κB in this phenomenon. Whilst this had been investigated to some extent in immune responsive cells such as microglia, macrophages and lymphocytes, it had not been directly investigated in astrocytes (Hotamisligil, 2017; O'Neill *et al.*, 2016; Robb *et al.*, 2019; Van den Bossche *et al.*, 2017).

Work presented in **Chapter 3** and **Chapter 4** established that immunometabolic responses are present in astrocytes and that NF-κB signalling was important in this response. Previous work by Gavillet *et al.* and Belenger *et al.* shows that pro-inflammatory cytokines increase $CO_2$ production and glucose uptake while decreasing glycogen stores in astrocytes after 48 hours, suggesting an increased use of the PPP and TCA cycle (Bélanger *et al.*, 2011b; Gavillet *et al.*, 2008). However, beyond this the role of cellular metabolism in astrocyte inflammation was relatively unexplored. Our data indicating that NF-κB signalling increased

glycolytic rate after 3 hours of treatment with LPS, and that limiting glycolysis with 2-DG decreased inflammatory outputs (pro-inflammatory cytokine production and NF-κB signalling) offers a significant contribution to this emerging field of study by demonstrating that intact glycolysis is necessary for the full acute inflammatory response of astrocytes following LPS stimulation.

After 24 hours treatment with LPS, astrocytes underwent a further metabolic adaptation: decreased glycolytic capacity and increased OXPHOS. The decrease in glycolytic capacity was likely to have been driven by the decrease in GLUT1 expression observed, which was dependent on intact NF-κB signalling. This decrease in GLUT1 expression was possibly a mechanism to restrict the ability of astrocytes to use glycolysis (Freemerman *et al.*, 2014). In macrophages and lymphocytes it has been shown that decreased GLUT1 expression reduces inflammation through suppressing glycolysis (Freemerman *et al.*, 2014; Siska *et al.*, 2016). As **Chapter 3** demonstrated, use of glycolysis was essential to maintain a pro-inflammatory response in astrocytes, the downregulation of GLUT1 and increased use of OXPHOS could be an anti-inflammatory mechanism, contributing to resolution of the pro-inflammatory response.

Together these data give strong evidence that astrocytes have dynamic immunometabolic responses, in part orchestrated by NF-κB signalling, as has been shown in other cell types (O'Neill *et al.*, 2016; Russell *et al.*, 2019). This finding is novel in astrocytes. I propose that these functions are mediated through an interaction between p53 and NF-κB, based on previous work by Mauro *et al*.

in fibroblasts (Mauro *et al.*, 2011), but further work would be necessary to specifically address this.

### 6.1.2 Therapeutic targeting of immunometabolism through NF-κB inhibition in astrocytes

As inflammation in astrocytes has been implicated in increasing the severity of some diseases, such as Alzheimer's disease, understanding the resolution of inflammation in astrocytes is important to enable development of new therapies to restrict chronic inflammation (Chun & Lee, 2018; Liu *et al.*, 2014a). The data presented in this thesis may suggest that NF-κB signalling is an appropriate target for therapeutically regulating glycolysis in pathologies such as highly glycolytic cancers. Supporting this, NF-κB is upregulated in glioblastomas, inhibition of which reduces human glioblastoma cell growth *in vitro* and tumour volume in mice *in vivo,* suggesting it is a suitable target (Puliyappadamba *et al.*, 2014; Robe *et al.*, 2004; Waters *et al.*, 2019). However, further studies (as described in the discussion of **Chapters 3 and 4**) would be needed to explore this new hypothesis.

A secondary finding presented in this body of work was that inhibition of NF-κB signalling reduced both glycolysis and OXPHOS independently of inflammation. This demonstrates that, in agreement with data from fibroblasts (Mauro *et al.*, 2011), NF-κB supports basal metabolic function in astrocytes in the absence of a pro-inflammatory stimulus (**Chapter 4**). Again, in astrocytes this finding is novel and may suggest that basal NF-κB signalling is important for normal astrocyte function. Supporting this, loss of NF-κB signalling *in vivo* reduces GLT-1 expression and glutamate cycling, which could result in excitotoxicity and

neuronal death (Ghosh *et al.*, 2011). Together these data suggest that normal astrocyte function relies on NF-κB signalling to maintain the CNS microenvironment. This highlights the need to be cautious with application of this as a therapy without further study, as inappropriate use could lead to significant consequences.

Although immunometabolism is an attractive therapeutic target due to the opportunity to re-purpose pre-existing drugs in new contexts, it is important to note that caution should be used with this approach. Inflammation is primarily a protective response, and inhibition of this may lead to increased disease pathology if not properly understood. Additionally, inappropriate inhibition of cellular metabolism could result in cellular energy deficits and premature cell death. With this is mind, it is important that further research is carried out to increase the current understanding of immunometabolism in astrocytes, to ensure these therapies can be applied appropriately and safely.

### 6.1.3 TSPO regulates cellular metabolism in astrocytes

In a related study I aimed to investigate translocator protein 18 kDa (TSPO) as a potential novel regulator of immunometabolism in astrocytes. TSPO is a promising therapeutic target for inflammatory disease in the CNS as it is not found in neurons (so targeting its activity would have less of an impact on these cells), and TSPO ligands have already been approved for use in humans (Li *et al.*, 2017; Ravikumar *et al.*, 2016). In this thesis, modulation of TSPO through pharmacological manipulation and genetic loss of expression altered cellular metabolism, increasing FAO and decreasing the use of glucose derivatives to

fuel the TCA cycle (**Chapter 5**). These findings are supported by an increasing body of published work (Gut *et al.*, 2013; Kim *et al.*, 2019; Li & Papadopoulos, 2015; Lin *et al.*, 2019; Tu *et al.*, 2016). Thus, the changes in TSPO expression in astrocytes during inflammation and diseases such as cancers and Alzheimer's disease may be driving the changes to cellular metabolism associated with these diseases.

As was expected from previously published data, TSPO was upregulated in astrocytes by 24 hours exposure to LPS (**Chapter 5**), possibly due to the metabolic changes reported in **Chapter 3** (Azrad *et al.*, 2019; Horiguchi *et al.*, 2019; Santoro *et al.*, 2016). This was supported by data showing that the glycolytic inhibitor 2-DG reduced TSPO expression, although further studies as described in **Chapter 5** would be important to more fully investigate the role of metabolism in TSPO regulation. This reiterates the involvement of cellular metabolism in inflammation in astrocytes. Interpreting this with our metabolic analysis, the increase in TSPO expression may be expected to decrease FAO and increase glycolysis and OXPHOS, as I have reported in **Chapter 3**. This metabolic reprogramming could support neuronal function during periods of stress as aerobic glycolysis and OXPHOS have been demonstrated to be essential for maintaining normal brain function (Dienel, 2019).

Pathways that regulate TSPO expression also regulate GLUT1 expression, which I have demonstrated to be an important regulator of glycolysis in astrocyte inflammation. For example, in **Chapter 3** and **Chapter 4** I found that GLUT1 expression was downregulated by prolonged NF-κB signalling. NF-κB is

downstream of the PI3K/Akt pathway (Dan *et al.*, 2008; Lawrence, 2009). In human retinal epithelial cells GLUT1 is downregulated by PI3K/Akt signalling (Kim *et al.*, 2007a). PI3K signalling also activates AP-1 which promotes TSPO expression, suggesting that the downregulation of GLUT1 and upregulation of TSPO may be linked during a pro-inflammatory stimulus (Rashid *et al.*, 2018; Shimoyama *et al.*, 2019). This is supported by our data demonstrating that these changes in expression both occur 24 hours after exposure to LPS. However, this is circumstantial evidence, so further studies are needed to directly confirm this hypothesis. Together these data provide further evidence that PI3K signalling integrates inflammatory and metabolic signalling through the downstream proteins it activates (Hawkins & Stephens, 2015).

While I discovered a novel interaction between TSPO and CPT-1A, the function of this interaction was not explored in this body of work. I propose that TSPO and CPT-1A interact in a larger complex including VDAC and hexokinase II, which have been previously reported to interact with TSPO (Arzoine *et al.*, 2009; Camara *et al.*, 2017; Pastorino & Hoek, 2008). I further hypothesise that this complex functions to integrate mitochondrial and glycolytic metabolism, based on the known functions of the proteins and data shown in this work. If this is demonstrated to be true, it may have implications for the possible application of TSPO ligands as therapeutics for metabolic diseases, as VDAC and hexokinase II are already being investigated in this role in peripheral tissues (Camara *et al.*, 2017; Roberts & Miyamoto, 2015). However further work is needed to explore this new hypothesis, as is detailed in **Chapter 5**.

### 6.1.4 TSPO as a potential novel regulator of immunometabolism

Although I have shown that metabolism and inflammation in astrocytes are intrinsically linked, metabolism appeared to change independently of inflammation when TSPO was manipulated within the time range studied, resulting in no change to the concentrations of the cytokines measured (**Chapter 5**). However, this was contrary to many published studies (Azrad *et al.*, 2019; Horiguchi *et al.*, 2019; Santoro *et al.*, 2016). I suggested that TSPO is a direct modulator of cellular metabolism, but not necessarily inflammation. However, due to conflicting evidence in the literature and the limited time points measured in the studies presented here, I cannot make strong conclusions around this hypothesis.

Further to this, I suggested that, unlike in macrophages and other cells in which TSPO is anti-inflammatory, FAO is not a regulator of immunometabolism in astrocytes, hence why I saw no change in cytokine release (Van den Bossche *et al.*, 2017). However, as I did not look at cytokine release or inflammatory signalling pathways at later time points I cannot comment on whether FAO affects inflammation later in the immunometabolic response. Significant further studies as described in **Chapter 5** would be necessary to strengthen these conclusions.

However, even though modulation of TSPO does not appear to affect the inflammatory profile of astrocytes at the time point examined thus far, many astrocyte functions are regulated by cellular metabolism, including those that support neuronal function, such as the synthesis of gliotransmitters and the recycling of neurotransmitters. Therefore, further studies into the impact that

modulation of TSPO may have on the wider CNS microenvironment, including gliotransmission and maintenance of the synaptic environment, may reveal more about the role of TSPO in astrocytes.

## 6.2 Limitations

Specific limitations of each study have been discussed within the relevant chapters. This section will detail the overarching limitations of the thesis as a whole.

### 6.2.1 Dependence on *in vitro* models

A major limitation of the studies presented was the sole use of *in vitro* models. These inherently take astrocytes out of the wider context of the diverse multicellular environment *in vivo*. The lack of neurotransmitters, cell-cell interactions, glial-derived factors, 3D morphology and hormones, among other factors, is likely to result in profound changes to astrocyte behaviour. However, for the exploratory research conducted in this study *in vitro* models were an appropriate starting point for our investigations and establish proof of principle prior to progressing to multicellular *in vitro* systems and the more complex *in vivo* environment. To take this study further, use of *in vivo* models would be necessary to study the effect of modulating astrocyte immunometabolism on neuronal function and whole-body physiology.

### 6.2.2 Limited range of inflammatory pathways studied

These studies used a reductionist approach, with no study of inflammatory pathways other than NF-κB. It is highly unlikely that NF-κB is the only pathway playing a role in astrocyte immunometabolism. For example, in many inflammatory diseases STAT3 has been shown to play a critical role in cytokine release and metabolic reprogramming (Demaria *et al.*, 2014; Kasembeli *et al.*, 2018; Kurdi *et al.*, 2018; Poli & Camporeale, 2015). Additionally, STAT3 is overexpressed in many cancers, including glioblastomas which I have previously mentioned to have metabolic perturbations and pro-inflammatory phenotypes (Demaria *et al.*, 2014; Yang Sheng *et al.*, 2019). Alternatively, MAPKs, which can be activated by inflammatory stimuli, have been shown to play a role in metabolic disorders (Papa *et al.*, 2019). Therefore, investigating the effect of other key signalling pathways on metabolism during inflammation, in particular STAT3, would be both interesting and relevant to explore in further studies.

### 6.2.3 No direct study of FAO in immunometabolism

Although suggestions were made that FAO does not play a role in inflammation in astrocytes, FAO in mouse primary astrocytes after treatment with LPS, or inflammatory outputs after modulating FAO function were not directly measured. Therefore, I cannot yet confidently comment on the importance of FAO to the inflammatory response in astrocytes. This would be an important study to follow up on, especially considering the apparent role of TSPO in modulating this metabolic pathway. Initial studies of the astrocyte FAO immunometabolic response to LPS using the Seahorse metabolic analyser, combining the study design from **Chapter 3** with the FAO Mito Stress Test used in **Chapter 5**, would

provide initial information to inform further studies. Results from this experiment would inform further experiments blocking FAO with etomoxir and/or promoting FAO through activating peroxisome proliferator activating protein activator, or another mechanism, and measuring inflammation to directly assess the effect of FAO metabolism on inflammation.

## 6.3 Outstanding questions and future directions

### 6.3.1 What is the effect of astrocyte glycolysis on the CNS microenvironment during inflammation?

One important question which requires addressing is the effect of blocking glycolysis in astrocytes on the wider CNS environment. As discussed in the introduction, astrocytes play an important role in maintaining CNS physiology and neuronal health. To answer this question, specifically blocking glycolysis in astrocytes during inflammation *in vivo* would be important. A targeted approach using genetic manipulation to restrict GLUT1 expression in astrocytes, or activity of glycolytic enzymes such as hexokinase II, and measuring end points such as circulating and cerebrospinal fluid cytokines, astrocyte ramification, astrocytic expression of glutamate and $K^+$ transporters, neuronal activity with electrophysiology and *cFos* expression, amongst others. This genetic modification would have to be inducible as long-term inhibition of astrocyte glycolysis is likely to have severely detrimental effects.

### 6.3.2 What is the effect of metabolic intermediates and products from astrocytes on the inflammatory response in the CNS?

Increasing evidence suggests that metabolic intermediates and products including succinate, citrate and lactate, are important inflammatory mediators (Murphy & O'Neill, 2018; Nolt *et al.*, 2018; Pucino *et al.*, 2019; Williams & O'Neill, 2018). Investigation into the production and role of these during inflammation in the CNS would be interesting. Of interest would be the impact of these molecules on the behaviour of other cells in the CNS. Lactate is known to be a gliotransmitter, but there is little exploration into the roles of other metabolic intermediates in modulating CNS neurotransmission and other functions (Gundersen *et al.*, 2015). Investigation of other metabolic intermediates as potential novel gliotransmitters may shed light on the control of astrocyte function during inflammation in the wider CNS network.

### 6.3.3 Does FAO play a role in the regulation of inflammation in astrocytes?

To explore the role of TSPO in inflammation further it would be important to measure FAO rate after treatment with LPS, and to investigate the importance of FAO in inflammation, as described above. This would go some way to exploring whether TSPO is directly involved in an immunometabolic regulatory response, or whether it just regulates metabolism in astrocytes. It would also be important to carry out the studies described in **Chapter 5**.

### 6.3.4 Does modulation of TSPO activity in astrocytes improve CNS health after an inflammatory stimulus?

As previously mentioned, a major limitation of this study was that astrocytes were investigated independently of other cell types. As astrocytes play an important role in regulating the CNS environment, the changes in metabolism caused by modulation or loss of TSPO may have an impact on the other cell types astrocytes interact with. To investigate this, *in vivo* work in animals with astrocyte-specific loss of TSPO challenged with LPS as an inflammatory stimulus followed by investigation of inflammatory markers, metabolic markers and neuronal function would be interesting.

## 6.4 Key conclusions arising from this thesis (fig. 6.4)

- Astrocyte metabolism is intrinsically linked to their inflammatory response, giving them 'immunometabolic' responses to inflammation.
- Astrocyte immunometabolism is regulated in part by NF-κB signalling.
- NF-κB signalling supports basal metabolism in astrocytes in the absence of a pro-inflammatory stimulus.
- TSPO expression promotes cellular glycolysis and OXPHOS in astrocytes.
- TSPO expression inhibits FAO in astrocytes.

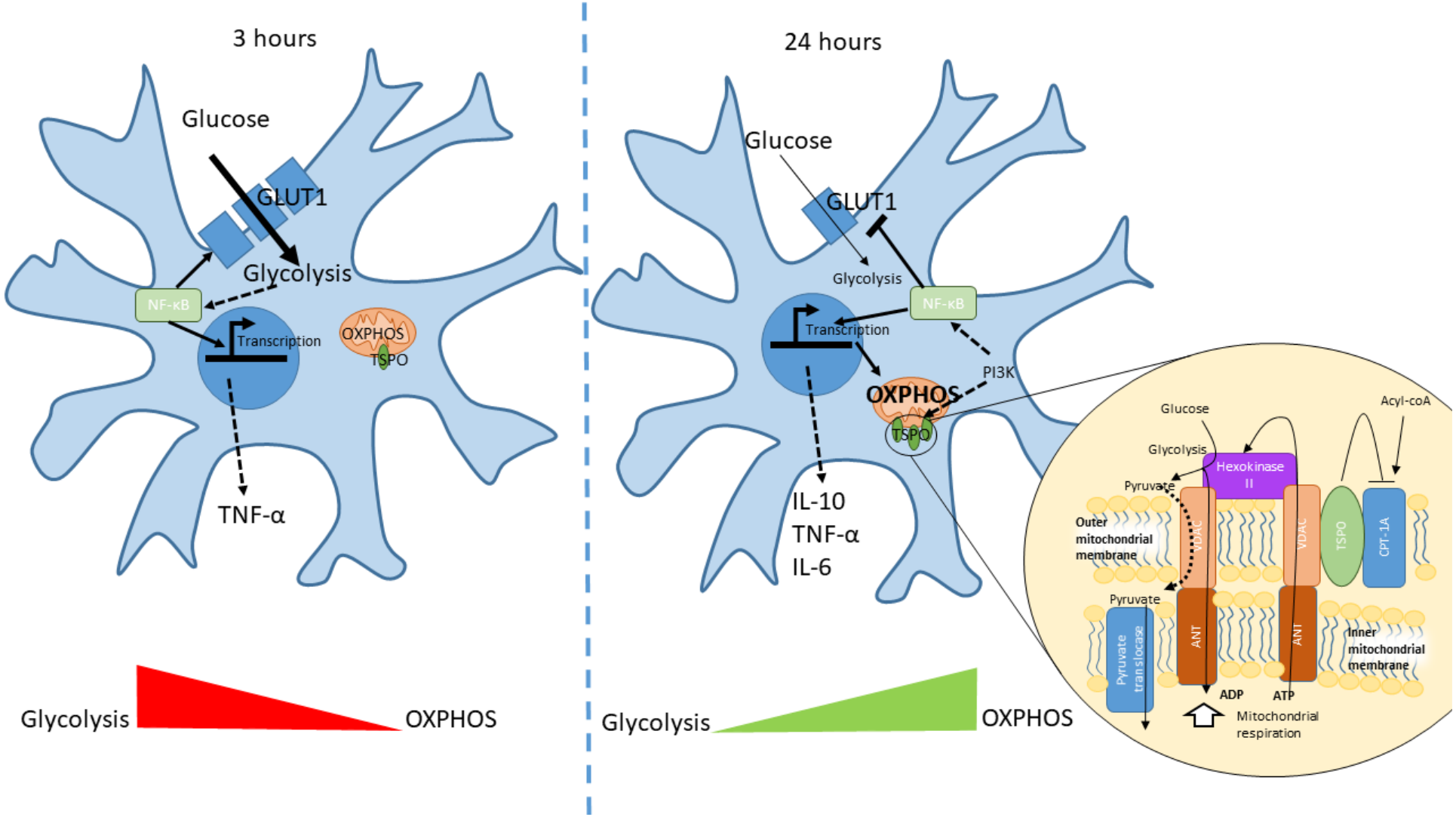
3 hours
Glucose
GLUT1
Glycolysis
NF-κB
Transcription
OXPHOS
TSPO
TNF-α
Glycolysis
OXPHOS
24 hours
Glucose
GLUT1
Glycolysis
NF-κB
Transcription
PI3K
OXPHOS
TSPO
IL-10
TNF-α
IL-6
Glycolysis
OXPHOS
Glucose
Acyl-coA
Glycolysis
Hexokinase II
Pyruvate
Outer mitochondrial membrane
VDAC
VDAC
TSPO
CPT-1A
Pyruvate
Pyruvate translocase
ANT
ANT
Inner mitochondrial membrane
ADP
ATP
Mitochondrial respiration

**Figure 6.4: Summary of thesis.** 3 hours after pro-inflammatory stimulus, astrocytes increase their use of glycolytic metabolism through nuclear factor kappa B (NF-κB) mediated mechanisms to allow synthesis of cytokines. 24 hours after pro-inflammatory stimulus, translocator protein 18 kDa (TSPO) expression is increased and NF-κB driven mechanisms decrease glycolytic rate through downregulation of glucose transporter GLUT1 expression. NF-κB signalling increases oxidative phosphorylation after 24 hours. TSPO may interact in a complex with other metabolic regulators to more closely integrate OXPHOS and glycolysis, and to limit FAO during inflammation.

# Appendices

## Appendix 1: Full representative immunoblots

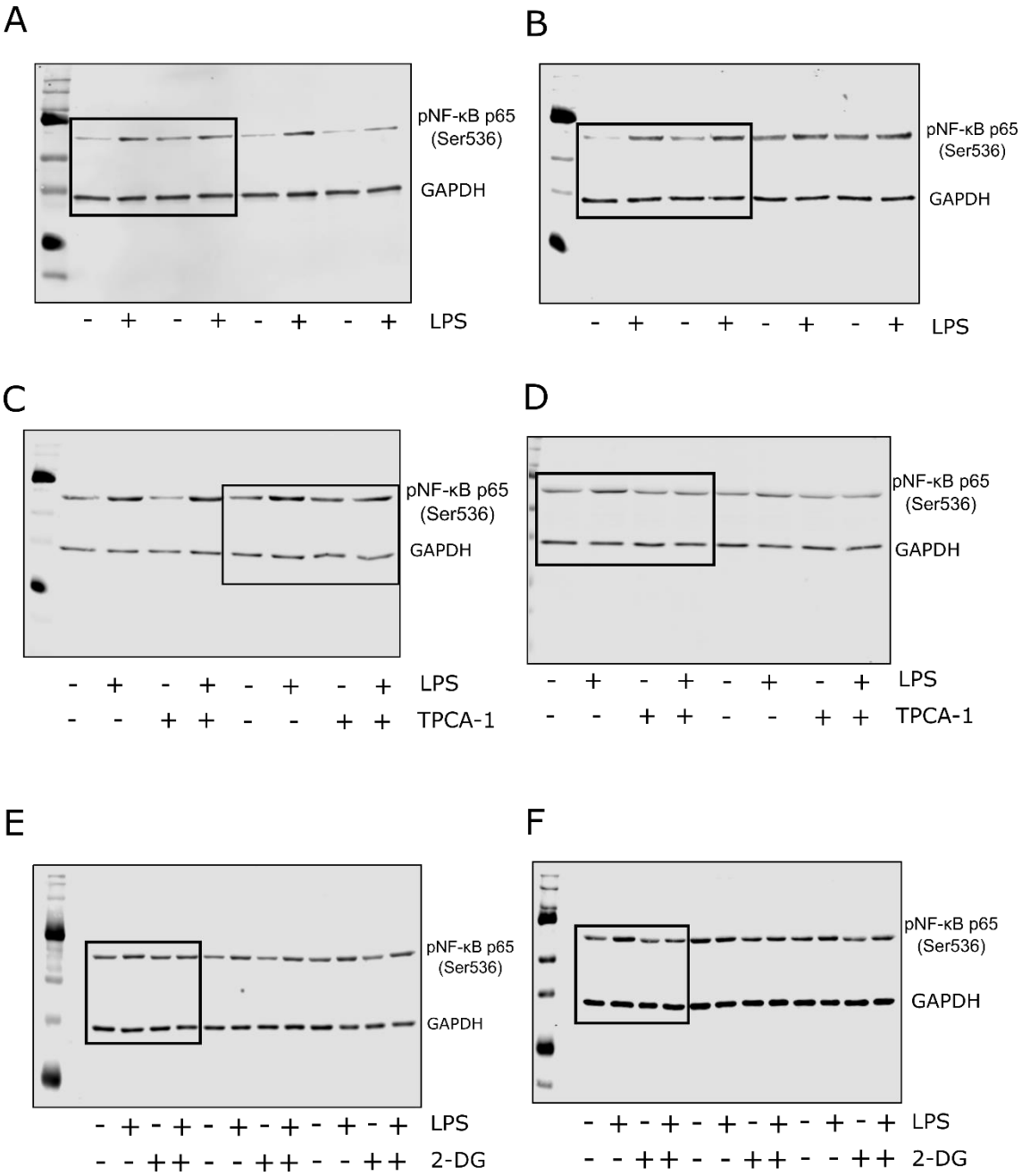

**Appendix 1.1: Full representative immunoblots probed with anti-phospho-NF-κB p65 (Ser536).** Immunoblots of treated mouse primary astrocyte (CRTAS) lysates. Bands of protein detected by anti-phospho-NF-κB (Ser536; Cell Signalling Technologies) were seen at the expected size of ~60 kDa. Anti-GAPDH (Protein Tech) loading control was used on all blots, and detected at the expected size of ~37 kDa. Boxes indicate cropped area for use in figures. **A.** CRTAS treated with 0.1 µg/mL lipopolysaccharide (LPS) for 3 hours. **B.** CRTAS treated with 0.1 µg/mL LPS for 24 hours. **C.** CRTAS pre-treated with 1 µM TPCA-1 for 2 hours ± 0.1 µg/mL LPS for 3 hours. **D.** CRTAS pre-treated with 1 µM TPCA-1 for 2 hours ± 0.1 µg/mL LPS for 24 hours. **E.** CRTAS pre-treated with 10 mM 2-deoxyglucose (2-DG) for 2 hours ± 0.1 µg/mL LPS for 3 hours. **F.** CRTAS pre-treated with 10 mM 2-deoxyglucose (2-DG) for 2 hours ± 0.1 µg/mL LPS for 24 hours.

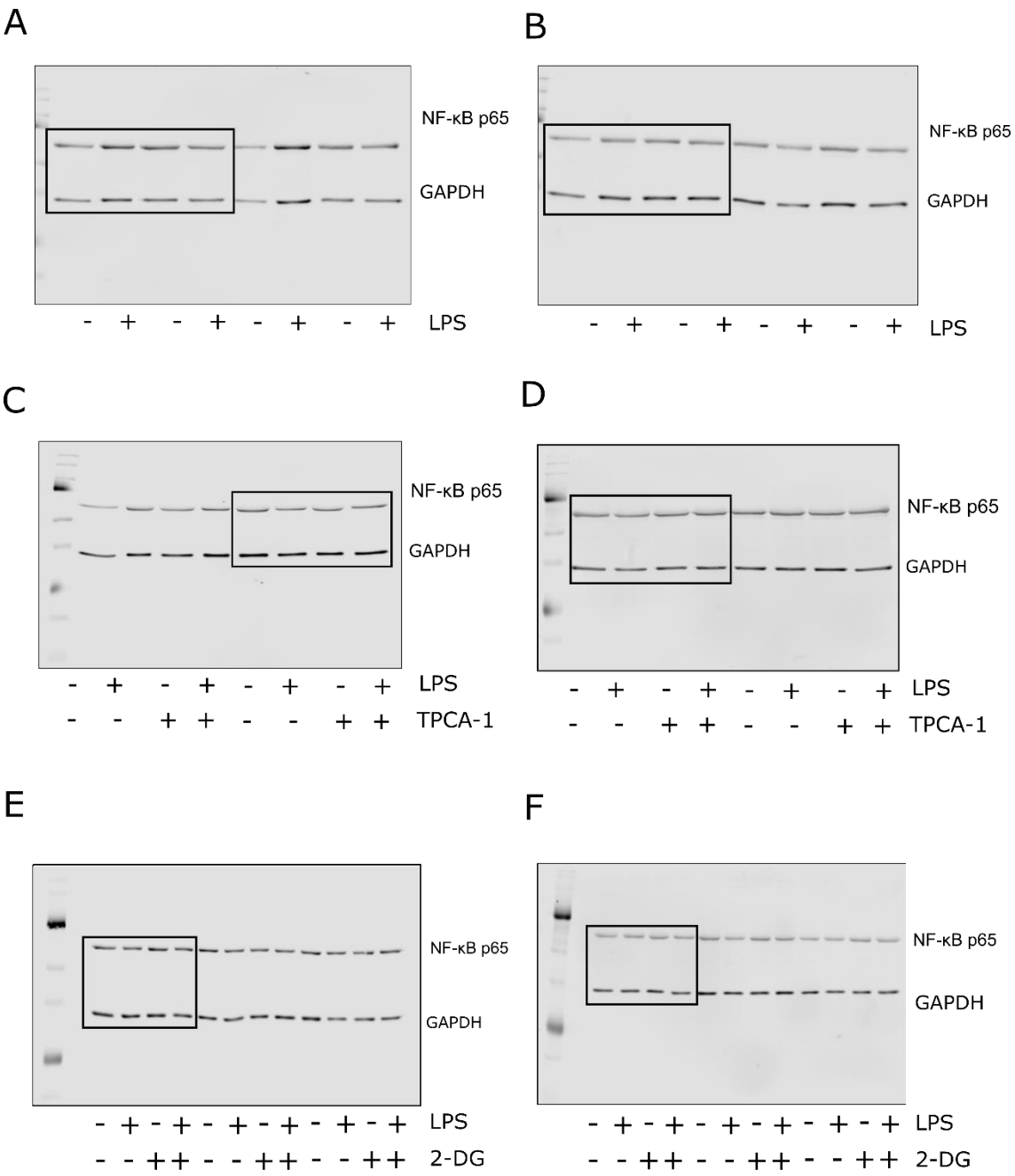
A
NF-κB p65
GAPDH
- + - + - + - + LPS
B
NF-κB p65
GAPDH
- + - + - + - + LPS
C
NF-κB p65
GAPDH
- + - + - + - + LPS
- - + + - - + + TPCA-1
D
NF-κB p65
GAPDH
- + - + - + - + LPS
- - + + - - + + TPCA-1
E
NF-κB p65
GAPDH
- + - + - + - + - + - + LPS
- - + + - - + + - - + + 2-DG
F
NF-κB p65
GAPDH
- + - + - + - + - + - + LPS
- - + + - - + + - - + + 2-DG

**Appendix 1.2: Full representative immunoblots probed with anti-NF-κB p65.** Immunoblots of treated mouse primary astrocyte (CRTAS) lysates. Bands of protein detected by anti-NF-κB (Cell Signalling Technologies) were seen at the expected size of ~60 kDa. Anti-GAPDH (Protein Tech) loading control was used on all blots, and detected at the expected size of ~37 kDa. Boxes indicate cropped area for use in figures. **A.** CRTAS treated with 0.1 µg/mL lipopolysaccharide (LPS) for 3 hours. **B.** CRTAS treated with 0.1 µg/mL LPS for 24 hours. **C.** CRTAS pre-treated with 1 µM TPCA-1 for 2 hours ± 0.1 µg/mL LPS for 3 hours. **D.** CRTAS pre-treated with 1 µM TPCA-1 for 2 hours ± 0.1 µg/mL LPS for 24 hours. **E.** CRTAS pre-treated with 10 mM 2-deoxyglucose (2-DG) for 2 hours ± 0.1 µg/mL LPS for 3 hours. **F.** CRTAS pre-treated with 10 mM 2-deoxyglucose (2-DG) for 2 hours ± 0.1 µg/mL LPS for 24 hours.

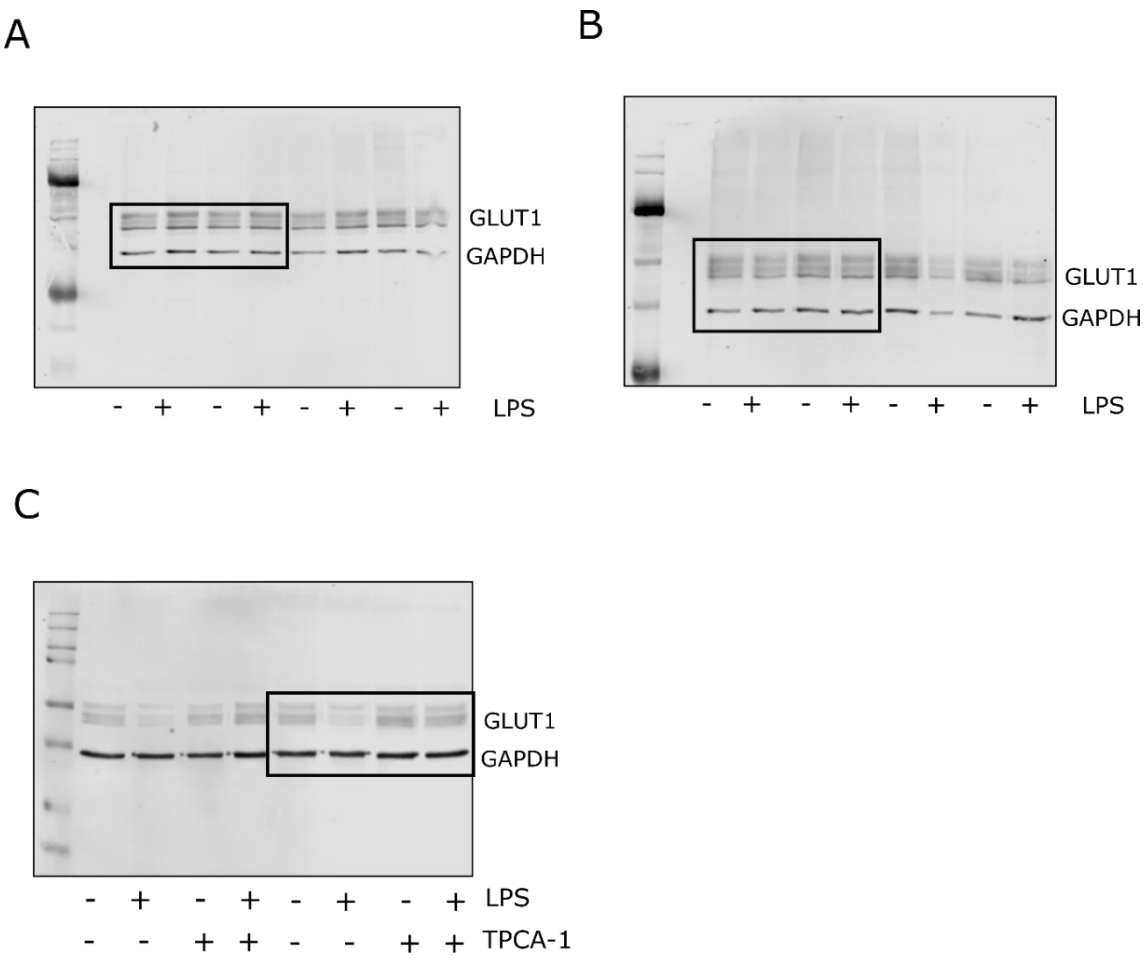


**Appendix 1.3: Full representative immunoblots probed with anti-GLUT1.** Immunoblots of treated mouse primary astrocyte (CRTAS) lysates. Bands of protein detected by anti-GLUT1 (Millipore) were seen at the expected size of ~50 kDa. Anti-GAPDH (Protein Tech) loading control was used on all blots, and detected at the expected size of ~37 kDa. Boxes indicate cropped area for use in figures. **A.** CRTAS treated with 0.1 µg/mL lipopolysaccharide (LPS) for 3 hours. **B.** CRTAS treated with 0.1 µg/mL LPS for 24 hours. **C.** CRTAS pre-treated with 1 µM TPCA-1 for 2 hours ± 0.1 µg/mL LPS for 24 hours.

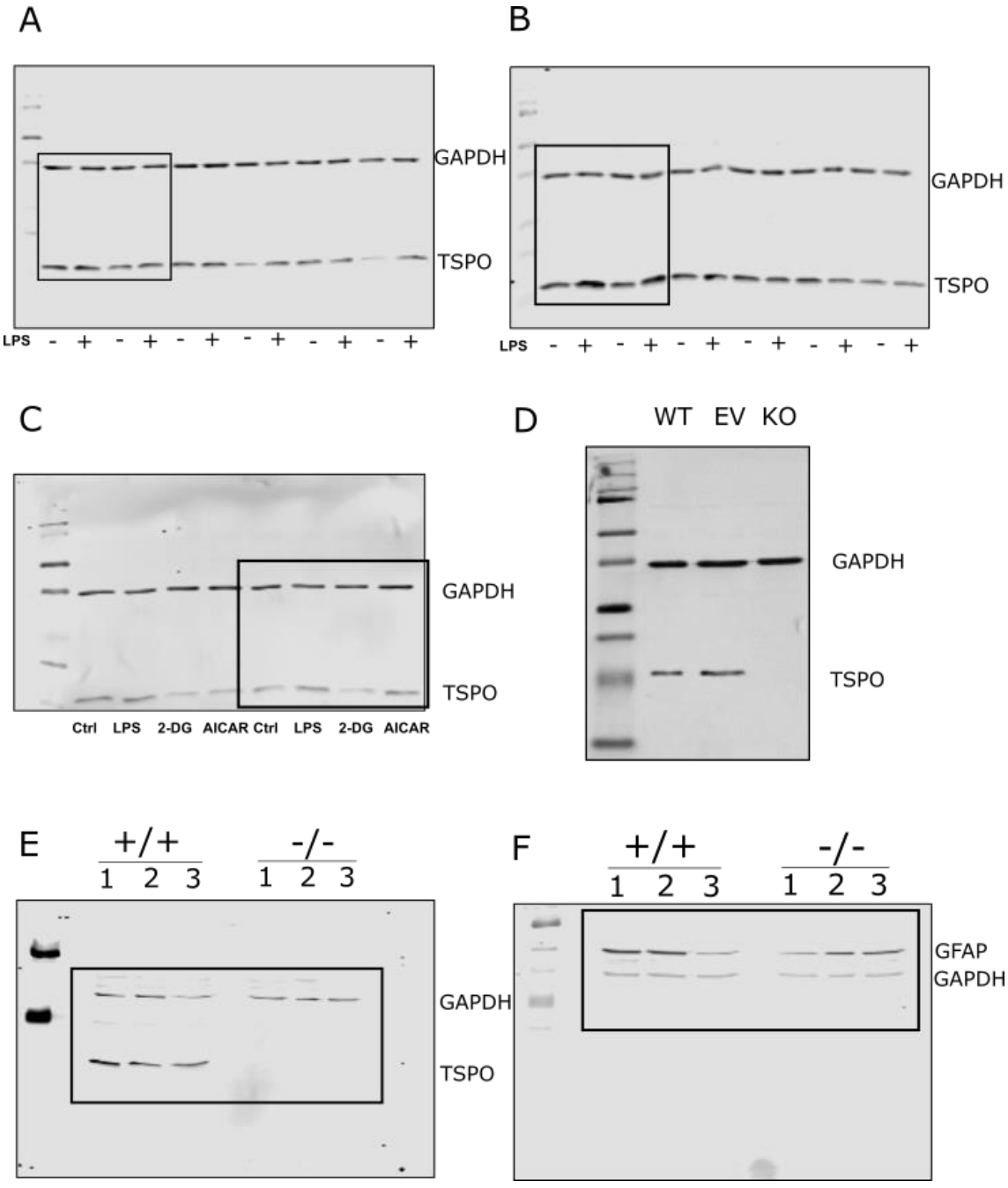
A
GAPDH
TSPO
LPS - + - + - + - + - + - +
B
GAPDH
TSPO
LPS - + - + - + - + - + - +
C
GAPDH
TSPO
Ctrl LPS 2-DG AICAR Ctrl LPS 2-DG AICAR
D
WT EV KO
GAPDH
TSPO
E
+/+
1 2 3
-/-
1 2 3
GAPDH
TSPO
F
+/+
1 2 3
-/-
1 2 3
GFAP
GAPDH

**Appendix 1.4: Full representative immunoblots probed with anti-TSPO.** Immunoblots of mouse primary astrocyte (CRTAS) or human astroglioma (U373) lysates. Bands of protein detected by anti-TSPO (Cell Signalling Technologies) were seen at the expected size of ~18 kDa. Bands of protein detected by anti-GFAP (Millipore) were seen at the expected size of ~50 kDa. Anti-GAPDH (Protein Tech) loading control was used on all blots, and detected at the expected size of ~37 kDa. Boxes indicate cropped area for use in figures. **A.** CRTAS treated with 0.1 µg/mL lipopolysaccharide (LPS) for 3 hours. **B.** CRTAS treated with 0.1 µg/mL LPS for 24 hours. **C.** CRTAS treated with 0.1 µg/mL LPS, 2-deoxyglucose (2-DG; 10 mM), or AMPK activator AICAR (1 µM) for 24 hours. **D.** U373 untransfected cells (WT), cells transfected with an empty CRISPR/Cas9 vector (EV), and transfected with a CRISPR/Cas9 vector containing guide RNA (KO). **E.** CRTAS from $TSPO^{+/+}$ and $TSPO^{-/-}$ mice. **F.** GFAP expression in CRTAS from $TSPO^{+/+}$ and $TSPO^{-/-}$ mice (same samples used in panels E and F).

# Appendix 2: Annotated MatLab script for mitochondrial network analysis

```
%pixelSizes is a cell array with one cell for each image
pixelSizes=cell(60,1);
%Loop through each image in turn
for i=61:63
%Read in image
imgin=sprintf('%d.tif',i);
img=imread(imgin);
%filtersize sets up parameters for local threshold filter
filtersizeX=round(((size(img,1))/200)^2);
filtersizeY=filtersizeX;
offset=20;
%minsize is cut-off size for small noisy objects
minsize=round(((size(img,1))/350)^2);
%Select red channel (change this if mitochondrial stain is in a different
%channel
imgR=img(:,:,1);
%Apply local threshold filter to the image
imgF=imfilter(imgR,fspecial('average',[filtersizeX,filtersizeY]),'replicate');
%Subtract filtered image from original
img2=imgR-(imgF+offset);
%Select all positive pixels
imgbw=im2bw(img2,0);
%Remove noise
imgbw2=bwareaopen(imgbw,minsize);
%Save output image
imgout=sprintf('%d_out.png',i);
```

```
imwrite(imgbw2,imgout);
%Create Otsu global threshold for comparison
imgT=im2bw(imgR,graythresh(imgR));
%Display results
subplot(2,2,1);imshow(imgR); title('Original');
subplot(2,2,2);imshow(imgF); title('Global threshold');
subplot(2,2,3);imshow(imgbw); title('Local threshold');
subplot(2,2,4);imshow(imgbw2); title('Noise removed');
%Save displayed results
saveas(gcf(),sprintf('%d_results.jpeg',i));
%Calculate object sizes
CC=bwconncomp(imgbw2);
%numPix is a vector containing the number of pixels in each object in the
%current image
numPix=cellfun(@numel,CC.PixelIdxList);
%number of objects in numPix
objects=length(numPix);
%mean number of pixels in each object in current image
pixMean=mean(numPix);
%median number of pixels in each object in current images
pixMedian=median(numPix);
%Object number, Mean value and Median value is copied into the appropriate
%cell for that image
pixelSizes{1,1}='ImageNumber';
pixelSizes{1,2}='No.Objects';
pixelSizes{1,3}='MeanPixels';
pixelSizes{1,4}='MedianPixels';
pixelSizes{i-59,1}=i;
pixelSizes{i-59,2}=objects;
pixelSizes{i-59,3}=pixMean;
```

```
pixelSizes{i-59,4}=pixMedian;
%Loop ends, go back and open next image...
end
%Export pixelSizes as .csv (Excel) file
xlswrite('MitoData.xls',pixelSizes);
```

# Appendix 3: Immunometabolic Changes in Glia – A Potential Role in the Pathophysiology of Obesity and Diabetes

Josephine L. Robb, Nicole A. Morrissey, Paul G. Weightman Potter, Hannah E. Smithers, Craig Beall, Kate L.J. Ellacott. **Neuroscience.** (2019)

DOI: 10.1016/j.neuroscience.2019.10.021

Abstract: Chronic low-grade inflammation is a feature of the pathophysiology of obesity and diabetes in the CNS as well as peripheral tissues. Glial cells are critical mediators of the response to inflammation in the brain. Key features of glia include their metabolic flexibility, sensitivity to changes in the CNS microenvironment, and ability to rapidly adapt their function accordingly. They are specialised cells which cooperate to promote and preserve neuronal health, playing important roles in regulating the activity of neuronal networks across the brain during different life stages. Increasing evidence points to a role of glia, most notably astrocytes and microglia, in the systemic regulation of energy and glucose homeostasis in the course of normal physiological control and during disease. Inflammation is an energetically expensive process that requires adaptive changes in cellular metabolism and, in turn, metabolic intermediates can also have immunomodulatory actions. Such “immunometabolic” changes in peripheral immune cells have been implicated in contributing to disease pathology in obesity and diabetes. This review will discuss the evidence for a role of immunometabolic changes in glial cells in the systemic regulation of energy and glucose homeostasis, and how this changes in the context of obesity and diabetes.

# Appendix 4: The metabolic response to inflammation in astrocytes is regulated by nuclear factor-kappa B signaling.

Josephine L. Robb, Nadia A. Hammad, Paul G. Weightman Potter, John K. Chilton, Craig Beall, Kate L.J. Ellacott. **Glia.** (2020)

DOI: 10.1002/glia.23835

Abstract: Inflammation and metabolism are intrinsically linked with inflammatory stimuli inducing metabolic changes in cells and, in turn, metabolic capacity determining cellular inflammatory responses. Although well characterized in peripheral immune cells there is comparatively less known about these “immunometabolic” responses in astrocytes. In this study we tested the hypothesis that the astrocytic inflammatory response driven by nuclear factor-kappa B (NF-κB) signaling is dependent on glycolytic metabolism. Using mouse primary cortical astrocyte cultures we assessed changes in cellular metabolism after exposure to lipopolysaccharide (LPS), with cytokine ELISAs and immunoblotting being used to measure inflammatory responses. Results indicate temporally distinct metabolic adaptations to proinflammatory stimulation in astrocytes: 3 hour LPS treatment increased glycolysis but did not alter mitochondrial metabolism, while following 24 hours of LPS treatment we observed increased oxidative phosphorylation, and decreased glycolytic capacity and glucose uptake partly due to reduced glucose transporter 1 (GLUT1) expression. Inhibition of NF-κB signaling with the IKK-beta inhibitor TPCA-1 prevented the LPS induced changes to glycolysis and oxidative phosphorylation. Furthermore, TPCA-1 treatment altered both glycolysis and oxidative phosphorylation independently from inflammatory stimulation, indicating a role for

NF-κB signaling in regulation of basal metabolism in astrocytes. Inhibition of glycolysis with 2-deoxyglucose significantly attenuated LPS-induced cytokine release and NF-κB phosphorylation, indicating that intact glycolysis is required for the full inflammatory response to LPS. Together our data indicate that astrocytes display immunometabolic responses to acute LPS-stimulation which may represent a potential therapeutic target for neuroinflammatory disorders.

# Appendix 5: Example flow cytometry gating data from TMRE uptake assay (Fig. 3.3.10)

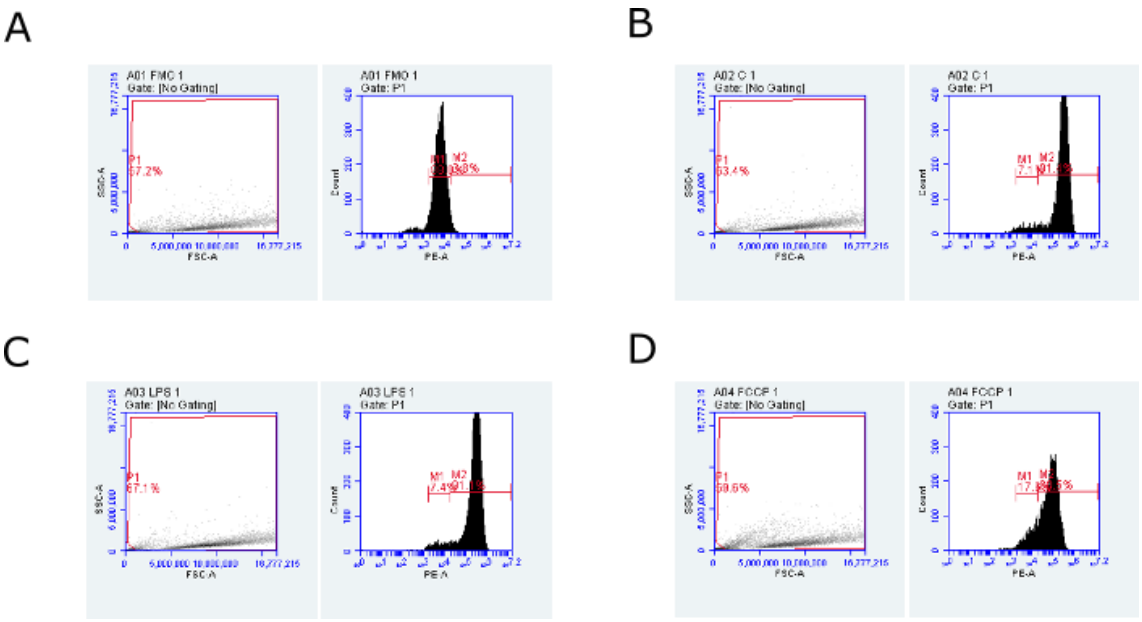


**Appendix 5. Representative data plots from TMRE dye uptake assays.** Cells were plated at a density of 3.5 x$10^5$ cells in 6 well dishes. After treatment with vehicle or lipopolysaccharide (0.1 µg/mL; LPS) cells were dissociated and incubated with FCCP (1 µM) or vehicle for 15 minutes prior to 30 minutes incubation with TMRE dye (100 nM) or vehicle and data collection on the BD Accuri C6 plus flow cytometer. Data from gate P1 Plot 1 was shown on Plot 2. Gate M1 Plot 2 was determined using the no TMRE stained control (FMO; **A**). Gate M2 started from the point gate M1 finished, and was used to determine stained cells. The mean of data in M2 was used as the TMRE dye uptake for the group. **A.** No TMRE stained control. **B.** vehicle treated control. **C.** 24 hour LPS treatment. **D.** FCCP treated depolarisation control.

# Reference list


Abboud, G., Choi, S.-C., Kanda, N., Zeumer-Spataro, L., Roopenian, D. C., & Morel, L. (2018). Inhibition of Glycolysis Reduces Disease Severity in an Autoimmune Model of Rheumatoid Arthritis. *Frontiers in Immunology, 9*, 1973-1973.

Adam-Vizi, V., & Chinopoulos, C. (2006). Bioenergetics and the formation of mitochondrial reactive oxygen species. *Trends in Pharmacological Sciences, 27*(12), 639-645.

Adams, K. L., & Gallo, V. (2018). The diversity and disparity of the glial scar. *Nature Neuroscience, 21*(1), 9-15.

Agarwal, E., Altman, B. J., Seo, J. H., Ghosh, J. C., Kossenkov, A. V., Tang, H.-Y., Krishn, S. R., Languino, L. R., Gabrilovich, D. I., Speicher, D. W., Dang, C. V., & Altieri, D. C. (2019). Myc-mediated transcriptional regulation of the mitochondrial chaperone TRAP1 controls primary and metastatic tumor growth. *Journal of Biological Chemistry, 294*(27), 10407-10414.

Alam, M. M., Lee, J., & Lee, S.-Y. (2017). Recent Progress in the Development of TSPO PET Ligands for Neuroinflammation Imaging in Neurological Diseases. *Nuclear medicine and molecular imaging, 51*(4), 283-296.

Albensi, B. C. (2019). What Is Nuclear Factor Kappa B (NF-κB) Doing in and to the Mitochondrion? *Frontiers in Cell and Developmental Biology, 7*, 154.

Aleyasin, H., Cregan, S. P., Iyirhiaro, G., O'Hare, M. J., Callaghan, S. M., Slack, R. S., & Park, D. S. (2004). Nuclear factor-(kappa)B modulates the p53 response in neurons exposed to DNA damage. *The Journal of neuroscience : the official journal of the Society for Neuroscience, 24*(12), 2963-2973.

Allen, N. J. (2014). Astrocyte Regulation of Synaptic Behavior. *Annual Review of Cell and Developmental Biology, 30*(1), 439-463.

Almeida, A., Moncada, S., & Bolaños, J. P. (2004). Nitric oxide switches on glycolysis through the AMP protein kinase and 6-phosphofructo-2-kinase pathway. *Nature Cell Biology, 6*(1), 45-51.

Alvarez, J. I., Katayama, T., & Prat, A. (2013). Glial influence on the blood brain barrier. *Glia, 61*(12), 1939-1958.

Amitani, M., Ohashi, A., Hatazawa, J., Gee, A., & Inoue, O. (2008). Effect of PK11195 on attenuating the enhancement of glucose utilization induced by quinolinic acid infusion in the rat brain. *Synapse, 62*(4), 253-258.

Angelova, P. R., & Abramov, A. Y. (2018). Role of mitochondrial ROS in the brain: from physiology to neurodegeneration. *FEBS Letters, 592*(5), 692-702.

Anholt, R. R., Pedersen, P. L., De Souza, E. B., & Snyder, S. H. (1986). The peripheral-type benzodiazepine receptor. Localization to the mitochondrial outer membrane. *The Journal of biological chemistry, 261*(2), 576-583.

Anrather, J., Racchumi, G., & Iadecola, C. (2006). NF-kappaB regulates phagocytic NADPH oxidase by inducing the expression of gp91phox. The *Journal of biological chemistry, 281*(9), 5657–5667.

Antico Arciuch, V. G., Elguero, M. E., Poderoso, J. J., & Carreras, M. C. (2012). Mitochondrial regulation of cell cycle and proliferation. *Antioxidants & redox signaling, 16*(10), 1150–1180.

Antonescu, C. N., McGraw, T. E., & Klip, A. (2014). Reciprocal regulation of endocytosis and metabolism. *Cold Spring Harbor perspectives in biology, 6*(7), a016964-a016964.

Arbo, B. D., Benetti, F., Garcia-Segura, L. M., & Ribeiro, M. F. (2015). Therapeutic actions of translocator protein (18kDa) ligands in experimental models of psychiatric disorders and neurodegenerative diseases. *The Journal of Steroid Biochemistry and Molecular Biology, 154*, 68-74.

Arif, T., Krelin, Y., & Shoshan-Barmatz, V. (2016). Reducing VDAC1 expression induces a non-apoptotic role for pro-apoptotic proteins in cancer cell differentiation. *Biochimica et Biophysica Acta (BBA) - Bioenergetics, 1857*(8), 1228-1242.

Arzoine, L., Zilberberg, N., Ben-Romano, R., & Shoshan-Barmatz, V. (2009). Voltage-dependent Anion Channel 1-based Peptides Interact with Hexokinase to Prevent Its Anti-apoptotic Activity. *Journal of Biological Chemistry, 284*(6), 3946-3955.

Assmann, N., O'Brien, K. L., Donnelly, R. P., Dyck, L., Zaiatz-Bittencourt, V., Loftus, R. M., Heinrich, P., Oefner, P. J., Lynch, L., Gardiner, C. M., Dettmer, K., & Finlay, D. K. (2017). Srebp-controlled glucose metabolism is essential for NK cell functional responses. *Nature immunology, 18*(11), 1197-1206.

Azoitei, N., Becher, A., Steinestel, K., Rouhi, A., Diepold, K., Genze, F., Simmet, T., & Seufferlein, T. (2016). PKM2 promotes tumor angiogenesis by regulating HIF-1α through NF-κB activation. *Molecular cancer, 15*, 3-3.

Azrad, M., Zeineh, N., Weizman, A., Veenman, L., & Gavish, M. (2019). The TSPO Ligands 2-Cl-MGV-1, MGV-1, and PK11195 Differentially Suppress the Inflammatory Response of BV-2 Microglial Cell to LPS. *International Journal of Molecular Sciences, 20*(3), 594.

Bader, S., Wolf, L., Milenkovic, V. M., Gruber, M., Nothdurfter, C., Rupprecht, R., & Wetzel, C. H. (2019). Differential effects of TSPO ligands on mitochondrial function in mouse microglia cells. *Psychoneuroendocrinology, 106*, 65-76.

Bae, K.-R., Shim, H.-J., Balu, D., Kim, S. R., & Yu, S.-W. (2014). Translocator Protein 18 kDa Negatively Regulates Inflammation in Microglia. *Journal of Neuroimmune Pharmacology, 9*(3), 424-437.

Baez, E., Guio-Vega, G. P., Echeverria, V., Sandoval-Rueda, D. A., & Barreto, G. E. (2017). 4′-Chlorodiazepam Protects Mitochondria in T98G Astrocyte Cell Line from Glucose Deprivation. *Neurotoxicity Research, 32*(2), 163-171.

Bak, L. K., Walls, A. B., Schousboe, A., & Waagepetersen, H. S. (2018). Astrocytic glycogen metabolism in the healthy and diseased brain. *Journal of Biological Chemistry, 293*(19), 7108-7116.

Banati, R. B., Middleton, R. J., Chan, R., Hatty, C. R., Wai-Ying Kam, W., Quin, C., Graeber, M. B., Parmar, A., Zahra, D., Callaghan, P., Fok, S., Howell, N. R., Gregoire, M., Szabo, A., Pham, T., Davis, E., & Liu, G.-J. (2014). Positron emission tomography and functional characterization of a complete PBR/TSPO knockout. *Nature communications, 5*(1), 5452.

Barron, A. M., Garcia-Segura, L. M., Caruso, D., Jayaraman, A., Lee, J.-W., Melcangi, R. C., & Pike, C. J. (2013). Ligand for Translocator Protein Reverses Pathology in a Mouse Model of Alzheimer's Disease. *The Journal of Neuroscience, 33*(20), 8891.

Basile, A. S., & Skolnick, P. (1986). Subcellular Localization of “Peripheral-Type” Binding Sites for Benzodiazepines in Rat Brain. *Journal of Neurochemistry, 46*(1), 305-308.

Batarseh, A., Giatzakis, C., & Papadopoulos, V. (2008). Phorbol-12-myristate 13-Acetate Acting through Protein Kinase Cε Induces Translocator Protein (18-kDa) Tspo Gene Expression. *Biochemistry, 47*(48), 12886-12899.

Batarseh, A., Li, J., & Papadopoulos, V. (2010). Protein kinase C epsilon regulation of translocator protein (18 kDa) Tspo gene expression is mediated through a MAPK pathway targeting STAT3 and c-Jun transcription factors. *Biochemistry, 49*(23), 4766-4778.

Batarseh, A., & Papadopoulos, V. (2010). Regulation of translocator protein 18 kDa (TSPO) expression in health and disease states. *Molecular and Cellular Endocrinology, 327*(1-2), 1-12.

Bazargani, N., & Attwell, D. (2016). Astrocyte calcium signaling: the third wave. *Nature Neuroscience, 19*(2), 182-189.

Becker, T., & Wagner, R. (2018). Mitochondrial Outer Membrane Channels: Emerging Diversity in Transport Processes. *BioEssays : news and reviews in molecular, cellular and developmental biology, 40*(7), e1800013-e1800013.

Beckers, L., Ory, D., Geric, I., Declercq, L., Koole, M., Kassiou, M., Bormans, G., & Baes, M. (2018). Increased Expression of Translocator Protein (TSPO) Marks Pro-inflammatory Microglia but Does Not Predict Neurodegeneration. *Molecular Imaging and Biology, 20*(1), 94-102.

Bélanger, M., Allaman, I., & Magistretti, Pierre J. (2011a). Brain Energy Metabolism: Focus on Astrocyte-Neuron Metabolic Cooperation. *Cell metabolism, 14*(6), 724-738.

Bélanger, M., Allaman, I., & Magistretti, P. J. (2011b). Differential effects of pro- and anti-inflammatory cytokines alone or in combinations on the metabolic profile of astrocytes. *Journal of Neurochemistry, 116*(4), 564-576.

BeltrandelRio, H., & Wilson, J. E. (1992). Coordinated regulation of cerebral glycolytic and oxidative metabolism, mediated by mitochondrially bound hexokinase dependent on intramitochondrially generated ATP. *Archives of Biochemistry and Biophysics, 296*(2), 667-677.

Berg J.M., Stryer L., Tymoczko J. (2002). *Biochemistry* (5 ed.). New York: W H Freeman.

Bhargavi, M., Sivan, S. K., & Potlapally, S. R. (2017). Identification of novel anti cancer agents by applying insilico methods for inhibition of TSPO protein. *Computational Biology and Chemistry, 68*, 43-55.

Bhoola, N. H., Mbita, Z., Hull, R., & Dlamini, Z. (2018). Translocator Protein (TSPO) as a Potential Biomarker in Human Cancers. *International Journal of Molecular Sciences, 19*(8), 2176.

Birrell, M. A., Hardaker, E., Wong, S., McCluskie, K., Catley, M., De Alba, J., Newton, R., Haj-Yahia, S., Pun, K. T., Watts, C. J., Shaw, R. J., Savage, T. J., & Belvisi, M. G. (2005). Ikappa-B kinase-2 inhibitor blocks inflammation in human airway smooth muscle and a rat model of asthma. *American journal of respiratory and critical care medicine, 172*(8), 962-971.

Biswas, L., Farhan, F., Reilly, J., Bartholomew, C., & Shu, X. (2018). TSPO Ligands Promote Cholesterol Efflux and Suppress Oxidative Stress and Inflammation in Choroidal Endothelial Cells. *International Journal of Molecular Sciences, 19*(12), 3740.

Blagih, J., Coulombe, F., Vincent, Emma E., Dupuy, F., Galicia-Vázquez, G., Yurchenko, E., Raissi, Thomas C., van der Windt, Gerritje J. W., Viollet, B., Pearce, Erika L., Pelletier, J., Piccirillo, Ciriaco A., Krawczyk, Connie M., Divangahi, M., & Jones, Russell G. (2015). The Energy Sensor AMPK Regulates T Cell Metabolic Adaptation and Effector Responses In Vivo. *Immunity, 42*(1), 41-54.

Bonora, M., Patergnani, S., Rimessi, A., De Marchi, E., Suski, J. M., Bononi, A., Giorgi, C., Marchi, S., Missiroli, S., Poletti, F., Wieckowski, M. R., & Pinton, P. (2012). ATP synthesis and storage. *Purinergic signalling, 8*(3), 343-357.

Bonsack, F., & Sukumari-Ramesh, S. (2018). TSPO: An Evolutionarily Conserved Protein with Elusive Functions. *International Journal of Molecular Sciences, 19*(6), 1694.

Bouillaud, F., Alves-Guerra, M.-C., & Ricquier, D. (2016). UCPs, at the interface between bioenergetics and metabolism. *Biochimica et Biophysica Acta (BBA) - Molecular Cell Research, 1863*(10), 2443-2456.

Braestrup, C., Nielsen, M., Biggio, G., & Squires, R. F. (1979). Neuronal localisation of benzodiazepine receptors in cerebellum. *Neuroscience letters, 13*(3), 219-224.

Braestrup, C., & Squires, R. F. (1977). Specific benzodiazepine receptors in rat brain characterized by high-affinity (3H)diazepam binding. *Proceedings of the National Academy of Sciences of the United States of America, 74*(9), 3805-3809.

Brambilla, R., Bracchi-Ricard, V., Hu, W.-H., Frydel, B., Bramwell, A., Karmally, S., Green, E. J., & Bethea, J. R. (2005). Inhibition of astroglial nuclear factor kappaB reduces inflammation and improves functional recovery after spinal cord injury. *The Journal of experimental medicine, 202*(1), 145-156.

Bribes, E., Carrière, D., Goubet, C., Galiègue, S., Casellas, P., & Joêlle, S.-L. (2004). Immunohistochemical Assessment of the Peripheral Benzodiazepine Receptor in Human Tissues. *Journal of Histochemistry & Cytochemistry, 52*(1), 19-28.

Brix, B., Mesters, J. R., Pellerin, L., & Jöhren, O. (2012). Endothelial cell-derived nitric oxide enhances aerobic glycolysis in astrocytes via HIF-1α-mediated target gene activation. *The Journal of neuroscience : the official journal of the Society for Neuroscience, 32*(28), 9727-9735.

Buckman, L. B., Thompson, M. M., Lippert, R. N., Blackwell, T. S., Yull, F. E., & Ellacott, K. L. J. (2014). Evidence for a novel functional role of astrocytes in the acute homeostatic response to high-fat diet intake in mice. *Molecular metabolism, 4*(1), 58-63.

Bundesen, L. Q., Scheel, T. A., Bregman, B. S., & Kromer, L. F. (2003). Ephrin-B2 and EphB2 regulation of astrocyte-meningeal fibroblast interactions in response to spinal cord lesions in adult rats. *Journal of neuroscience, 23*(21), 7789–7800.

Bushong, E. A., Martone, M. E., Jones, Y. Z., & Ellisman, M. H. (2002). Protoplasmic Astrocytes in CA1 Stratum Radiatum Occupy Separate Anatomical Domains. *The Journal of Neuroscience, 22*(1), 183.

Buskila, Y., Bellot-Saez, A., & Morley, J. W. (2019). Generating Brain Waves, the Power of Astrocytes. *Frontiers in neuroscience, 13*, 1125.

Caggiu, E., Arru, G., Hosseini, S., Niegowska, M., Sechi, G., Zarbo, I. R., & Sechi, L. A. (2019). Inflammation, Infectious Triggers, and Parkinson's Disease. *Frontiers in Neurology, 10*, 122.

Caito, S. W., Yu, Y., & Aschner, M. (2014). Differential inflammatory response to acrylonitrile in rat primary astrocytes and microglia. *NeuroToxicology, 42*, 1-7.

Calle, P., Torrico, S., Muñoz, A., & Hotter, G. (2019). CPT1a downregulation protects against cholesterol-induced fibrosis in tubular epithelial cells by

downregulating TGFβ-1 and inflammasome. *Biochemical and Biophysical Research Communications, 517*(4), 715-721.

Calmettes, G., John, S. A., Weiss, J. N., & Ribalet, B. (2013). Hexokinase–mitochondrial interactions regulate glucose metabolism differentially in adult and neonatal cardiac myocytes. *The Journal of General Physiology, 142*(4), 425-436.

Camara, A. K. S., Zhou, Y., Wen, P.-C., Tajkhorshid, E., & Kwok, W.-M. (2017). Mitochondrial VDAC1: A Key Gatekeeper as Potential Therapeutic Target. *Frontiers in Physiology, 8*, 460.

Campbell, J. M., Stephenson, M. D., de Courten, B., Chapman, I., Bellman, S. M., & Aromataris, E. (2018). Metformin Use Associated with Reduced Risk of Dementia in Patients with Diabetes: A Systematic Review and Meta-Analysis. *Journal of Alzheimer's disease : JAD, 65*(4), 1225-1236.

Campiani, G., Nacci, V., Fiorini, I., De Filippis, M. P., Garofalo, A., Ciani, S. M., Greco, G., Novellino, E., Williams, D. C., Zisterer, D. M., Woods, M. J., Mihai, C., Manzoni, C., & Mennini, T. (1996). Synthesis, biological activity, and SARs of pyrrolobenzoxazepine derivatives, a new class of specific "peripheral-type" benzodiazepine receptor ligands. *Journal of medicinal chemistry, 39*(18), 3435-3450.

Cao, S., Zhang, X., Edwards, J. P., & Mosser, D. M. (2006). NF-kappaB1 (p50) homodimers differentially regulate pro- and anti-inflammatory cytokines in macrophages. *The Journal of biological chemistry, 281*(36), 26041-26050.

Carmona, M. A., Murai, K. K., Wang, L., Roberts, A. J., & Pasquale, E. B. (2009). Glial ephrin-A3 regulates hippocampal dendritic spine morphology and glutamate transport. *Proceedings of the National Academy of Sciences of the United States of America, 106*(30), 12524-12529.

Casalotti, S. O., Pelaia, G., Yakovlev, A. G., Csikós, T., Grayson, D. R., & Krueger, K. E. (1992). Structure of the rat gene encoding the mitochondrial benzodiazepine receptor. *Gene, 121*(2), 377-382.

Caslin, H. L., Taruselli, M. T., Haque, T., Pondicherry, N., Baldwin, E. A., Barnstein, B. O., & Ryan, J. J. (2018). Inhibiting Glycolysis and ATP Production Attenuates IL-33-Mediated Mast Cell Function and Peritonitis. *Frontiers in Immunology, 9*, 3026-3026.

Chang, C.-H., Curtis, J. D., Maggi, L. B., Jr., Faubert, B., Villarino, A. V., O'Sullivan, D., Huang, S. C.-C., van der Windt, G. J. W., Blagih, J., Qiu,

J., Weber, J. D., Pearce, E. J., Jones, R. G., & Pearce, E. L. (2013). Posttranscriptional control of T cell effector function by aerobic glycolysis. *Cell, 153*(6), 1239-1251.

Chang, Y. J., McCabe, R. T., Rennert, H., Budarf, M. L., Sayegh, R., Emanuel, B. S., Skolnick, P., & Strauss, J. F., 3rd. (1992). The human "peripheral-type" benzodiazepine receptor: regional mapping of the gene and characterization of the receptor expressed from cDNA. *DNA and cell biology, 11*(6), 471-480.

Chapalain, A., Chevalier, S., Orange, N., Murillo, L., Papadopoulos, V., & Feuilloley, M. G. J. (2009). Bacterial ortholog of mammalian translocator protein (TSPO) with virulence regulating activity. *PloS one, 4*(6), e6096-e6096.

Chaudhary, D., & Miller, D. M. (1995). The c-myc Promoter Binding Protein (MBP-1) and TBP Bind Simultaneously in the Minor Groove of the c-myc P2 Promoter. *Biochemistry, 34*(10), 3438-3445.

Chávez, C. E., Oyarzún, J. E., Avendaño, B. C., Mellado, L. A., Inostroza, C. A., Alvear, T. F., & Orellana, J. A. (2019). The Opening of Connexin 43 Hemichannels Alters Hippocampal Astrocyte Function and Neuronal Survival in Prenatally LPS-Exposed Adult Offspring. *Frontiers in cellular neuroscience, 13*, 460.

Chen, L., Deng, H., Cui, H., Fang, J., Zuo, Z., Deng, J., Li, Y., Wang, X., & Zhao, L. (2017). Inflammatory responses and inflammation-associated diseases in organs. *Oncotarget, 9*(6), 7204-7218.

Chistyakov, D. V., Azbukina, N. V., Astakhova, A. A., Goriainov, S. V., Chistyakov, V. V., & Sergeeva, M. G. (2018). Sex-Mediated Differences in LPS Induced Alterations of TNFα, IL-10 Expression, and Prostaglandin Synthesis in Primary Astrocytes. *International Journal of Molecular Sciences, 19*(9), 2793.

Choi, S. S., Lee, H. J., Lim, I., Satoh, J.-i., & Kim, S. U. (2014). Human Astrocytes: Secretome Profiles of Cytokines and Chemokines. *PloS one, 9*(4), e92325.

Choi, Y. M., & Kim, K. H. (2015). Etifoxine for pain patients with anxiety. *The Korean journal of pain, 28*(1), 4-10.

Chun, H., & Lee, C. J. (2018). Reactive astrocytes in Alzheimer's disease: A double-edged sword. *Neuroscience research, 126*, 44-52.

Cimmino F, Avitabile M, Lasorsa VA, et al. HIF-1 transcription activity: HIF1A driven response in normoxia and in hypoxia. (2019) *BMC Med Genet. 20*(1):37.

Cino, M., & Del Maestro, R. F. (1989). Generation of hydrogen peroxide by brain mitochondria: The effect of reoxygenation following postdecapitative ischemia. *Archives of Biochemistry and Biophysics, 269*(2), 623-638.

Cleary, J., Johnson, K. M., Opipari, A. W., & Glick, G. D. (2007). Inhibition of the mitochondrial F1F0-ATPase by ligands of the peripheral benzodiazepine receptor. *Bioorganic & Medicinal Chemistry Letters, 17*(6), 1667-1670.

Cogswell, P. C., Kashatus, D. F., Keifer, J. A., Guttridge, D. C., Reuther, J. Y., Bristow, C., Roy, S., Nicholson, D. W., & Baldwin, A. S. (2003). NF-κB and IκBα are found in the mitochondria: evidence for regulation of mitochondrial gene expression by NF-κB. *Journal of Biological Chemistry, 278*(5), 2963-2968.

Colasanti, A., Owen, D. R., Grozeva, D., Rabiner, E. A., Matthews, P. M., Craddock, N., & Young, A. H. (2013). Bipolar Disorder is associated with the rs6971 polymorphism in the gene encoding 18kDa Translocator Protein (TSPO). *Psychoneuroendocrinology, 38*(11), 2826-2829.

Collart, M. A., Baeuerle, P., & Vassalli, P. (1990). Regulation of tumor necrosis factor alpha transcription in macrophages: involvement of four kappa B-like motifs and of constitutive and inducible forms of NF-kappa B. *Molecular and Cellular Biology, 10*(4), 1498-1506.

Colombini, M. (2012). VDAC structure, selectivity, and dynamics. *Biochimica et biophysica acta, 1818*(6), 1457-1465.

Colombo, E., & Farina, C. (2016). Astrocytes: Key Regulators of Neuroinflammation. *Trends in Immunology, 37*(9), 608-620.

Cooney, S. J., Bermudez-Sabogal, S. L., & Byrnes, K. R. (2013). Cellular and temporal expression of NADPH oxidase (NOX) isotypes after brain injury. *Journal of neuroinflammation, 10*, 155.

Cope, A. P. (2002). Studies of T-cell activation in chronic inflammation. *Arthritis research, 4 Suppl 3*(Suppl 3), S197-S211.

Costa, B., Pini, S., Martini, C., Abelli, M., Gabelloni, P., Landi, S., Muti, M., Gesi, C., Lari, L., Cardini, A., Galderisi, S., Mucci, A., Lucacchini, A., & Cassano, G. B. (2009). Ala147Thr substitution in translocator protein is associated

with adult separation anxiety in patients with depression. *Psychiatric Genetics, 19*(2).

Cotrina, M. L., Lin, J. H., Alves-Rodrigues, A., Liu, S., Li, J., Azmi-Ghadimi, H., Kang, J., Naus, C. C., & Nedergaard, M. (1998). Connexins regulate calcium signaling by controlling ATP release. *Proceedings of the National Academy of Sciences of the United States of America, 95*(26), 15735-15740.

Covelo, A., & Araque, A. (2018). Neuronal activity determines distinct gliotransmitter release from a single astrocyte. *eLife, 7*, e32237.

D'Ignazio, L., Bandarra, D., & Rocha, S. (2016). NF-κB and HIF crosstalk in immune responses. *The FEBS Journal, 283*(3), 413-424.

Dan, H. C., Cooper, M. J., Cogswell, P. C., Duncan, J. A., Ting, J. P. Y., & Baldwin, A. S. (2008). Akt-dependent regulation of NF-κB is controlled by mTOR and Raptor in association with IKK. *Genes & development, 22*(11), 1490-1500.

Daneman, R., & Prat, A. (2015). The blood-brain barrier. *Cold Spring Harbor perspectives in biology, 7*(1), a020412.

Daugherty, D. J., Selvaraj, V., Chechneva, O. V., Liu, X.-B., Pleasure, D. E., & Deng, W. (2013). A TSPO ligand is protective in a mouse model of multiple sclerosis. *EMBO molecular medicine, 5*(6), 891-903.

DeBerardinis, R. J., & Chandel, N. S. (2016). Fundamentals of cancer metabolism. *Science advances, 2*(5), e1600200-e1600200.

Demaria, M., Camporeale, A., & Poli, V. (2014). STAT3 and metabolism: how many ways to use a single molecule? *International journal of cancer, 135*(9), 1997-2003.

Devraj, G., Beerlage, C., Brüne, B., & Kempf, V. A. (2017). Hypoxia and HIF-1 activation in bacterial infections. *Microbes and infection, 19*(3), 144–156.

Devraj, K., Klinger, M. E., Myers, R. L., Mokashi, A., Hawkins, R. A., & Simpson, I. A. (2011). GLUT-1 glucose transporters in the blood-brain barrier: differential phosphorylation. *Journal of neuroscience research, 89*(12), 1913–1925.

Dhir, A., & Rogawski, M. A. (2012). Role of neurosteroids in the anticonvulsant activity of midazolam. *British Journal of Pharmacology, 165*(8), 2684-2691.

Dienel, G. A. (2019). Brain Glucose Metabolism: Integration of Energetics with Function. *Physiological reviews, 99*(1), 949-1045.

Douglass, J. D., Dorfman, M. D., Fasnacht, R., Shaffer, L. D., & Thaler, J. P. (2017). Astrocyte IKKβ/NF-κB signaling is required for diet-induced obesity and hypothalamic inflammation. *Molecular metabolism, 6*(4), 366-373.

Dozio, V., & Sanchez, J.-C. (2018). Profiling the proteomic inflammatory state of human astrocytes using DIA mass spectrometry. *Journal of Neuroinflammation, 15*(1), 331.

Dresselhaus, E. C., & Meffert, M. K. (2019). Cellular Specificity of NF-κB Function in the Nervous System. *Frontiers in Immunology, 10*, 1043-1043.

Dumitru, C., Kabat, A. M., & Maloy, K. J. (2018). Metabolic Adaptations of CD4(+) T Cells in Inflammatory Disease. *Frontiers in Immunology, 9*, 540-540.

Dupont, A.-C., Largeau, B., Santiago Ribeiro, M. J., Guilloteau, D., Tronel, C., & Arlicot, N. (2017). Translocator Protein-18 kDa (TSPO) Positron Emission Tomography (PET) Imaging and Its Clinical Impact in Neurodegenerative Diseases. *International Journal of Molecular Sciences, 18*(4), 785.

Edison, P., Donat, C. K., & Sastre, M. (2018). In vivo Imaging of Glial Activation in Alzheimer's Disease. *Frontiers in Neurology, 9*, 625.

Engelhardt, B. (2008). Immune cell entry into the central nervous system: Involvement of adhesion molecules and chemokines. *Journal of the Neurological Sciences, 274*(1), 23-26.

Escoll, P., & Buchrieser, C. (2018). Metabolic reprogramming of host cells upon bacterial infection: Why shift to a Warburg-like metabolism? *The FEBS Journal, 285*(12), 2146-2160.

Everts, B., Amiel, E., Huang, S. C.-C., Smith, A. M., Chang, C.-H., Lam, W. Y., Redmann, V., Freitas, T. C., Blagih, J., van der Windt, G. J. W., Artyomov, M. N., Jones, R. G., Pearce, E. L., & Pearce, E. J. (2014). TLR-driven early glycolytic reprogramming via the kinases TBK1-IKKε supports the anabolic demands of dendritic cell activation. *Nature immunology, 15*(4), 323-332.

Falkowska, A., Gutowska, I., Goschorska, M., Nowacki, P., Chlubek, D., & Baranowska-Bosiacka, I. (2015). Energy Metabolism of the Brain, Including the Cooperation between Astrocytes and Neurons, Especially in the Context of Glycogen Metabolism. *International Journal of Molecular Sciences, 16*(11).

Fan, J., Lindemann, P., Feuilloley, M. G. J., & Papadopoulos, V. (2012). Structural and Functional Evolution of the Translocator Protein (18 kDa). *Current Molecular Medicine, 12*(4), 369-386.

Fan, J., Zirkin, B., & Papadopoulos, V. (2018a). Response to Letter to the Editor: "Dubious Conclusions on TSPO Function". *Endocrinology, 159*(7), 2530-2531.

Fan, K., Lin, L., Ai, Q., Wan, J., Dai, J., Liu, G., Tang, L., Yang, Y., Ge, P., Jiang, R., & Zhang, L. (2018b). Lipopolysaccharide-Induced Dephosphorylation of AMPK-Activated Protein Kinase Potentiates Inflammatory Injury via Repression of ULK1-Dependent Autophagy. *Frontiers in Immunology, 9*, 1464.

Fang, D., & Maldonado, E. N. (2018). VDAC Regulation: A Mitochondrial Target to Stop Cell Proliferation. *Advances in cancer research, 138*, 41-69.

Fang, J., Zhou, S., Fan, J., & Yan, S. (2015). Roles of glucose transporter-1 and the phosphatidylinositol 3-kinase/protein kinase B pathway in cancer radioresistance. *Molecular Medicine Reports, 11*, 1573-1581.

Farges, R., Joseph-Liauzun, E., Shire, D., Caput, D., Le Fur, G., & Ferrara, P. (1994). Site-directed mutagenesis of the peripheral benzodiazepine receptor: identification of amino acids implicated in the binding site of Ro5-4864. *Molecular Pharmacology, 46*(6), 1160.

Farhy-Tselnicker, I., & Allen, N. J. (2018). Astrocytes, neurons, synapses: a tripartite view on cortical circuit development. *Neural Development, 13*(1), 7.

Faubert, B., Boily, G., Izreig, S., Griss, T., Samborska, B., Dong, Z., Dupuy, F., Chambers, C., Fuerth, B. J., Viollet, B., Mamer, O. A., Avizonis, D., DeBerardinis, R. J., Siegel, P. M., & Jones, R. G. (2013). AMPK is a negative regulator of the Warburg effect and suppresses tumor growth in vivo. *Cell metabolism, 17*(1), 113-124.

Fernández-Moncada, I., Ruminot, I., Robles-Maldonado, D., Alegría, K., Deitmer, J. W., & Barros, L. F. (2018). Neuronal control of astrocytic respiration through a variant of the Crabtree effect. *Proceedings of the National Academy of Sciences, 115*(7), 1623.

Ferrarese, C., Pierpaoli, C., Linfante, I., Bobo, R. H., Guthrie, B., Kufta, C., Duhaney, M. O., Melisi, J., & Fulham, M. J. (1994). Peripheral

benzodiazepine receptors and glucose metabolism in human gliomas. *Journal of neuro-oncology, 22*(1), 15-22.

Fiebig, C., Keiner, S., Ebert, B., Schäffner, I., Jagasia, R., Lie, D. C., & Beckervordersandforth, R. (2019). Mitochondrial Dysfunction in Astrocytes Impairs the Generation of Reactive Astrocytes and Enhances Neuronal Cell Death in the Cortex Upon Photothrombotic Lesion. *Frontiers in Molecular Neuroscience, 12*, 40.

Flachbartová, Z., & Kovacech, B. (2013). Mortalin - a multipotent chaperone regulating cellular processes ranging from viral infection to neurodegeneration. *Acta virologica, 57*(1), 3-15.

Foo, Lynette C., Allen, Nicola J., Bushong, Eric A., Ventura, P. B., Chung, W.-S., Zhou, L., Cahoy, John D., Daneman, R., Zong, H., Ellisman, Mark H., & Barres, Ben A. (2011). Development of a Method for the Purification and Culture of Rodent Astrocytes. *Neuron, 71*(5), 799-811.

Fox, C. J., Hammerman, P. S., & Thompson, C. B. (2005). Fuel feeds function: energy metabolism and the T-cell response. *Nature Reviews Immunology, 5*(11), 844-852.

Frauwirth, K. A., Riley, J. L., Harris, M. H., Parry, R. V., Rathmell, J. C., Plas, D. R., Elstrom, R. L., June, C. H., & Thompson, C. B. (2002). The CD28 Signaling Pathway Regulates Glucose Metabolism. *Immunity, 16*(6), 769-777.

Freemerman, A. J., Johnson, A. R., Sacks, G. N., Milner, J. J., Kirk, E. L., Troester, M. A., Macintyre, A. N., Goraksha-Hicks, P., Rathmell, J. C., & Makowski, L. (2014). Metabolic reprogramming of macrophages: glucose transporter 1 (GLUT1)-mediated glucose metabolism drives a proinflammatory phenotype. *The Journal of biological chemistry, 289*(11), 7884-7896.

Frugier, T., Conquest, A., McLean, C., Currie, P., Moses, D., & Goldshmit, Y. (2012). Expression and activation of EphA4 in the human brain after traumatic injury. *Journal of neuropathology and experimental neurology, 71*(3), 242–250.

Fu, Y., Wang, D., Wang, H., Cai, M., Li, C., Zhang, X., Chen, H., Hu, Y., Zhang, X., Ying, M., He, W., & Zhang, J. (2020). TSPO deficiency induces mitochondrial dysfunction, leading to hypoxia, angiogenesis, and a

growth-promoting metabolic shift toward glycolysis in glioblastoma. *Neuro-Oncology, 22*(2):240–252

Fujioka, S., Schmidt, C., Sclabas, G. M., Li, Z., Pelicano, H., Peng, B., Yao, A., Niu, J., Zhang, W., Evans, D. B., Abbruzzese, J. L., Huang, P., & Chiao, P. J. (2004). Stabilization of p53 is a novel mechanism for proapoptotic function of NF-kappaB. *The Journal of biological chemistry, 279*(26), 27549-27559.

Gaber, T., Strehl, C., & Buttgereit, F. (2017). Metabolic regulation of inflammation. *Nature Reviews Rheumatology, 13*(5), 267-279.

Galiègue, S., Casellas, P., Kramar, A., Tinel, N., & Simony-Lafontaine, J. (2004). Immunohistochemical Assessment of the Peripheral Benzodiazepine Receptor in Breast Cancer and Its Relationship with Survival. *Clinical Cancer Research, 10*(6), 2058.

Gao, X., Wang, H., Yang, J. J., Liu, X., & Liu, Z.-R. (2012). Pyruvate kinase M2 regulates gene transcription by acting as a protein kinase. *Molecular Cell, 45*(5), 598-609.

Garg, R., Blando, J., Perez, C. J., Wang, H., Benavides, F. J., & Kazanietz, M. G. (2012). Activation of Nuclear Factor κB (NF-κB) in Prostate Cancer Is Mediated by Protein Kinase C ϵ (PKCϵ). *Journal of Biological Chemistry, 287*(44), 37570-37582.

Gatliff, J., East, D., Crosby, J., Abeti, R., Harvey, R., Craigen, W., Parker, P., & Campanella, M. (2014). TSPO interacts with VDAC1 and triggers a ROS-mediated inhibition of mitochondrial quality control. *Autophagy, 10*(12), 2279-2296.

Gatliff, J., East, D. A., Singh, A., Alvarez, M. S., Frison, M., Matic, I., Ferraina, C., Sampson, N., Turkheimer, F., & Campanella, M. (2017). A role for TSPO in mitochondrial Ca(2+) homeostasis and redox stress signaling. *Cell death & disease, 8*(6), e2896-e2896.

Gavillet, M., Allaman, I., & Magistretti, P. J. (2008). Modulation of astrocytic metabolic phenotype by proinflammatory cytokines. *Glia, 56*(9), 975-989.

Gavish, M., Bachman, I., Shoukrun, R., Katz, Y., Veenman, L., Weisinger, G., & Weizman, A. (1999). Enigma of the peripheral benzodiazepine receptor. *Pharmacological reviews, 51*(4), 629-650.

Genda, E. N., Jackson, J. G., Sheldon, A. L., Locke, S. F., Greco, T. M., O'Donnell, J. C., Spruce, L. A., Xiao, R., Guo, W., Putt, M., Seeholzer, S.,

Ischiropoulos, H., & Robinson, M. B. (2011). Co-compartmentalization of the astroglial glutamate transporter, GLT-1, with glycolytic enzymes and mitochondria. *The Journal of neuroscience : the official journal of the Society for Neuroscience, 31*(50), 18275-18288.

Ghosh, M., Yang, Y., Rothstein, J. D., & Robinson, M. B. (2011). Nuclear factor-κB contributes to neuron-dependent induction of glutamate transporter-1 expression in astrocytes. *The Journal of neuroscience : the official journal of the Society for Neuroscience, 31*(25), 9159-9169.

Giatzakis, C., Batarseh, A., Dettin, L., & Papadopoulos, V. (2007). The role of Ets transcription factors in the basal transcription of the translocator protein (18 kDa). *Biochemistry, 46*(16), 4763-4774.

Giatzakis, C., & Papadopoulos, V. (2004). Differential utilization of the promoter of peripheral-type benzodiazepine receptor by steroidogenic versus nonsteroidogenic cell lines and the role of Sp1 and Sp3 in the regulation of basal activity. *Endocrinology, 145*(3), 1113-1123.

Göbel, J., Motori, E., & Bergami, M. (2018). Spatiotemporal control of mitochondrial network dynamics in astroglial cells. *Biochemical and Biophysical Research Communications, 500*(1), 17-25.

Goetzman, E. S., & Prochownik, E. V. (2018). The Role for Myc in Coordinating Glycolysis, Oxidative Phosphorylation, Glutaminolysis, and Fatty Acid Metabolism in Normal and Neoplastic Tissues. *Frontiers in endocrinology, 9*, 129-129.

Goldfine, A. B., Fonseca, V., Jablonski, K. A., Pyle, L., Staten, M. A., Shoelson, S. E., & Team, T.-T. D. S. (2010). The effects of salsalate on glycemic control in patients with type 2 diabetes: a randomized trial. *Annals of internal medicine, 152*(6), 346-357.

Goldfine, A. B., Silver, R., Aldhahi, W., Cai, D., Tatro, E., Lee, J., & Shoelson, S. E. (2008). Use of Salsalate to Target Inflammation in the Treatment of Insulin Resistance and Type 2 Diabetes. *Clinical and Translational Science, 1*(1), 36-43.

Gomes, L. C., Di Benedetto, G., & Scorrano, L. (2011). Essential amino acids and glutamine regulate induction of mitochondrial elongation during autophagy. *Cell Cycle, 10*(16), 2635-2639.

Gong, C.-Y., Zhou, A.-L., Mao, J.-H., Hu, Y.-E., & Geng, J.-S. (2014). The role of Toll-like receptor 4 on inflammation and Aβ formation in cortex astrocytes. *Sheng li xue bao : [Acta physiologica Sinica], 66*(6), 631-638.

Gong, J., Szego, É. M., Leonov, A., Benito, E., Becker, S., Fischer, A., Zweckstetter, M., Outeiro, T., & Schneider, A. (2019). Translocator Protein Ligand Protects against Neurodegeneration in the MPTP Mouse Model of Parkinsonism. *The Journal of Neuroscience, 39*(19), 3752.

González-Reyes, R. E., Nava-Mesa, M. O., Vargas-Sánchez, K., Ariza-Salamanca, D., & Mora-Muñoz, L. (2017). Involvement of Astrocytes in Alzheimer's Disease from a Neuroinflammatory and Oxidative Stress Perspective. *Frontiers in molecular neuroscience, 10*, 427.

Gorina, R., Font-Nieves, M., Márquez-Kisinousky, L., Santalucia, T., & Planas, A. M. (2011). Astrocyte TLR4 activation induces a proinflammatory environment through the interplay between MyD88-dependent NFκB signaling, MAPK, and Jak1/Stat1 pathways. *Glia, 59*(2), 242-255.

Graves, J. A., Wang, Y., Sims-Lucas, S., Cherok, E., Rothermund, K., Branca, M. F., Elster, J., Beer-Stolz, D., Van Houten, B., Vockley, J., & Prochownik, E. V. (2012). Mitochondrial structure, function and dynamics are temporally controlled by c-Myc. *PloS one, 7*(5), e37699-e37699.

Grimm, A., Lejri, I., Hallé, F., Schmitt, M., Götz, J., Bihel, F., & Eckert, A. (2019). Mitochondria modulatory effects of new TSPO ligands in a cellular model of tauopathies. *Journal of Neuroendocrinology, n/a*(n/a), e12796.

Guidotti, A., Forchetti, C. M., Corda, M. G., Konkel, D., Bennett, C. D., & Costa, E. (1983). Isolation, characterization, and purification to homogeneity of an endogenous polypeptide with agonistic action on benzodiazepine receptors. *Proceedings of the National Academy of Sciences, 80*(11), 3531.

Gumaa, K. A., & McLean, P. (1969). A possible interrelationship between binding of hexokinase and the site of ATP formation in Krebs ascites cells. *Biochemical and Biophysical Research Communications, 36*(5), 771-779.

Gundersen, V., Storm-Mathisen, J., & Bergersen, L. H. (2015). Neuroglial Transmission. *Physiological reviews, 95*(3), 695-726.

Guo, Y., Kalathur, R. C., Liu, Q., Kloss, B., Bruni, R., Ginter, C., Kloppmann, E., Rost, B., & Hendrickson, W. A. (2015). Structure and activity of tryptophan-rich TSPO proteins. *Science, 347*(6221), 551.

Gut, P., Baeza-Raja, B., Andersson, O., Hasenkamp, L., Hsiao, J., Hesselson, D., Akassoglou, K., Verdin, E., Hirschey, M. D., & Stainier, D. Y. R. (2013). Whole-organism screening for gluconeogenesis identifies activators of fasting metabolism. *Nature Chemical Biology, 9*(2), 97-104.

Hamilton, J. A., Vairo, G., & Lingelbach, S. R. (1986). CSF-1 stimulates glucose uptake in murine bone marrow-derived macrophages. *Biochemical and Biophysical Research Communications, 138*(1), 445-454.

Han, D., Wei, W., Chen, X., Zhang, Y., Wang, Y., Zhang, J., Wang, X., Yu, T., Hu, Q., Liu, N., & You, Y. (2015). NF-κB/RelA-PKM2 mediates inhibition of glycolysis by fenofibrate in glioblastoma cells. *Oncotarget, 6*(28), 26119-26128.

Harada, K., Kamiya, T., & Tsuboi, T. (2016). Gliotransmitter Release from Astrocytes: Functional, Developmental, and Pathological Implications in the Brain. *Frontiers in neuroscience, 9*, 499.

Hardwick, M., Fertikh, D., Culty, M., Li, H., Vidic, B., & Papadopoulos, V. (1999). Peripheral-type benzodiazepine receptor (PBR) in human breast cancer: correlation of breast cancer cell aggressive phenotype with PBR expression, nuclear localization, and PBR-mediated cell proliferation and nuclear transport of cholesterol. *Cancer Research, 59*(4), 831-842.

Hatty, C. R., Le Brun, A. P., Lake, V., Clifton, L. A., Liu, G. J., James, M., & Banati, R. B. (2014). Investigating the interactions of the 18kDa translocator protein and its ligand PK11195 in planar lipid bilayers. *Biochimica et Biophysica Acta (BBA) - Biomembranes, 1838*(3), 1019-1030.

Hawkins, P. T., & Stephens, L. R. (2015). PI3K signalling in inflammation. *Biochimica et biophysica acta, 1851*(6), 882-897.

Hayden, M. S., & Ghosh, S. (2008). Shared Principles in NF-κB Signaling. *Cell, 132*(3), 344-362.

Headland, S. E., & Norling, L. V. (2015). The resolution of inflammation: Principles and challenges. *Seminars in Immunology, 27*(3), 149-160.

Herzig, S., & Shaw, R. J. (2018). AMPK: guardian of metabolism and mitochondrial homeostasis. *Nature reviews. Molecular cell biology, 19*(2), 121-135.

Hirvonen, J., Roivainen, A., Virta, J., Helin, S., Någren, K., & Rinne, J. O. (2010). Human biodistribution and radiation dosimetry of 11C-(R)-PK11195, the

prototypic PET ligand to image inflammation. *European Journal of Nuclear Medicine and Molecular Imaging, 37*(3), 606-612.

Horiguchi, Y., Ohta, N., Yamamoto, S., Koide, M., & Fujino, Y. (2019). Midazolam suppresses the lipopolysaccharide-stimulated immune responses of human macrophages via translocator protein signaling. *International immunopharmacology, 66*, 373-382.

Hotamisligil, G. S. (2017). Foundations of Immunometabolism and Implications for Metabolic Health and Disease. *Immunity, 47*(3), 406-420.

Hu J., Nakano H., Sakurai H., & Colburn N. (2004). Insufficient p65 phosphorylation at S536 specifically contributes to the lack of NF-kB activation and transformation in resistant JB6 cells. *Carcinogenesis, 25*(10), 1991-2003.

Huenchuguala, S., Muñoz, P., & Segura-Aguilar, J. (2017). The Importance of Mitophagy in Maintaining Mitochondrial Function in U373MG Cells. Bafilomycin A1 Restores Aminochrome-Induced Mitochondrial Damage. *ACS chemical neuroscience, 8*(10), 2247-2253.

Hurst, S., Hoek, J., & Sheu, S.-S. (2017). Mitochondrial Ca(2+) and regulation of the permeability transition pore. *Journal of bioenergetics and biomembranes, 49*(1), 27-47.

Huynh, A., DuPage, M., Priyadharshini, B., Sage, P. T., Quiros, J., Borges, C. M., Townamchai, N., Gerriets, V. A., Rathmell, J. C., Sharpe, A. H., Bluestone, J. A., & Turka, L. A. (2015). Control of PI(3) kinase in Treg cells maintains homeostasis and lineage stability. *Nature immunology, 16*(2), 188-196.

Iatmanen-Harbi, S., Senicourt, L., Papadopoulos, V., Lequin, O., & Lacapere, J.-J. (2019). Characterization of the High-Affinity Drug Ligand Binding Site of Mouse Recombinant TSPO. *International Journal of Molecular Sciences, 20*(6), 1444.

Ignatenko, O., Chilov, D., Paetau, I., de Miguel, E., Jackson, C. B., Capin, G., Paetau, A., Terzioglu, M., Euro, L., & Suomalainen, A. (2018). Loss of mtDNA activates astrocytes and leads to spongiotic encephalopathy. *Nature communications, 9*(1), 70.

Ilkan, Z., & Akar, F. G. (2018). The Mitochondrial Translocator Protein and the Emerging Link Between Oxidative Stress and Arrhythmias in the Diabetic Heart. *Frontiers in Physiology, 9*, 1518.

Infantino, V., Iacobazzi, V., Palmieri, F., & Menga, A. (2013). ATP-citrate lyase is essential for macrophage inflammatory response. *Biochemical and Biophysical Research Communications, 440*(1), 105-111.

Issop, L., Ostuni, M. A., Lee, S., Laforge, M., Péranzi, G., Rustin, P., Benoist, J.-F., Estaquier, J., Papadopoulos, V., & Lacapère, J.-J. (2016). Translocator Protein-Mediated Stabilization of Mitochondrial Architecture during Inflammation Stress in Colonic Cells. *PloS one, 11*(4), e0152919-e0152919.

Jackson, J. G., O'Donnell, J. C., Takano, H., Coulter, D. A., & Robinson, M. B. (2014). Neuronal activity and glutamate uptake decrease mitochondrial mobility in astrocytes and position mitochondria near glutamate transporters. *The Journal of neuroscience : the official journal of the Society for Neuroscience, 34*(5), 1613-1624.

Jackson, J. G., & Robinson, M. B. (2015). Reciprocal Regulation of Mitochondrial Dynamics and Calcium Signaling in Astrocyte Processes. *The Journal of neuroscience : the official journal of the Society for Neuroscience, 35*(45), 15199-15213.

Jaipuria, G., Leonov, A., Giller, K., Vasa, S. K., Jaremko, Ł., Jaremko, M., Linser, R., Becker, S., & Zweckstetter, M. (2017). Cholesterol-mediated allosteric regulation of the mitochondrial translocator protein structure. *Nature communications, 8*, 14893-14893.

Jäkel, S., & Dimou, L. (2017). Glial Cells and Their Function in the Adult Brain: A Journey through the History of Their Ablation. *Frontiers in cellular neuroscience, 11*, 24.

James, M.L., Sellari, S., Kassiou, M. (2006). Development of Ligands for the Peripheral Benzodiazepine Receptor. *Current medicinal chemistry, 13,* 1991-2001.

Jamin, N., Neumann, J.-M., Ostuni, M. A., Vu, T. K. N., Yao, Z.-X., Murail, S., Robert, J.-C., Giatzakis, C., Papadopoulos, V., & Lacapère, J.-J. (2005). Characterization of the cholesterol recognition amino acid consensus sequence of the peripheral-type benzodiazepine receptor. *Molecular endocrinology, 19*(3), 588-594.

Janczar, K., Su, Z., Raccagni, I., Anfosso, A., Kelly, C., Durrenberger, Pascal F., Gerhard, A., & Roncaroli, F. (2015). The 18-kDa mitochondrial translocator

protein in gliomas: from the bench to bedside. *Biochemical Society Transactions, 43*(4), 579-585.

Jaremko, L., Jaremko, M., Giller, K., Becker, S., & Zweckstetter, M. (2014). Structure of the mitochondrial translocator protein in complex with a diagnostic ligand. *Science, 343*(6177), 1363-1366.

Jernberg, J. N., Bowman, C. E., Wolfgang, M. J., & Scafidi, S. (2017). Developmental regulation and localization of carnitine palmitoyltransferases (CPTs) in rat brain. *Journal of Neurochemistry, 142*(3), 407-419.

Ji, L., Arcinas, M., & Boxer, L. M. (1994). NF-kappa B sites function as positive regulators of expression of the translocated c-myc allele in Burkitt's lymphoma. *Molecular and Cellular Biology, 14*(12), 7967-7974.

Jiang, T., & Cadenas, E. (2014). Astrocytic metabolic and inflammatory changes as a function of age. *Aging Cell, 13*(6), 1059-1067.

Jiang X., Takahashi N., Ando K., Otsuka T., Tetsuka T., & Okamoto T. (2003). NF-kappa B p65 transactivation domain is involved in the NF-kappa B-inducing kinase pathway. *Biochem Biophys Res Commun*., *301*(2):583–590.

John, S., Weiss, J. N., & Ribalet, B. (2011). Subcellular localization of hexokinases I and II directs the metabolic fate of glucose. *PloS one, 6*(3), e17674-e17674.

Johnson, R. F., & Perkins, N. D. (2012). Nuclear factor-κB, p53, and mitochondria: regulation of cellular metabolism and the Warburg effect. *Trends in biochemical sciences, 37*(8), 317-324.

Johnson, R. F., Witzel, I.-I., & Perkins, N. D. (2011). p53-Dependent Regulation of Mitochondrial Energy Production by the RelA Subunit of NF-κB. *Cancer Research, 71*(16), 5588.

Johnson, E., Dammer, E. B., Duong, D. M., Ping, L., Zhou, M., Yin, L., Higginbotham, L. A., Guajardo, A., White, B., Troncoso, J. C., Thambisetty, M., Montine, T. J., Lee, E. B., Trojanowski, J. Q., Beach, T. G., Reiman, E. M., Haroutunian, V., Wang, M., Schadt, E., Zhang, B., … Seyfried, N. T. (2020). Large-scale proteomic analysis of Alzheimer's disease brain and cerebrospinal fluid reveals early changes in energy

metabolism associated with microglia and astrocyte activation. *Nature medicine*, 10.1038/s41591-020-0815-6. Advance online publication.

Jung, J., Zeng, H., & Horng, T. (2019). Metabolism as a guiding force for immunity. *Nature Cell Biology, 21*(1), 85-93.

Kaltschmidt, B., Widera, D., & Kaltschmidt, C. (2005). Signaling via NF-kappaB in the nervous system. *Biochimica et biophysica acta, 1745*(3), 287–299.

Karlstetter, M., Nothdurfter, C., Aslanidis, A., Moeller, K., Horn, F., Scholz, R., Neumann, H., Weber, B. H. F., Rupprecht, R., & Langmann, T. (2014). Translocator protein (18 kDa) (TSPO) is expressed in reactive retinal microglia and modulates microglial inflammation and phagocytosis. *Journal of Neuroinflammation, 11*, 3-3.

Kasembeli, M. M., Bharadwaj, U., Robinson, P., & Tweardy, D. J. (2018). Contribution of STAT3 to Inflammatory and Fibrotic Diseases and Prospects for its Targeting for Treatment. *International Journal of Molecular Sciences, 19*(8), 2299.

Katz, Y., Weizman, R., Weizman, A., & Gavish, M. (1992). Disulfiram and diethyldithiocarbamate are competitive inhibitors at the peripheral benzodiazepine receptor. *The Journal of pharmacology and experimental therapeutics, 262*(1), 394-397.

Kawauchi, K., Araki, K., Tobiume, K., & Tanaka, N. (2008a). Activated p53 induces NF-κB DNA binding but suppresses its transcriptional activation. *Biochemical and Biophysical Research Communications, 372*(1), 137-141.

Kawauchi, K., Araki, K., Tobiume, K., & Tanaka, N. (2008b). p53 regulates glucose metabolism through an IKK-NF-κB pathway and inhibits cell transformation. *Nature Cell Biology, 10*(5), 611-618.

Kelly, B., & O'Neill, L. A. J. (2015). Metabolic reprogramming in macrophages and dendritic cells in innate immunity. *Cell research, 25*(7), 771-784.

Kielian T. (2006). Toll-like receptors in central nervous system glial inflammation and homeostasis. *Journal of neuroscience research, 83*(5), 711–730.

Kim, D.-I., Lim, S.-K., Park, M.-J., Han, H.-J., Kim, G.-Y., & Park, S. H. (2007a). The involvement of phosphatidylinositol 3-kinase /Akt signaling in high glucose-induced downregulation of GLUT-1 expression in ARPE cells. *Life Sciences, 80*(7), 626-632.

Kim, E., Lee, J.-H., Ntambi, J. M., & Hyun, C.-K. (2011). Inhibition of stearoyl-CoA desaturase1 activates AMPK and exhibits beneficial lipid metabolic effects in vitro. *European journal of pharmacology, 672*(1-3), 38-44.

Kim, J.-w., Gao, P., Liu, Y.-C., Semenza, G. L., & Dang, C. V. (2007b). Hypoxia-Inducible Factor 1 and Dysregulated c-Myc Cooperatively Induce Vascular Endothelial Growth Factor and Metabolic Switches Hexokinase 2 and Pyruvate Dehydrogenase Kinase 1. *Molecular and Cellular Biology, 27*(21), 7381.

Kim, M. T., & Harty, J. T. (2014). Impact of Inflammatory Cytokines on Effector and Memory CD8+ T Cells. *Frontiers in Immunology, 5*, 295.

Kim, S., Kim, N., Park, S., Jeon, Y., Lee, J., Yoo, S.-J., Lee, J.-W., Moon, C., Yu, S.-W., & Kim, E.-K. (2019). Tanycytic TSPO inhibition induces lipophagy to regulate lipid metabolism and improve energy balance. *Autophagy*, 1-21.

Kinney, J. W., Bemiller, S. M., Murtishaw, A. S., Leisgang, A. M., Salazar, A. M., & Lamb, B. T. (2018). Inflammation as a central mechanism in Alzheimer's disease. *Alzheimer's & dementia, 4*, 575-590.

Kita, A., Kohayakawa, H., Kinoshita, T., Ochi, Y., Nakamichi, K., Kurumiya, S., Furukawa, K., & Oka, M. (2004). Antianxiety and antidepressant-like effects of AC-5216, a novel mitochondrial benzodiazepine receptor ligand. *British Journal of Pharmacology, 142*(7), 1059-1072.

Klee, K., Storti, F., Barben, M., Samardzija, M., Langmann, T., Dunaief, J., & Grimm, C. (2019). Systemic knockout of Tspo in mice does not affect retinal morphology, function and susceptibility to degeneration. *Experimental Eye Research, 188*, 107816.

Koenig, A. M., Mechanic-Hamilton, D., Xie, S. X., Combs, M. F., Cappola, A. R., Xie, L., Detre, J. A., Wolk, D. A., & Arnold, S. E. (2017). Effects of the Insulin Sensitizer Metformin in Alzheimer Disease: Pilot Data From a Randomized Placebo-controlled Crossover Study. *Alzheimer disease and associated disorders, 31*(2), 107-113.

Koivunen, P., Hirsilä, M., Remes, A. M., Hassinen, I. E., Kivirikko, K. I., & Myllyharju, J. (2007). Inhibition of Hypoxia-inducible Factor (HIF) Hydroxylases by Citric Acid Cycle Intermediates: possible links between cell metabolism and stabilization of HIF. *Journal of Biological Chemistry, 282*(7), 4524-4532.

Kolikova, J., Afzalov, R., Giniatullina, A., Surin, A., Giniatullin, R., & Khiroug, L. (2006). Calcium-dependent trapping of mitochondria near plasma membrane in stimulated astrocytes. *Brain Cell Biology, 35*(1), 75-86.

Korkhov, V. M., Sachse, C., Short, J. M., & Tate, C. G. (2010). Three-dimensional structure of TspO by electron cryomicroscopy of helical crystals. *Structure, 18*(6), 677-687.

Krämer, D. K., Al-Khalili, L., Guigas, B., Leng, Y., Garcia-Roves, P. M., & Krook, A. (2007). Role of AMP Kinase and PPARδ in the Regulation of Lipid and Glucose Metabolism in Human Skeletal Muscle. *Journal of Biological Chemistry, 282*(27), 19313-19320.

Krawczyk, C. M., Holowka, T., Sun, J., Blagih, J., Amiel, E., DeBerardinis, R. J., Cross, J. R., Jung, E., Thompson, C. B., Jones, R. G., & Pearce, E. J. (2010). Toll-like receptor-induced changes in glycolytic metabolism regulate dendritic cell activation. *Blood, 115*(23), 4742-4749.

Kudin, A. P., Bimpong-Buta, N. Y.-B., Vielhaber, S., Elger, C. E., & Kunz, W. S. (2004). Characterization of Superoxide-producing Sites in Isolated Brain Mitochondria. *Journal of Biological Chemistry, 279*(6), 4127-4135.

Kuehne, A., Emmert, H., Soehle, J., Winnefeld, M., Fischer, F., Wenck, H., Gallinat, S., Terstegen, L., Lucius, R., Hildebrand, J., & Zamboni, N. (2015). Acute Activation of Oxidative Pentose Phosphate Pathway as First-Line Response to Oxidative Stress in Human Skin Cells. *Molecular Cell, 59*(3), 359-371.

Kumagai, A. K., Dwyer, K. J., & Pardridge, W. M. (1994). Differential glycosylation of the GLUT1 glucose transporter in brain capillaries and choroid plexus. *Biochimica et biophysica acta, 1193*(1), 24–30.

Kurdi, M., Zgheib, C., & Booz, G. W. (2018). Recent Developments on the Crosstalk Between STAT3 and Inflammation in Heart Function and Disease. *Frontiers in Immunology, 9*, 3029.

Lacapère, J.-J., Delavoie, F., Li, H., Péranzi, G., Maccario, J., Papadopoulos, V., & Vidic, B. (2001). Structural and Functional Study of Reconstituted Peripheral Benzodiazepine Receptor. *Biochemical and Biophysical Research Communications, 284*(2), 536-541.

Laforge, M., Rodrigues, V., Silvestre, R., Gautier, C., Weil, R., Corti, O., & Estaquier, J. (2016). NF-κB pathway controls mitochondrial dynamics. *Cell death and differentiation, 23*(1), 89-98.

Lagarde, J., Sarazin, M., & Bottlaender, M. (2018). In vivo PET imaging of neuroinflammation in Alzheimer's disease. *Journal of neural transmission, 125*(5), 847-867.

Largeau, B., Dupont, A.-C., Guilloteau, D., Santiago-Ribeiro, M.-J., & Arlicot, N. (2017). TSPO PET Imaging: From Microglial Activation to Peripheral Sterile Inflammatory Diseases? *Contrast media & molecular imaging, 2017*, 6592139-6592139.

Lavisse, S., Guillermier, M., Hérard, A.-S., Petit, F., Delahaye, M., Van Camp, N., Ben Haim, L., Lebon, V., Remy, P., Dollé, F., Delzescaux, T., Bonvento, G., Hantraye, P., & Escartin, C. (2012). Reactive astrocytes overexpress TSPO and are detected by TSPO positron emission tomography imaging. *The Journal of neuroscience : the official journal of the Society for Neuroscience, 32*(32), 10809-10818.

Lawrence, T. (2009). The nuclear factor NF-kappaB pathway in inflammation. *Cold Spring Harbor perspectives in biology, 1*(6), a001651-a001651.

Le Fur, G., Vaucher, N., Perrier, M. L., Flamier, A., Benavides, J., Renault, C., Dubroeucq, M. C., Guérémy, C., & Uzan, A. (1983). Differentiation between two ligands for peripheral benzodiazepine binding sites, [3H]R05-4864 and [3H]PK 11195, by thermodynamic studies. *Life Sciences, 33*(5), 449-457.

Lee, C. H., Kim, H. J., Lee, Y.-S., Kang, G. M., Lim, H. S., Lee, S.-H., Song, D. K., Kwon, O., Hwang, I., Son, M., Byun, K., Sung, Y. H., Kim, S., Kim, J. B., Choi, E. Y., Kim, Y.-B., Kim, K., Kweon, M.-N., Sohn, J.-W., & Kim, M.-S. (2018). Hypothalamic Macrophage Inducible Nitric Oxide Synthase Mediates Obesity-Associated Hypothalamic Inflammation. *Cell reports, 25*(4), 934-946.e935.

Lee, I.-K. (2014). The role of pyruvate dehydrogenase kinase in diabetes and obesity. *Diabetes & metabolism journal, 38*(3), 181-186.

Lee, J.-W., Nam, H., & Yu, S.-W. (2016). Systematic Analysis of Translocator Protein 18 kDa (TSPO) Ligands on Toll-like Receptors-mediated Pro-inflammatory Responses in Microglia and Astrocytes. *Experimental neurobiology, 25*(5), 262-268.

Lee, K., Kerner, J., & Hoppel, C. L. (2011). Mitochondrial carnitine palmitoyltransferase 1a (CPT1a) is part of an outer membrane fatty acid

transfer complex. *The Journal of biological chemistry, 286*(29), 25655-25662.

Lee, M. K. S., Al-Sharea, A., Shihata, W. A., Bertuzzo Veiga, C., Cooney, O. D., Fleetwood, A. J., Flynn, M. C., Claeson, E., Palmer, C. S., Lancaster, G. I., Henstridge, D. C., Hamilton, J. A., & Murphy, A. J. (2019). Glycolysis Is Required for LPS-Induced Activation and Adhesion of Human CD14(+)CD16(-) Monocytes. *Frontiers in Immunology, 10*, 2054-2054.

Lejri, I., Grimm, A., Hallé, F., Abarghaz, M., Klein, C., Maitre, M., Schmitt, M., Bourguignon, J.-J., Mensah-Nyagan, A. G., Bihel, F., & Eckert, A. (2019). TSPO Ligands Boost Mitochondrial Function and Pregnenolone Synthesis. *Journal of Alzheimer's disease, 72*(4), 1045-1058.

Li, F., Liu, J., Zheng, Y., Garavito, R. M., & Ferguson-Miller, S. (2015). Protein structure. Crystal structures of translocator protein (TSPO) and mutant mimic of a human polymorphism. *Science, 347*(6221), 555-558.

Li, F., Wang, Y., Zeller, K. I., Potter, J. J., Wonsey, D. R., O'Donnell, K. A., Kim, J.-W., Yustein, J. T., Lee, L. A., & Dang, C. V. (2005). Myc stimulates nuclearly encoded mitochondrial genes and mitochondrial biogenesis. *Molecular and Cellular Biology, 25*(14), 6225-6234.

Li, H., & Papadopoulos, V. (1998). Peripheral-type benzodiazepine receptor function in cholesterol transport. Identification of a putative cholesterol recognition/interaction amino acid sequence and consensus pattern. *Endocrinology, 139*(12), 4991-4997.

Li, J., & Papadopoulos, V. (2015). Translocator protein (18kDa) as a pharmacological target in adipocytes to regulate glucose homeostasis. *Biochemical Pharmacology, 97*(1), 99-110.

Li, L., Jin, X., Zhang, H., & Yin, J. (2018). Protective effect of picroliv against lipopolysaccharide-induced cognitive dysfunction and neuroinflammation by attenuating TLR4/NFκB pathway. *Folia neuropathologica, 56*(4), 337-345.

Li, M., Ren, H., Sheth, K. N., Shi, F.-D., & Liu, Q. (2017). A TSPO ligand attenuates brain injury after intracerebral hemorrhage. *FASEB journal, 31*(8), 3278-3287.

Li, N., Zhang, X., Dong, H., Zhang, S., Sun, J., & Qian, Y. (2016). Lithium Ameliorates LPS-Induced Astrocytes Activation Partly via Inhibition of Toll-Like Receptor 4 Expression. *Cellular physiology and biochemistry :*

*international journal of experimental cellular physiology, biochemistry, and pharmacology, 38*(2), 714-725.

Liddelow, S. A., & Barres, B. A. (2017). Reactive Astrocytes: Production, Function, and Therapeutic Potential. *Immunity, 46*(6), 957-967.

Lin, D., Chang, Y. J., Strauss, J. F., & Miller, W. L. (1993). The human peripheral renzodiazepine receptor gene: Cloning and characterization of alternative splicing in normal tissues and in a patient with congenital lipoid adrenal hyperplasia. *Genomics, 18*(3), 643-650.

Lin, Y.-M., Sun, H.-Y., Chiu, W.-T., Su, H.-C., Chien, Y.-C., Chang, H.-A., Chong, L.-W., Chang, H.-C., Young, K.-C., Bai, C.-H., & Tsao, C.-W. (2019). Etifoxine, a TSPO Ligand, Worsens Hepatitis C-Related Insulin Resistance but Relieves Lipid Accumulation. *BioMed research international, 2019*, 3102414-3102414.

Liu, C., Cui, G., Zhu, M., Kang, X., & Guo, H. (2014a). Neuroinflammation in Alzheimer's disease: chemokines produced by astrocytes and chemokine receptors. *International journal of clinical and experimental pathology, 7*(12), 8342-8355.

Liu, G.-J., Middleton, R. J., & Banati, R. B. (2017a). Subcellular distribution of the 18kDa translocator protein and transcript variant PBR-S in human cells. *Gene, 613*, 45-56.

Liu, G.-J., Middleton, R. J., Hatty, C. R., Kam, W. W.-Y., Chan, R., Pham, T., Harrison-Brown, M., Dodson, E., Veale, K., & Banati, R. B. (2014b). The 18 kDa Translocator Protein, Microglia and Neuroinflammation. *Brain Pathology, 24*(6), 631-653.

Liu, G.-J., Middleton, R. J., Kam, W. W.-Y., Chin, D. Y., Hatty, C. R., Chan, R. H. Y., & Banati, R. B. (2017b). Functional gains in energy and cell metabolism after TSPO gene insertion. *Cell cycle, 16*(5), 436-447.

Liu, H.-T., Akita, T., Shimizu, T., Sabirov, R. Z., & Okada, Y. (2009). Bradykinin-induced astrocyte-neuron signalling: glutamate release is mediated by ROS-activated volume-sensitive outwardly rectifying anion channels. *The Journal of physiology, 587*(10), 2197-2209.

Liu, L., Lu, Y., Martinez, J., Bi, Y., Lian, G., Wang, T., Milasta, S., Wang, J., Yang, M., Liu, G., Green, D. R., & Wang, R. (2016). Proinflammatory signal suppresses proliferation and shifts macrophage metabolism from Myc-

dependent to HIF1α-dependent. *Proceedings of the National Academy of Sciences, 113*(6), 1564.

Liu, T., Zhang, L., Joo, D., & Sun, S.-C. (2017c). NF-κB signaling in inflammation. *Signal Transduction and Targeted Therapy, 2*(1), 17023.

Loftus, R. M., & Finlay, D. K. (2016). Immunometabolism: Cellular Metabolism Turns Immune Regulator. *Journal of Biological Chemistry, 291*(1), 1-10.

Londhe, P., Yu, P. Y., Ijiri, Y., Ladner, K. J., Fenger, J. M., London, C., Houghton, P. J., & Guttridge, D. C. (2018). Classical NF-κB Metabolically Reprograms Sarcoma Cells Through Regulation of Hexokinase 2. *Frontiers in Oncology, 8*, 104.

Long, Y. C., & Zierath, J. R. (2006). AMP-activated protein kinase signaling in metabolic regulation. *The Journal of Clinical Investigation, 116*(7), 1776-1783.

Lopez-Fabuel, I., Le Douce, J., Logan, A., James, A. M., Bonvento, G., Murphy, M. P., Almeida, A., & Bolaños, J. P. (2016). Complex I assembly into supercomplexes determines differential mitochondrial ROS production in neurons and astrocytes. *Proceedings of the National Academy of Sciences*, 201613701.

Lu, Y.-C., Yeh, W.-C., & Ohashi, P. S. (2008). LPS/TLR4 signal transduction pathway. *Cytokine, 42*(2), 145-151.

Lukasiuk, K., Kaczmarek, L., & Condorelli, D. F. (1995). Inducible and constitutive transcription factor NF-kB-like DNA binding activities in rat brain cells cultured in vitro. *Neurochemistry International, 26*(2), 173-178.

Macheda, M. L., Rogers, S., & Best, J. D. (2005). Molecular and cellular regulation of glucose transporter (GLUT) proteins in cancer. *Journal of Cellular Physiology, 202*(3), 654-662.

Macintyre, Andrew N., Gerriets, Valerie A., Nichols, Amanda G., Michalek, Ryan D., Rudolph, Michael C., Deoliveira, D., Anderson, Steven M., Abel, E. D., Chen, Benny J., Hale, Laura P., & Rathmell, Jeffrey C. (2014). The Glucose Transporter Glut1 Is Selectively Essential for CD4 T Cell Activation and Effector Function. *Cell metabolism, 20*(1), 61-72.

Maedera, S., Mizuno, T., Ishiguro, H., Ito, T., Soga, T., & Kusuhara, H. (2019). GLUT6 is a lysosomal transporter that is regulated by inflammatory stimuli and modulates glycolysis in macrophages. *FEBS Letters, 593*(2), 195-208.

Mages, K., Grassmann, F., Jägle, H., Rupprecht, R., Weber, B. H. F., Hauck, S. M., & Grosche, A. (2019). The agonistic TSPO ligand XBD173 attenuates the glial response thereby protecting inner retinal neurons in a murine model of retinal ischemia. *Journal of Neuroinflammation, 16*(1), 43.

Mahmoud, S., Gharagozloo, M., Simard, C., & Gris, D. (2019). Astrocytes Maintain Glutamate Homeostasis in the CNS by Controlling the Balance between Glutamate Uptake and Release. *Cells, 8*(2).

Majewski, N., Nogueira, V., Bhaskar, P., Coy, P. E., Skeen, J. E., Gottlob, K., Chandel, N. S., Thompson, C. B., Robey, R. B., & Hay, N. (2004). Hexokinase-Mitochondria Interaction Mediated by Akt Is Required to Inhibit Apoptosis in the Presence or Absence of Bax and Bak. *Molecular Cell, 16*(5), 819-830.

Makinoshima, H., Takita, M., Saruwatari, K., Umemura, S., Obata, Y., Ishii, G., Matsumoto, S., Sugiyama, E., Ochiai, A., Abe, R., Goto, K., Esumi, H., & Tsuchihara, K. (2015). Signaling through the Phosphatidylinositol 3-Kinase (PI3K)/Mammalian Target of Rapamycin (mTOR) Axis Is Responsible for Aerobic Glycolysis mediated by Glucose Transporter in Epidermal Growth Factor Receptor (EGFR)-mutated Lung Adenocarcinoma. *Journal of Biological Chemistry, 290*(28), 17495-17504.

Maranzana, E., Barbero, G., Falasca, A. I., Lenaz, G., & Genova, M. L. (2013). Mitochondrial respiratory supercomplex association limits production of reactive oxygen species from complex I. *Antioxidants & redox signaling, 19*(13), 1469-1480.

Marginedas-Freixa, I., Hattab, C., Bouyer, G., Halle, F., Chene, A., Lefevre, S. D., Cambot, M., Cueff, A., Schmitt, M., Gamain, B., Lacapere, J. J., Egee, S., Bihel, F., Le Van Kim, C., & Ostuni, M. A. (2016). TSPO ligands stimulate ZnPPIX transport and ROS accumulation leading to the inhibition of P. falciparum growth in human blood. *Scientific reports, 6*, 33516-33516.

Márquez, S., Fernández, J. J., Mancebo, C., Herrero-Sánchez, C., Alonso, S., Sandoval, T. A., Rodríguez Prados, M., Cubillos-Ruiz, J. R., Montero, O., Fernández, N., & Sánchez Crespo, M. (2019). Tricarboxylic Acid Cycle Activity and Remodeling of Glycerophosphocholine Lipids Support Cytokine Induction in Response to Fungal Patterns. *Cell reports, 27*(2), 525-536.e524.

Mason, S. (2017). Lactate Shuttles in Neuroenergetics—Homeostasis, Allostasis and Beyond. *Frontiers in neuroscience, 11*, 43.

Mathupala, S. P., Ko, Y. H., & Pedersen, P. L. (2006). Hexokinase II: Cancer's double-edged sword acting as both facilitator and gatekeeper of malignancy when bound to mitochondria. *Oncogene, 25*(34), 4777-4786.

Matoba, S., Kang, J.-G., Patino, W. D., Wragg, A., Boehm, M., Gavrilova, O., Hurley, P. J., Bunz, F., & Hwang, P. M. (2006). p53 Regulates Mitochondrial Respiration. *Science, 312*(5780), 1650.

Matthews, P. M. (2019). Chronic inflammation in multiple sclerosis — seeing what was always there. *Nature Reviews Neurology, 15*(10), 582-593.

Matute, C., Domercq, M., & Sánchez-Gómez, M.-V. (2006). Glutamate-mediated glial injury: Mechanisms and clinical importance. *Glia, 53*(2), 212-224.

Mauro, C., Leow, S. C., Anso, E., Rocha, S., Thotakura, A. K., Tornatore, L., Moretti, M., De Smaele, E., Beg, A. A., Tergaonkar, V., Chandel, N. S., & Franzoso, G. (2011). NF-κB controls energy homeostasis and metabolic adaptation by upregulating mitochondrial respiration. *Nature Cell Biology, 13*(10), 1272-1279.

McCommis, K. S., & Finck, B. N. (2015). Mitochondrial pyruvate transport: a historical perspective and future research directions. *The Biochemical journal, 466*(3), 443-454.

McEnery, M. W., Dawson, T. M., Verma, A., Gurley, D., Colombini, M., & Snyder, S. H. (1993). Mitochondrial voltage-dependent anion channel. Immunochemical and immunohistochemical characterization in rat brain. *Journal of Biological Chemistry, 268*(31), 23289-23296.

McGettrick, A. F., & O'Neill, L. A. J. (2013). How metabolism generates signals during innate immunity and inflammation. *The Journal of biological chemistry, 288*(32), 22893-22898.

McNeela, A. M., Bernick, C., Hines, R. M., & Hines, D. J. (2018). TSPO regulation in reactive gliotic diseases. *Journal of Neuroscience Research, 96*(6), 978-988.

Meares, G. P., Qin, H., Liu, Y., Holdbrooks, A. T., & Benveniste, E. N. (2013). AMP-activated protein kinase restricts IFN-γ signaling. *Journal of immunology, 190*(1), 372-380.

Menk, A. V., Scharping, N. E., Moreci, R. S., Zeng, X., Guy, C., Salvatore, S., Bae, H., Xie, J., Young, H. A., Wendell, S. G., & Delgoffe, G. M. (2018).

Early TCR Signaling Induces Rapid Aerobic Glycolysis Enabling Distinct Acute T Cell Effector Functions. *Cell reports, 22*(6), 1509-1521.

Michalek, R. D., Gerriets, V. A., Jacobs, S. R., Macintyre, A. N., MacIver, N. J., Mason, E. F., Sullivan, S. A., Nichols, A. G., & Rathmell, J. C. (2011). Cutting Edge: Distinct Glycolytic and Lipid Oxidative Metabolic Programs Are Essential for Effector and Regulatory $CD4^+$ T Cell Subsets. *The Journal of Immunology, 186*(6), 3299.

Michelle, L. J., Silvia, S., & Michael, K. (2006). Development of Ligands for the Peripheral Benzodiazepine Receptor. *Current Medicinal Chemistry, 13*(17), 1991-2001.

Michl, J., Ohlbaum, D. J., & Silverstein, S. C. (1976). 2-Deoxyglucose selectively inhibits Fc and complement receptor-mediated phagocytosis in mouse peritoneal macrophages. I. Description of the inhibitory effect. *The Journal of experimental medicine, 144*(6), 1465-1483.

Migheli, A., Piva, R., Atzori, C., Troost, D., & Schiffer, D. (1997). c-Jun, JNK/SAPK Kinases and Transcription Factor NF-κB Are Selectively Activated in Astrocytes, but not Motor Neurons, in Amyotrophic Lateral Sclerosis. *Journal of Neuropathology & Experimental Neurology, 56*(12), 1314-1322.

Milenkovic, V., Rupprecht, R., & Wetzel, H. (2015). The Translocator Protein 18 kDa (TSPO) and Its Role in Mitochondrial Biology and Psychiatric Disorders. *Mini-Reviews in Medicinal Chemistry, 15*(5), 366-372.

Milenkovic, V. M., Bader, S., Sudria-Lopez, D., Siebert, R., Brandl, C., Nothdurfter, C., Weber, B. H. F., Rupprecht, R., & Wetzel, C. H. (2018). Effects of genetic variants in the TSPO gene on protein structure and stability. *PloS one, 13*(4), e0195627.

Millet, P., Vachharajani, V., McPhail, L., Yoza, B., & McCall, C. E. (2016). GAPDH Binding to TNF-α mRNA Contributes to Posttranscriptional Repression in Monocytes: A Novel Mechanism of Communication between Inflammation and Metabolism. *Journal of immunology, 196*(6), 2541-2551.

Mills, E. L., Kelly, B., Logan, A., Costa, A. S. H., Varma, M., Bryant, C. E., Tourlomousis, P., Däbritz, J. H. M., Gottlieb, E., Latorre, I., Corr, S. C., McManus, G., Ryan, D., Jacobs, H. T., Szibor, M., Xavier, R. J., Braun, T., Frezza, C., Murphy, M. P., & O'Neill, L. A. (2016). Succinate

Dehydrogenase Supports Metabolic Repurposing of Mitochondria to Drive Inflammatory Macrophages. *Cell, 167*(2), 457-470.e413.

Miyamoto, S., Murphy, A. N., & Brown, J. H. (2008). Akt mediates mitochondrial protection in cardiomyocytes through phosphorylation of mitochondrial hexokinase-II. *Cell Death & Differentiation, 15*(3), 521-529.

Miyazawa, N., Hamel, E., & Diksic, M. (1998). Assessment of the peripheral benzodiazepine receptors in human gliomas by two methods. *Journal of neuro-oncology, 38*(1), 19-26.

Morgan, M. J., & Liu, Z.-g. (2011). Crosstalk of reactive oxygen species and NF-κB signaling. *Cell research, 21*(1), 103-115.

Moriyama, H., Moriyama, M., Ozawa, T., Tsuruta, D., Iguchi, T., Tamada, S., Nakatani, T., Nakagawa, K., & Hayakawa, T. (2018). Notch Signaling Enhances Stemness by Regulating Metabolic Pathways Through Modifying p53, NF-κB, and HIF-1α. *Stem Cells and Development, 27*(13), 935-947.

Mørkholt, A. S., Wiborg, O., Nieland, J. G. K., Nielsen, S., & Nieland, J. D. (2017). Blocking of carnitine palmitoyl transferase 1 potently reduces stress-induced depression in rat highlighting a pivotal role of lipid metabolism. *Scientific reports, 7*(1), 2158-2158.

Mosser, D. M., & Edwards, J. P. (2008). Exploring the full spectrum of macrophage activation. *Nature reviews. Immunology, 8*(12), 958-969.

Motori, E., Puyal, J., Toni, N., Ghanem, A., Angeloni, C., Malaguti, M., Cantelli-Forti, G., Berninger, B., Conzelmann, K.-K., Götz, M., Winklhofer, Konstanze F., Hrelia, S., & Bergami, M. (2013). Inflammation-Induced Alteration of Astrocyte Mitochondrial Dynamics Requires Autophagy for Mitochondrial Network Maintenance. *Cell metabolism, 18*(6), 844-859.

Movafagh, S., Crook, S., & Vo, K. (2015). Regulation of hypoxia-inducible factor-1a by reactive oxygen species: new developments in an old debate. *Journal of cellular biochemistry, 116*(5), 696-703.

Muhammad, T., Ikram, M., Ullah, R., Rehman, S. U., & Kim, M. O. (2019). Hesperetin, a Citrus Flavonoid, Attenuates LPS-Induced Neuroinflammation, Apoptosis and Memory Impairments by Modulating TLR4/NF-κB Signaling. *Nutrients, 11*(3), 648.

Mukherjee, S., & Das, S. K. (2012). Translocator protein (TSPO) in breast cancer. *Current Molecular Medicine, 12*(4), 443-457.

Murail, S., Robert, J.-C., Coïc, Y.-M., Neumann, J.-M., Ostuni, M. A., Yao, Z.-X., Papadopoulos, V., Jamin, N., & Lacapère, J.-J. (2008). Secondary and tertiary structures of the transmembrane domains of the translocator protein TSPO determined by NMR. Stabilization of the TSPO tertiary fold upon ligand binding. *Biochimica et biophysica acta, 1778*(6), 1375-1381.

Murphy-Royal, C., Dupuis, J., Groc, L., & Oliet, S. H. R. (2017). Astroglial glutamate transporters in the brain: Regulating neurotransmitter homeostasis and synaptic transmission. *Journal of Neuroscience Research, 95*(11), 2140-2151.

Murphy, Michael P. (2008). How mitochondria produce reactive oxygen species. *Biochemical Journal, 417*(1), 1-13.

Murphy, M. P., & O'Neill, L. A. J. (2018). Krebs Cycle Reimagined: The Emerging Roles of Succinate and Itaconate as Signal Transducers. *Cell, 174*(4), 780-784.

Musman, J., Paradis, S., Panel, M., Pons, S., Barau, C., Caccia, C., Leoni, V., Ghaleh, B., & Morin, D. (2017). A TSPO ligand prevents mitochondrial sterol accumulation and dysfunction during myocardial ischemia-reperfusion in hypercholesterolemic rats. *Biochemical Pharmacology, 142*, 87-95.

Nair, S., Sobotka, K. S., Joshi, P., Gressens, P., Fleiss, B., Thornton, C., Mallard, C., & Hagberg, H. (2019). Lipopolysaccharide-induced alteration of mitochondrial morphology induces a metabolic shift in microglia modulating the inflammatory response in vitro and in vivo. *Glia, 67*(6), 1047-1061.

Nakamura, K., Yamada, K., Iwayama, Y., Toyota, T., Furukawa, A., Takimoto, T., Terayama, H., Iwahashi, K., Takei, N., Minabe, Y., Sekine, Y., Suzuki, K., Iwata, Y., Pillai, A., Nakamoto, Y., Ikeda, K., Yoshii, M., Fukunishi, I., Yoshikawa, T., & Mori, N. (2006). Evidence that variation in the peripheral benzodiazepine receptor (PBR) gene influences susceptibility to panic disorder. *American Journal of Medical Genetics Part B: Neuropsychiatric Genetics, 141B*(3), 222-226.

Namgaladze, D., Lips, S., Leiker, T. J., Murphy, R. C., Ekroos, K., Ferreiros, N., Geisslinger, G., & Brüne, B. (2014). Inhibition of macrophage fatty acid β-oxidation exacerbates palmitate-induced inflammatory and endoplasmic reticulum stress responses. *Diabetologia, 57*(5), 1067-1077.

Nan, J., Du, Y., Chen, X., Bai, Q., Wang, Y., Zhang, X., Zhu, N., Zhang, J., Hou, J., Wang, Q., & Yang, J. (2014). TPCA-1 is a direct dual inhibitor of STAT3 and NF-κB and regresses mutant EGFR-associated human non-small cell lung cancers. *Molecular cancer therapeutics, 13*(3), 617-629.

Nan, J., Hu, H., Sun, Y., Zhu, L., Wang, Y., Zhong, Z., Zhao, J., Zhang, N., Wang, Y., Wang, Y., Ye, J., Zhang, L., Hu, X., Zhu, W., & Wang, J. a. (2017). TNFR2 Stimulation Promotes Mitochondrial Fusion via Stat3- and NF-kB-Dependent Activation of OPA1 Expression. *Circulation research, 121*(4), 392-410.

Narayan, N., Mandhair, H., Smyth, E., Dakin, S. G., Kiriakidis, S., Wells, L., Owen, D., Sabokbar, A., & Taylor, P. (2017). The macrophage marker translocator protein (TSPO) is down-regulated on pro-inflammatory 'M1' human macrophages. *PloS one, 12*(10), e0185767-e0185767.

Nedergaard, M., & Verkhratsky, A. (2012). Artifact versus reality — How astrocytes contribute to synaptic events. *Glia, 60*(7), 1013-1023.

Nelson D., Cox M. (2017). *Lehninger Principles of Biochemistry* (7 ed.). New York: W.H. Freeman.

Newcombe, E. A., Camats-Perna, J., Silva, M. L., Valmas, N., Huat, T. J., & Medeiros, R. (2018). Inflammation: the link between comorbidities, genetics, and Alzheimer's disease. *Journal of Neuroinflammation, 15*(1), 276.

Nisr, R. B., Shah, D. S., Ganley, I. G., & Hundal, H. S. (2019). Proinflammatory NFkB signalling promotes mitochondrial dysfunction in skeletal muscle in response to cellular fuel overloading. *Cellular and Molecular Life Sciences, 76*(24), 4887-4904.

Nolt, B., Tu, F., Wang, X., Ha, T., Winter, R., Williams, D. L., & Li, C. (2018). Lactate and Immunosuppression in Sepsis. *Shock, 49*(2), 120-125.

Norata, Giuseppe D., Caligiuri, G., Chavakis, T., Matarese, G., Netea, Mihai G., Nicoletti, A., O'Neill, Luke A. J., & Marelli-Berg, Federica M. (2015). The Cellular and Molecular Basis of Translational Immunometabolism. *Immunity, 43*(3), 421-434.

Nwaobi, S. E., Cuddapah, V. A., Patterson, K. C., Randolph, A. C., & Olsen, M. L. (2016). The role of glial-specific Kir4.1 in normal and pathological states of the CNS. *Acta Neuropathologica, 132*(1), 1-21.

O'Beirne, G. B., Woods, M. J., & Williams, D. C. (1990). Two subcellular locations for peripheral-type benzodiazepine acceptors in rat liver. *European Journal of Biochemistry, 188*(1), 131-138.

O'Neill, L. A. J., Kishton, R. J., & Rathmell, J. (2016). A guide to immunometabolism for immunologists. *Nature Reviews Immunology, 16*(9), 553-565.

Obame, F. N., Zini, R., Souktani, R., Berdeaux, A., & Morin, D. (2007). Peripheral Benzodiazepine Receptor-Induced Myocardial Protection is Mediated by Inhibition of Mitochondrial Membrane Permeabilization. *Journal of Pharmacology and Experimental Therapeutics, 323*(1), 336.

Oberheim, N. A., Takano, T., Han, X., He, W., Lin, J. H. C., Wang, F., Xu, Q., Wyatt, J. D., Pilcher, W., Ojemann, J. G., Ransom, B. R., Goldman, S. A., & Nedergaard, M. (2009). Uniquely hominid features of adult human astrocytes. *The Journal of neuroscience : the official journal of the Society for Neuroscience, 29*(10), 3276-3287.

Oeckinghaus, A., & Ghosh, S. (2009). The NF-kappaB family of transcription factors and its regulation. *Cold Spring Harbor perspectives in biology, 1*(4), a000034-a000034.

Oke, B. O., Suarez-Quian, C. A., Riond, J., Ferrara, P., & Papadopoulos, V. (1992). Cell surface localization of the peripheral-type benzodiazepine receptor (PBR) in adrenal cortex. *Molecular and Cellular Endocrinology, 87*(1), R1-R6.

Olmos, G., & Lladó, J. (2014). Tumor necrosis factor alpha: a link between neuroinflammation and excitotoxicity. *Mediators of inflammation, 2014*, 861231-861231.

Owen, D. R., Fan, J., Campioli, E., Venugopal, S., Midzak, A., Daly, E., Harlay, A., Issop, L., Libri, V., Kalogiannopoulou, D., Oliver, E., Gallego-Colon, E., Colasanti, A., Huson, L., Rabiner, E. A., Suppiah, P., Essagian, C., Matthews, P. M., & Papadopoulos, V. (2017a). TSPO mutations in rats and a human polymorphism impair the rate of steroid synthesis. *The Biochemical journal, 474*(23), 3985-3999.

Owen, D. R., Guo, Q., Kalk, N. J., Colasanti, A., Kalogiannopoulou, D., Dimber, R., Lewis, Y. L., Libri, V., Barletta, J., Ramada-Magalhaes, J., Kamalakaran, A., Nutt, D. J., Passchier, J., Matthews, P. M., Gunn, R. N., & Rabiner, E. A. (2014). Determination of [11C]PBR28 Binding Potential

in vivo: A First Human TSPO Blocking Study. *Journal of Cerebral Blood Flow & Metabolism, 34*(6), 989-994.

Owen, D. R., Narayan, N., Wells, L., Healy, L., Smyth, E., Rabiner, E. A., Galloway, D., Williams, J. B., Lehr, J., Mandhair, H., Peferoen, L. A., Taylor, P. C., Amor, S., Antel, J. P., Matthews, P. M., & Moore, C. S. (2017b). Pro-inflammatory activation of primary microglia and macrophages increases 18 kDa translocator protein expression in rodents but not humans. *Journal of cerebral blood flow and metabolism : official journal of the International Society of Cerebral Blood Flow and Metabolism, 37*(8), 2679-2690.

Owen, D. R., Yeo, A. J., Gunn, R. N., Song, K., Wadsworth, G., Lewis, A., Rhodes, C., Pulford, D. J., Bennacef, I., Parker, C. A., StJean, P. L., Cardon, L. R., Mooser, V. E., Matthews, P. M., Rabiner, E. A., & Rubio, J. P. (2012). An 18-kDa translocator protein (TSPO) polymorphism explains differences in binding affinity of the PET radioligand PBR28. *Journal of cerebral blood flow and metabolism : official journal of the International Society of Cerebral Blood Flow and Metabolism, 32*(1), 1-5.

Øyehaug, L., Østby, I., Lloyd, C. M., Omholt, S. W., & Einevoll, G. T. (2012). Dependence of spontaneous neuronal firing and depolarisation block on astroglial membrane transport mechanisms. *Journal of Computational Neuroscience, 32*(1), 147-165.

Pahl, H. L. (1999). Activators and target genes of Rel/NF-κB transcription factors. *Oncogene, 18*(49), 6853-6866.

Pahwa R, S. A., Jialal I. (2019). *Chronic Inflammation*.

Palmieri, F., & Monné, M. (2016). Discoveries, metabolic roles and diseases of mitochondrial carriers: A review. *Biochimica et biophysica acta, 1863*(10), 2362-2378.

Palsson-McDermott, Eva M., Curtis, Anne M., Goel, G., Lauterbach, Mario A. R., Sheedy, Frederick J., Gleeson, Laura E., van den Bosch, Mirjam W. M., Quinn, Susan R., Domingo-Fernandez, R., Johnston, Daniel G. W., Jiang, J.-k., Israelsen, William J., Keane, J., Thomas, C., Clish, C., Vander Heiden, M., Xavier, Ramnik J., & O'Neill, Luke A. J. (2015). Pyruvate Kinase M2 Regulates Hif-1α Activity and IL-1β Induction and Is a Critical Determinant of the Warburg Effect in LPS-Activated Macrophages. *Cell metabolism, 21*(1), 65-80.

Panickar, K. S., Jayakumar, A. R., Rao, K. V. R., & Norenberg, M. D. (2009). Ammonia-induced activation of p53 in cultured astrocytes: Role in cell swelling and glutamate uptake. *Neurochemistry International, 55*(1), 98-105.

Papa, S., Choy, P. M., & Bubici, C. (2019). The ERK and JNK pathways in the regulation of metabolic reprogramming. *Oncogene, 38*(13), 2223-2240.

Papadopoulos, V., Amri, H., Boujrad, N., Cascio, C., Culty, M., Garnier, M., Hardwick, M., Li, H., Vidic, B., Brown, A. S., Reversa, J. L., Bernassau, J. M., & Drieu, K. (1997). Peripheral benzodiazepine receptor in cholesterol transport and steroidogenesis. *Steroids, 62*(1), 21-28.

Papadopoulos, V., Baraldi, M., Guilarte, T. R., Knudsen, T. B., Lacapère, J.-J., Lindemann, P., Norenberg, M. D., Nutt, D., Weizman, A., Zhang, M.-R., & Gavish, M. (2006). Translocator protein (18kDa): new nomenclature for the peripheral-type benzodiazepine receptor based on its structure and molecular function. *Trends in Pharmacological Sciences, 27*(8), 402-409.

Papadopoulos, V., Boujrad, N., Ikonomovic, M. D., Ferrara, P., & Vidic, B. (1994). Topography of the Leydig cell mitochondrial peripheral-type benzodiazepine receptor. *Molecular and Cellular Endocrinology, 104*(1), R5-R9.

Papadopoulos, V., Fan, J., & Zirkin, B. (2018). Translocator protein (18 kDa): an update on its function in steroidogenesis. *Journal of Neuroendocrinology, 30*(2), e12500.

Papadopoulos, V., Mukhin, A. G., Costa, E., & Krueger, K. E. (1990). The peripheral-type benzodiazepine receptor is functionally linked to Leydig cell steroidogenesis. *The Journal of biological chemistry, 265*(7), 3772-3779.

Paradis, S., Leoni, V., Caccia, C., Berdeaux, A., & Morin, D. (2013). Cardioprotection by the TSPO ligand 4'-chlorodiazepam is associated with inhibition of mitochondrial accumulation of cholesterol at reperfusion. *Cardiovascular Research, 98*(3), 420-427.

Park, J., Choi, H., Min, J.-S., Park, S.-J., Kim, J.-H., Park, H.-J., Kim, B., Chae, J.-I., Yim, M., & Lee, D.-S. (2013). Mitochondrial dynamics modulate the expression of pro-inflammatory mediators in microglial cells. *Journal of Neurochemistry, 127*(2), 221-232.

Park J.Y., Lee K.H., Park H.S., & Choi S.J. (2017) LPS Sensing Mechanism of Human Astrocytes: Evidence of Functional TLR4 Expression and Requirement of Soluble CD14. *J Bacteriol Virol. 47*(4):189-198.

Parpura, V., & Verkhratsky, A. (2012). Astrocytes revisited: concise historic outlook on glutamate homeostasis and signaling. *Croatian medical journal, 53*(6), 518-528.

Parra, V., Verdejo, H. E., Iglewski, M., del Campo, A., Troncoso, R., Jones, D., Zhu, Y., Kuzmicic, J., Pennanen, C., Lopez-Crisosto, C., Jaña, F., Ferreira, J., Noguera, E., Chiong, M., Bernlohr, D. A., Klip, A., Hill, J. A., Rothermel, B. A., Abel, E. D., Zorzano, A., & Lavandero, S. (2014). Insulin Stimulates Mitochondrial Fusion and Function in Cardiomyocytes via the Akt-mTOR-NFκB-Opa-1 Signaling Pathway. *Diabetes, 63*(1), 75.

Pasquale, E. B. (2008). Eph-Ephrin Bidirectional Signaling in Physiology and Disease. *Cell, 133*(1), 38-52.

Pastorino, J. G., & Hoek, J. B. (2008). Regulation of hexokinase binding to VDAC. *Journal of bioenergetics and biomembranes, 40*(3), 171-182.

Pastorino, J. G., Shulga, N., & Hoek, J. B. (2002). Mitochondrial Binding of Hexokinase II Inhibits Bax-induced Cytochrome c Release and Apoptosis. *Journal of Biological Chemistry, 277*(9), 7610-7618.

Pellerin, L., & Magistretti, P. J. (1994). Glutamate uptake into astrocytes stimulates aerobic glycolysis: a mechanism coupling neuronal activity to glucose utilization. *Proceedings of the National Academy of Sciences of the United States of America, 91*(22), 10625-10629.

Pennock, N. D., White, J. T., Cross, E. W., Cheney, E. E., Tamburini, B. A., & Kedl, R. M. (2013). T cell responses: naive to memory and everything in between. *Advances in physiology education, 37*(4), 273-283.

Perevoshchikova, I. V., Zorov, S. D., Kotova, E. A., Zorov, D. B., & Antonenko, Y. N. (2010). Hexokinase inhibits flux of fluorescently labeled ATP through mitochondrial outer membrane porin. *FEBS Letters, 584*(11), 2397-2402.

Perkins, N. D. (2007). Integrating cell-signalling pathways with NF-κB and IKK function. *Nature Reviews Molecular Cell Biology, 8*(1), 49-62.

Pfeiffer, T., Schuster, S., & Bonhoeffer, S. (2001). Cooperation and Competition in the Evolution of ATP-Producing Pathways. *Science, 292*(5516), 504.

Podolin, P. L., Callahan, J. F., Bolognese, B. J., Li, Y. H., Carlson, K., Davis, T. G., Mellor, G. W., Evans, C., & Roshak, A. K. (2005). Attenuation of murine

collagen-induced arthritis by a novel, potent, selective small molecule inhibitor of IkappaB Kinase 2, TPCA-1 (2-[(aminocarbonyl)amino]-5-(4-fluorophenyl)-3-thiophenecarboxamide), occurs via reduction of proinflammatory cytokines and antigen-induced T cell Proliferation. *The Journal of pharmacology and experimental therapeutics, 312*(1), 373-381.

Poli, V., & Camporeale, A. (2015). STAT3-Mediated Metabolic Reprograming in Cellular Transformation and Implications for Drug Resistance. *Frontiers in Oncology, 5*, 121.

Pozzo, E. D., Tremolanti, C., Costa, B., Giacomelli, C., Milenkovic, V. M., Bader, S., Wetzel, C. H., Rupprecht, R., Taliani, S., Settimo, F. D., & Martini, C. (2019). Microglial Pro-Inflammatory and Anti-Inflammatory Phenotypes Are Modulated by Translocator Protein Activation. *International Journal of Molecular Sciences, 20*(18), 4467.

Priego, N., & Valiente, M. (2019). The Potential of Astrocytes as Immune Modulators in Brain Tumors. *Frontiers in immunology, 10,* 1314.

Pucino, V., Certo, M., Bulusu, V., Cucchi, D., Goldmann, K., Pontarini, E., Haas, R., Smith, J., Headland, S. E., Blighe, K., Ruscica, M., Humby, F., Lewis, M. J., Kamphorst, J. J., Bombardieri, M., Pitzalis, C., & Mauro, C. (2019). Lactate Buildup at the Site of Chronic Inflammation Promotes Disease by Inducing CD4+ T Cell Metabolic Rewiring. *Cell metabolism, 30*(6), 1055-1074.e1058.

Puliyappadamba, V. T., Hatanpaa, K. J., Chakraborty, S., & Habib, A. A. (2014). The role of NF-κB in the pathogenesis of glioma. *Molecular & cellular oncology, 1*(3), e963478-e963478.

Rambold, A. S., Kostelecky, B., Elia, N., & Lippincott-Schwartz, J. (2011). Tubular network formation protects mitochondria from autophagosomal degradation during nutrient starvation. *Proceedings of the National Academy of Sciences, 108*(25), 10190.

Rambold, A. S., & Pearce, E. L. (2018). Mitochondrial Dynamics at the Interface of Immune Cell Metabolism and Function. *Trends in Immunology, 39*(1), 6-18.

Rashid, K., Geissl, L., Wolf, A., Karlstetter, M., & Langmann, T. (2018). Transcriptional regulation of Translocator protein (18 kDa) (TSPO) in microglia requires Pu.1, Ap1 and Sp factors. *Biochimica et Biophysica Acta (BBA) - Gene Regulatory Mechanisms, 1861*(12), 1119-1133.

Ratter, J. M., Rooijackers, H. M. M., Hooiveld, G. J., Hijmans, A. G. M., de Galan, B. E., Tack, C. J., & Stienstra, R. (2018). In vitro and in vivo Effects of Lactate on Metabolism and Cytokine Production of Human Primary PBMCs and Monocytes. *Frontiers in Immunology, 9*, 2564.

Ravanan, P., Srikumar, I. F., & Talwar, P. (2017). Autophagy: The spotlight for cellular stress responses. *Life Sciences, 188*, 53-67.

Ravikumar, B., Crawford, D., Dellovade, T., Savinainen, A., Graham, D., Liere, P., Oudinet, J.-P., Webb, M., & Hering, H. (2016). Differential efficacy of the TSPO ligands etifoxine and XBD-173 in two rodent models of Multiple Sclerosis. *Neuropharmacology, 108*, 229-237.

Ray, R., & Miller, D. M. (1991). Cloning and characterization of a human c-myc promoter-binding protein. *Molecular and Cellular Biology, 11*(4), 2154-2161.

Reid, M. A., Lowman, X. H., Pan, M., Tran, T. Q., Warmoes, M. O., Ishak Gabra, M. B., Yang, Y., Locasale, J. W., & Kong, M. (2016). IKKβ promotes metabolic adaptation to glutamine deprivation via phosphorylation and inhibition of PFKFB3. *Genes & development, 30*(16), 1837-1851.

Remels, A. H. V., Gosker, H. R., Verhees, K. J. P., Langen, R. C. J., & Schols, A. M. W. J. (2015). TNF-α-Induced NF-κB Activation Stimulates Skeletal Muscle Glycolytic Metabolism Through Activation of HIF-1α. *Endocrinology, 156*(5), 1770-1781.

Reyes, R. C., & Parpura, V. (2008). Mitochondria modulate Ca2+-dependent glutamate release from rat cortical astrocytes. *The Journal of neuroscience : the official journal of the Society for Neuroscience, 28*(39), 9682-9691.

Rhoads, J. P., Major, A. S., & Rathmell, J. C. (2017). Fine tuning of immunometabolism for the treatment of rheumatic diseases. *Nature Reviews Rheumatology, 13*(5), 313-320.

Riond, J., Mattei, M. G., Kaghad, M., Dumont, X., Guillemot, J. C., Le Fur, G., Caput, D., & Ferrara, P. (1991). Molecular cloning and chromosomal localization of a human peripheral-type benzodiazepine receptor. *European Journal of Biochemistry, 195*(2), 305-311.

Robb, J. L., Morrissey, N. A., Weightman Potter, P. G., Smithers, H. E., Beall, C., & Ellacott, K. L. J. (2019). Immunometabolic Changes in Glia – A Potential Role in the Pathophysiology of Obesity and Diabetes. *Neuroscience*.

Robe, P. A., Bentires-Alj, M., Bonif, M., Rogister, B., Deprez, M., Haddada, H., Khac, M.-T. N., Jolois, O., Erkmen, K., Merville, M.-P., Black, P. M., & Bours, V. (2004). In vitro and in vivo activity of the nuclear factor-kappaB inhibitor sulfasalazine in human glioblastomas. *Clinical cancer research : an official journal of the American Association for Cancer Research, 10*(16), 5595-5603.

Roberts, D. J., & Miyamoto, S. (2015). Hexokinase II integrates energy metabolism and cellular protection: Akting on mitochondria and TORCing to autophagy. *Cell death and differentiation, 22*(2), 248-257.

Robey, R. B., & Hay, N. (2006). Mitochondrial hexokinases, novel mediators of the antiapoptotic effects of growth factors and Akt. *Oncogene, 25*(34), 4683-4696.

Rodríguez-Prados, J.-C., Través, P. G., Cuenca, J., Rico, D., Aragonés, J., Martín-Sanz, P., Cascante, M., & Boscá, L. (2010). Substrate Fate in Activated Macrophages: A Comparison between Innate, Classic, and Alternative Activation. *The Journal of Immunology, 185*(1), 605.

Romanyukha, A. A., Rudnev, S. G., & Sidorov, I. A. (2006). Energy cost of infection burden: An approach to understanding the dynamics of host–pathogen interactions. *Journal of Theoretical Biology, 241*(1), 1-13.

Romeo, E., Cavallaro, S., Korneyev, A., Kozikowski, A. P., Ma, D., Polo, A., Costa, E., & Guidotti, A. (1993). Stimulation of brain steroidogenesis by 2-aryl-indole-3-acetamide derivatives acting at the mitochondrial diazepam-binding inhibitor receptor complex. *The Journal of pharmacology and experimental therapeutics, 267*(1), 462-471.

Rosciszewski, G., Cadena, V., Murta, V., Lukin, J., Villarreal, A., Roger, T., & Ramos, A. J. (2018). Toll-Like Receptor 4 (TLR4) and Triggering Receptor Expressed on Myeloid Cells-2 (TREM-2) Activation Balance Astrocyte Polarization into a Proinflammatory Phenotype. *Molecular neurobiology, 55*(5), 3875-3888.

Rossignol, R., Gilkerson, R., Aggeler, R., Yamagata, K., Remington, S. J., & Capaldi, R. A. (2004). Energy Substrate Modulates Mitochondrial Structure and Oxidative Capacity in Cancer Cells. *Cancer Research, 64*(3), 985.

Rostovtseva, T., & Colombini, M. (1996). ATP Flux Is Controlled by a Voltage-gated Channel from the Mitochondrial Outer Membrane. *Journal of Biological Chemistry, 271*(45), 28006-28008.

Rupprecht, R., Papadopoulos, V., Rammes, G., Baghai, T. C., Fan, J., Akula, N., Groyer, G., Adams, D., & Schumacher, M. (2010). Translocator protein (18 kDa) (TSPO) as a therapeutic target for neurological and psychiatric disorders. *Nature Reviews Drug Discovery, 9*(12), 971-988.

Russell, D. G., Huang, L., & VanderVen, B. C. (2019). Immunometabolism at the interface between macrophages and pathogens. *Nature reviews. Immunology, 19*(5), 291-304.

Ryan, D. G., & O'Neill, L. A. J. (2017). Krebs cycle rewired for macrophage and dendritic cell effector functions. *FEBS Letters, 591*(19), 2992-3006.

Sag, D., Carling, D., Stout, R. D., & Suttles, J. (2008). Adenosine 5′-Monophosphate-Activated Protein Kinase Promotes Macrophage Polarization to an Anti-Inflammatory Functional Phenotype. *The Journal of Immunology, 181*(12), 8633.

Sakurai H., Chiba H., Miyoshi H., Sugita T., & Toriumi W. (1999) IkappaB kinases phosphorylate NF-kappaB p65 subunit on serine 536 in the transactivation domain. *J Biol Chem. 274*(43):30353–30356.

Salminen, A., Hyttinen, J. M. T., & Kaarniranta, K. (2011). AMP-activated protein kinase inhibits NF-κB signaling and inflammation: impact on healthspan and lifespan. *Journal of molecular medicine, 89*(7), 667-676.

Samsoondar, J., P., Burke Amy, C., Sutherland Brian, G., Telford Dawn, E., Sawyez Cynthia, G., Edwards Jane, Y., Pinkosky Stephen, L., Newton Roger, S., & Huff Murray, W. (2017). Prevention of Diet-Induced Metabolic Dysregulation, Inflammation, and Atherosclerosis in Ldlr−/− Mice by Treatment With the ATP-Citrate Lyase Inhibitor Bempedoic Acid. *Arteriosclerosis, Thrombosis, and Vascular Biology, 37*(4), 647-656.

Santoro, A., Mattace Raso, G., Taliani, S., Da Pozzo, E., Simorini, F., Costa, B., Martini, C., Laneri, S., Sacchi, A., Cosimelli, B., Calignano, A., Da Settimo, F., & Meli, R. (2016). TSPO-ligands prevent oxidative damage and inflammatory response in C6 glioma cells by neurosteroid synthesis. *European Journal of Pharmaceutical Sciences, 88*, 124-131.

Sarkar, S., Malovic, E., Harischandra, D. S., Ngwa, H. A., Ghosh, A., Hogan, C., Rokad, D., Zenitsky, G., Jin, H., Anantharam, V., Kanthasamy, A. G., &

Kanthasamy, A. (2018). Manganese exposure induces neuroinflammation by impairing mitochondrial dynamics in astrocytes. *NeuroToxicology, 64*, 204-218.

Satoh, A., Gukovskaya, A. S., Nieto, J. M., Cheng, J. H., Gukovsky, I., Reeve, J. R., Shimosegawa, T., & Pandol, S. J. (2004). PKC-δ and -ε regulate NF-κB activation induced by cholecystokinin and TNF-α in pancreatic acinar cells. *American Journal of Physiology-Gastrointestinal and Liver Physiology, 287*(3), G582-G591.

Schildge, S., Bohrer, C., Beck, K., & Schachtrup, C. (2013). Isolation and culture of mouse cortical astrocytes. *Journal of visualized experiments : JoVE*(71), 50079.

Schindelin, J., Arganda-Carreras, I., Frise, E., Kaynig, V., Longair, M., Pietzsch, T., Preibisch, S., Rueden, C., Saalfeld, S., Schmid, B., Tinevez, J.-Y., White, D. J., Hartenstein, V., Eliceiri, K., Tomancak, P., & Cardona, A. (2012). Fiji: an open-source platform for biological-image analysis. *Nature methods, 9*(7), 676-682.

Schmitt, C., Strazielle, N., & Ghersi-Egea, J.-F. (2012). Brain leukocyte infiltration initiated by peripheral inflammation or experimental autoimmune encephalomyelitis occurs through pathways connected to the CSF-filled compartments of the forebrain and midbrain. *Journal of Neuroinflammation, 9*, 187.

Schneider, C. A., Rasband, W. S., & Eliceiri, K. W. (2012). NIH Image to ImageJ: 25 years of image analysis. *Nature methods, 9*(7), 671-675.

Schulze, R. J., Sathyanarayan, A., & Mashek, D. G. (2017). Breaking fat: The regulation and mechanisms of lipophagy. *Biochimica et biophysica acta. Molecular and cell biology of lipids, 1862*(10 Pt B), 1178-1187.

Schwartzenberg-Bar-Yoseph, F., Armoni, M., & Karnieli, E. (2004). The Tumor Suppressor p53 Down-Regulates Glucose Transporters GLUT1 and GLUT4 Gene Expression. *Cancer Research, 64*(7), 2627-2633.

Seki, S. M., & Gaultier, A. (2017). Exploring Non-Metabolic Functions of Glycolytic Enzymes in Immunity. *Frontiers in Immunology, 8*, 1549-1549.

Selak, M. A., Armour, S. M., MacKenzie, E. D., Boulahbel, H., Watson, D. G., Mansfield, K. D., Pan, Y., Simon, M. C., Thompson, C. B., & Gottlieb, E. (2005). Succinate links TCA cycle dysfunction to oncogenesis by inhibiting HIF-α prolyl hydroxylase. *Cancer Cell, 7*(1), 77-85.

Selvaraj, V., & Stocco, D. M. (2018). Letter to the Editor: Dubious Conclusions on TSPO Function. *Endocrinology, 159*(7), 2528-2529.

Selvaraj, V., & Tu, L. N. (2016). Current status and future perspectives: TSPO in steroid neuroendocrinology. *The Journal of endocrinology, 231*(1), R1-R30.

Selvaraj, V., Tu, L. N., & Stocco, D. M. (2016). Crucial Role Reported for TSPO in Viability and Steroidogenesis is a Misconception. Commentary: Conditional Steroidogenic Cell-Targeted Deletion of TSPO Unveils a Crucial Role in Viability and Hormone-Dependent Steroid Formation. *Frontiers in endocrinology, 7*, 91-91.

Sena, L. A., Li, S., Jairaman, A., Prakriya, M., Ezponda, T., Hildeman, D. A., Wang, C.-R., Schumacker, P. T., Licht, J. D., Perlman, H., Bryce, P. J., & Chandel, N. S. (2013). Mitochondria are required for antigen-specific T cell activation through reactive oxygen species signaling. *Immunity, 38*(2), 225-236.

Sharma, J. N., Al-Omran, A., & Parvathy, S. S. (2007). Role of nitric oxide in inflammatory diseases. *Inflammopharmacology, 15*(6), 252-259.

Shehadeh, M., Palzur, E., Apel, L., & Soustiel, J. F. (2019). Reduction of Traumatic Brain Damage by Tspo Ligand Etifoxine. *International Journal of Molecular Sciences, 20*(11), 2639.

Sheng, W. S., Hu, S., Feng, A., & Rock, R. B. (2013). Reactive oxygen species from human astrocytes induced functional impairment and oxidative damage. *Neurochemical research, 38*(10), 2148-2159.

Shi, L., Jiang, Q., Bushkin, Y., Subbian, S., & Tyagi, S. (2019). Biphasic Dynamics of Macrophage Immunometabolism during Mycobacterium tuberculosis Infection. *mBio, 10*(2), e02550-02518.

Shi, L. Z., Wang, R., Huang, G., Vogel, P., Neale, G., Green, D. R., & Chi, H. (2011). HIF1α–dependent glycolytic pathway orchestrates a metabolic checkpoint for the differentiation of TH17 and Treg cells. *The Journal of experimental medicine, 208*(7), 1367-1376.

Shimoyama, S., Furukawa, T., Ogata, Y., Nikaido, Y., Koga, K., Sakamoto, Y., Ueno, S., & Nakamura, K. (2019). Lipopolysaccharide induces mouse translocator protein (18 kDa) expression via the AP-1 complex in the microglial cell line, BV-2. *PloS one, 14*(9), e0222861-e0222861.

Shoshan-Barmatz, V., Pittala, S., & Mizrachi, D. (2019). VDAC1 and the TSPO: Expression, Interactions, and Associated Functions in Health and Disease States. *International Journal of Molecular Sciences, 20*(13), 3348.

Šileikytė, J., Blachly-Dyson, E., Sewell, R., Carpi, A., Menabò, R., Di Lisa, F., Ricchelli, F., Bernardi, P., & Forte, M. (2014). Regulation of the Mitochondrial Permeability Transition Pore by the Outer Membrane Does Not Involve the Peripheral Benzodiazepine Receptor (Translocator Protein of 18 kDa (TSPO)). *Journal of Biological Chemistry, 289*(20), 13769-13781.

Singer, K., Cheng, W.-C., Kreutz, M., Ho, P.-C., & Siska, P. J. (2018). Immunometabolism in cancer at a glance. *Disease Models & Mechanisms, 11*(8), dmm034272.

Siska, P. J., van der Windt, G. J. W., Kishton, R. J., Cohen, S., Eisner, W., MacIver, N. J., Kater, A. P., Weinberg, J. B., & Rathmell, J. C. (2016). Suppression of Glut1 and Glucose Metabolism by Decreased Akt/mTORC1 Signaling Drives T Cell Impairment in B Cell Leukemia. *Journal of immunology, 197*(6), 2532-2540.

Snezhkina, A. V., Kudryavtseva, A. V., Kardymon, O. L., Savvateeva, M. V., Melnikova, N. V., Krasnov, G. S., & Dmitriev, A. A. (2019). ROS Generation and Antioxidant Defense Systems in Normal and Malignant Cells. *Oxidative medicine and cellular longevity, 2019,* 6175804.

Sofroniew, M. V. (2013). Multiple Roles for Astrocytes as Effectors of Cytokines and Inflammatory Mediators. *The Neuroscientist, 20*(2), 160-172.

Sofroniew, M. V. (2015). Astrocyte barriers to neurotoxic inflammation. *Nature reviews. Neuroscience, 16*(5), 249-263.

Sommermann, T. G., O'Neill, K., Plas, D. R., & Cahir-McFarland, E. (2011). IKKβ and NF-κB transcription govern lymphoma cell survival through AKT-induced plasma membrane trafficking of GLUT1. *Cancer Research, 71*(23), 7291-7300.

Son, Y.-H., Jeong, Y.-T., Lee, K.-A., Choi, K.-H., Kim, S.-M., Rhim, B.-Y., & Kim, K. (2008). Roles of MAPK and NF-κB in Interleukin-6 Induction by Lipopolysaccharide in Vascular Smooth Muscle Cells. *Journal of Cardiovascular Pharmacology, 51*(1).

Sparacio, S. M., Zhang, Y., Vilcek, J., & Benveniste, E. N. (1992). Cytokine regulation of interleukin-6 gene expression in astrocytes involves

activation of an NF-κB-like nuclear protein. *Journal of Neuroimmunology, 39*(3), 231-242.

Sridharan, S., Raffel, J., Nandoskar, A., Record, C., Brooks, D. J., Owen, D., Sharp, D., Muraro, P. A., Gunn, R., & Nicholas, R. (2019). Confirmation of Specific Binding of the 18-kDa Translocator Protein (TSPO) Radioligand [18F]GE-180: a Blocking Study Using XBD173 in Multiple Sclerosis Normal Appearing White and Grey Matter. *Molecular Imaging and Biology, 21*(5), 935-944.

Stamatovic, S. M., Shakui, P., Keep, R. F., Moore, B. B., Kunkel, S. L., Van Rooijen, N., & Andjelkovic, A. V. (2005). Monocyte Chemoattractant Protein-1 Regulation of Blood–Brain Barrier Permeability. *Journal of Cerebral Blood Flow & Metabolism, 25*(5), 593-606.

Sun, L., Shukair, S., Naik, T. J., Moazed, F., & Ardehali, H. (2008). Glucose Phosphorylation and Mitochondrial Binding Are Required for the Protective Effects of Hexokinases I and II. *Molecular and Cellular Biology, 28*(3), 1007.

Sun, S. C. (2017). The non-canonical NF-κB pathway in immunity and inflammation. *Nature reviews. Immunology, 17*(9), 545-558.

Supplie, L. M., Düking, T., Campbell, G., Diaz, F., Moraes, C. T., Götz, M., Hamprecht, B., Boretius, S., Mahad, D., & Nave, K.-A. (2017). Respiration-Deficient Astrocytes Survive As Glycolytic Cells *In Vivo*. *The Journal of Neuroscience, 37*(16), 4231.

Taïb, B., Bouyakdan, K., Hryhorczuk, C., Rodaros, D., Fulton, S., & Alquier, T. (2013). Glucose regulates hypothalamic long-chain fatty acid metabolism via AMP-activated kinase (AMPK) in neurons and astrocytes. *The Journal of biological chemistry, 288*(52), 37216-37229.

Tallman, J. F., Thomas, J. W., & Gallager, D. W. (1978). GABAergic modulation of benzodiazepine binding site sensitivity. *Nature, 274*(5669), 383-385.

Tang, D., Kang, R., Coyne, C. B., Zeh, H. J., & Lotze, M. T. (2012). PAMPs and DAMPs: signal 0s that spur autophagy and immunity. *Immunological reviews, 249*(1), 158-175.

Tannahill, G. M., Curtis, A. M., Adamik, J., Palsson-McDermott, E. M., McGettrick, A. F., Goel, G., Frezza, C., Bernard, N. J., Kelly, B., Foley, N. H., Zheng, L., Gardet, A., Tong, Z., Jany, S. S., Corr, S. C., Haneklaus, M., Caffrey, B. E., Pierce, K., Walmsley, S., Beasley, F. C., Cummins, E., Nizet, V.,

Whyte, M., Taylor, C. T., Lin, H., Masters, S. L., Gottlieb, E., Kelly, V. P., Clish, C., Auron, P. E., Xavier, R. J., & O'Neill, L. A. J. (2013). Succinate is an inflammatory signal that induces IL-1β through HIF-1α. *Nature, 496*(7444), 238-242.

Tarassishin, L., Suh, H. S., & Lee, S. C. (2014). LPS and IL-1 differentially activate mouse and human astrocytes: role of CD14. *Glia, 62*(6), 999–1013

Thapa, B., & Lee, K. (2019). Metabolic influence on macrophage polarization and pathogenesis. *BMB reports, 52*(6), 360-372.

Tilleux, S., & Hermans, E. (2007). Neuroinflammation and regulation of glial glutamate uptake in neurological disorders. *Journal of Neuroscience Research, 85*(10), 2059-2070.

Tilstra, J. S., Gaddy, D. F., Zhao, J., Davé, S. H., Niedernhofer, L. J., Plevy, S. E., & Robbins, P. D. (2014). Pharmacologic IKK/NF-κB inhibition causes antigen presenting cells to undergo TNFα dependent ROS-mediated programmed cell death. *Scientific reports, 4*, 3631-3631.

Tong, X., Ao, Y., Faas, G. C., Nwaobi, S. E., Xu, J., Haustein, M. D., Anderson, M. A., Mody, I., Olsen, M. L., Sofroniew, M. V., & Khakh, B. S. (2014). Astrocyte Kir4.1 ion channel deficits contribute to neuronal dysfunction in Huntington's disease model mice. *Nature Neuroscience, 17*(5), 694-703.

Tonon, M.-C., Vaudry, H., Chuquet, J., Guillebaud, F., Fan, J., Masmoudi-Kouki, O., Vaudry, D., Lanfray, D., Morin, F., Prevot, V., Papadopoulos, V., Troadec, J.-D., & Leprince, J. (2019). Endozepines and their receptors: Structure, functions and pathophysiological significance. *Pharmacology & therapeutics*, 107386-107386.

Tornatore, L., Thotakura, A. K., Bennett, J., Moretti, M., & Franzoso, G. (2012). The nuclear factor kappa B signaling pathway: integrating metabolism with inflammation. *Trends in Cell Biology, 22*(11), 557-566.

Tounai, H., Hayakawa, N., Kato, H., & Araki, T. (2007). Immunohistochemical Study on Distribution of NF-κB and p53 in Gerbil Hippocampus after Transient Cerebral Ischemia: Effect of Pitavastatin. *Metabolic Brain Disease, 22*(1), 89.

Tremblay, M. E., Cookson, M. R., & Civiero, L. (2019). Glial phagocytic clearance in Parkinson's disease. Molecular neurodegeneration, 14(1), 16.

Tu, L. N., Morohaku, K., Manna, P. R., Pelton, S. H., Butler, W. R., Stocco, D. M., & Selvaraj, V. (2014). Peripheral Benzodiazepine Receptor/Translocator Protein Global Knockout Mice are Viable with no Effects on Steroid Hormone Biosynthesis. *Journal of Biological Chemistry*, *289*, 27444-27454

Tu, L. N., Zhao, A. H., Hussein, M., Stocco, D. M., & Selvaraj, V. (2016). Translocator Protein (TSPO) Affects Mitochondrial Fatty Acid Oxidation in Steroidogenic Cells. *Endocrinology, 157*(3), 1110-1121.

Twig, G., & Shirihai, O. S. (2011). The interplay between mitochondrial dynamics and mitophagy. *Antioxidants & redox signaling, 14*(10), 1939-1951.

Vafai, S. B., & Mootha, V. K. (2012). Mitochondrial disorders as windows into an ancient organelle. *Nature, 491*(7424), 374-383.

Vainshtein, A., Veenman, L., Shterenberg, A., Singh, S., Masarwa, A., Dutta, B., Island, B., Tsoglin, E., Levin, E., Leschiner, S., Maniv, I., Pe'er, L., Otradnov, I., Zubedat, S., Aga-Mizrachi, S., Weizman, A., Avital, A., Marek, I., & Gavish, M. (2015). Quinazoline-based tricyclic compounds that regulate programmed cell death, induce neuronal differentiation, and are curative in animal models for excitotoxicity and hereditary brain disease. *Cell death discovery, 1*, 15027-15027.

Van den Bossche, J., O'Neill, L. A., & Menon, D. (2017). Macrophage Immunometabolism: Where Are We (Going)? *Trends in Immunology, 38*(6), 395-406.

van der Windt, G. J. W., Everts, B., Chang, C.-H., Curtis, J. D., Freitas, T. C., Amiel, E., Pearce, E. J., & Pearce, E. L. (2012). Mitochondrial respiratory capacity is a critical regulator of CD8+ T cell memory development. *Immunity, 36*(1), 68-78.

van Uden, P., Kenneth, N. S., & Rocha, S. (2008). Regulation of hypoxia-inducible factor-1alpha by NF-kappaB. *The Biochemical journal, 412*(3), 477-484.

Vander Heiden, M. G., Cantley, L. C., & Thompson, C. B. (2009). Understanding the Warburg Effect: The Metabolic Requirements of Cell Proliferation. *Science, 324*(5930), 1029.

Vardjan, N., Chowdhury, H. H., Horvat, A., Velebit, J., Malnar, M., Muhič, M., Kreft, M., Krivec, Š. G., Bobnar, S. T., Miš, K., Pirkmajer, S., Offermanns, S., Henriksen, G., Storm-Mathisen, J., Bergersen, L. H., & Zorec, R.

(2018). Enhancement of Astroglial Aerobic Glycolysis by Extracellular Lactate-Mediated Increase in cAMP. *Frontiers in Molecular Neuroscience, 11*, 148.

Vats, D., Mukundan, L., Odegaard, J. I., Zhang, L., Smith, K. L., Morel, C. R., Wagner, R. A., Greaves, D. R., Murray, P. J., & Chawla, A. (2006). Oxidative metabolism and PGC-1beta attenuate macrophage-mediated inflammation. *Cell metabolism, 4*(1), 13-24.

Veenman, L., Shandalov, Y., & Gavish, M. (2008). VDAC activation by the 18 kDa translocator protein (TSPO), implications for apoptosis. *Journal of bioenergetics and biomembranes, 40*(3), 199-205.

Veenman, L., Vainshtein, A., Yasin, N., Azrad, M., & Gavish, M. (2016). Tetrapyrroles as Endogenous TSPO Ligands in Eukaryotes and Prokaryotes: Comparisons with Synthetic Ligands. *International Journal of Molecular Sciences, 17*(6), 880.

Veiga, S., Carrero, P., Pernia, O., Azcoitia, I., & Garcia-Segura, L. M. (2007). Translocator protein (18 kDa) is involved in the regulation of reactive gliosis. *Glia, 55*(14), 1426-1436.

Vergadi, E., Ieronymaki, E., Lyroni, K., Vaporidi, K., & Tsatsanis, C. (2017). Akt Signaling Pathway in Macrophage Activation and M1/M2 Polarization. *The Journal of Immunology, 198*(3), 1006.

Verkhratsky, A., Parpura, V., Vardjan, N., & Zorec, R. (2019). Physiology of Astroglia. In A. Verkhratsky, M. S. Ho, R. Zorec, & V. Parpura (Eds.), *Neuroglia in Neurodegenerative Diseases* (pp. 45-91). Singapore: Springer Singapore.

Viola, A., Munari, F., Sánchez-Rodríguez, R., Scolaro, T., & Castegna, A. (2019). The Metabolic Signature of Macrophage Responses. *Frontiers in Immunology, 10*, 1462-1462.

Vittoria, I., Ciro Leonardo, P., & Vito, I. (2019). Metabolic Routes in Inflammation: The Citrate Pathway and its Potential as Therapeutic Target. *Current Medicinal Chemistry, 26*(40), 7104-7116.

Vlachaki Walker, J. M., Robb, J. L., Cruz, A. M., Malhi, A., Weightman Potter, P. G., Ashford, M. L. J., McCrimmon, R. J., Ellacott, K. L. J., & Beall, C. (2017). AMP-activated protein kinase (AMPK) activator A-769662 increases intracellular calcium and ATP release from astrocytes in an

AMPK-independent manner. *Diabetes, Obesity and Metabolism, 19*(7), 997-1005.

Votyakova, T. V., & Reynolds, I. J. (2001). ΔΨm-Dependent and -independent production of reactive oxygen species by rat brain mitochondria. *Journal of Neurochemistry, 79*(2), 266-277.

Wager, L. C. M., & Wormley, F. L., Jr. (2014). Classical versus alternative macrophage activation: the Ying and the Yang in host defense against pulmonary fungal infections. *Mucosal Immunology, 7*(5), 1023-1035.

Wai, T., & Langer, T. (2016). Mitochondrial Dynamics and Metabolic Regulation. *Trends in Endocrinology & Metabolism, 27*(2), 105-117.

Wang, F., Zhang, S., Vuckovic, I., Jeon, R., Lerman, A., Folmes, C. D., Dzeja, P. P., & Herrmann, J. (2018). Glycolytic Stimulation Is Not a Requirement for M2 Macrophage Differentiation. *Cell metabolism, 28*(3), 463-475.e464.

Wang, H., Sharma, L., Lu, J., Finch, P., Fletcher, S., & Prochownik, E. V. (2015). Structurally diverse c-Myc inhibitors share a common mechanism of action involving ATP depletion. *Oncotarget, 6*(18), 15857-15870.

Wang, R., Dillon, Christopher P., Shi, Lewis Z., Milasta, S., Carter, R., Finkelstein, D., McCormick, Laura L., Fitzgerald, P., Chi, H., Munger, J., & Green, Douglas R. (2011). The Transcription Factor Myc Controls Metabolic Reprogramming upon T Lymphocyte Activation. *Immunity, 35*(6), 871-882.

Wang, S., Liu, R., Yu, Q., Dong, L., Bi, Y., & Liu, G. (2019). Metabolic reprogramming of macrophages during infections and cancer. *Cancer Letters, 452*, 14-22.

Wang, T., Liu, H., Lian, G., Zhang, S.-Y., Wang, X., & Jiang, C. (2017). HIF1α-Induced Glycolysis Metabolism Is Essential to the Activation of Inflammatory Macrophages. *Mediators of inflammation, 2017*, 9029327-9029327.

Waters, M. R., Gupta, A. S., Mockenhaupt, K., Brown, L. N., Biswas, D. D., & Kordula, T. (2019). RelB acts as a molecular switch driving chronic inflammation in glioblastoma multiforme. *Oncogenesis, 8*(6), 37.

Weiss, J. M., Downie, S. A., Lyman, W. D., & Berman, J. W. (1998). Astrocyte-Derived Monocyte-Chemoattractant Protein-1 Directs the Transmigration of Leukocytes Across a Model of the Human Blood-Brain Barrier. *The Journal of Immunology, 161*(12), 6896.

Werry, E. L., Bright, F. M., Piguet, O., Ittner, L. M., Halliday, G. M., Hodges, J. R., Kiernan, M. C., Loy, C. T., Kril, J. J., & Kassiou, M. (2019). Recent Developments in TSPO PET Imaging as A Biomarker of Neuroinflammation in Neurodegenerative Disorders. *International Journal of Molecular Sciences, 20*(13), 3161.

Whitton, P. S. (2007). Inflammation as a causative factor in the aetiology of Parkinson's disease. *British Journal of Pharmacology, 150*(8), 963-976.

Wieman, H. L., Wofford, J. A., & Rathmell, J. C. (2007). Cytokine stimulation promotes glucose uptake via phosphatidylinositol-3 kinase/Akt regulation of Glut1 activity and trafficking. *Molecular biology of the cell, 18*(4), 1437-1446.

Williams, N. C., & O'Neill, L. A. J. (2018). A Role for the Krebs Cycle Intermediate Citrate in Metabolic Reprogramming in Innate Immunity and Inflammation. *Frontiers in Immunology, 9*, 141-141.

Williamson, R. T. (1901). On the Treatment of Glycosuria and Diabetes Mellitus with Sodium Salicylate. *British medical journal, 1*(2100), 760-762.

Wilson, E. H., Weninger, W., & Hunter, C. A. (2010). Trafficking of immune cells in the central nervous system. *The Journal of Clinical Investigation, 120*(5), 1368-1379.

Wilson, J. E. (2003). Isozymes of mammalian hexokinase: structure, subcellular localization and metabolic function. *Journal of Experimental Biology, 206*(12), 2049.

World Health Organisation. (2019). Dementia. Retrieved from https://www.who.int/news-room/fact-sheets/detail/dementia

Ensembl. (2020). Transcript: TSPO-202. Retrieved from http://www.ensembl.org/Homo_sapiens/Transcript/Summary?db=core;g=ENSG00000100300;r=22:43151935-43163241;t=ENST00000337554

Xie, M., Yu, Y., Kang, R., Zhu, S., Yang, L., Zeng, L., Sun, X., Yang, M., Billiar, T. R., Wang, H., Cao, L., Jiang, J., & Tang, D. (2016). PKM2-dependent glycolysis promotes NLRP3 and AIM2 inflammasome activation. *Nature communications, 7*, 13280.

Xu, C.-Y., Zhang, W.-S., Zhang, H., Cao, Y., & Zhou, H.-Y. (2019). The Role of Connexin-43 in the Inflammatory Process: A New Potential Therapy to Influence Keratitis. *Journal of ophthalmology, 2019*, 9312827-9312827.

Yang, J. S., Wei, H. X., Chen, P. P., & Wu, G. (2018). Roles of Eph/ephrin bidirectional signaling in central nervous system injury and recovery. *Experimental and therapeutic medicine, 15*(3), 2219–2227.

Yang, L., Xie, M., Yang, M., Yu, Y., Zhu, S., Hou, W., Kang, R., Lotze, M. T., Billiar, T. R., Wang, H., Cao, L., & Tang, D. (2014). PKM2 regulates the Warburg effect and promotes HMGB1 release in sepsis. *Nature communications, 5*, 4436-4436.

Yang Sheng, H., Xu, H., & Xin Hua, L. (2019). STAT3: A Potential Drug Target for Tumor and Inflammation. *Current Topics in Medicinal Chemistry, 19*(15), 1305-1317.

Yao, Y., & Tsirka, S. E. (2014). Monocyte chemoattractant protein-1 and the blood-brain barrier. *Cellular and molecular life sciences : CMLS, 71*(4), 683-697.

Yeliseev, A. A., & Kaplan, S. (1995). A Sensory Transducer Homologous to the Mammalian Peripheral-type Benzodiazepine Receptor Regulates Photosynthetic Membrane Complex Formation in Rhodobacter sphaeroides 2.4.1. *Journal of Biological Chemistry, 270*(36), 21167-21175.

Yeliseev, A. A., Krueger, K. E., & Kaplan, S. (1997). A mammalian mitochondrial drug receptor functions as a bacterial "oxygen" sensor. *Proceedings of the National Academy of Sciences of the United States of America, 94*(10), 5101-5106.

Yellen, G. (2018). Fueling thought: Management of glycolysis and oxidative phosphorylation in neuronal metabolism. *The Journal of Cell Biology, 217*(7), 2235-2246.

Yeung, S. J., Pan, J., & Lee, M. H. (2008). Roles of p53, Myc and HIF-1 in Regulating Glycolysis — the Seventh Hallmark of Cancer. *Cellular and Molecular Life Sciences, 65*(24), 3981.

Yi, C., Mei, X., Ezan, P., Mato, S., Matias, I., Giaume, C., & Koulakoff, A. (2016). Astroglial connexin43 contributes to neuronal suffering in a mouse model of Alzheimer's disease. *Cell Death & Differentiation, 23*(10), 1691-1701.

Zamanian, J. L., Xu, L., Foo, L. C., Nouri, N., Zhou, L., Giffard, R. G., & Barres, B. A. (2012). Genomic analysis of reactive astrogliosis. *The Journal of neuroscience : the official journal of the Society for Neuroscience, 32*(18), 6391-6410.

Zattoni, M., Mura, M. L., Deprez, F., Schwendener, R. A., Engelhardt, B., Frei, K., & Fritschy, J.-M. (2011). Brain infiltration of leukocytes contributes to the pathophysiology of temporal lobe epilepsy. *The Journal of neuroscience : the official journal of the Society for Neuroscience, 31*(11), 4037-4050.

Zemirli, N., Pourcelot, M., Ambroise, G., Hatchi, E., Vazquez, A., & Arnoult, D. (2014). Mitochondrial hyperfusion promotes NF-κB activation via the mitochondrial E3 ligase MULAN. *The FEBS Journal, 281*(14), 3095-3112.

Zha, X., Hu, Z., Ji, S., Jin, F., Jiang, K., Li, C., Zhao, P., Tu, Z., Chen, X., Di, L., Zhou, H., & Zhang, H. (2015). NFκB up-regulation of glucose transporter 3 is essential for hyperactive mammalian target of rapamycin-induced aerobic glycolysis and tumor growth. *Cancer Letters, 359*(1), 97-106.

Zhang, J., Jia, L., Lin, W., Yip, Y. L., Lo, K. W., Lau, V. M. Y., Zhu, D., Tsang, C. M., Zhou, Y., Deng, W., Lung, H. L., Lung, M. L., Cheung, L. M., & Tsao, S. W. (2017a). Epstein-Barr Virus-Encoded Latent Membrane Protein 1 Upregulates Glucose Transporter 1 Transcription via the mTORC1/NF-κB Signaling Pathways. *Journal of virology, 91*(6), e02168-02116.

Zhang, M.-R., Kumata, K., Maeda, J., Yanamoto, K., Hatori, A., Okada, M., Higuchi, M., Obayashi, S., Suhara, T., & Suzuki, K. (2007). 11C-AC-5216: A Novel PET Ligand for Peripheral Benzodiazepine Receptors in the Primate Brain. *Journal of Nuclear Medicine, 48*(11), 1853-1861.

Zhang, Y., Reichel, J. M., Han, C., Zuniga-Hertz, J. P., & Cai, D. (2017b). Astrocytic Process Plasticity and IKKβ/NF-κB in Central Control of Blood Glucose, Blood Pressure, and Body Weight. *Cell metabolism, 25*(5), 1091-1102.

Zhao, A. H., Tu, L. N., Mukai, C., Sirivelu, M. P., Pillai, V. V., Morohaku, K., Cohen, R., & Selvaraj, V. (2016). Mitochondrial Translocator Protein (TSPO) Function Is Not Essential for Heme Biosynthesis. *The Journal of biological chemistry, 291*(4), 1591-1603.

Zhao, R.-Z., Jiang, S., Zhang, L., & Yu, Z.-B. (2019). Mitochondrial electron transport chain, ROS generation and uncoupling (Review). *International journal of molecular medicine, 44*(1), 3-15.

Zheng, M., Son, M., Park, C., Park, J., Jo, E., Yoon, W., Park, S., Hwang, B., Lim, K. (2005). Transcriptional repression of vimentin gene expression by pyrroline dithiocarbamate during 12-O-tetradecanoylphorbol-13-acetate-dependent differentiation of HL-60 cells. *Oncology Reports, 14*, 713-717.

Zhong, Z., Umemura, A., Sanchez-Lopez, E., Liang, S., Shalapour, S., Wong, J., He, F., Boassa, D., Perkins, G., Ali, Syed R., McGeough, Matthew D., Ellisman, Mark H., Seki, E., Gustafsson, Asa B., Hoffman, Hal M., Diaz-Meco, Maria T., Moscat, J., & Karin, M. (2016). NF-κB Restricts Inflammasome Activation via Elimination of Damaged Mitochondria. *Cell, 164*(5), 896-910.

Zhou, C.-H., Zhu, Y.-Z., Zhao, P.-P., Xu, C.-M., Zhang, M.-X., Huang, H., Li, J., Liu, L., & Wu, Y.-Q. (2015). Propofol Inhibits Lipopolysaccharide-Induced Inflammatory Responses in Spinal Astrocytes via the Toll-Like Receptor 4/MyD88-Dependent Nuclear Factor-κB, Extracellular Signal-Regulated Protein Kinases1/2, and p38 Mitogen-Activated Protein Kinase Pathways. *Anesthesia & Analgesia, 120*(6).

Ziello, J. E., Jovin, I. S., & Huang, Y. (2007). Hypoxia-Inducible Factor (HIF)-1 regulatory pathway and its potential for therapeutic intervention in malignancy and ischemia. *The Yale journal of biology and medicine, 80*(2), 51–60.